

POLYMER ELECTROLYTES FOR LITHIUM BATTERIES:
AN IMPROVEMENT IN IONIC CONDUCTIVITY AND LITHIUM DENDRITE
RESISTANCE

A Dissertation

Presented to the Faculty of the Graduate School
of Cornell University

In Partial Fulfillment of the Requirements for the Degree of
Doctor of Philosophy

by

Qi Zheng

August 2017

© 2017 Qi Zheng

POLYMER ELECTROLYTES FOR LITHIUM BATTERIES:
AN IMPROVEMENT IN IONIC CONDUCTIVITY AND LITHIUM DENDRITE
RESISTANCE

Qi Zheng, Ph. D.

Cornell University 2017

Rechargeable lithium-ion batteries are widely used in portable devices and electric vehicles. The electrolyte, composed of organic liquid and lithium salt, is a critical part of the battery that conducts ions during charging and discharging. Because of the flammability of the organic liquid, conventional electrolytes cause safety concerns, especially under thermal runaway conditions. Moreover, liquid electrolytes are not fully compatible with lithium metal, a promising high capacity anode material for future lithium batteries, because of the uneven electrodeposition of Li (Li dendrites). Solid polymer electrolytes (SPEs) have been reported as promising candidates to replace liquid electrolytes with advantages on processability, mechanical strength, and non-flammability. However, the low ionic conductivity of SPEs at room temperature preclude their practical application. This dissertation describes studies intended to improve the ionic conductivity and Li dendrite suppression of a series of poly(ethylene oxide) (PEO) and polyether based polymer electrolytes.

We first did a systematic property-structure relationship study on a family of cross-linked hydrocarbon/PEO electrolytes by tuning the crystallinity of the hydrocarbon backbone. We were able to develop a hydrogenated polynorbornene backbone that increased the ionic conductivity to $\sim 10^{-3}$ S/cm at room temperature without significant sacrifice on its Li dendrite resistance. With the help of theoretical

chemists, we then synthesized an alternating copolymer of ethylene oxide (EO) and trimethylene oxide (TMO), which was predicted to have higher ionic conductivity than that of PEO at room temperature. The cyclic ether monomer of this alternating polymer was prepared from a novel ester-to-ether reduction. A series of EO/TMO random copolymers were also synthesized for comparison. One of the EO/TMO random copolymers showed an ionic conductivity of 10^{-4} S/cm at room temperature, among the highest ionic conductivities reported for SPEs. Finally, we explored further the application of the ester-to-ether reduction on some polyesters and successfully synthesized polyethers that have never been accessed before.

We anticipate that the polymer electrolytes described in this work will provide useful insights for future design of SPEs and the concept of direct synthesis of polyethers from polyesters may help prepare new polyethers for SPE and other applications.

BIOGRAPHICAL SKETCH

Qi Zheng was born in Suzhou, China, a beautiful garden city with a history of more than 2500 years, on October 6, 1989. He had his first chemistry class with Ms. Huifang Wu when he was a 3rd year middle school student and became fascinated about the power of chemistry. He then started to do some simple chemistry experiments at home, including the preparation of oxygen from potassium permanganate and burning the carpet with hydrogen peroxide (accidently). After graduating from middle school in 2005, he went to Suzhou High School of Jiangsu Province for his high school education. He participated in the Chemistry Olympiad competition and won the first prize of Jiangsu province twice during high school, which helped him to get admitted to Nanjing University free from entrance examinations after his graduation in 2008.

In Nanjing University, he was admitted to the Kuang Yaming Honors School, where he had multidisciplinary trainings in math, physics, chemistry, and biology for the first two years. Because of his love of chemistry, he chose chemistry as his major in his junior year without any hesitation. After learned a lot about chemistry, he decided to conduct some original researches of chemistry and joined Prof. Jinglin Zuo's group as an undergraduate researcher. Prof. Zuo was an expert in coordination chemistry and the naive reason he joined Zuo's group was simply because he loved the beautiful colors of coordination compounds. His project in Zuo's lab was on the synthesis and characterization of molecular magnets based on organometallic complex. He had a great time there synthesizing ligands and growing crystals. Because of his interest in chemistry research and curiosity of the outside world, he decided to pursue a PhD degree in USA. He got offers from UIUC, UMN, TAMU, and Cornell. Because Cornell is a

prestigious ivy league school and one of his favorite writers – Hu Shih graduated from Cornell, he decided to take the offer from Cornell in the spring of 2012.

After his undergraduate research, he became more mature and decided to conduct researches that will have practical applications. In Cornell, he joined the group of Prof. Geoffrey Coates, where he worked on the development of polymer electrolytes for lithium batteries during his Ph.D. study because both polymers and lithium batteries have gained wide applications. During his stay in Coates lab, he enjoyed his everyday with the best group members in the world. He also had the privilege to collaborate with exceptional scientists both within and outside of Cornell. Upon completion of his Ph.D., he will step into the real world and move to the great city of Pittsburgh, where he will begin his career as a research chemist at PPG Industries.

To my parents and Na for all your support and love

ACKNOWLEDGMENTS

First and foremost, I would like to thank my advisor Prof. Geoff Coates. Joining his lab is the single best decision I've ever made during my entire Ph.D. career. He is the most supportive advisor I could ever imagine. He supported me when I couldn't teach one course I would like to teach. "I think I got it worked out. Let's see what happens by tomorrow", he said in his email. He supported me to try any reactions I was interested and always celebrated with me when the reaction worked and mourned with me when it didn't. He supported me when I was puzzled and upset about the experiments. We spent many Saturday afternoons in the conference room brainstorming new ideas. He supported me when I was publishing my first paper. He spent a lot of money to have a copy editor carefully editing my manuscript and taught me how to improve my scientific writing. He supported me when I was looking for jobs. He connected me with previous group members and provided valuable information about my future employer. He even indirectly supported me to find my girlfriend, Na. Na said she found my contact information from our group website because it was updated and looked well-organized. Geoff is an incredible scientist, manager, and advisor. His recent election to the National Academy of Sciences is another great example to demonstrate who he is. It's my great honor to work with him for the past five years. I'll miss you Geoff!

I also want to thank Prof. Héctor Abruña, Prof. Song Lin, and Prof. William Dichtel for serving on my committee. Prof. Abruña was always willing to talk to me about my research and I was also lucky to have Na, his student, as my girlfriend. He was even kind enough to introduce Na and me to his house for his summer party twice. I can still remember the delicious food, stunning art crafts from all over the world, and the beautiful wine cellar. Although I did not get a chance to engage a lot with Prof. Lin, I have always been an admirer of his research. I'll never forget the day when Prof. Lin

gave his faulty candidate talk – it was the best I have ever attended. His exceptional presentation skills and elegant researches deeply impressed me. I have had the chance to briefly collaborated with Prof. Dichtel on a covalent organic framework (COF) project. His sharp intuition of chemistry greatly inspired me and I wish him all the best in Northwestern.

I owe a huge debt of gratitude to Dr. Anne LaPointe for all her support during my Ph.D. career. She is the go-to person in the lab if I have any questions. She helped me editing my paper manuscript. She gave a lot of invaluable advices during my job hunting and connected me with my future employer. I couldn't thank her more for what she has done for me.

I would like to thank Kelly Case, our great group assistant, not only because she keeps our group running by ordering supplies and chemicals, and shipping my samples out but also because of all the conversations I had with her. She is such a kind and great person to talk to. I enjoyed listening to all the stories she had at Cornell, the history of this department, and her interest about watching pandas and collecting magnets from Oakwood.

I enjoyed my every day at Coates lab because of the best group members in the world. I must thank Dr. Rachna Khurana first. She was my mentor when I joined the group and my Ph.D. project was based on the work she pioneered. She taught me how to synthesize monomers, how to cast membranes, and how to characterize them. She is an amazing chemist and I'm grateful for her helps. I would like to thank Dr. Tulaza Vaidya for sharing her secret on communicating with people and hosting me during my visit to Dow. Dr. Yuki Jung was in the same collaboration I had and she taught me a lot on how to coordinate with my collaborators, and I'm thankful to her for all her advices. I would like to thank Dr. Masato Mizutani for sparing his dry EO to me for my reactions and all his kind helps and suggestions. Dr. Brandon Tiegs have always been helpful and

I'm grateful for his enormous help when our glove box was down. I would like to thank Prof. Hegui Gong for his support and insights during his visit here. Other past group members I want to acknowledge includes: Dr. Chad Ellis, Dr. Rocco Girolamo, Dr. Angie DiCiccio, Dr. Michael Mulzer, "C", Dr. Kristina Hugar, Dr. Ian Childers, Dr. Tam Truong, Dr. Nate Van Zee, Mr. Jeff Marvin, and Dr. Julie Whitehead.

I would like to thank Kyle, Jessica, and Dave for accompanying me over the past five years. We went to the Cornell at the same time; we took our first class together; and now we are going to graduate at the same time. Congratulations! Dr Wei You, although you have just stayed here for one year, I have already owed you a lot. Your helps in research, thesis writing, and life are all invaluable to me. Good luck in your job hunting next year! I would like to thank Dr. James Eagen for all the helpful suggestions you gave to me. Dr. Brooks Abel and Dr. Kristine Klimovica, you have just joined the group for a few months and I hope you will enjoy your stay in this group. Maria, you are one of kindest people I've ever met. You helped me on GPCs, on glove boxes, on job applications, on manuscript preparations, on many many other things. I enjoyed every talk I had with you. Michelle, Xiaopeng, and Lilli, you are all doing incredibly good jobs and I'm looking forward to reading about your research in the future. Aran, Omar, and Ting-Wei, you are all going to be Masters very soon and I wish you all the best in your future research. Hillis and Bryce, it was a great pleasure to teach you for a while and I have no doubt that you will do outstanding jobs in the future. Sam, it's a great pleasure working in the same lab with you. Good luck in Princeton! Ahmed, you are already a legend and keep your big smile. Good luck in Oxford! Anna, I hope you will enjoy your last year in Coates group.

I've been fortunate to collaborate with extraordinary professors, postdoc fellows, and graduate students both in and outside Cornell. These include: Prof. Lynden Archer, Prof. Nitash Balsara, Prof. Tom Miller, Prof. Rachel Segalman, Dr. Lin Ma, Dr. Mike

Webb, Dr. Brett Savoie, Danielle Pesko, Emily Davidson. I would like to thank Dr. Ivan Keresztes for helps in NMR techniques and Tony Condo in mass spectroscopy.

I have to thank all my other friends at Cornell here – Lihai Qian, Yi Xu, Naigeng Chen, Yuxing Tang, Xiaoyu Zhang, Huichan Zhao, Tianshu Liu, Liang Chen, Xuetian Ma, Saien Xie, Jia Tian, Xiaodong Wang, Ningmu Zou, Niankai Fu, Wei Hao, Dong Ren, Luxi Shen, Yuhui Zhou, Zirong Zhang, Yugang Zhang, Miao Wang, Xiangyu Wu, Yao Yang, Xinran Feng, Kaori Kubo, Sine Somsinee, Saba Parvez, Won Jung, Yun Ma, Janis Jermarks.

I would like to thank financial support from the Cornell Chemistry Department for my teaching assistantship and NSF DMREF program for my research assistantship.

Last but not least, I want to thank my parents for their consistent and unconditional support and love over my life. I couldn't finish my Ph.D. study without the love from my girlfriend, Na, who is an angel sent by the god. I remember she waited me for many "10 minutes" to let me finish my work in the lab. I remember she accompanied me for 3 hours under the sunlight for entering the career fair. I remember I practiced my job interview in front of her. I remember she celebrated with me at Yellowstone when I found my paper was accepted. I remember every days and nights I spent with her and I'll cherish every second spent with her in the future.

To finish my acknowledgement, I would like to thank Cornell by quoting what President Martha E. Pollack said during her first commencement address, "Cornell will always be a part of you and you will always be a part of Cornell."

TABLE OF CONTENTS

Biographical Sketch	v
Acknowledgements	viii
Table of Contents	xii
List of Figures	xv
List of Tables	xxii
List of Abbreviations	xxiv
List of Symbols	xxvii

Chapter 1 An overview of polymer electrolytes for lithium batteries

1.1	Introduction	2
1.2	Lithium batteries	3
1.3	Liquid Electrolytes	7
1.4	Polymer electrolytes	10
1.4.1	The discovery of polymer electrolytes	10
1.4.2	General considerations	11
1.4.2.1	Ionic conductivity	11
1.4.2.2	Voltage stability	13
1.4.2.3	Transference number	14
1.4.2.4	Lithium dendrite suppression	16
1.5	Types of polymer electrolytes.	17
1.5.1	Dry (solid) polymer electrolytes	17
1.5.1.1	Polyethers	17
1.5.1.2	Polycarbonates	21
1.5.1.3	Polyesters	23
1.5.1.4	Si-containing polymers	24
1.5.1.5	B-containing polymers	25
1.5.1.6	N-containing polymers	26
1.5.1.7	S-containing polymers	27
1.5.1.8	F-containing polymers	27
1.5.2	Gel polymer electrolytes	28
1.5.2.1	Liquid plasticizer in gel polymer electrolytes	28
1.5.2.2	Polymer matrix in gel polymer electrolytes	30
1.5.3	Composite polymer electrolytes	31
1.6	Conclusions	33
	References	34

Chapter 2 Structure–property study of cross-linked hydrocarbon/poly(ethylene oxide) electrolytes with superior conductivity and dendrite resistance

2.1	Abstract	43
2.2	Introduction	44
2.3	Results and Discussions	46
2.4	Conclusions	61

2.5	Experimental	62
2.5.1	General Considerations	62
2.5.2	Materials	63
2.5.3	Synthesis of PEO Crosslinkers	64
2.5.3.1	Preparation of endo/exo-bicyclo[2.2.1]hept-5-en-2-ylmethanol (2)	64
2.5.3.2	Preparation of endo/exo-5-(((4-(bromomethyl)benzyl)oxy)methyl)bicyclo[2.2.1]hept-2-ene (3)	67
2.5.3.3	Preparation of bis-norbornene terminated PEO crosslinker (1a)	70
2.5.4	Synthesis of the Cross-Linked Solid Polymer Electrolytes (SPEs)	72
2.5.4.1	Di-Norbornene Terminated PEO Crosslinker	72
2.5.4.2	Nomenclature of hPNB-PEO, PCOD-PEO Cross-Linked Solid Polymer Electrolyte	73
2.5.4.3	Sample procedure for the synthesis of hPNB-PEO, PCOD-PEO cross-linked system:	75
2.5.5	Control Experiment	76
2.5.6	Differential Scanning Calorimetry (DSC)	78
2.5.7	DC Ionic conductivity and VTF fitting	80
2.5.8	Galvanostatic Cycling Measurements	85
2.5.9	Galvanostatic Polarization Measurements	86
2.5.10	Rheology	86
2.5.11	SEM of the lithium metal after short-circuit	89
2.5.12	Electrochemical Impedance Spectroscopy (EIS)	90
2.5.13	Density measurements	91
2.5.14	Li transference number	92
2.5.15	Battery device test	93
	References	95

Chapter 3 Alternating and random copolymers of ethylene oxide and trimethylene oxide as solid polymer electrolytes for lithium batteries

3.1	Abstract	98
3.2	Introduction	99
3.3	Results and Discussions	102
3.4	Conclusions	115
3.5	Experimental	116
3.5.1	General	116
3.5.2	Materials	117
3.5.3	Synthesis	118
3.5.3.1	Synthesis of 1,4-dioxepan-5-one	118
3.5.3.2	Synthesis of 1,4-dioxepane	120
3.5.3.3	Polymerization of 1,4-dioxepane	122
3.5.3.4	Copolymerization of ethylene oxide (EO) and trimethylene oxide (TMO)	124
3.5.4	Thermal properties of the polymers and the electrolytes	126
3.5.5	Ionic conductivities	127

References	132
------------	-----

Chapter 4 Indium catalyzed reduction of polyesters to polyethers

4.1	Abstract	135
4.2	Introduction	136
4.3	Results and Discussions	137
4.3.1	Model reaction on poly(ϵ -caprolactone) (PCL)	137
4.3.2	Substrate scope	142
4.3.3	Catalyst screening	145
4.4	Conclusions	147
4.5	Experimental	148
4.5.1	General	148
4.5.2	Materials	149
4.5.3	Synthesis	150
4.5.3.1	Reduction on poly(γ -butyrolactone) (PBL, 1a)	150
4.5.3.2	Reduction on poly(δ -valerolactone) (PVL, 1b)	154
4.5.3.3	Reduction on poly(ϵ -caprolactone) (PCL, 1c)	158
4.5.3.4	Reduction on poly(6-methyl- ϵ -caprolactone) (1g)	160
4.5.3.5	Synthesis of (rac-tBuSalcy)InBr	166
4.5.4	Reaction temperature screening	167
References		169

Appendix A Synthesis of poly(1,3,6-trioxocane), poly(styrene-*b*-1,3,6-trioxocane), and their applications as polymer electrolytes

A.1	Introduction	171
A.2	Results and discussions	172
A.3	Experimental	178
A.3.1	General	178
A.3.2	Materials	180
A.3.3	Synthesis	181
A.3.3.1	Synthesis of 1,3,6-trioxocane	181
A.3.3.2	Synthesis of poly(1,3,6-trioxocane)	183
A.3.3.3	Synthesis of 2-hydroxyethyl 2-bromoisobutyrate (HEBI)	185
A.3.3.4	Synthesis of hydroxyl terminated polystyrene (PS-OH)	187
A.3.3.5	Synthesis of polystyrene- <i>b</i> -poly(1,3,6-trioxocane) (PS- <i>b</i> -P(MO-2EO))	189
A.3.4	GPC traces	191
References		192

LIST OF FIGURES

Figure 1.1	A scheme of a Li-ion battery during discharging.	3
Figure 1.2	A comparison on performance metrics of rechargeable batteries.	4
Figure 1.3	Schematic description for the growth of dendrite crystals on a Li surface. Figure reproduced from reference 6.	6
Figure 1.4	Mechanism of ion transport in PEO (adapted from reference 19).	11
Figure 1.5	Voltammogram obtained at 1 mV/s for P(STFSILi)- <i>b</i> -PEO- <i>b</i> -P(STFSILi) with 31 wt% P(STFSILi) (red curve) at 80 °C. For comparison, the voltammogram obtained in the same conditions with the neutral copolymer PS-PEO-PS with 30 wt% PS laden with LiTFSI at [EO]/[Li] = 25 (blue curve) is also given. (adapted from reference 36)	15
Figure 1.6	Structures of polyoxetane based polymers. ⁵³	21
Figure 1.7	Dependence on the concentration of the ionic conductivity at 60 °C and T_g for (a) PEO– and (b) PEC–LiTFSI electrolytes. (adapted from reference 63)	23
Figure 2.1	Cross-linked polyethylene/poly(ethylene oxide) (PE-PEO) solid polymer electrolyte (SPE). ¹⁰	46
Figure 2.2	Hydrogenated polynorbornene–polyethylene oxide (hPNB-PEO) and polycyclooctadiene–polyethylene oxide (PCOD-PEO) cross-linked polymer electrolyte synthesis and nomenclature.	48
Figure 2.3	Ionic conductivity of unplasticized polymer electrolyte with different numbers of ethylene oxide (EO) units in the cross-linker and various [cross-linker]:[monomer] ratios at 25 °C. The data for PE-PEO SPEs are from Reference 10.	50
Figure 2.4	Ionic conductivity of plasticized polymer electrolyte as a function of wt % of PEG 275 at 25 °C. All membranes had approximately 80 EO cross-linker units (70 for PE-PEO, ¹⁰ 88 for hPNB-PEO, and 75 for PCOD-PEO), [1a]:[NB] or [1b]:[COD] ratios of 1:15, and [EO]:[Li] compositions of 20:1. Error bars are smaller than the size of the data points. The data for PE-PEO SPEs are from Reference 10.	51

Figure 2.5	Galvanostatic cycling tests. Plot of C_d for polymer electrolytes. All samples were tested with a current density (J) of 0.26 mA/cm ² at 90 °C. Error bars are 33 h for hPNB-PEO and 67 h for PCOD-PEO. PE-PEO, PS-b-PEO, and PEO values are from the literature. ¹⁰⁻¹¹	56
Figure 2.6	Galvanostatic polarization tests. Plot of short-circuit time (t_{sc}) as a function of J at 90 °C. All membranes were plasticized with 32 wt % PEG 275 and had approximately 80 EO cross-linker units (70 for PE-PEO, ¹⁰ 88 for hPNB-PEO, and 75 for PCOD-PEO), [1a]:[NB] or [1b]:[COD] ratios of 1:15, and [EO]:[Li] composition of 20:1.	57
Figure 2.7	Scanning electron microscopy images of a short-circuited Li anode after galvanostatic (a) polarization (0.40 mA/cm ²) and (c) cycling (0.26 mA/cm ²) test with hPNB-PEO electrolyte (plasticized with 32 wt % PEG 275) and (b) polarization (0.40 mA/cm ²) and (d) cycling (0.26 mA/cm ²) test with PCOD-PEO electrolyte (plasticized with 32 wt % PEG 275).	58
Figure 2.8	Dynamic shear measurements on (a) hPNB-PEO and (b) PCOD-PEO electrolytes. All membranes were plasticized with 32 wt % PEG 275 and had approximately 80 EO cross-linker units (88 for hPNB-PEO and 75 for PCOD-PEO), [1a]:[NB] or [1b]:[COD] ratios of 1:15, and [EO]:[Li] compositions of 20:1.	60
Figure 2.9	General scheme for the synthesis of crosslinker 1a .	64
Figure 2.10	¹ H NMR spectrum of 2 in CDCl ₃ . Signal at 7.26 ppm is the residual CHCl ₃ .	66
Figure 2.11	¹³ C NMR spectrum of 2 in CDCl ₃ . Signal at 77.16 ppm is the residue CHCl ₃ .	66
Figure 2.12	¹ H NMR spectrum of 3 in CDCl ₃ . Signal at 7.26 ppm is the residual CHCl ₃ .	69
Figure 2.13	¹³ C NMR spectrum of 3 in CDCl ₃ . Signal at 77.16 ppm is the residual CHCl ₃ .	69
Figure 2.14	¹ H NMR spectrum of 1a in CDCl ₃ . Signal at 7.26 ppm is the residual CHCl ₃ .	71
Figure 2.15	¹³ C NMR spectrum of 1a in CDCl ₃ . Signal at 77.16 ppm is the residual CHCl ₃ .	71
Figure 2.16	MALDI-TOF mass spectrum of 1a with dithranol as the matrix.	72
Figure 2.17	A scheme of a Li-ion battery during discharging.	73

Figure 2.18	^1H NMR spectrum of hydrogenated film in CDCl_3 . Signal at 7.26 ppm is the residual CHCl_3 .	78
Figure 2.19	Real part of the ionic conductivity and $\tan(\delta)$ vs. frequency plot for $(^{8,5}\text{hPNB}_{0.11})(^{88,5}\text{PEO}_{0.46,0.43})$.	81
Figure 2.20	Galvanostatic cycling curve obtained for hPNB-PEO with 32 wt % plasticizer at fixed current density for 0.26 mA/cm^2 and 90°C . The short circuit time (t_{SC}) is pointed out; C_d value is 1638 C/cm^2 .	85
Figure 2.21	Voltage profile of galvanostatic polarization of hPNB-PEO system at fixed current density of 0.26 mA/cm^2 at 90°C . The short circuit time is determined at the moment when the sudden voltage drop is observed.	86
Figure 2.22	Rheological measurements on hPNB-PEO system with different weight% of the plasticizer at 90°C . All films had [NB]:[1a] ratio of 15:1 and [EO]:[Li] composition of 20:1. Storage modulus $G'(\omega)$ is shown with filled symbols, and the loss modulus $G''(\omega)$ is shown with hollow symbols. (a) 0 wt %, (b) 16 wt%, (c) 24 wt %, (d) 32 wt %, and (e) 40 w % PEG275 plasticizer in the cross-linked films.	87
Figure 2.23	Rheological measurements on PCOD-PEO system with different weight% of the plasticizer at 90°C . All films had [COD]:[1b] ratio of 15:1 and [EO]:[Li] composition of 20:1. Storage modulus $G'(\omega)$ is shown with filled symbols, and the loss modulus $G''(\omega)$ is shown with hollow symbols. (a) 0 wt %, (b) 16 wt%, (c) 24 wt %, (d) 32 wt %, and (e) 40 wt % PEG275 plasticizer in the cross-linked films.	88
Figure 2.24	SEM images of lithium metal after short-circuit. Galvanostatic polarization of hPNB-PEO system at (a) 0.26 mA/cm^2 ; (b) 0.4 mA/cm^2 ; (c) 1 mA/cm^2 ; (d) Galvanostatic cycling of hPNB-PEO system at 0.26 mA/cm^2 ; Galvanostatic polarization of PCOD-PEO system at (e) 0.26 mA/cm^2 ; (f) 0.4 mA/cm^2 ; (g) 1 mA/cm^2 ; (h) Galvanostatic cycling of PCOD-PEO system at 0.26 mA/cm^2 . Scale bar = $20 \mu\text{m}$.	89
Figure 2.25	(a) Impedance spectra for hPNB-PEO electrolytes with varied plasticizer weight at 18°C . (b) Impedance for hPNB-PEO with 32 wt % plasticizer at variable temperature. (c) Impedance spectra for PCOD-PEO electrolytes with varied plasticizer weight at 18°C . (d) Impedance for PCOD-PEO with 32 wt % plasticizer at variable temperature.	91

Figure 2.26	(a) Initial and steady state impedance spectra of lithium symmetric cell for unplasticized hPNB-PEO. (b) Steady state current measurement for unplasticized hPNB-PEO.	93
Figure 2.27	Charge/discharge profile of LiCoO ₂ /hPNB/Li battery at a discharge rate of 0.5 C.	94
Figure 3.1	Mean-square displacement (MSD) of a lithium cation obtained from KMC trajectories using the CS-DBP model. (adapted from reference 1).	100
Figure 3.2	Synthesis of 1,4-dioxepane	103
Figure 3.3	Mechanism of the cationic ring-opening polymerization of 1,4-dioxepane	106
Figure 3.4	Quantitative ¹³ C-NMR of alternating (a) and random (b) copolymers of EO and TMO	108
Figure 3.5	Ionic conductivity of PEO, PTMO and EO-TMO copolymers with variable temperatures at $r = 0.08$.	111
Figure 3.6	Ionic conductivity of PEO, PTMO and EO-TMO copolymers with different salt concentrations at 27 °C (a) and 90 °C (b).	112
Figure 3.7	¹ H-NMR spectrum of 1,4-dioxepan-5-one. Signal at 7.26 ppm is the residue CHCl ₃ .	119
Figure 3.8	¹³ C-NMR spectrum of 1,4-dioxepan-5-one. Signal at 77.16 ppm is the residue CHCl ₃ .	119
Figure 3.9	¹ H-NMR spectrum of 1,4-dioxepane. Signal at 7.26 ppm is the residue CHCl ₃ .	121
Figure 3.10	¹³ C-NMR spectrum of 1,4-dioxepane. Signal at 77.16 ppm is the residue CHCl ₃ .	121
Figure 3.11	¹ H-NMR spectrum of poly(1,4-dioxepane). Signal at 7.26 ppm is the residue CHCl ₃ .	123
Figure 3.12	¹³ C-NMR spectrum of poly(1,4-dioxepane). Signal at 77.16 ppm is the residue CHCl ₃ .	123
Figure 3.13	¹ H-NMR spectrum of poly(EO-co-TMO). Signal at 7.26 ppm is the residue CHCl ₃ .	125
Figure 3.14	¹³ C-NMR spectrum of poly(EO-co-TMO). Signal at 77.16 ppm is the residue CHCl ₃ .	125
Figure 3.15	Ionic conductivity of EO-TMO polymers as a function of $1000/(T-T_g+50)$ with $r = 0.08$.	129

Figure 3.16	Reduced ionic conductivity of EO-TMO polymers as a function of Li salt concentrations.	130
Figure 4.1	Proposed mechanism of indium catalyzed hydrosilylation on polyester	140
Figure 4.2	^1H -NMR spectrum of 1a . Signal at 7.26 ppm is the residue CHCl_3 .	151
Figure 4.3	^{13}C -NMR spectrum of 1a . Signal at 77.16 ppm is the residue CHCl_3 .	151
Figure 4.4	^1H -NMR spectrum of 2a . Signal at 7.26 ppm is the residue CHCl_3 .	153
Figure 4.5	^{13}C -NMR spectrum of 2a . Signal at 77.16 ppm is the residue CHCl_3 .	153
Figure 4.6	^1H -NMR spectrum of 1b . Signal at 7.26 ppm is the residue CHCl_3 .	155
Figure 4.7	^{13}C -NMR spectrum of 1b . Signal at 77.16 ppm is the residue CHCl_3 .	155
Figure 4.8	^1H -NMR spectrum of 2b . Signal at 7.26 ppm is the residue CHCl_3 .	157
Figure 4.9	^{13}C -NMR spectrum of 2b . Signal at 77.16 ppm is the residue CHCl_3 .	157
Figure 4.10	^1H -NMR spectrum of 2c . Signal at 7.26 ppm is the residue CHCl_3 .	159
Figure 4.11	^{13}C -NMR spectrum of 2c . Signal at 77.16 ppm is the residue CHCl_3 .	159
Figure 4.12	^1H -NMR spectrum of 6-methyl- ϵ -caprolactone. Signal at 7.26 ppm is the residue CHCl_3 .	161
Figure 4.13	^{13}C -NMR spectrum of 6-methyl- ϵ -caprolactone. Signal at 77.16 ppm is the residue CHCl_3 .	161
Figure 4.14	^1H -NMR spectrum of 1g . Signal at 7.26 ppm is the residue CHCl_3 .	163
Figure 4.15	^{13}C -NMR spectrum of 1g . Signal at 77.16 ppm is the residue CHCl_3 .	163
Figure 4.16	^1H -NMR spectrum of 2g . Signal at 7.26 ppm is the residue CHCl_3 .	165

Figure 4.17	^{13}C -NMR spectrum of 2g . Signal at 77.16 ppm is the residue CHCl_3 .	165
Figure 4.18	^1H -NMR spectrum of (<i>rac</i> - <i>t</i> BuSalcy)InBr. Signal at 7.26 ppm is the residue CHCl_3 .	167
Figure 4.19	GPC traced of reaction temperature screening. The molecular weights were calibrated with monodisperse polystyrene standards.	168
Figure A.1	Experimental connectivity, f_{exp} (defined as $f_{\text{exp}} = \sigma_r(\text{polymer})/\sigma_r(\text{PEO})$, with increasing x_{O} (mol% of O) at $r = 0.08$ (defined as $r = [\text{Li}]:[\text{O}]$) and $T - T_g = 75$ K. (adapted from reference ³).	172
Figure A.2	Ionic conductivity of PEO and P(MO-2EO) with increasing r ($[\text{Li}]:[\text{O}]$) at 90 °C.	174
Figure A.3	Transference number t_{Li^+} of PEO and P(MO-2EO) with increasing r ($[\text{Li}]:[\text{O}]$) at 90 °C.	174
Figure A.4	Effective ionic conductivity (σ_{eff}) of PEO and P(MO-2EO) with increasing r ($[\text{Li}]:[\text{O}]$) at 90 °C.	175
Figure A.5	Synthesis of PS- <i>b</i> -P(MO-2EO) block copolymer.	176
Figure A.6	^1H -NMR spectrum of 1,3,6-trioxocane. Signal at 7.26 ppm is the residue CHCl_3 .	182
Figure A.7	^{13}C -NMR spectrum of 1,3,6-trioxocane. Signal at 77.16 ppm is the residue CHCl_3 .	182
Figure A.8	^1H -NMR spectrum of poly(1,3,6-trioxocane). Signal at 7.26 ppm is the residue CHCl_3 .	184
Figure A.9	^{13}C -NMR spectrum of poly(1,3,6-trioxocane). Signal at 77.16 ppm is the residue CHCl_3 .	184
Figure A.10	^1H -NMR spectrum of HEBI. Signal at 7.26 ppm is the residue CHCl_3 .	186
Figure A.11	^{13}C -NMR spectrum of HEBI. Signal at 77.16 ppm is the residue CHCl_3 .	186
Figure A.12	^1H -NMR spectrum of PS-OH. Signal at 7.26 ppm is the residue CHCl_3 .	188
Figure A.13	^{13}C -NMR spectrum of PS-OH. Signal at 77.16 ppm is the residue CHCl_3 .	188

Figure A.14	^1H -NMR spectrum of (PS- <i>b</i> -P(MO-2EO)). Signal at 7.26 ppm is the residue CHCl_3 .	190
Figure A.15	^{13}C -NMR spectrum of (PS- <i>b</i> -P(MO-2EO)). Signal at 77.16 ppm is the residue CHCl_3 .	190
Figure A.16	GPC traces of PS-OH and PS- <i>b</i> -P(MO-2EO).	191
Figure A.17	The GPC trace of the crude mixture of Table A.1 entry 3.	191

LIST OF TABLES

Table 1.1	Common lithium salts as electrolyte solutes	7
Table 1.2	Common organic carbonates as electrolyte solvents	8
Table 1.3	Structurally modified PEO-based solid polymer electrolyte	18
Table 2.1	Compositions and Vogel–Tammann–Fulcher fitting parameters of plasticized hydrogenated polynorbornene–polyethylene oxide (hPNB-PEO) and polycyclooctadiene–polyethylene oxide (PCOD-PEO) solid polymer electrolytes (SPEs)	53
Table 2.2	Di-norbornene terminated PEO crosslinker.	73
Table 2.3	Composition and thermal properties of Unplasticized hPNB-PEO Cross-Linked SPEs ^a	79
Table 2.4	Composition and thermal properties of Unplasticized PCOD-PEO Cross-Linked SPEs ^a	80
Table 2.5	DC ionic Conductivities of Unplasticized hPNB-PEO Cross-Linked SPEs ^a	82
Table 2.6	DC ionic Conductivities of Unplasticized PCOD-PEO Cross-Linked SPEs ^a	83
Table 2.7	DC ionic Conductivities of Plasticized hPNB-PEO Cross-Linked SPEs ^a	84
Table 2.8	DC ionic Conductivities of Plasticized PCOD-PEO Cross-Linked SPEs ^a	84
Table 2.9	Density of the hPNB and PCOD SPEs	92
Table 3.1	Regio-selective cationic ring-opening polymerization of 1,4-dioxepane	105
Table 3.2	Synthesis and thermal properties of EO-TMO copolymers	109
Table 3.3	Glass transition temperatures of EO-TMO polymer and electrolytes	126
Table 3.4	DC ionic Conductivities of Unplasticized PCOD-PEO Cross-Linked SPEs ^a	128

Table 4.1	Polyester to polyether reduction on poly(ϵ -caprolactone) ^a (PCL) through indium catalyzed hydrosilylation	141
Table 4.2	Substrate scope of polyester to polyether reduction	143
Table 4.3	Catalyst screening on polyester to polyether reduction on poly(ϵ -caprolactone) ^a (PCL)	146
Table A.1	Synthesis of P(MO-2EO)	173

LIST OF ABBREVIATIONS

Atom-transfer radical polymerization	ATRP
Cationic ring-opening polymerization	cROP
Chemically specific dynamic bonder percolation	CS-DBP
Diethyl carbonate	DEC
Dimethyl carbonate	DMC
Differential scanning calorimetry	DSC
Ethylene carbonate	EC
Ethylmethyl carbonate	EMC
Ethylene oxide	EO
Gel permeation chromatography	GPC
Gel polymer electrolyte	GPE
Gel polymer electrolyte	GPE
2-Hydroxyethyl 2-bromoisobutyrate	HEBI
Hydrogenated polynorbornene	hPNB
High resolution mass spectroscopy	HRMS
Ionic liquids	IL
Lithium bis(trifluoromethanesulfonyl)imide	LiTFSI
Lithium-metal based battery	LMB
Matrix-assisted laser desorption/ionization	MALDI
Methyl trifluoromethanesulfonate	MeOTf
Nuclear magnetic resonance	NMR
Poly-3-hydroxybutyrate	P3HB
Poly(acrylonitrile)	PAN
Poly(γ -butyrolactone)	PBL
Propylene carbonate	PC

Poly(ϵ -caprolactone)	PCL
Polycyclooctadiene	PCOD
Polydispersity index	PDI
Poly(dimethyl siloxane)	PDMS
Poly(1,4-dioxepan-5-one)	PDXO
Polyethylene	PE
Poly(ethylene carbonate)	PEC
Poly(ethylene glycol)	PEG
Polyethylenimine	PEI
Poly(ethylene oxide)	PEO
Poly(ethylene sulfide)	PES
Polylactic acid	PLA
Propylmethyl carbonate	PMC
Poly(methyl methacrylate)	PMMA
Poly(propylene oxide)	PPO
Polystyrene	PS
Hydroxyl terminated polystyrene	PS-OH
Poly(trimethylene carbonate)	PTMC
Poly(vinylidene fluoride- <i>co</i> -hexafluoropropylene)	PVDF-HFP
Poly(δ -valerolactone)	PVL
Ring opening metathesis polymerization	ROMP
Solid electrolyte interface	SEI
Scanning electron microscopy	SEM
Succinonitrile	SN
Solid polymer electrolyte	SPE
Tetrahydrofuran	THF

Trimethylene oxide

TMO

Vogel-Tammann-Fulcher

VTF

LIST OF SYMBOLS

R_b	Bulk resistance
C_d	Charge passed before short-circuits
T_c	Cold crystallization temperature
J	Current density
σ_{eff}	Effective ionic conductivity
ΔH_{fus}	Enthalpy of fusion
T_g	Glass transition temperature
R_i	Interfacial resistance
σ	Ionic conductivity
r	Lithium salt concentration [Li]:[O]
$t_{\text{Li}+}$	Lithium transference number
T_m	Melting temperature
μ	Mobility
x_{O}	Mol% of oxygen atoms
M_n	Number average molecular weight
\bar{D}	Polydispersity index
σ_r	Reduced ionic conductivity
G''	Shear loss modulus
G'	Shear storage modulus
t_{sc}	Short-circuit time

CHAPTER 1

An overview of polymer electrolytes for lithium batteries

Chapter 1

An overview of polymer electrolytes for lithium batteries

1.1 Introduction

Lithium-ion batteries have gained tremendous success in portable devices, such as laptops and cellphones. More recently, the development of electric vehicles has promised more prosperous future of lithium-ion batteries. While the Li-ion battery is attractive in its high energy density, open circuit voltage, and charge/discharge efficiency, there are still rooms for improvement, such as the removal of flammable liquid electrolytes and the increase of energy density by applying Li-metal anodes. Solid polymer electrolytes (SPEs) have gained wide interest since 1970s as promising candidates to replace liquid electrolytes. Although SPEs have advantages on flexibility, processability, mechanical strength, and non-flammability, their low ionic conductivity at room temperature remain the biggest barrier for practical applications. Besides of the ionic conductivity, several other issues need to be addressed for SPEs, including Li transference number, voltage stability, and Li dendrite suppression. This chapter reviews the history of polymer electrolyte development and briefly discusses different types of polymer electrolytes, including solid polymer electrolytes, gel polymer electrolytes, and composite polymer electrolytes. Future directions of polymer electrolyte development are also discussed.

1.2 Lithium batteries

Batteries are devices that can convert chemical energy into electrical energy. Based on their rechargeability, batteries can be categorized into primary batteries and secondary batteries. Primary batteries are discarded after used once because the chemical reactions are irreversible, which is a huge waste of resources and environmentally unfriendly. Secondary (rechargeable) batteries can be discharged and charged multiple times to realize continuous energy conversions. Main groups of rechargeable batteries include lead-acid, Ni-Cd, Ni-metal hydride and lithium-ion batteries. A rechargeable battery is composed of three main parts – a cathode, an anode and an electrolyte. When the battery is discharged, positive species (cations) are transported from anodes to cathodes through electrolytes inside the battery and electrons

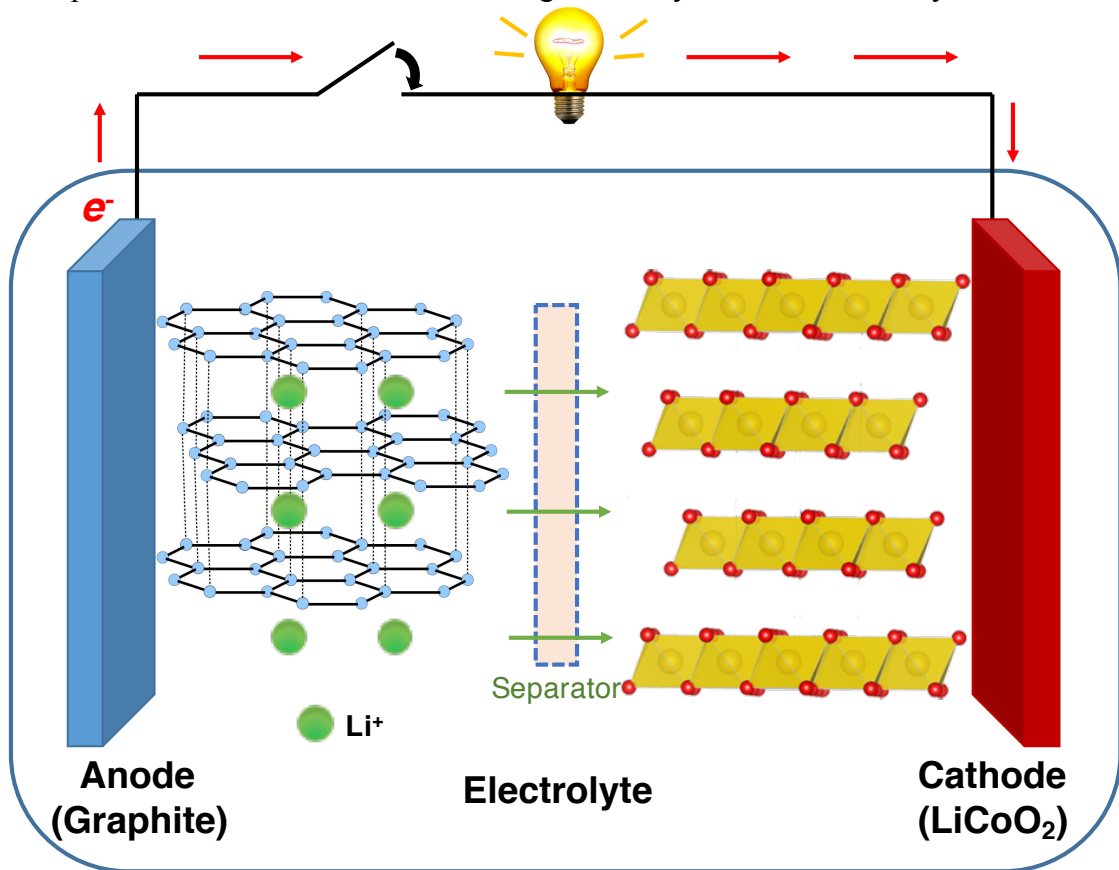


Figure 1.1 A scheme of a Li-ion battery during discharging.

flow spontaneously from anodes to cathodes through external circuit. (Figure 1.1) The transportation directions are reversed when the battery is charged.

The performance metrics of a battery can be quantitatively evaluated based on some key parameters. (Figure 1.2) Specific energy and energy density denote the amount of energy a battery can release when discharging per unit mass and per unit volume, respectively. Specific power characterizes how quick the energy stored can be released. Charge/discharge efficiency demonstrates the efficiency of the battery based on the ratio of the amount of output energy to input energy. Cell voltage is determined by the electrochemical potential difference between the anode and cathode. The economic cost can be normalized by the amount of energy released per US dollar.

Among all the main rechargeable batteries, lithium-ion batteries outperform all

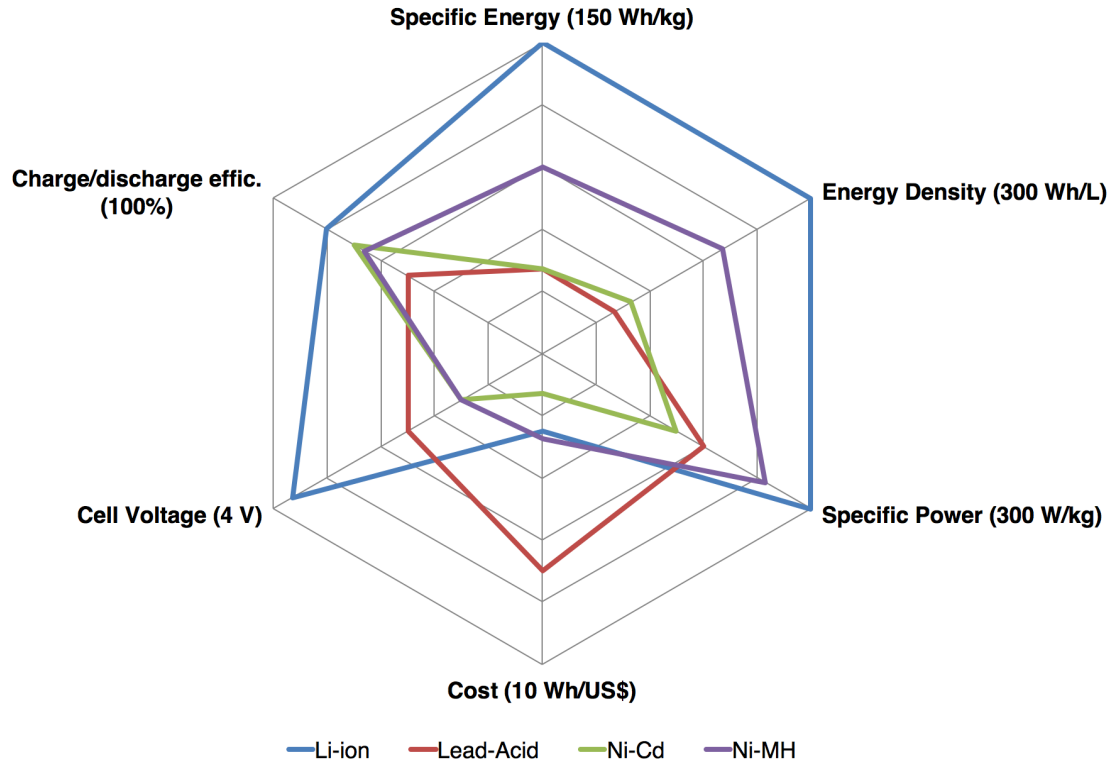
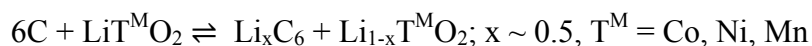


Figure 1.2 A comparison on performance metrics of rechargeable batteries.

the other batteries on most of the metrics and have been widely used in portable devices and electric vehicles. The idea of lithium-ion batteries was first proposed by Whittingham back in the 1970s.¹ He used titanium (IV) sulfide as the cathode and lithium metal as the anode. However, the battery could not be commercialized because of the high cost of titanium (IV) sulfide and safety issues with metallic lithium, but the idea of using intercalated compounds as electrode materials laid the foundation of the modern Li-ion battery technology. In 1977, Basu demonstrated the electrochemical intercalation of lithium in graphite,² which led to the usage of lithium intercalated graphite (LiC₆) anode in today's commercialized lithium-ion batteries. The cathode material – LiCoO₂ was developed two years later by Godshall³ and Goodenough⁴. Finally, Sony commercialized the first rechargeable Li-ion battery in 1991 and revolutionized the consumer electronics market, indirectly leading to the significant development of cellphones and laptop computers. The reversible redox process in Li-ion batteries is shown below:



Unlike the cathode and anode materials which were well-developed before the debut of the first Li-ion battery, it took longer time to develop a suitable electrolyte for Li-ion battery. In 1994, Tarascon⁵ developed a solution of 1.0 M LiPF₆ in 1:1 (v/v) mixture of ethylene carbonate (EC) and dimethyl carbonate (DMC) that serves as today's electrolyte in Li-ion batteries.

Cathodes, anodes and electrolytes are all under rapid developments in recent years. The improvement on cathodes have been mostly on utilizing S or O₂ to increase the specific capacity of the electrode. The long-term goal on the anode is to replace

lithium intercalated graphite with metallic lithium, which will increase the capacity of the anode by an order of magnitude. The challenge in applying metallic lithium is the lithium dendrite growth that causes battery failure over prolonged cycles.⁶ Li dendrites are tree-like structures that generated because of the uneven Li dissolution during discharging and Li deposition during charging. The dendritic Li can detach from the lithium substrate to form isolated Li, which is highly reactive; or penetrates the separator to contact the cathode, which causes battery shorts. The holy-grail on electrolytes is to develop a solid electrolyte that can replace the inflammable organic liquid electrolyte and suppress lithium dendrites to produce an all-solid battery.

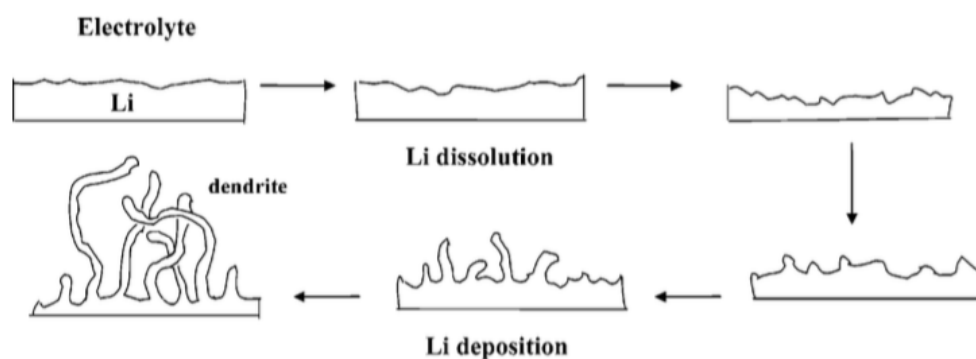


Figure 1.3 Schematic description for the growth of dendrite crystals on a Li surface. Figure reproduced from reference 6.

1.3 Liquid Electrolytes

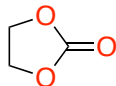
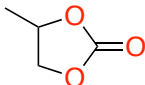
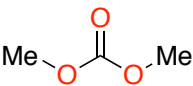
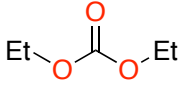
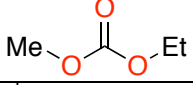
The function of electrolytes in Li-ion batteries is to conduct Li ions during charging and discharging. An aqueous electrolyte is not available because the high voltage (~ 3.7 V) of a typical Li-ion battery can oxidize the water. A conventional electrolyte is composed of a Li salt solute and an organic solvent that dissolves the Li salt. Table 1.1 (adapted from reference 6) summarizes common Li salts used in the electrolyte.

Table 1.1 Common lithium salts as electrolyte solutes

Salt	T_m (°C)	Al-Corrosion	σ (mS/cm) in PC	σ (mS/cm) in EC/DMC
LiBF ₄	293	N	3.4	4.9
LiPF ₆	200	N	5.8	10.7
LiAsF ₆	340	N	5.7	11.1
LiClO ₄	236	N	5.6	8.4
Li ⁺ CF ₃ SO ₃ ⁻ (LiOTf)	>300	Y	1.7	–
Li ⁺ [N(SO ₂ CF ₃) ₂] ⁻ (LiTFSI)	234	Y	5.1	9.0

The selection of a right lithium salt as the electrolyte solute is a great example to show how complicated the internal environment is inside a battery. LiBF₄ and LiOTf have poor ionic conductivities; LiAsF₆ is toxic and environmentally unfriendly; LiClO₄ is too oxidative and can react with the organic liquid; LiTFSI can corrode the Al current collector. The success of the LiPF₆ was achieved by a combination of a series well-balanced properties, not by a single outstanding feature. LiTFSI, although corroding Al, remains a widely used salt in electrolyte research because of its high dissociation constant and good solubility in various organic liquids.

Table 1.2 Common organic carbonates as electrolyte solvents

Carbonates	Structure	T_m (°C) ^a	T_b (°C) ^b	η (cP) ^c at 25 °C	T_f (°C) ^d	ϵ^e at 25 °C
EC		36	248	1.9 ^f	160	90
PC		-50	242	2.5	132	65
DMC		5	91	0.6 ^g	18	3
DEC		-74	126	0.8	31	3
EMC		-53	110	0.7	–	3

^aMelting point. ^bBoiling point. ^cViscosity. ^dFlash point. ^eDielectric constant. ^fMeasured at 40 °C. ^gMeasured at 20 °C.

The solvents for the electrolytes have been overwhelmingly based on organic carbonates. Table 1.2 (adapted from reference 6) summarizes common organic carbonates used in electrolytes. Propylene carbonate (PC) was first observed to enable lithium electrodeposition from a solution of LiClO₄ in PC, which resulted in extensive investigation.⁷ PC has a wide liquid range (wide usage temperature), high dielectric constant (high Li-ion conductivity), and static stability with lithium. However, later study demonstrated that the cycling efficiency of PC electrolytes is only <85 %, resulting in capacity fading of lithium cells.⁷ Yeager and coworkers identified that this is caused by PC reduction on newly formed lithium surfaces.⁸ Ethylene carbonate (EC), an analogue of PC, despite having a higher dielectric constant than PC, was never favored as an electrolyte solvent because of its high melting point (~36 °C). Scrosati and Pistoia first exploited a mixture of EC/PC as the electrolyte solvent to suppress the melting point of EC.⁹ Finally, the fundamental difference of EC as an electrolyte solvent compared to PC was demonstrated in 1990 by Dahn and co-workers¹⁰ that EC can form

an effective protective film solid electrolyte interface (SEI) on a graphitic anode to prevent sustained electrolyte decomposition while this cannot be realized with PC. The composition and the reason for the effectiveness of the SEI have attracted extensive research interests but remains unsolved. The EC was further formulated to lower the melting point and dimethyl carbonate (DMC) was identified by Tarascon *et al.*⁵ as the ideal cosolvent with EC to obtain low viscosity, high ionic conductivity and wide electrochemical stability window. Some other linear carbonates were also explored, including diethyl carbonate (DEC),¹¹ ethylmethyl carbonate (EMC)¹² and propylmethyl carbonate (PMC).¹³ No significant differences were found compared to DMC.

1.4 Polymer electrolytes

1.4.1 The discovery of polymer electrolytes

One of the key drawbacks of today's liquid electrolytes is their flammability. As discussed in Section 1.3, dimethyl carbonate (DMC) was added as a cosolvent to reduce the melting point of ethylene carbonate (EC). However, DMC has a low boiling point (91 °C) and flashing point (18 °C) (Table 1.2) and it can be ignited under a thermal runaway condition. In 2016, a series of explosions on Samsung Galaxy Note7 cellphones resulted in the recall of the product.¹⁴ Investigations showed that the explosions were caused by weakened separation between cathodes and anodes, leading to a cell short circuit and ignition of the electrolyte.¹⁵ Replacing flammable organic liquids with ionic conductive solids to achieve an all-solid Li-ion battery has been a “holy grail” for many researchers. Solid polymers, in contrast to liquids, have the advantage of being non-flammable, lightweight, and flexible and are viewed as promising candidates to replace liquid electrolytes.

In 1973, Wright *et al.*¹⁶ first discovered that alkali metal salt can be dissolved in poly(ethylene oxide) (PEO) to form a complex. Later, Armand and co-workers first proposed the use of lithium salt doped PEO as solid polymer electrolytes for battery applications.¹⁷ The ion transport mechanism was proposed to be a combination of segmental motion of PEO chains and breaking/forming of Li-O bonds.^{6, 18-19} The breaking/forming process can happen either intrachainly or interchainly. Figure 1.4 demonstrated the intrachain and interchain hopping of lithium ions in PEO matrix. The lithium ion conductivity of PEO is near 10^{-3} S/cm at 90 °C,²⁰ which is close to that of

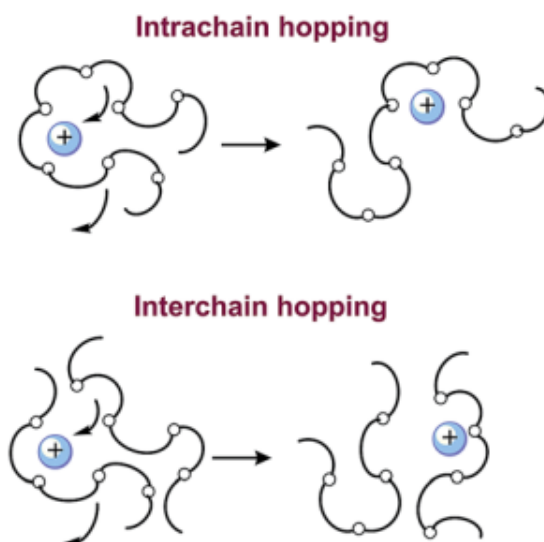


Figure 1.4 Mechanism of ion transport in PEO (adapted from reference 19).

conventional liquid electrolytes at room temperature. However, at room temperature, the conductivity of PEO dropped significantly to $\sim 10^{-5}$ S/cm because of its high melting point ($T_m \sim 65$ °C),²⁰ preventing the practical use of PEO electrolytes. For successful operation of a battery, several criterions need to be met: (a) high ionic conductivity ($\sigma > 10^{-4}$ S/cm at room temperature is desired²¹), (b) wide voltage stability window (> 4.5 V for conventional Li-ion batteries, > 5.0 V for high potential cathode batteries), (c) good mechanical properties, (d) chemical and thermal stability, (e) high cation transference number (faster transport of cations compared to anions), and (f) good contact with electrodes.²²

1.4.2 General considerations

1.4.2.1 Ionic conductivity

After the initial discovery of the low room temperature ionic conductivity of PEO, various methods have been examined to elevate it, including structural

modification²³ and additive addition.^{21, 23} However, the most severe barrier for practical applications of solid polymer electrolytes (SPEs) remains the low room temperature conductivity, or more precisely, the trade-off between conductivity and mechanical property. As discussed in section 1.4.1, the transport of Li ions takes place in the amorphous region of the polymer and is directly related to the polymer chain mobility,²⁴ which is often characterized by the glass transition temperature (T_g). A generally accepted relation between ionic conductivities and T_g can be described by the Vogel-Tammann-Fulcher (VTF) equation:

$$\sigma = AT^{-1/2} \exp \left[-\frac{B}{R(T-T_0)} \right] \quad \text{Equation 1.1}$$

where A is the pre-exponential factor that's related to ion mobility, B is the apparent activation energy, R is the gas content, and T_0 is the ideal T_g , which is selected to be 50 K below the experimental T_g values of the SPE.²⁵⁻²⁷ Thus, lower the T_g of the SPE has been a main method to increase the conductivity, but with the trade-off of deteriorating the mechanical strength of the SPE. Bruce and co-workers²⁸ challenged the mainstream view of confined conduction in amorphous region and showed that crystalline polymer can also conduct lithium ions in a crankshaft-like motion. Shriver and co-workers²⁹ reported that a rigid polyester – poly((1,3-dioxolan-2-one-4,5-diylloxalate), with a T_m of 132 C, can be doped with LiOTf to obtain a solid polymer electrolyte with a high ionic conductivity of 10^{-4} S/cm at room temperature. More research on Li conduction in crystalline region may help to increase conductivities without sacrificing mechanical properties.

1.4.2.2 Voltage stability

Electrochemical stability within the voltage window of lithium-ion batteries are essential for polymer electrolytes. The instability of electrolytes will cause reactions with electrode materials and capacity fading over prolonged cycles. The voltage window of polymer electrolytes should be higher than the electrode potential so that overpotentials during charging can be compensated. Although conventional lithium-ion batteries with LiCoO_2 cathodes have an operation voltage of 3.7 V, charging voltage can be as high as 4.2 V, requiring polymer electrolytes to be stable in the potential range of 0 – 4.5 V. New cathode materials, such as $\text{LiCu}_x\text{Mn}_{2-x}\text{O}_4$ ³⁰ and $\text{LiNi}_x\text{Co}_{1-x}\text{PO}_4$ ³¹ with higher operation potentials (~ 5 V), were developed to achieve higher energy density of the battery. However, the practical usage of these high voltage cathodes was limited by the voltage stability of the electrolytes. PEO-LiTFSI SPEs have been reported to be stable up to 4.5 V versus Li^+/Li at room temperature.³² Greenbaum and co-workers³³ did an electrochemical stability study on PEO-LiTFSI and PEO-LiOTf. They discovered that a PEO sample with LiTFSI exhibited dramatically decreased voltage stability compared to an analogous PEO sample with LiOTf. The salt concentration (Li:O ratio) also has a significant impact on voltage stability with increasing instability on more concentrated samples. Both discoveries suggested that unlike liquid electrolyte, where the voltage stability is determined by both the Li salt and the organic solvent, the Li salt (or more precisely the anions of the Li salt) determines the voltage stability in PEO-based SPEs.³⁴

Two strategies were applied to improve the voltage stability of Li salt anions. One strategy was to develop new anions that can tolerate higher potentials. Kita and co-

workers³⁵ examined a series of anions with long fluoroalkyl chains. They determined the oxidation potentials for LiCF_3SO_3 , $\text{LiC}_4\text{F}_9\text{SO}_3$, and $\text{LiC}_8\text{F}_{17}\text{SO}_3$ to be 4.8, 6.0, and 6.5 V versus Li^+/Li respectively in PC electrolytes. However, the longer fluoroalkyl anions decrease the ionic conductivity and their voltage stabilities in SPEs is yet to know. The other strategy was to bind the anions onto polymer backbones to yield “single-ion” conductors. Bouchet and co-workers³⁶ synthesized a triblock copolymer $\text{P}(\text{STFSiLi})\text{-}b\text{-PEO}\text{-}b\text{-P}(\text{STFSiLi})$, where STFSiLi was a styrene monomer with TFSI anion bonded. They compared the electrochemical stability of $\text{P}(\text{STFSiLi})\text{-}b\text{-PEO}\text{-}b\text{-P}(\text{STFSiLi})$ to that of LiTFSI doped ($[\text{EO}]:[\text{Li}] = 25$) $\text{PS}\text{-}b\text{-PEO}\text{-}b\text{-PS}$ with 30 wt% PS (polystyrene). The single-ion conductor was stable up to 5 V versus Li^+/Li while the conductor with free salt was stable up to only 3.8 V at 80 °C (Figure 1.5). The binding of anions onto the polymer backbone eliminated the contact between anions and electrodes, thus preventing the oxidation of the anions. However, the single-ion conductor generally has significantly lower ionic conductivities compared to its binary salt version.

1.4.2.3 Transference number

The measured conductivity is contributed by the migration of both cations and anions in an electrolyte with binary salt. However, in a Li-ion battery, the rate of charging and discharging is only determined by the fraction of current carried by Li^+ ions. The portion of current carried by lithium ions is referred to as Li^+ transference number (t_{Li^+}) and defined as:

$$t_{\text{Li}^+} = \frac{\mu_{\text{Li}^+}}{\sum_i \mu_i} \quad \text{Equation 1.2}$$

where i stands for an ion in the electrolyte whose mobility is denoted as μ_i , and μ_{Li^+} is

the mobility of lithium ions.

In PEO-based polymer electrolytes, the t_{Li^+} mostly falls in the range of 0.2 – 0.3 in diluted salt region ($[\text{EO}]:[\text{Li}] = 50:1 - 5:1$).³⁷ This is caused by the strong chelation between oxygens on the PEO backbone with lithium cations. A significantly less than 1 transference number is not desired because the fast anion movement will lead to anion accumulation near the electrode, causing polarization during charging/discharging and facilitating lithium dendrite growth. To increase the t_{Li^+} , two strategies were developed. The first strategy was to add Lewis acidic additives, including metal oxide nanoparticles²¹ (increase the t_{Li^+} to 0.6) and organic boranes³⁸ (increase the t_{Li^+} to 0.85). The increase of t_{Li^+} was realized by neutralizing the Lewis basicity of PEO with Lewis acids and weakening the interactions between PEO backbones and Li^+ cations. The

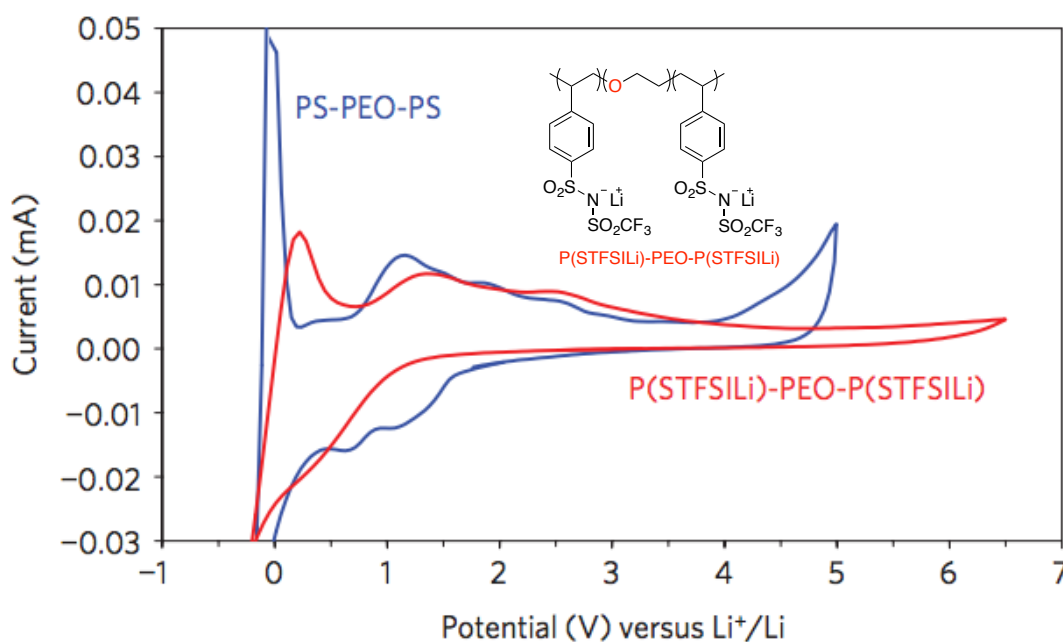


Figure 1.5 Voltammogram obtained at 1 mV/s for P(STFSiLi)-*b*-PEO-*b*-P(STFSiLi) with 31 wt% P(STFSiLi) (red curve) at 80 °C. For comparison, the voltammogram obtained in the same conditions with the neutral copolymer PS-PEO-PS with 30 wt% PS laden with LiTFSI at $[\text{EO}]/[\text{Li}] = 25$ (blue curve) is also given. (adapted from reference 36)

second strategy was to develop “single-ion” conductors as discussed in section 1.4.2.2, where the migration of anions was completely suppressed and the t_{Li^+} should theoretically be 1. In the case of P(STFSiLi)-*b*-PEO-*b*-P(STFSiLi) shown in section 1.4.2.2, the transference number of Li^+ was measured to be 0.85, slightly below the expected value of unity.

1.4.2.4 Lithium dendrite suppression

As mentioned in section 1.2, the formation of lithium dendrites over prolonged cycles is one of the primary modes of failure in rechargeable Li-metal batteries. Two main theories have been proposed to understand dendrite growth mechanisms. Chazalviel³⁹ proposed that anion depletion at the electrode causes large electric field gradients near the lithium electrode, leading to enhanced electrodeposition and dendrite growth. His theory suggested that higher ionic conductivity and reduced anion mobility will mitigate the anion depletion and delay the dendrite growth. This theory was further developed by Tikerkar *et al.*⁴⁰ and their calculation suggested that even a low fraction of immobilized anions (10 %) should significantly increase the stability of lithium electrodeposits. The other theory was proposed by Newman and Monroe⁴¹ that SPEs with high shear modulus ($G' > 7$ GPa) will physically force the lithium electrodeposition process and suppress the dendrite growth. This theory was partially supported by Balsara *et al.*⁴² who designed block copolymers of polystyrene-*b*-poly(ethylene oxide) (PS-*b*-PEO) with variable shear modulus ($G' \sim 0.1$ GPa) and proved positive correlations between shear modulus and Li dendrite resistance. However, Newman and Monroe’s theory was also challenged by Coates *et al.*²⁰ who designed a cross-linked

polymer of polyethylene (PE) and poly(ethylene oxide) (PEO) with extremely low shear modules ($G' \sim 0.1$ MPa) compared to that of PS-*b*-PEO. The dendrite suppression of the cross-linked material was about an order of magnitude higher than that of PS-*b*-PEO, suggesting high shear modules was not essential.

1.5 Types of polymer electrolytes.

Based on the chemical composition, polymer electrolytes can be categorized into three classes: a) Dry (solid) polymer electrolytes, where no additive (plasticizer, filler) is added and the polymer chain conducts the Li-ion directly; b) Gel polymer electrolytes, where liquid plasticizers (small organic molecules, oligomers) are added to the polymer matrix and the Li-ions are conducted mostly by the plasticizers; c) Composite polymer electrolytes, where solid fillers (ceramics, inorganic metal oxide) are presented and the Li-ions are conducted mostly by the fillers. In gel polymer electrolytes and composite polymer electrolytes, the polymer matrix is not necessarily involved into the Li-ion conduction and can serve solely as a mechanical support to the material.

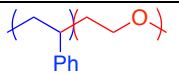
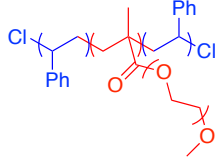
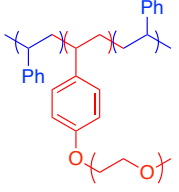
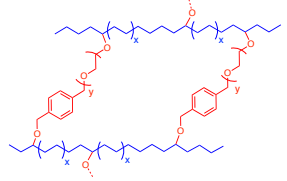
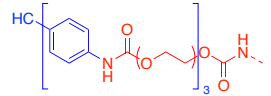
1.5.1 Dry (solid) polymer electrolytes

1.5.1.1 Polyethers

Polyethers, especially PEO-based polyethers remain the most extensively studied solid polymer electrolytes. Batteries with PEO as the electrolyte need to be kept at >65 °C (T_m of PEO) for normal operation, as in the case of Bluecar⁴³, which renders concerns both economically- and safety-related. Besides of adding plasticizers to suppress the crystallinity (will be addressed in section 1.5.2), structural modification

has been a main strategy to suppress the crystallinity. Table 1.3 summarizes some of the block and cross-linked copolymers of PEO, and their highest ionic conductivities are reported as well.

Table 1.3 Structurally modified PEO-based solid polymer electrolyte

Entry	Polymer	Structure	Li salt	Conductivity (S/cm) at Temperature	Reference
1	PS- <i>b</i> -PEO		LiTFSI	2.5×10^{-4} S/cm at 90 °C	44
2	PS- <i>b</i> -(PMMA- <i>g</i> -PEO)- <i>b</i> -PS		LiClO ₄	2.0×10^{-4} S/cm at 30 °C	23
3	PS- <i>b</i> -(PS- <i>g</i> -PEO)- <i>b</i> -PS		LiTFSI	2.5×10^{-5} S/cm at 25 °C	45
4	PE- <i>c</i> -PEO		LiTFSI	2.3×10^{-5} S/cm at 25 °C	20
5	Triisocyanate- <i>c</i> -PEO		LiOTf	3.2×10^{-5} S/cm at 60 °C	46

Block copolymers with PEO on the backbone normally have low ionic conductivities at room temperature. One classical example, polystyrene-*b*-poly(ethylene oxide) (PS-*b*-PEO), was developed by Balsara and co-workers.⁴⁴ The ionic conductivity of PS-*b*-PEO reached 10^{-4} S/cm at 90 °C, which was too low for room temperature applications. Block copolymers with PEO on the backbones significantly increase the rigidity of the PEO, leading to decreased chain mobility and ionic conductivity. An alternative strategy was to graft PEO on the side chains. Niitani *et al.*²³ designed a polystyrene-*b*-poly(methyl methacrylate)-*b*-polystyrene with PEO grafted on the poly(methyl methacrylate) block (PS-*b*-(PMMA-*g*-PEO)-*b*-PS). A conductivity of 10^{-4} S/cm at room temperature was obtained for this polymer. However, the M_n of the PEO block was only 1000 Da, suggesting that the high ionic conductivity was likely contributed by the low molecular weight. When the M_n of the PEO block was increased to 200 kDa as in the work of Sakai,⁴⁵ the room temperature conductivity quickly dropped back to the order of 10^{-5} S/cm. Besides of block copolymers, cross-linking was another strategy to increase the conductivity without sacrificing the mechanical strength. A conventional method was to cross-link the PEO by triisocyanate through an A₂-B₃ cross-linking process.⁴⁶ Coates *et al.*²⁰ also reported cross-linked PEO realized by ring opening metathesis polymerization (ROMP). The room temperature ionic conductivities of both materials were on the order of 10^{-5} S/cm. Extensive research and rational design are required to increase room temperature ionic conductivities of PEO-based polymers for real applications.

Polymers of epoxides have also been studied as polymer electrolytes. Poly(propylene oxide) (PPO), although a close cousin of PEO and amorphous at room

temperature, exhibited ionic conductivities ($\sim 10^{-7}$ S/cm) at least an order of magnitude lower than that of PEO.⁴⁷ The dramatic differences on conductivities of PEO and PPO were because of two reasons: 1. lower ionic dissociation of Li salt because of lower dielectric constant of PPO compared to PEO; 2. weaker donor power from O because of the bulky methyl group.⁴⁸ Copolymers of PEO and PPO have been designed and studied by Wieczorek and co-workers.⁴⁹ Room temperature ionic conductivity as high as 10^{-4} S/cm was achieved with LiBF₄ as the lithium salt. However, molecular weight of this polymer was not reported and it's difficult to exclude low molecular weight contributions. Other epoxides, including PEO-graft poly (glycidyl ether),⁵⁰ poly(allyl glycidyl ether),⁵¹ and their copolymers with PEO, have also been extensively studied but none of them exceeded 10^{-4} S/cm on room temperature ionic conductivities.

In addition to 3-membered cyclic ethers, there were a few reports on polyethers from other cyclic ethers. Tsutsumi *et al.*⁵²⁻⁵³ developed a family of substituted oxetane (4-membered cyclic ether) monomers with pendant cyano groups. (Figure 1.6) Homopolymers of these oxetane monomers were too sticky to form a free-standing film. SPE were obtained by mixing the oxetane polymer with poly(vinylidene fluoride-*co*-hexafluoropropylene) (PVDF-HFP, acting as a binder) and LiBF₄, exhibiting a room temperature ionic conductivity as high as 2×10^{-4} S/cm. As far as we know, there is no report on unsubstituted polyoxetane as polymer electrolytes, probably because of the expensiveness of the oxetane monomer. Besides of polyoxetane, polytetrahydrofuran (polyTHF, 5-membered cyclic ether) and poly(1,3-dioxolane) (5-membered cyclic acetal) have been studied as polymer electrolytes. However, their room temperature conductivities were both on the order of 10^{-6} S/cm.⁵⁴ Quantum chemical studies⁵⁵

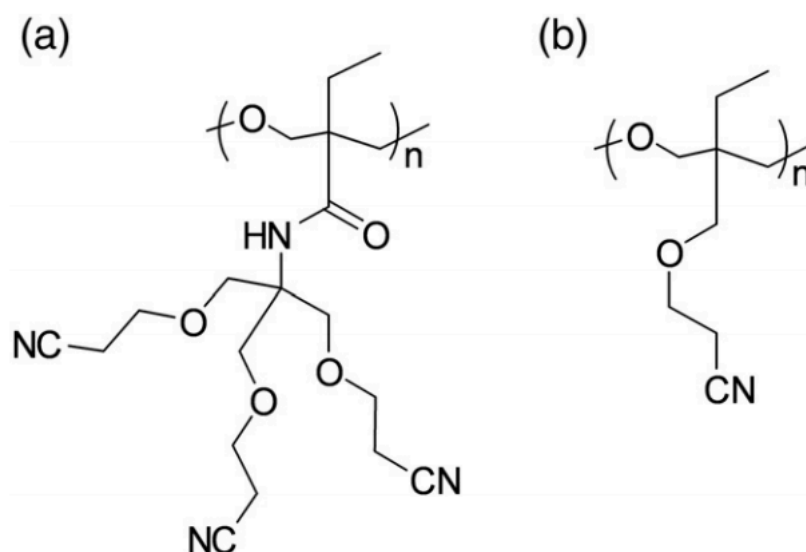


Figure 1.6 Structures of polyoxetane based polymers.⁵³

showed that the energy barrier for Li^+ transport between coordination sites in polyoxetane was smaller than that in PEO and a recent report by Miller *et al.*⁵⁶ demonstrated that the alternating copolymer poly(ethylene oxide-*alt*-oxetane) exhibited even faster Li^+ diffusion than PEO. Both theoretical studies suggest that more studies are needed for polyethers other than PEO and PEO-based solid polymer electrolytes.

1.5.1.2 Polycarbonates

Since the wide application of organic carbonates as the solvent of liquid electrolytes, researchers have long dreamed of using polycarbonates as solid polymer electrolytes. Unfortunately, polycarbonates differ dramatically from small molecule carbonates. The typical dielectric constant of polycarbonates, such as poly(propylene carbonate), is close to 3, less than that of PEO ($\epsilon \sim 5$) and significantly less than that of its monomer PC ($\epsilon \sim 65$). The low dielectric constant of polycarbonates leads to low conductivities in general.

Brandell and co-workers⁵⁷ reported a high molecular weight poly(trimethylene carbonate) (PTMC) with extremely low room temperature conductivities (10^{-9} S/cm). The room temperature ionic conductivity was improved to 10^{-5} S/cm by incorporating a small fraction of ϵ -caprolactone repeating units into PTMC.⁵⁸ However, the synthesis of PTMC was achieved by ring-opening polymerization of trimethylene carbonate, which made structural modification difficult. Tominaga *et al.*⁵⁹⁻⁶⁴ took the advantage of epoxide/ CO_2 alternating copolymerization and designed a family of poly(ethylene carbonate)s (PECs) by using different epoxides. A conductivity of 10^{-4} S/cm was achieved for PEC and pushed to close to 10^{-3} S/cm when ether linkages were incorporated into PEC at 60 °C. An interesting trend in polycarbonate electrolytes was that the T_g of the electrolytes decreased and the ionic conductivity increased with increasing Li salt concentration, exactly the opposite compared to PEO-based electrolytes. (Figure 1.7) The highest conductivity for PECs was obtained with a Li salt concentration of 188 mol% while for PEO it was close to 5 mol%. This is due to different mechanism of Li salt dissolution in the polymer.⁶³ In PEO, the Li salt is dissolved by chelation from ether oxygens. Concentrated Li salt cross-links polymer chains, leading to increased T_g and decreased ionic conductivity. In PEC, the dipole moment of the carbonate group is strong enough to dissociate the Li salt, leading to less chelation and the breakage of the interchain interactions. Thus, the trend of the T_g and the conductivity was the opposite compared to PEO. The Li transference number in PEC (~ 0.6) was also significantly higher than that in PEO, further suggesting less chelation presented in PEC.

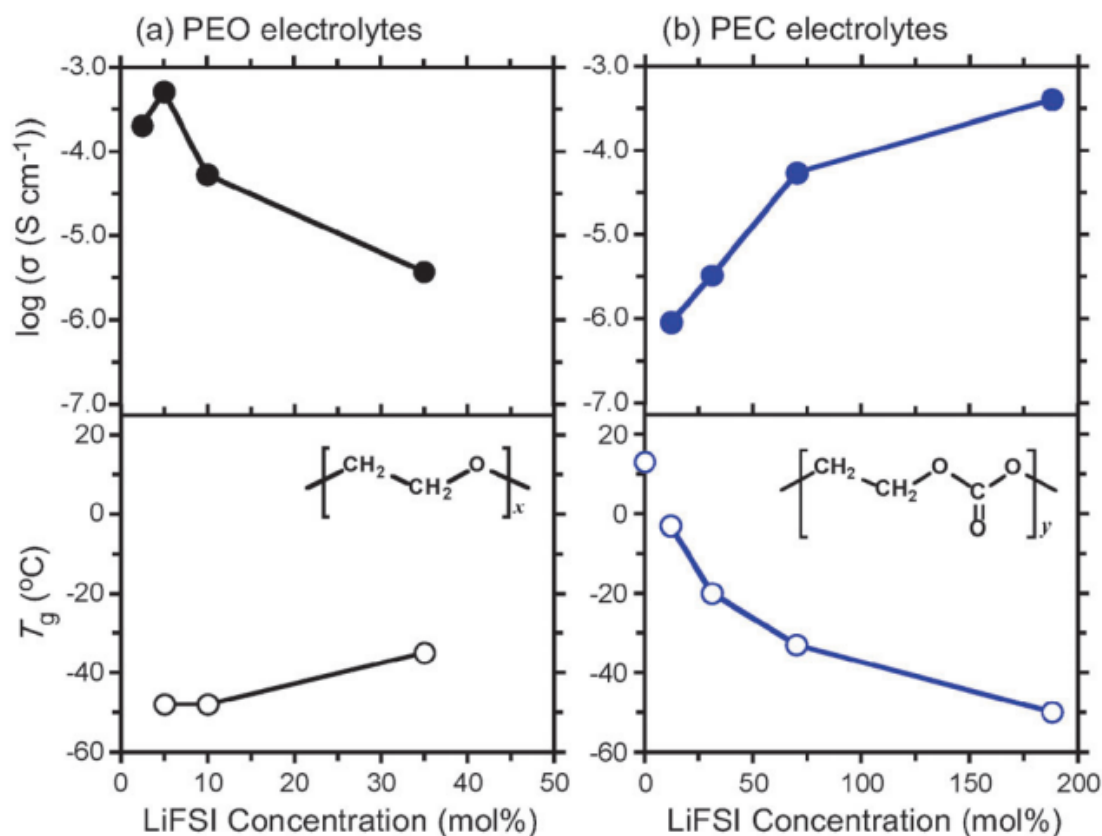


Figure 1.7 Dependence on the concentration of the ionic conductivity at 60 $^\circ\text{C}$ and T_g for (a) PEO– and (b) PEC–LiTFSI electrolytes. (adapted from reference 63)

1.5.1.3 Polyesters

Shortly after the discovery of salt conductive properties of PEO, researchers started to study salt conductive properties of other polymers. Shriver *et al.*^{65–66} screened several new polymer electrolyte system and reported the first polyester based lithium conducting SPE – poly(ethylene succinate). Although expecting the polar ester group will facilitate ionic conductivities, the Li conductivity is only 10^{-7} S/cm at 41 $^\circ\text{C}$ (with LiBF_4) and 10^{-5} S/cm at 90 $^\circ\text{C}$ (with LiClO_4).⁶⁷ Inspired by the discovery of the coupling between ionic conductivity and T_g of the polymer, oligo(ethylene glycol) linkages were incorporated between ester groups to lower the T_g of the polyester and improve the room

temperature ionic conductivity to the order of 10^{-5} S/cm.⁶⁸⁻⁶⁹ Polylactones were also briefly studied, such as poly(β -propiolactone)⁷⁰ and poly(ϵ -caprolactone)⁵⁸, but no significant improvement on room temperature ionic conductivity was achieved. Contrary to lowering the T_g of the polyester, Shriver *et al.*²⁹ further developed an unusual class of polyesters with both high rigidity and room temperature ionic conductivity. The polymer was synthesized by reacting dibromoethylene carbonate with $\text{Ag}_2\text{C}_2\text{O}_4$. The resulted carbonate-containing polyester had a high T_m of 132 °C but the room temperature ionic conductivity was as high as 10^{-4} S/cm. It was possible that the ion transport was facilitated by polar cyclic carbonate groups and decoupled from the segmental motion in this rigid polyester.

Besides of improving ionic conductivities, ion transport mechanism for polyester electrolytes was also investigated and compared to that for PEO-based electrolytes. Recently, Miller and co-workers⁷¹ conducted a systematic computational and experimental investigation of Li ion transport mechanism in a series of polyesters synthesized by alternating ring-opening polymerization of cyclic anhydride and epoxides. A concept “connectivity”, defined as the density of 3 Å connections between solvation sites, was applied to evaluate the efficiency of hopping. Computational simulation showed PEO had an order of magnitude higher connectivity than that of polyesters, which helped to understand the reason of high conductivities in PEO and design new polyester structures.

1.5.1.4 Si-containing polymers

Poly(dimethyl siloxane) (PDMS) has one of the lowest T_g s (−125 °C) of any

polymers.⁷² Many researchers expected that incorporating siloxane groups may help to lower the T_g of the polymer electrolyte, thus increasing the ionic conductivity. In 1984, Watanabe and co-workers synthesized poly(dimethyl siloxane-*co*-ethylene oxide) to decrease the T_g of PEO and increase the room temperature ionic conductivity to 2.6×10^{-4} S/cm.⁷³ Hooper *et al.*⁷⁴ developed a comb polymer with polysiloxane backbone and oligo(ethylene oxide) pendants. The room temperature ionic conductivity of this polymer was also on the order of 10^{-4} S/cm. Various of other pendant groups were examined, including cyclic carbonate⁷⁵ and alkyl cyanide groups.⁷⁶ One drawback of siloxane based polymer electrolytes is their poor mechanical strength due to the low T_g , which can be improved by cross-linking.⁷⁷⁻⁷⁸ However, neither the cross-linking nor pendant variation helps to improve the room temperature ionic conductivity to 10^{-3} S/cm.

A more recent trend was to synthesize single-ion conductors based on polysiloxane backbones. Shriver *et al.*⁷⁹ developed a single-ion conductor with polysiloxane backbones, pendant tri(ethylene glycol), and anchored LiOTf salt. Similar single-ion conductor was designed by Colby and co-workers⁸⁰ with polysiloxane backbones, pendant cyclic carbonate, and anchored lithium tetra(pentafluorophenyl) borate salt. Although expecting the T_g of polysiloxane may help to improve the ionic conductivity, both single-ion conductors had poor room temperature conductivities in the range of $10^{-7} - 10^{-6}$ S/cm.

1.5.1.5 B-containing polymers

Boron and boron-based molecules, with strong electron-deficiency, exhibit rare non-metal Lewis acidity. Boron-containing polymer electrolytes were expected to trap

anions of the Li salt and increase the Li transference number. Fujinami *et al.*⁸¹ reported a polymer electrolyte incorporating boroxine ring groups with oligo(ethylene oxide) spacers. This polymer electrolyte had a room temperature ionic conductivity of 10^{-5} S/cm and an enhanced Li transference number of 0.75 with LiOTf salt. Besides of borate esters, alkylborane groups were also investigated. Ohno and co-workers⁸²⁻⁸³ synthesized a class of alkylborane containing polymer electrolytes by hydroboration reactions between mesitylborane and diallyl oligo(ethylene glycol). Similar borate ester polymers were also synthesized by reacting mesitylborane with oligo(ethylene glycol). Although the conductivities of both classes of polymers were low ($10^{-7} - 10^{-6}$ S/cm at 25 °C), they compared the Li transference numbers of the polymers and discovered that the t_{Li^+} s for alkylborane polymers ($t_{\text{Li}^+} \sim 0.78 - 0.80$) were significantly higher than that for boron ester polymers ($t_{\text{Li}^+} \sim 0.35 - 0.50$), which was expected because the alkylborane group was more electron-deficient. However, due to the high reactivity and dynamic exchange in alkylborane, the practical application of alkylborane polymer electrolytes is limited.

1.5.1.6 N-containing polymers

After the discovery of PEO-based polymer electrolytes, polyethylenimine (PEI), N-version of PEO, was explored as a polymer electrolyte. Davis *et al.*⁸⁴ first investigated PEI ionic conductivity with various of lithium salt, followed by more detailed study from Fujita *et al.*⁸⁵ on both high molecular weight PEI and poly(N-methylethylenimine). Unfortunately, the room temperature conductivity of PEI was extremely low (10^{-7} S/cm) due to the strong Lewis basicity of nitrogens and N-H hydrogen bonds.

Another N-containing polymer was based on polyphosphazene backbones.

Seminal work from Shirver and Allcock *et al.*⁸⁶ on poly(bis-2-(2-methoxyethoxy)ethoxyphosphazene) demonstrated higher conductivity ($\sim 10^{-5}$ S/cm) than PEO at room temperature. The reason to use polyphosphazene is similar to that of polysiloxane backbones: lower the T_g of the polymer and increase the conductivity. However, polymer electrolytes with polyphosphazenes backbones also lack the mechanical properties, precluding practical application in the battery.

1.5.1.7 S-containing polymers

Sulfur is a weaker Lewis base compared to oxygen. Polymer electrolytes with S should have less chelation to Li compared to O. On the other side, because S is heavier than O, polymers with S normally have higher T_g and T_m compared to their O derivatives. Unlike PEO, poly(ethylene sulfide) (PES), analogue of PEO, has extremely high T_m (220 °C) and is insoluble in most of the organic solvents.⁸⁷ MacDonald and coworkers⁸⁸ partially substituted oxygens in PEO with S and did a systematic variation of S mol% content in the polymer. The highest room temperature ionic conductivity, still lower than 10^{-5} S/cm, was recorded with 20 % S-substituted polymer and LiOTf. A recent paper by Tew *et al.*⁸⁹ took the advantage of thiol-ene click reaction and synthesized a series of poly(ether-thioethers) polymer. The poly(ether-thioethers) polymer was then oxidized to poly(ether-sulfoxide) and poly(ether-sulfone) polymers. Despite various modifications, the room temperature ionic conductivities of the three sulfur-containing polymers were all lower than 10^{-5} S/cm.

1.5.1.8 F-containing polymers

Fluorine-containing polymers are relatively new for polymer electrolytes largely

due to the difficulties in synthesis. Fluorine has the highest electronegativity and can significantly change the property of the polymer when incorporated. DeSimone and Balsara *et al.*⁹⁰ examined a series of perfluorinated PEO with different molecular weight. Although the room temperature conductivity was not high ($\sim 10^{-5}$ S/cm), the perfluorinated polymer exhibited the highest lithium transference number ($t_{\text{Li}^+} = 0.91$) ever reported for solution containing lithium salts. The authors proposed two possible reasons for the near-unity transference number: (a) fluorine-containing backbones interacted with fluorine-containing TFSI⁻ anions and their mobility was reduced; (b) the strong electron withdrawing effect of fluorine reduced the Lewis basicity of the oxygen atoms and weakened their binding strength to Li^+ , thus facilitating cation transport. More fluorine-containing polymers need to be developed to rigorously evaluate the effect from fluorine atoms.

1.5.2 Gel polymer electrolytes

Unlike dry (solid) polymer electrolyte, where the polymer directly contributes the Li transport, the polymer in gel polymer electrolyte does not necessarily conduct Li ions and the Li ions are conducted mostly by liquid electrolytes swallowed by the polymer. Gel polymer electrolytes are conventionally composed of a polymer host and a liquid plasticizer.

1.5.2.1 Liquid plasticizer in gel polymer electrolytes

There are three main liquid plasticizers in gel polymer electrolytes (GPE): (a) small molecule organic solvent, such as ethylene carbonate, propylene carbonate; (b) ionic liquids; (c) oligomers of ethylene glycol.

Organic carbonates are the frequently used plasticizers. Frech and Mellander *et al.*⁹¹⁻⁹³ did systematic studies on the effect of EC and PC plasticizers on PEO–LiOTf electrolytes. The conductivity of (PEO)₉·LiOTf complex was improved from 2.5×10^{-5} S/cm to 9×10^{-4} S/cm (with EC) and 5.2×10^{-5} S/cm (with PC) at 60 °C. A polymer electrolyte⁹⁴ composed of PEO, PVDF-HFP, LiClO₄, and a mixture of EC and PC was reported to have a high ionic conductivity (1.25×10^{-3} S/cm) at 30 °C. The crystalline regions of PEO became amorphous when plasticizers were added, leading to significant improvement on the ionic conductivity. In addition to liquid electrolyte, solid organic molecules were recently developed as a new class of plasticizers. Armand and co-workers⁹⁵ first reported the ionic conduction in succinonitrile (SN), a plastic crystalline material with a T_m of 62 °C and a dielectric constant of 55. The SN-LiTFSI mixture exhibited an extremely high ionic conductivity (3×10^{-3} S/cm) at room temperature. Further application of SN as a plasticizer in PEO-LiTFSI also demonstrated significant improvement on conductivities, reaching 10^{-3} S/cm at room temperature.⁹⁶

Ionic liquids (IL) are molten salts at room temperature because of their low melting points. They typically are composed of a bulky organic cation and an inorganic anion. Researchers became interested in replacing organic liquid electrolyte with ILs because of several advantages: lower vapor pressure, higher polar environment, and non-flammability. Two main classes of ILs have been extensively studied: imidazolium based ILs, such as 1-ethyl-3-methylimidazolium TFSI salt (EMI-TFSI)⁹⁷ and 1-butyl-3-methylimidazolium TFSI salt (BMI-TFSI);⁹⁸ pyrrolidinium based ILs, such as N-butyl-N-methylpyrrolidinium.⁹⁹ The ionic conductivity was normally increased to 10^{-4} S/cm at room temperature with IL plasticizers.

Low molecular weight poly(ethylene glycol) (PEG) have also been used as plasticizers. Park and co-workers¹⁰⁰ incorporated PEG ($M_n = 250$ Da) and PEO based cross-linked electrolyte into pores of a non-woven PE matrix. The resulting material displayed conductivity of 3×10^{-4} S/cm at room temperature. Similar strategy was taken by Coates *et al.*²⁰ to increase the conductivity of a PE/PEO cross-linked polymer electrolyte to 10^{-4} S/cm at room temperature.

1.5.2.2 Polymer matrix in gel polymer electrolytes

Besides of PEO, several other polymers have served as polymer host for gel polymer electrolytes, including poly(acrylonitrile) (PAN) and poly(vinylidene fluoride-hexafluoro propylene) (PVDF-HFP).

Watanabe and co-workers¹⁰¹ first studied EC and PC plasticized PAN as gel polymer electrolytes. Abraham and Alamgir¹⁰² optimized the composition of PAN gel polymers and reported a fully amorphous gel of PAN-LiClO₄ in EC with an ionic conductivity of 10^{-3} S/cm at room temperature. It's noteworthy that the lithium transference number in PAN-based GPEs can be more than 0.5 because of the removal of oxygen atoms. Infrared and Raman spectroscopy revealed that lithium ions can strongly interact with the CN groups in PAN. One main drawback of PAN based GPE was its poor compatibility with lithium metal anode¹⁰³ which prevents its practical application in Li metal batteries.

PVDF-HFP electrolytes with EC/DEC as the plasticizer and LiTFSI as the salt were first reported by Saito *et al.*¹⁰⁴ Ionic conductivity as high as 10^{-2} S/cm was obtained for PVDF-HFP GPE at room temperature, making PVDF-HFP one of the most used

matrix for GPE.

1.5.3 Composite polymer electrolytes

Scrosati *et al.*²¹ first reported the addition of Ti_2O and Al_2O_3 nanoparticles into PEO electrolytes to increase its conductivity to 10^{-5} S/cm at room temperature. The resulted composite polymer electrolytes not only have improved ionic conductivities but also increased Li transference number. Although the mechanism of these nanoparticles on the ionic conductivity is not clear yet, Scrosati *et al.*¹⁰⁵ proposed it's due to the suppression on polymer crystallinity.

Besides of inorganic fillers, a more recent trend on composite polymer electrolyte is to blend polymers with ceramics. Some ceramics are known to be good solid lithium conductors with high ionic conductivities ($10^{-3} - 10^{-2}$ S/cm) at room temperature.¹⁰⁶ However, ceramics lithium conductor are normally thick pellets, brittle, and hard to process. Researchers have envisioned that a combination of ceramics and polymers will result in materials with both high ionic conductivity and processability. Recently, DeSimone and Balsara *et al.*¹⁰⁷ mixed perfluorinated PEO polymer with $\text{Li}_2\text{S} \cdot 25\text{P}_2\text{S}_5$ conducting glass to obtained a composite polymer electrolyte. The resulting electrolytes exhibited a conductivity of 10^{-4} at room temperature, as well as a close to unity Li transference number. Another example was reported by Goodenough and co-workers.¹⁰⁸ They developed an electrolyte with sandwiched structures (polymer/ceramic/polymer), where the polymer was a pre-synthesized cross-linked poly(ethylene glycol) methyl ether acrylate membrane and the ceramic was $\text{Li}_{1.3}\text{Al}_{0.3}\text{Ti}_{1.7}(\text{PO}_4)_3$. Although the conductivity of the sandwiched electrolyte was not

high (10^{-4} S/cm at 65 °C), it showed excellent voltage stability up to 4.8 V, notably high Coulombic efficiency of 99.8–100% over 640 cycles, and no obvious dendrite formation in a Li/electrolyte/LiFePO₄ cell after 640 cycles.

In summary, polymer-ceramic composite electrolytes are a relatively new but promising area because of their increased ionic conductivity, high Li transference number, improved mechanical property and non-flammability. However, more studies are needed before practical applications of these composite electrolytes.

1.6 Conclusions

Since the first discovery of PEO-based polymer electrolytes four decades ago, little progress has been made on the practical applications of polymer electrolytes and PEO remains the optimal polymer electrolyte despite extensive studies on non-PEO electrolytes. The seemingly insurmountable barrier for SPEs' application is still its low ionic conductivity at room temperature compared to liquid electrolytes. In addition, voltage stability, Li transference number, and dendrite suppression are also issues that SPEs need to address. Although GPEs have achieved successful applications in commercialized Li-ion batteries, the safety risk of GPEs are no less than that of liquid electrolytes because of the liquid plasticizers in GPEs.

However, several new directions of polymer electrolytes development have emerged in recent years. One direction is to develop new polymer electrolytes predicted by theoretical calculations⁷¹ or machine learnings¹⁰⁹ and another direction is to develop hybrid materials of polymers and ceramics. Even so, the development of high performance SPE is still a challenging research topic. An in-depth understanding of Li transport mechanism, systematic structure-property relationship studies, characterizations with state-of-the-art characterization techniques, and interdisciplinary collaboration will likely to promote the breakthrough of this field.

REFERENCES

- (1) Whittingham, M. S. *Science* **1976**, *192*, 1126–1127.
- (2) Zanini, M.; Basu, S.; Fischer, J. E. *Carbon* **1978**, *16*, 211–212.
- (3) Godshall, N. A.; Raistrick, I. D.; Huggins, R. A. *Mater. Res. Bull.* **1980**, *15*, 561–570.
- (4) Mizushima, K.; Jones, P. C.; Wiseman, P. J.; Goodenough, J. B. *Mater. Res. Bull.* **1980**, *15*, 783–789.
- (5) Guyomard, D.; Tarascon, J. M. *J. Electrochem. Soc.* **1993**, *140*, 3071–3081.
- (6) Xu, K. *Chem. Rev.* **2004**, *104*, 4303–4418.
- (7) Rauh, R. D.; Brummer, S. B. *Electrochim. Acta* **1977**, *22*, 75–83.
- (8) Aurbach, D.; Daroux, M. L.; Faguy, P. W.; Yeager, E. *J. Electrochem. Soc.* **1987**, *134*, 1611–1620.
- (9) Pistoia, G.; Rossi, M. D.; Scrosati, B. *J. Electrochem. Soc.* **1970**, *117*, 500–502.
- (10) Fong, R. a.; Sacken, U. v.; Dahn, J. R. *J. Electrochem. Soc.* **1990**, *137*, 2009–2013.
- (11) Aurbach, D.; Ein-Eli, Y.; Markovsky, B.; Zaban, A.; Luski, S.; Carmeli, Y.; Yamin, H. *J. Electrochem. Soc.* **1995**, *142*, 2882–2890.
- (12) Ein-Eli, Y.; Thomas, S. R.; Koch, V.; Aurbach, D.; Markovsky, B.; Schechter, A. *J. Electrochem. Soc.* **1996**, *143*, L273–L277.
- (13) Ein-Eli, Y.; McDevitt, S. F.; Aurbach, D.; Markovsky, B.; Schechter, A. *J. Electrochem. Soc.* **1997**, *144*, L180–L184.
- (14) Samsung Expands Recall to All Galaxy Note7 Devices.
<http://www.samsung.com/us/note7recall/>.

- (15) Samsung pins explosive Galaxy Note 7 on battery flaw.
<https://www.cnet.com/news/samsung-galaxy-note-7-explosion-battery-manufacturing-error/>.
- (16) Fenton, D. E.; Parker, J. M.; Wright, P. V. *Polymer* **1973**, *14*, 589.
- (17) Armand, M. *Adv. Mater.* **1990**, *2*, 278–286.
- (18) Manuel Stephan, A. *Eur. Polym. J.* **2006**, *42*, 21–42.
- (19) Xue, Z.; He, D.; Xie, X. *J. Mater. Chem. A* **2015**, *3*, 19218–19253.
- (20) Khurana, R.; Schaefer, J. L.; Archer, L. A.; Coates, G. W. *J. Am. Chem. Soc.* **2014**, *136*, 7395–7402.
- (21) Scrosati, B.; Croce, F.; Appetecchi, G. B.; Persi, L. *Nature* **1998**, *394*, 456–458.
- (22) Dias, F. B.; Plomp, L.; Veldhuis, J. B. J. *J. Power Sources* **2000**, *88*, 169–191.
- (23) Niitani, T.; Shimada, M.; Kawamura, K.; Kanamura, K. *J. Power Sources* **2005**, *146*, 386–390.
- (24) Berthier, C.; Gorecki, W.; Minier, M.; Armand, M. B.; Chabagno, J. M.; Rigaud, P. *Solid State Ionics* **1983**, *11*, 91–95.
- (25) Fulcher, G. S. *J. Am. Ceram. Soc.* **1925**, *8*, 789–794.
- (26) Tammann, G.; Hesse, W. *Z. Anorg. Allg. Chem.* **1926**, *156*, 245–257.
- (27) Vogel, H. *Phys. Z* **1921**, *22*, 645–646.
- (28) Gadjourova, Z.; Andreev, Y. G.; Tunstall, D. P.; Bruce, P. G. *Nature* **2001**, *412*, 520–523.
- (29) Wei, X.; Shriver, D. F. *Chem. Mater.* **1998**, *10*, 2307–2308.
- (30) Ein-Eli, Y.; Howard, J., W. F. *J. Electrochem. Soc.* **1997**, *144*, L205–L207.
- (31) Wolfenstine, J.; Allen, J. *J. Power Sources* **2004**, *136*, 150–153.

- (32) Xia, Y.; Fujieda, T.; Tatsumi, K.; Prosini, P. P.; Sakai, T. *J. Power Sources* **2001**, *92*, 234–243.
- (33) Cheung, I. W.; Chin, K. B.; Greene, E. R.; Smart, M. C.; Abbrent, S.; Greenbaum, S. G.; Prakash, G. K. S.; Surampudi, S. *Electrochim. Acta* **2003**, *48*, 2149–2156.
- (34) Armand, M. *Solid State Ionics* **1983**, *9-10*, 745–754.
- (35) Kita, F.; Sakata, H.; Sinomoto, S.; Kawakami, A.; Kamizori, H.; Sonoda, T.; Nagashima, H.; Nie, J.; Pavlenko, N. V.; Yagupolskii, Y. L. *J. Power Sources* **2000**, *90*, 27–32.
- (36) Bouchet, R.; Maria, S.; Meziane, R.; Aboulaich, A.; Lienafa, L.; Bonnet, J. P.; Phan, T. N.; Bertin, D.; Gigmes, D.; Devaux, D.; Denoyel, R.; Armand, M. *Nat. Mater.* **2013**, *12*, 452–457.
- (37) Pożyczka, K.; Marzantowicz, M.; Dygas, J. R.; Krok, F. *Electrochim. Acta* **2017**, *227*, 127–135.
- (38) Ciosek, M.; Marcinek, M.; Żukowska, G.; Wieczorek, W. *Electrochim. Acta* **2009**, *54*, 4487–4493.
- (39) Chazalviel, J. N. *Phys. Rev. A* **1990**, *42*, 7355–7367.
- (40) Tikekar, M. D.; Archer, L. A.; Koch, D. L. *J. Electrochem. Soc.* **2014**, *161*, A847–A855.
- (41) Monroe, C.; Newman, J. *J. Electrochem. Soc.* **2005**, *152*, A396–A404.
- (42) Stone, G. M.; Mullin, S. A.; Teran, A. A.; Hallinan, D. T.; Minor, A. M.; Hexemer, A.; Balsara, N. P. *J. Electrochem. Soc.* **2012**, *159*, A222–A227.
- (43) Bluecar. https://en.wikipedia.org/wiki/Bollor%C3%A9_Bluecar.

- (44) Singh, M.; Odusanya, O.; Wilmes, G. M.; Eitouni, H. B.; Gomez, E. D.; Patel, A. J.; Chen, V. L.; Park, M. J.; Fragouli, P.; Iatrou, H.; Hadjichristidis, N.; Cookson, D.; Balsara, N. P. *Macromolecules* **2007**, *40*, 4578–4585.
- (45) Wang, C.; Sakai, T.; Watanabe, O.; Hirahara, K.; Nakanishi, T. *J. Electrochem. Soc.* **2003**, *150*, A1166–A1170.
- (46) Laik, B.; Legrand, L.; Chausse, A.; Messina, R. *Electrochim. Acta* **1998**, *44*, 773–780.
- (47) Watanabe, M.; Sanui, K.; Ogata, N.; Inoue, F.; Kobayashi, T.; Ohtaki, Z. *Polym. J.* **1984**, *16*, 711–716.
- (48) Kim, D.-W.; Ryoo, B.-K.; Park, J.-K.; Maeng, K.-S.; Hwang, T.-S. *Polym. J.* **1992**, *24*, 509–518.
- (49) Przyłuski, J.; Wieczorek, W. *Solid State Ionics* **1992**, *53-56*, 1071–1076.
- (50) Motogami, K.; Kono, M.; Mori, S.; Watanabe, M.; Ogata, N. *Electrochim. Acta* **1992**, *37*, 1725–1727.
- (51) Barteau, K. P.; Wolffs, M.; Lynd, N. A.; Fredrickson, G. H.; Kramer, E. J.; Hawker, C. J. *Macromolecules* **2013**, *46*, 8988–8994.
- (52) Tsutsumi, H.; Suzuki, A. *Solid State Ionics* **2014**, *262*, 761–764.
- (53) Nakano, Y.; Tsutsumi, H. *Solid State Ionics* **2014**, *262*, 774–777.
- (54) Alamgir, M.; Moulton, R. D.; Abraham, K. M. *Electrochim. Acta* **1991**, *36*, 773–782.
- (55) Redfern, P. C.; Curtiss, L. A. *J. Power Sources* **2002**, *110*, 401–405.
- (56) Webb, M. A.; Savoie, B. M.; Wang, Z.-G.; Miller Iii, T. F. *Macromolecules* **2015**, *48*, 7346–7358.

- (57) Sun, B.; Mindemark, J.; Edström, K.; Brandell, D. *Solid State Ionics* **2014**, *262*, 738–742.
- (58) Mindemark, J.; Sun, B.; Törmä, E.; Brandell, D. *J. Power Sources* **2015**, *298*, 166–170.
- (59) Tominaga, Y.; Shimomura, T.; Nakamura, M. *Polymer* **2010**, *51*, 4295–4298.
- (60) Nakamura, M.; Tominaga, Y. *Electrochim. Acta* **2011**, *57*, 36–39.
- (61) Tominaga, Y.; Nanthana, V.; Tohyama, D. *Polym. J.* **2012**, *44*, 1155–1158.
- (62) Morioka, T.; Nakano, K.; Tominaga, Y. *Macromol. Rapid Commun.* **2017**, *38*, 1600652.
- (63) Tominaga, Y.; Yamazaki, K. *Chem. Commun.* **2014**, *50*, 4448–4450.
- (64) Tominaga, Y. *Polym. J.* **2016**, *49*, 291–299.
- (65) Shriver, D.; Papke, B.; Ratner, M.; Dupon, R.; Wong, T.; Brodwin, M. *Solid State Ionics* **1981**, *5*, 83–88.
- (66) Dupon, R.; Papke, B. L.; Ratner, M. A.; Shriver, D. F. *J. Electrochem. Soc.* **1984**, *131*, 586–589.
- (67) Watanabe, M.; Rikukawa, M.; Sanui, K.; Ogata, N.; Kato, H.; Kobayashi, T.; Ohtaki, Z. *Macromolecules* **1984**, *17*, 2902–2908.
- (68) Kim, D.-W.; Park, J.-K.; Gong, M.-S. *J. Polym. Sci., Part B: Polym. Phys.* **1995**, *33*, 1323–1331.
- (69) Manaresi, P.; Bignozzi, M. C.; Pilati, F.; Munari, A.; Mastragostino, M.; Meneghello, L.; Chiolle, A. *Polymer* **1993**, *34*, 2422–2426.
- (70) Watanabe, M.; Togo, M.; Sanui, K.; Ogata, N.; Kobayashi, T.; Ohtaki, Z. *Macromolecules* **1984**, *17*, 2908–2912.

- (71) Webb, M. A.; Jung, Y.; Pesko, D. M.; Savoie, B. M.; Yamamoto, U.; Coates, G. W.; Balsara, N. P.; Wang, Z. G.; Miller, T. F., 3rd *ACS Cent. Sci.* **2015**, *1*, 198–205.
- (72) Lötters, J. C.; Olthuis, W.; Veltink, P. H.; Bergveld, P. *J. Micromech. Microeng.* **1997**, *7*, 145–147.
- (73) Nagaoka, K.; Naruse, H.; Shinohara, I.; Watanabe, M. *J. Polym. Sci.: Polym. Lett. Ed.* **1984**, *22*, 659–663.
- (74) Hooper, R.; Lyons, L. J.; Mapes, M. K.; Schumacher, D.; Moline, D. A.; West, R. *Macromolecules* **2001**, *34*, 931–936.
- (75) Li, J.; Lin, Y.; Yao, H.; Yuan, C.; Liu, J. *ChemSusChem* **2014**, *7*, 1901–1908.
- (76) Lee, Y. S.; Song, G. S.; Kang, Y.; Suh, D. H. *Electrochim. Acta* **2004**, *50*, 311–316.
- (77) Zhang, Z.; Fang, S. *Electrochim. Acta* **2000**, *45*, 2131–2138.
- (78) Kuo, P.-L.; Hou, S.-S.; Lin, C.-Y.; Chen, C.-C.; Wen, T.-C. *J. Polym. Sci., Part A: Polym. Chem.* **2004**, *42*, 2051–2059.
- (79) Siska, D. P.; Shriver, D. F. *Chem. Mater.* **2001**, *13*, 4698–4700.
- (80) Liang, S.; Choi, U. H.; Liu, W.; Runt, J.; Colby, R. H. *Chem. Mater.* **2012**, *24*, 2316–2323.
- (81) Mehta, M. A.; Fujinami, T. *Chem. Lett.* **1997**, *26*, 915–916.
- (82) Matsumi, N.; Sugai, K.; Ohno, H. *Macromolecules* **2003**, *36*, 2321–2326.
- (83) Matsumi, N.; Sugai, K.; Ohno, H. *Macromolecules* **2002**, *35*, 5731–5733.
- (84) Chiang, C.; Davis, G.; Harding, C.; Takahashi, T. *Solid State Ionics* **1986**, *18-19*, 300–305.

- (85) Tanaka, R.; Fujita, T.; Nishibayashi, H.; Saito, S. *Solid State Ionics* **1993**, *60*, 119–123.
- (86) Blonsky, P. M.; Shriver, D. F.; Austin, P.; Allcock, H. R. *J. Am. Chem. Soc.* **1984**, *106*, 6854–6855.
- (87) Takahashi, Y.; Tadokoro, H.; Chatani, Y. *J. Macromol. Sci. B* **1968**, *2*, 361–367.
- (88) Narang, S. C.; MacDonald, D. D. Novel solid polymer electrolytes. US Patent 5061581, Oct. 29, 1991.
- (89) Sarapas, J. M.; Tew, G. N. *Macromolecules* **2016**, *49*, 1154–1162.
- (90) Wong, D. H.; Thelen, J. L.; Fu, Y.; Devaux, D.; Pandya, A. A.; Battaglia, V. S.; Balsara, N. P.; DeSimone, J. M. *Proc. Natl. Acad. Sci.* **2014**, *111*, 3327–3331.
- (91) Chintapalli, S.; Frech, R. *Macromolecules* **1996**, *29*, 3499–3506.
- (92) Frech, R.; Chintapalli, S. *Solid State Ionics* **1996**, *85*, 61–66.
- (93) Bandara, L. R. A. K.; Dissanayake, M. A. K. L.; Mellander, B. E. *Electrochim. Acta* **1998**, *43*, 1447–1451.
- (94) Fan, L.; Dang, Z.; Nan, C.-W.; Li, M. *Electrochim. Acta* **2002**, *48*, 205–209.
- (95) Alarco, P. J.; Abu-Lebdeh, Y.; Abouimrane, A.; Armand, M. *Nat. Mater.* **2004**, *3*, 476–481.
- (96) Fan, L.-Z.; Maier, J. *Electrochem. Commun.* **2006**, *8*, 1753–1756.
- (97) Zhu, C.; Cheng, H.; Yang, Y. *J. Electrochem. Soc.* **2008**, *155*, A569–A575.
- (98) Choi, J.; Cheruvally, G.; Kim, Y.; Kim, J.; Manuel, J.; Raghavan, P.; Ahn, J.; Kim, K.; Ahn, H.; Choi, D. *Solid State Ionics* **2007**, *178*, 1235–1241.
- (99) Shin, J.; Henderson, W. A.; Passerini, S. *Electrochem. Commun.* **2003**, *5*, 1016–1020.

- (100) Lee, Y. M.; Ko, D.-H.; Lee, J. Y.; Park, J.-K. *Electrochim. Acta* **2006**, *52*, 1582–1587.
- (101) Watanabe, M.; Kanba, M.; Nagaoka, K.; Shinohara, I. *J. Appl. Polym. Sci.* **1982**, *27*, 4191–4198.
- (102) Abraham, K. M.; Alamgir, M. *J. Electrochem. Soc.* **1990**, *137*, 1657–1658.
- (103) Croce, F.; Scrosati, B. *J. Power Sources* **1993**, *43*, 9–19.
- (104) Capiglia, C.; Saito, Y.; Kataoka, H.; Kodama, T.; Quartarone, E.; Mustarelli, P. *Solid State Ionics* **2000**, *131*, 291–299.
- (105) Capuano, F.; Croce, F.; Scrosati, B. *J. Electrochem. Soc.* **1991**, *138*, 1918–1922.
- (106) Fergus, J. W. *J. Power Sources* **2010**, *195*, 4554–4569.
- (107) Villaluenga, I.; Wujcik, K. H.; Tong, W.; Devaux, D.; Wong, D. H.; DeSimone, J. M.; Balsara, N. P. *Proc. Natl. Acad. Sci.* **2016**, *113*, 52–57.
- (108) Zhou, W.; Wang, S.; Li, Y.; Xin, S.; Manthiram, A.; Goodenough, J. B. *J. Am. Chem. Soc.* **2016**, *138*, 9385–9388.
- (109) Nosengo, N.; Ceder, G. *Nature* **2016**, *533*, 22–25.

CHAPTER 2

Structure–property study of cross-linked hydrocarbon/poly(ethylene oxide)
electrolytes with superior conductivity and dendrite resistance

Reprinted with permission from
Chemical Science **2016**, 7, 6932–6838.

Copyright © 2016 by the Royal Society of Chemistry

Chapter 2

Structure–property study of cross-linked hydrocarbon/poly(ethylene oxide) electrolytes with superior conductivity and dendrite resistance

2.1 Abstract

Lithium dendrite growth is a fundamental problem that precludes the practical use of lithium metal batteries. Solid polymer electrolytes (SPEs) have been widely studied to resist the growth of lithium dendrites but the underlying mechanisms are still unclear. Most SPEs sacrifice high ionic conductivities for increased dendrite suppression performance by using components with high mechanical stiffness. We report a class of cross-linked hydrocarbon/poly(ethylene oxide) SPEs with both high ionic conductivities (approaching 1×10^{-3} S/cm at 25 °C) and superior dendrite suppression characteristics. A systematic structure-property study shows that the crystallinity of the hydrocarbon backbones plays a key role in regulating size and morphology of lithium dendrites, as well as the ability to suppress their growth.

2.2 Introduction

The possibility of replacing the lithiated graphitic carbon LiC_6 anode in lithium-ion batteries with metallic lithium has been the subject of extensive research because metallic lithium has a specific capacity approximately 10 times that of conventional lithiated graphite (3800 mA h g^{-1} vs 380 mA h g^{-1}).¹⁻² A fundamental problem with metallic lithium anodes is their propensity to form rough, dendritic electrodeposits during cell recharge. While catastrophic cell failure due to dendrite-induced short circuits and the potential for thermal runaway are often cited as the main consequences of rough electrodeposition, an equally important problem is increased reactivity between electrodeposits and liquid electrolytes, which lowers cell efficiency and ultimately leads to premature failure over prolonged cycling.^{1, 3-4} Many strategies have been developed to solve the problem of rough Li electrodeposition, including coating Li anodes with polymers,⁵ introducing additives into the electrolyte,⁶⁻⁸ inserting an interlayer between the anode and the electrolyte,⁹ and careful design of solid polymer electrolytes.¹⁰⁻¹³

Among all these strategies, self-assembled nanostructured electrolyte architectures produced by block copolymers,¹²⁻¹³ offers a particularly versatile platform for dendrite inhibition. Archer *et al.* reported a cross-linked material of hairy silica nanoparticles and poly(propylene oxide), which can be cycled for more than 1000 hours in a lithium symmetric cell at a current density (J) of 0.2 mA/cm^2 .¹⁴ A similar cross-linked material between polyhedral oligomeric silsesquioxane (POSS) and poly(ethylene glycol) (PEG) was synthesized by Li and co-workers.¹⁵ This material has

a C_d (total charge passed at cell failure in a galvanostatic cycling test) of 2800 C/cm² at $J = 0.3$ mA/cm². These two examples are believed to be the state-of-the-art of Li dendrite suppression for solid polymer electrolytes. Recently, Balsara and co-workers¹¹ reported high shear moduli polystyrene-*block*-poly(ethylene oxide) (PS-*b*-PEO) polymers that exhibited improved dendrite growth resistance. This work validated the Monroe and Newman's model¹⁶⁻¹⁷ for dendrite growth inhibition. Their model predicts that a surface layer with high shear modulus ($G' > 7$ GPa) can physically suppress the growth of lithium dendrites. Recently, our group¹⁰ developed a family of PE-PEO cross-linked SPEs (see Figure 2.1) that showed exceptional Li dendrite suppression, which in some cases was one magnitude higher than that of PS-*b*-PEO as deduced by C_d in a galvanostatic cycling test. Significantly, the shear moduli of the best-performing cross-linked PE-PEO SPEs were three magnitudes lower than that of PS-*b*-PEO (~ 0.1 MPa compared with ~ 0.1 GPa), which suggests that a high shear modulus is not essential for good Li dendrite resistance. Moreover, the ionic conductivity of these SPEs were two orders of magnitude higher than PS-*b*-PEO at room temperature, making them promising for practical use at ambient temperatures.

The role of the PE main chain with respect to the improved dendrite resistance of the PE-PEO cross-linked is currently unclear. To investigate the effect of the physical properties of these polymer main chains on the exceptional overall Li dendrite resistance of the materials, we prepared a series of PEO cross-linked polymers with main chains comprising semicrystalline hydrogenated polynorbornene (hPNB) and amorphous, unsaturated polycyclooctadiene (PCOD). This composition allowed us to systematically vary the crystallinity of the materials and thereby the mechanical stiffness of the main

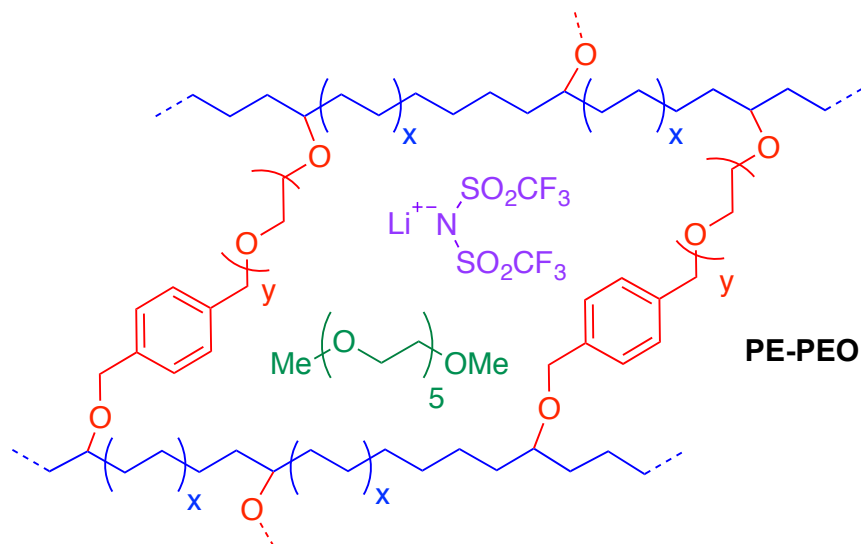


Figure 2.1 Cross-linked polyethylene/poly(ethylene oxide) (PE-PEO) solid polymer electrolyte (SPE).¹⁰

chain. Although the Li-metal battery dendrite phenomenon is known for more than 50 years, none of the presented remedies are able to tackle both the safety issue as well as the low cycling performance. Despite the extensive research that has been performed on the fundamentals of dendrite growth,^{4, 16-18} the underlying mechanisms are still not clear. In this work, our goal is to gain better understanding regarding the structure-property relationships of the polymer main chain on the Li dendrite resistance of the materials. The results of this study are reported herein.

2.3 Results and Discussions

The goal of the study was to determine how the physical properties of SPEs comprising hydrocarbon backbones with varied crystallinity compare with those of previously reported highly crystalline PE-PEO SPEs, and to systematically evaluate how these properties influence the capability of SPEs to retard dendrite growth. Atactic hPNB (melting temperature (T_m): 143 °C) and PCOD (no T_m) were selected because they are semicrystalline¹⁹ and amorphous,

respectively. The comparison of PCOD, hPNB, and PE hydrocarbon chains permitted a complete study of the crystallinity effects of backbones in hydrocarbon/PEO cross-linked SPEs.

Cross-linked polymers with incorporated PEO segments are usually synthesized with UV irradiation²⁰ or by reacting PEO with tri-isocyanates.²¹ However, these methods offer little structural control of the synthesized polymers. Building on our recent work on cross-linked alkaline anion-exchange membranes,²² we developed a tandem catalyst system with Grubbs' and Crabtree's catalysts. This system allows orthogonal catalysis of ring-opening metathesis polymerization to form polymers containing cross-linked PEO (Figure 2.1) that can undergo subsequent olefin hydrogenation to tune the crystallinity of the hydrocarbon backbones.

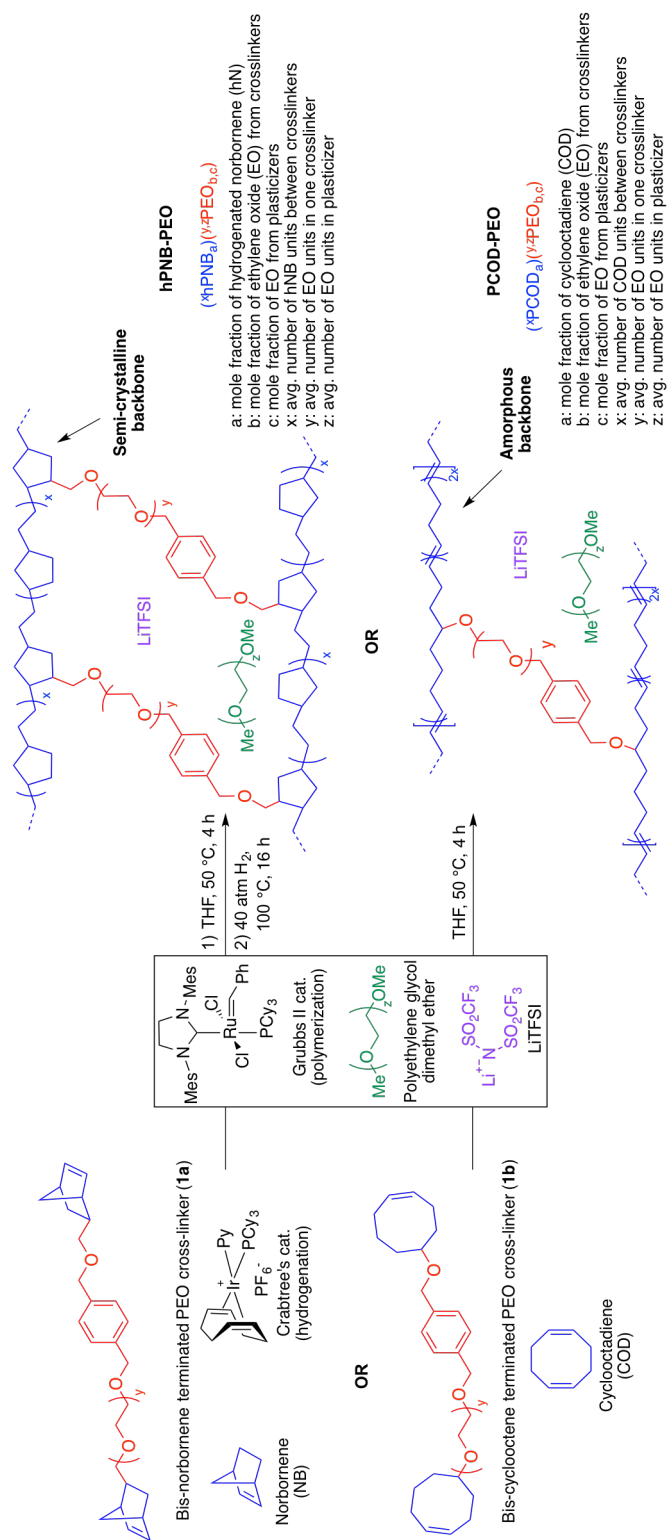


Figure 2.2 Hydrogenated polynorbornene-polyethylene oxide (hPNB-PEO) and polycyclooctadiene-polyethylene oxide (PCOD-PEO) cross-linked polymer electrolyte synthesis and nomenclature.

Norbornene- or cyclooctene-terminated PEO cross-linkers (**1a**, **1b**) were synthesized via anionic ring-opening polymerization of ethylene oxide (EO). Macromonomer **1a** was copolymerized with norbornene in a Teflon-coated mold with Grubbs' second-generation catalyst and lithium bis(trifluoromethane)sulfonimide as a lithium salt in THF (Figure 2.2). Macromonomer **1b** was copolymerized with cyclooctadiene by using the same procedure. Translucent thin membranes were obtained after evaporating THF at 50 °C for 4 h. Membranes prepared from **1a** and norbornene were then hydrogenated with Crabtree's catalyst under 40 atm hydrogen gas at 100 °C for 16 h. The number of EO repeating units in the cross-linkers (ca. 40, 80, and 140 units via anionic ring-opening polymerization) and the [**1a**]:[NB] or [**1b**]:[COD] ratios (1:7, 1:10, 1:15 via ring-opening metathesis polymerization) were varied to prepare materials with a range of compositions. Nine different hPNB-PEO and PCOD-PEO SPEs were made (see 2.5 for details). The ionic conductivities of these SPEs at room temperature were quantified from the plateau conductivity in dielectric measurements and compared with those of the analogous PE-PEO SPEs (Figure 2.3).

As reported earlier for the PE-PEO SPEs, the number of EO units in the cross-linker played a key role in determining the ionic conductivity for hPNB-PEO and PCOD-PEO SPEs as well. Among the tested SPEs, electrolytes containing 80 EO cross-linker units showed maximum conductivity. In the polymers with 40 EO cross-linker units, the crystallinity of the PEO segments was completely suppressed by either the cross-linking structure or the backbones (no T_m observed; see 2.5). Segmental movements of the chain were also significantly reduced, which led to relatively low conductivity. With 140 EO units, PEO segments resumed being crystalline, hampering

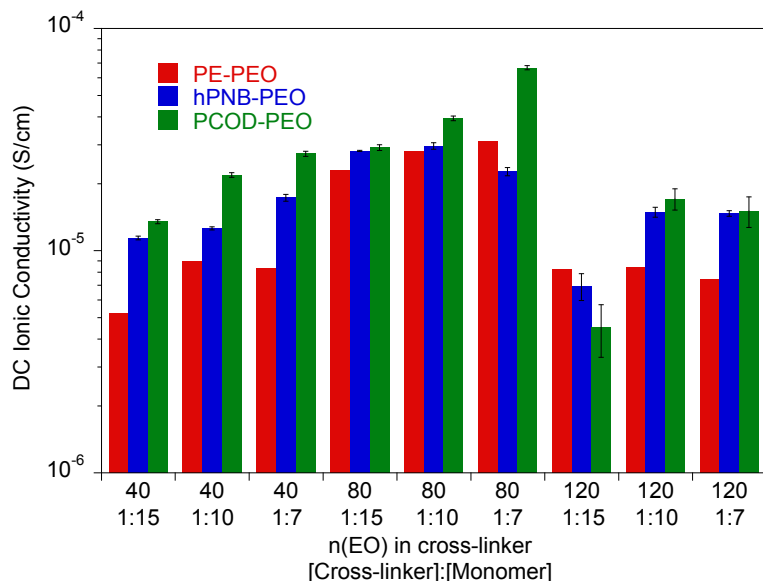


Figure 2.3 Ionic conductivity of unplasticized polymer electrolyte with different numbers of ethylene oxide (EO) units in the cross-linker and various [cross-linker]:[monomer] ratios at 25 °C. The data for PE-PEO SPEs are from Reference 10.

the room-temperature conductivity. Therefore, cross-linkers containing 80 EO units lie between the two extremes and give the highest conductivities.

Ionic conductivity of the SPEs showed an interesting dependence on the crystallinity of the polymer backbones when the cross-linking density was varied. For crystalline backbones such as PE and hPNB, no substantial changes were observed when the spacing of the cross-linkers was changed. However, for the amorphous PCOD backbone, conductivity increased with closer cross-linker spacing (higher [1b]:[COD] ratio). We hypothesize that crystalline backbones limit the segmental movement of PEO segments, whereas an amorphous backbone facilitates motion. Closer spacing of the cross-linkers would not improve Li-ion transport in frozen PEO chains but would greatly improve Li interchain transport in movable PEO chains. The overall conductivity was found to be inversely related to the degree of backbone crystallinity.

To improve the conductivity further, we used various amounts of poly(ethylene

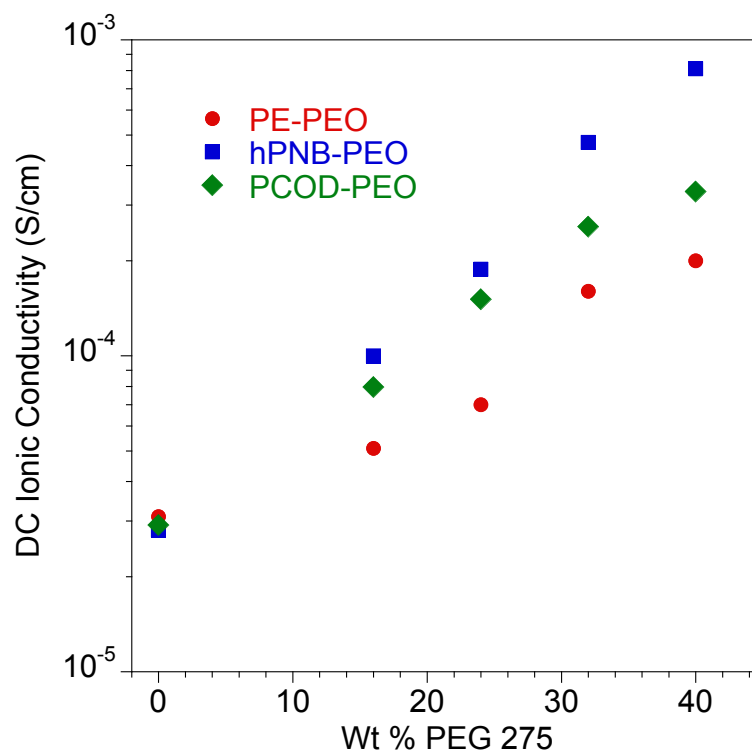


Figure 2.4 Ionic conductivity of plasticized polymer electrolyte as a function of wt % of PEG 275 at 25 °C. All membranes had approximately 80 EO cross-linker units (70 for PE-PEO,¹⁰ 88 for hPNB-PEO, and 75 for PCOD-PEO), [1a]:[NB] or [1b]:[COD] ratios of 1:15, and [EO]:[Li] compositions of 20:1. Error bars are smaller than the size of the data points. The data for PE-PEO SPEs are from Reference 10.

glycol) dimethyl ether (**PEG**; molecular weight, 275 Da; 16, 24, 32, 40 wt %) to plasticize the SPEs with approximately 80 EO repeating cross-linker units and 1:15 for [1a]:[NB] or [1b]:[COD] concentration ratios. The number of EO repeating cross-linker units and [1a]:[NB] or [1b]:[COD] concentration ratios were chosen to be consistent with our previous studies¹⁰ so that we can make comparisons among different systems. The compositions and thermal properties of the plasticized samples are reported in Table 2.1.

The addition of plasticizers greatly decreased the glass transition temperature (T_g) of PEO segments in the SPEs. For hPNB-PEO, T_g dropped from −48 °C (Table 2.1,

entry 1) to $-70\text{ }^{\circ}\text{C}$ in the presence of 40 wt % **PEG** (Table 2.1, entry 5). A decrease was also observed for PCOD-PEO, for which T_g changed from $-41\text{ }^{\circ}\text{C}$ (0 wt %, Table 2.1, entry 6) to $-55\text{ }^{\circ}\text{C}$ (40 wt %, entry 10). Significant decreases were also observed in cold crystallization temperature, and T_m for PEO segments, indicating that the crystallinity was greatly suppressed by **PEG** oligomers. However, T_m of the hPNB segments was not affected significantly by plasticizers. The relative percent crystallinity is in the range of 4.3 % to 6.4 % (ΔH_{fus} for pure hPNB is 65.4 J/g^{19}), which is slightly lower than what we observed in PE-PEO¹⁰ (5.1 % to 6.9 %). The absolute value of ΔH_{fus} is lower in hPNB-PEO than in PE-PEO, which confirms that the hPNB-PEO has a lower crystallinity compared to PE-PEO. Figure 2.4 reports the room temperature ionic conductivities of plasticized cross-linked hPNB-PEO, PCOD-PEO, and PE-PEO systems. Ionic conductivity increased with increasing **PEG** loading. Notably, the conductivity of 40 wt % plasticized hPNB-PEO reached $8.1 \times 10^{-4}\text{ S/cm}$, almost one order of magnitude higher than the minimum conductivity ($1 \times 10^{-4}\text{ S/cm}$) required for SPEs use in commercial batteries at ambient temperature.

Table 2.1 Compositions and Vogel–Tammann–Fulcher fitting parameters of plasticized hydrogenated polynorbornene–polyethylene oxide (hPNB-PEO) and polycyclooctadiene–polyethylene oxide (PCOD-PEO) solid polymer electrolytes (SPEs)
hPNB

Entry	Plasticized SPE ^a	Weight % of PEG ^b	segments ^c		PEO segments ^c				
			T_m^d (°C)	ΔH_{fus}^d (J/g)	T_g^d (°C)	T_c^d (°C)	T_m^d (°C)	ΔH_{fus}^d (J/g)	E_a (kJ/mol)
1	(^{8.5} hPNB _{0.25})(^{88.0} PEO _{0.75,0})	0	92	2.8	-48	-6	32	27.9	10.0
2	(^{8.5} hPNB _{0.14})(^{88.5} PEO _{0.64,0.22})	16	101	4.2	-60	-27	28	42.7	9.7
3	(^{8.5} hPNB _{0.13})(^{88.5} PEO _{0.57,0.30})	24	95	3.6	-64	-31	25	35.9	9.6
4	(^{8.5} hPNB _{0.11})(^{88.5} PEO _{0.46,0.43})	32	94	3.0	-69	-40	22	31.9	8.8
5	(^{8.5} hPNB _{0.09})(^{88.5} PEO _{0.38,0.54})	40	89	3.0	-70	-35	20	34.1	8.6
6	(^{8.5} PCOD _{0.17})(^{75.0} PEO _{0.83,0})	0	n.d. ^e	n.d. ^e	-41	n.d. ^e	n.d. ^e	n.d. ^e	8.6
7	(^{8.5} PCOD _{0.13})(^{75.5} PEO _{0.66,0.21})	16	n.d. ^e	n.d. ^e	-46	n.d. ^e	n.d. ^e	n.d. ^e	8.1
8	(^{8.5} PCOD _{0.11})(^{75.5} PEO _{0.57,0.32})	24	n.d. ^e	n.d. ^e	-50	n.d. ^e	n.d. ^e	n.d. ^e	8.2
9	(^{8.5} PCOD _{0.10})(^{75.5} PEO _{0.48,0.43})	32	n.d. ^e	n.d. ^e	-51	n.d. ^e	n.d. ^e	n.d. ^e	7.8
10	(^{8.5} PCOD _{0.08})(^{75.5} PEO _{0.39,0.53})	40	n.d. ^e	n.d. ^e	-55	n.d. ^e	n.d. ^e	n.d. ^e	8.1

^aSee for nomenclatures. All films have [EO]:[Li] compositions of 20:1, where EO indicates ethylene oxide units in the cross-linker.

^bWt % of PEG plasticizer = (mass of PEG) / [(mass of PEG) + (mass of PEO from cross-linker) + (mass of norbornene) + (mass of LiTFSI)] × 100. ^cThermal properties data for hPNB and PEO segments. ^dGlass transition temperature (T_g), cold crystallization temperature (T_c), melting temperature (T_m), and enthalpy of fusion (ΔH_{fus}) were determined with differential scanning calorimetry from the second heat cycle. ^eNot detected.

Both plasticized hPNB-PEO and PCOD-PEO SPEs exhibited higher ionic conductivities than those of PE-PEO SPEs at the same **PEG** loading. We attribute this increase to the lower crystallinity of the backbones, which allows better segmental movement of PEO chains, and thus faster Li ion transport. Variable-temperature ionic conductivities from 10 °C to 100 °C with an increment of 15 °C were also measured for entries 1–10 in Table 2.1 (see 2.5 for details). The data can be well-described with the Vogel–Tammann–Fulcher equation (Equation 2.1), which is widely used to describe the temperature dependence of ionic conductivity for polymers:²³

$$\sigma = A \exp \left[\frac{-E_a}{R(T-T_0)} \right] \quad \text{Equation 2.1}$$

where σ is the ionic conductivity, A is the prefactor, E_a is the activation energy, R is the gas content, and T_0 is the ideal T_g , which was selected to be 50 K below the experimental T_g values of SPEs. The Vogel–Tammann–Fulcher parameters are summarized in Table 1. The activation energy dropped with increasing wt % of **PEG** in the hPNB-PEO system, but no clear trends were observed in the PCOD-PEO system. The decrease in activation energy of the former system is expected because the plasticizer helps lower the energy barrier for Li ion conduction. The prefactor A increases with increasing wt % of **PEG** in both the hPNB-PEO and the PCOD-PEO systems. A is proportional to the number of charge carriers. The higher wt % of **PEG** provides more solvation centers, matching the increase in A .

To investigate the lifetime of lithium-metal-based batteries (LMB), we carried out galvanostatic lithium plate/strip electrochemical cycling measurements in symmetric Li/SPE/Li cells with a 3 h lithium plating followed by a 3 h lithium stripping at a current density (J) of 0.26 mA/cm² and 90 °C. The 3 h period mimics the

charge/discharge profiles of typical cells and ensures that the quantities of lithium transported during each cycle are sufficient to create dendrites large enough to short-circuit the cell.^{10, 24} The temperature was chosen to be consistent with earlier experiments. This temperature is above the T_m s of PEO segments so that a good conductivity can be achieved but below the T_m s of hydrocarbon backbones in PE-PEO and hPNB-PEO so that the crystallinity was maintained. Under these conditions, the conductivities of the hPNB-PEO and PCOD-PEO are nearly identical, allowing us to remove the trivial influence of electrolyte conductivity on dendrite suppression features of the copolymers. The effects of the various backbones in the three SPEs on suppressing dendrite growth was quantified by the total charge passed, C_d , at the time of cell failure as a result of dendrite-induced short-circuits. hPNB-PEO had a C_d value of 1630 C/cm², which is similar to that for PE-PEO (1790 C/cm²) reported in our earlier paper.¹⁰ Thus, lithium dendrite resistance is not significantly changed when semicrystalline hPNB is used instead of crystalline PE, but the conductivity is three times higher than that of PE-PEO at ambient temperature. When the crystallinity is further suppressed by modifying the backbone with PCOD, C_d decreases to approximately half that of PE-PEO.

A more aggressive galvanostatic polarization procedure was used to further characterize lithium electrodeposition and LMB cell failure in symmetric lithium cells polarized at a fixed J . The short-circuit time (t_{sc}) was defined as the time at which a sudden voltage drop occurred (see Figure 2.21).²⁵ The t_{sc} values for the crosslinked SPEs were measured at variable current densities (0.26–1.0 mA/cm²) at 90 °C, and the results are shown in Figure 2.6. Duplicate measurements were performed for each sample at

each specified J value. Consistent with the findings in lithium plate/strip cycling measurement, the t_{sc} values of these cross-linked SPEs with hydrocarbon backbones were significantly higher than those of all other SPEs reported to date. PE-PEO had a t_{sc} higher than that of hPNB-PEO, and PCOD-PEO had the lowest t_{sc} . Unlike in galvanostatic cycling measurements, where hPNB-PEO had a comparable C_d value to PE-PEO, hPNB-PEO had significantly lower t_{sc} than PE-PEO in galvanostatic polarization measurements, especially at high current densities. We attribute this phenomenon to the more aggressive conditions of galvanostatic polarization procedures.

The data for galvanostatic tests indicates that the polymer crystallinity plays a significant role in delaying the dendrite growth. We hypothesize that backbones with

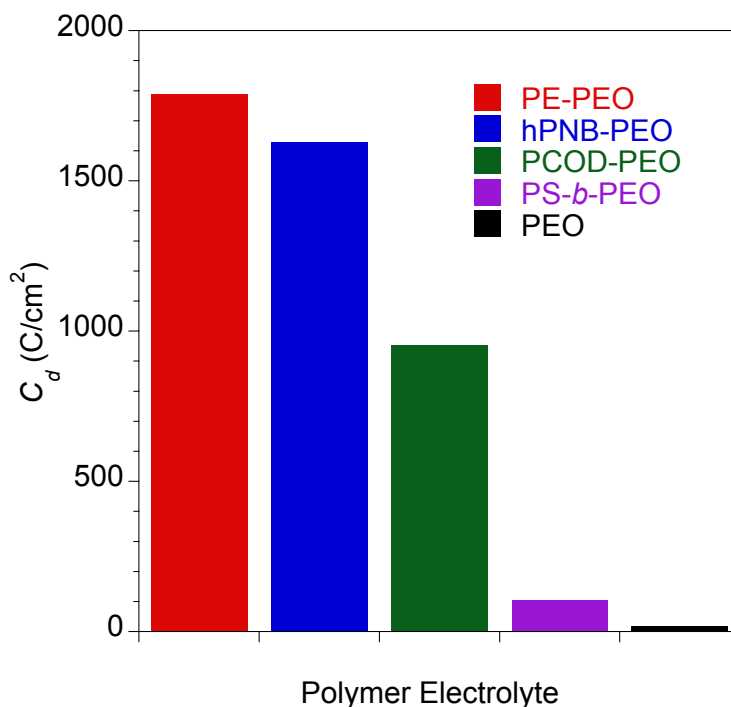


Figure 2.5 Galvanostatic cycling tests. Plot of C_d for polymer electrolytes. All samples were tested with a current density (J) of 0.26 mA/cm² at 90 °C. Error bars are 33 h for hPNB-PEO and 67 h for PCOD-PEO. PE-PEO, PS-*b*-PEO, and PEO values are from the literature.¹⁰⁻¹¹

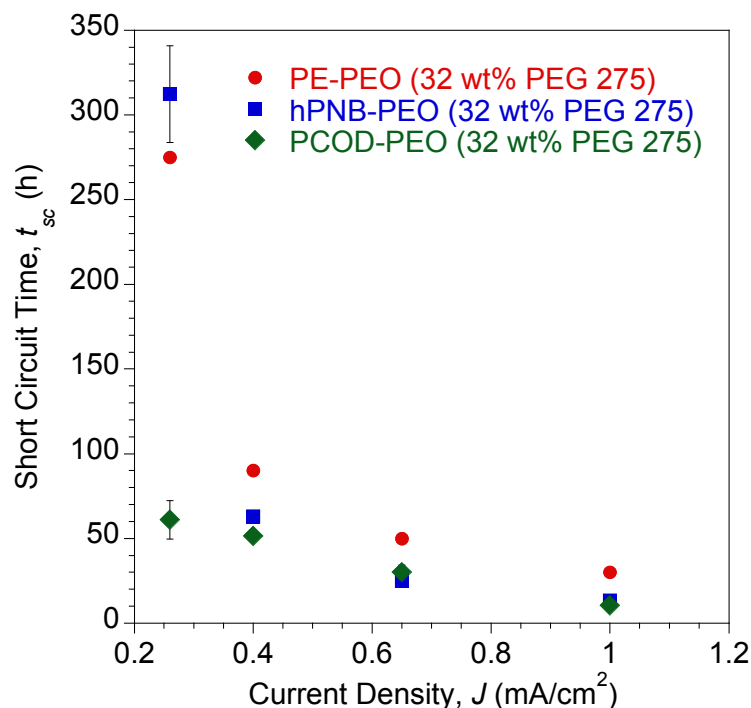


Figure 2.6 Galvanostatic polarization tests. Plot of short-circuit time (t_{sc}) as a function of J at 90 °C. All membranes were plasticized with 32 wt % PEG 275 and had approximately 80 EO cross-linker units (70 for PE-PEO,¹⁰ 88 for hPNB-PEO, and 75 for PCOD-PEO), [1a]:[NB] or [1b]:[COD] ratios of 1:15, and [EO]:[Li] composition of 20:1.

greater crystallinity create better-defined nanopore structures in the networks to provide enhanced resistance to the growth of micron-scale lithium dendrites, which increases C_d values (Figure 2.5, 2.6).²⁶ This hypothesis was further examined through post-mortem scanning electron microscopy to characterize the lithium metal anode and observe the morphology of the lithium surface after short-circuiting (Figure 2.7). Figure 2.7 a and c show the morphology of the lithium deposition in hPNB-PEO after a short-circuiting event during polarization and cycling measurement respectively. Figure 2.7 b and d display the SEM pictures of PCOD-PEO, after a short-circuiting event during galvanostatic polarization and cycling measurements respectively. Small ramified electrodeposits (<10 μm) were observed for hPNB-PEO, whereas much larger

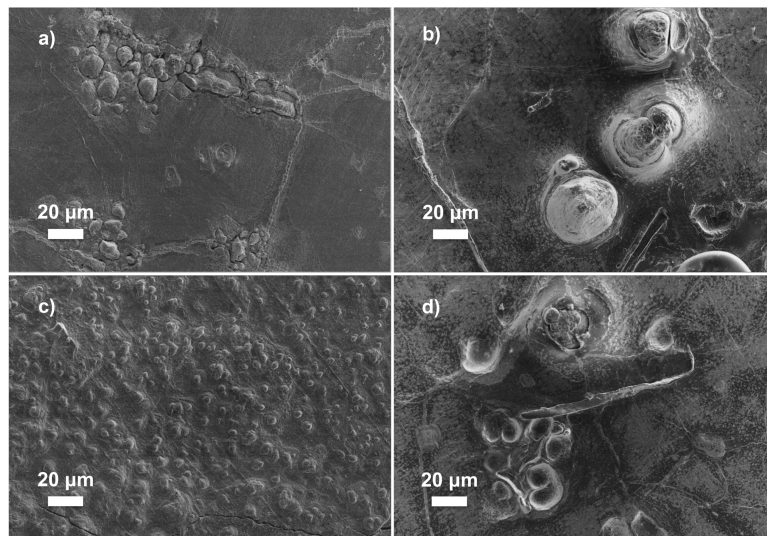


Figure 2.7 Scanning electron microscopy images of a short-circuited Li anode after galvanostatic (a) polarization (0.40 mA/cm^2) and (c) cycling (0.26 mA/cm^2) test with hPNB-PEO electrolyte (plasticized with 32 wt % PEG 275) and (b) polarization (0.40 mA/cm^2) and (d) cycling (0.26 mA/cm^2) test with PCOD-PEO electrolyte (plasticized with 32 wt % PEG 275).

protrusions ($>40 \text{ }\mu\text{m}$) were observed for PCOD-PEO. These results may be due to the higher crystallinity in hPNB-PEO compared with that of PCOD-PEO. The dendrites grow by creating splay-like openings in the softer PCOD-PEO membrane to produce large structures, whereas the crystallites in hPNB-PEO produce materials with stronger main-chain domains and hence higher splay resistance, permitting only smaller dendrites to penetrate the membrane.

Notably, the lithium dendrite resistance of the modified PEO system with different backbones is still much higher than those reported for other SPEs: PS-*b*-PEO¹¹ has a C_d value of 105 C/cm^2 , and the C_d of standard PEO¹⁰ (molecular weight, 900 kDa) is $\sim 20 \text{ C/cm}^2$. Figure 2.8 shows the shear moduli for the respective materials. The moduli of the **PEG**-plasticized hPNB-PEO and PCOD-PEO both exhibit only weak dependence on frequency, and the elastic shear modulus G' is at least an order of magnitude greater than the loss modulus G'' . Both observations are consistent with

expectations of materials with network structures, with cross-link spacing of approximately 4.8 nm for hPNB-PEO and 11.3 nm for PCOD-PEO. As in our previous studies of PE-PEO networks, an order of magnitude higher C_d values are obtained for materials with rather modest shear moduli ($G' \sim 10^5$ Pa at 90 °C) in both PE-PEO and hPNB-PEO. Even PCOD-PEO, which has a G' one order of magnitude lower than that of hPNB-PEO, has a C_d that is much higher than those of most reported systems.¹¹ However, the earlier conjecture that the C_d of hPNB-PEO is higher than that of PCOD-PEO because the main chain is stiffer and gives the material greater resistance to dendrite penetration is supported by the higher modulus of the former material, meaning that the mechanical properties of the materials do matter, but the effect in these networks is likely more complex than that captured in the solid separator model studied by Monroe and Newman.¹⁶⁻¹⁷ The systems developed in our lab produce very promising hydrocarbon/PEO cross-linked SPEs with high lithium dendrite resistance. In particular, hPNB-PEO is of special interest for Li metal based high energy density batteries due to both high lithium dendrite resistance and high conductivity.

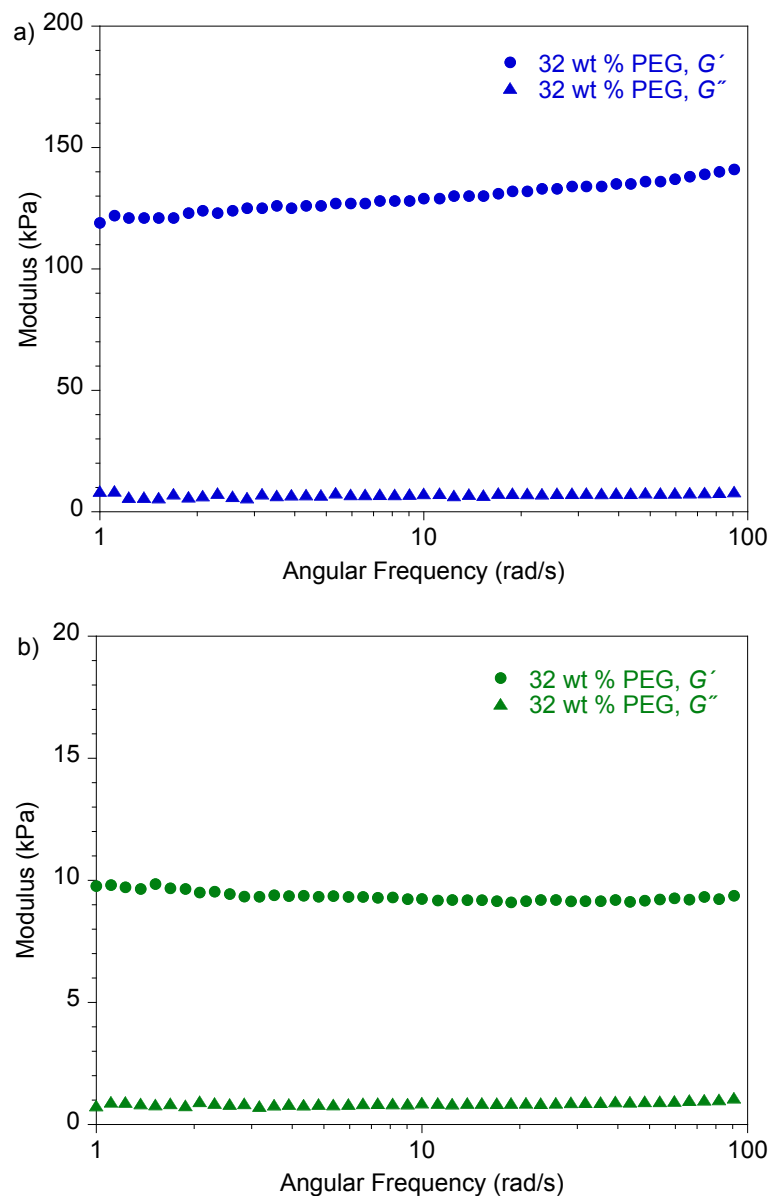


Figure 2.8 Dynamic shear measurements on (a) hPNB-PEO and (b) PCOD-PEO electrolytes. All membranes were plasticized with 32 wt % PEG 275 and had approximately 80 EO cross-linker units (88 for hPNB-PEO and 75 for PCOD-PEO), [1a]:[NB] or [1b]:[COD] ratios of 1:15, and [EO]:[Li] compositions of 20:1.

2.4 Conclusions

We developed two new hydrocarbon/PEO cross-linked SPEs: hPNB-PEO and PCOD-PEO. hPNB-PEO shows exceptionally high ionic conductivity at room temperature (approaching 10^{-3} S/cm) and significant lithium dendrite suppression. PCOD-PEO retains half of the hPNB-PEO C_d value even though its shear modulus is an order of magnitude lower than that of PE-PEO. This result suggests that a high shear modulus is not essential for good lithium dendrite suppression. Our systematic comparison of hydrocarbon backbones suggests that crystallinity plays a central role in the size and morphology of lithium dendrites. We believe that these hydrocarbon/PEO cross-linked systems with high conductivity and good lithium dendrite resistance are promising candidate SPEs for future batteries that use Li metal anodes. We are currently performing battery device testing and morphology studies to further characterize the microstructures of these materials.

2.5 Experimental

2.5.1 General Considerations

All air and water sensitive reactions were carried out under dry nitrogen conditions. ^1H NMR spectra were collected on a Varian INOVA 500MHz spectrometer and referenced with residue non-deuterated solvent shifts ($\text{CHCl}_3 = 7.26$ ppm). ^{13}C NMR spectra were collected on a Varian INOVA (^{13}C , 125 MHz) spectrometer and referenced to chloroform (δ 77.16 ppm). High resolution mass spectrometry (DART-HRMS) analyses were performed on a Thermo Scientific Exactive Orbitrap MS system equipped with an Ion Sense DART ion source. Matrix-assisted laser desorption/ionization time-of-flight mass spectrometry (MALDI-TOF MS) analyses were performed on a Waters MALDI Micro MX using dithranol as the matrix.

Gel permeation chromatography (GPC) analyses were carried out using an Agilent PL-GPC 50 integrated system, equipped with UV and refractive index detectors, and 2 PL gel Mini-MIX C columns (5 micron, 4.6 mm ID). The GPC columns were eluted with tetrahydrofuran at 30 °C at 0.3 mL/min and were calibrated with monodisperse polystyrene standards. Differential scanning calorimetry (DSC) analyses of polymer samples were performed on a TA Instruments Q1000 instrument equipped with liquid nitrogen cooling system. Polymer samples were made in aluminum pans and heated under nitrogen from -100 °C to 180 °C at a rate of 10 °C per minute and then cooled to -100 °C at a rate of 10 °C per minute, followed heating to 180 °C at a rate of 10 °C per minute. The glass transition temperature (T_g) and the melting temperature (T_m) were recorded from the second heating run.

The thickness of the cross-linked solid polymer electrolytes for all measurement purposes was measured with a Marathon CO030025 electronic digital micrometer. The conductivity data of the polymer electrolytes was obtained over a range of frequency (0.1 to 3×10^6 Hz) and temperature (10 °C to 100 °C) using a Novocontrol Dielectric Broadband Spectrometer fitted with a Quatro temperature control system. Conductivity measurements were performed using blocking/solid polymer electrolyte (SPE)/blocking cell orientation, using gold plated stainless steel electrodes.

2.5.2 Materials

Sodium hydride (95%), bicyclo[2.2.1]hept-5-ene-2-carboxaldehyde (95%), sodium borohydride, benzyl bromide, dithranol, Grubbs' 2nd generation catalyst and Crabtree's catalyst were purchased from Sigma-Aldrich and used as received. Bis(trifluoromethane)sulfonimide lithium salt, LiTFSI (99.95% trace metals basis), was purchased from Sigma-Aldrich and dried in vacuo at 90 °C for 24 h and transferred directly into the glove box. Norbornene (99%) and 1,5-cyclooctadiene ($\geq 99\%$) were purchased from Sigma-Aldrich and dried over calcium hydride at 60 °C for 2 days and then distilled and transferred into the glove box. Ethylene oxide was purchased from Sigma-Aldrich and dried over *n*-BuLi for 1h before use. Poly(ethylene glycol) dimethyl ether, PEG275 (M_n (NMR) = 275 Da; M_n (Sigma-Aldrich label) = 250 Da) was bought from Sigma-Aldrich, dried over activated 3 Å sieves for 48 hours, and degassed by three freeze-pump-thaw cycles before use. Dibromo-*p*-xylene (97%) was purchased from Alfa Aesar and used as received. Sodium hydroxide and sodium chloride were purchased from Mallinckrodt and used as received. HPLC grade tetrahydrofuran was

purchased from Fischer Scientific and dried over an alumina column and degassed by three freeze-pump-thaw cycles before use. Chloroform was dried over P₂O₅ and distilled prior to use. Hydrogen (99.99%) was purchased from Airgas. CDCl₃ was purchased from Cambridge Isotope Laboratories (CIL) and used as received. Bis-cyclooctene terminated PEO cross-linker (**1b**) was synthesized as reported.¹⁰ Potassium naphthalenide in THF was prepared from naphthalene and potassium at a concentration of 0.31 M (titrated with a standard benzoic acid solution until a persistent green color was observed as an end-point of the titration) and degassed by three freeze pump thaw cycles before use.

2.5.3 Synthesis of PEO Crosslinkers

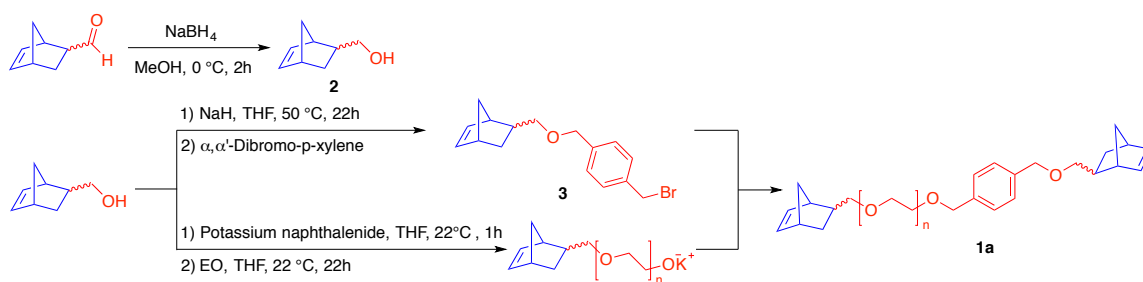


Figure 2.9 General scheme for the synthesis of crosslinker **1a**.

2.5.3.1 Preparation of endo/exo-bicyclo[2.2.1]hept-5-en-2-ylmethanol (**2**)

Following a literature procedure,²⁷ to a solution of bicyclo[2.2.1]hept-5-ene-2-carboxaldehyde (mixture of *endo* (67%) and *exo* (33%), 5.15 g, 42.2 mmol) in methanol (30 mL) was added dropwise a suspension of sodium borohydride (0.80 g, 21 mmol) in 2 M aqueous NaOH solution (20 mL) at 0 °C. The mixture was stirred for 2 h. The pH was then brought to 6 with 30 wt % H₂SO₄. Methanol was removed under vacuum and the residue was extracted with Et₂O (50 mL×3). The organic layer was washed with

saturated NaHCO₃ (50 mL×3) and dried over anhydrous Na₂SO₄. Solvent was removed under vacuum and the residue was further purified by vacuum distillation (0.25 torr, 58 °C). The product was a viscous yellow oil (3.22 g, 61%).

¹H NMR (500 MHz, CDCl₃) *endo*: δ 6.16 – 6.13 (m, 1H), 5.97 – 5.94 (m, 1H), 3.43 – 3.36 (m, 1H), 3.29 – 3.21 (m, 1H), 2.93 (br s, 1H), 2.81 (br s, 1H), 2.33 – 2.24 (m, 1H), 1.85 – 1.78 (m, 1H), 1.47 – 1.41 (m, 1H), 1.36 – 1.21 (m, 1H), 0.55 – 0.49 (m, 1H); *exo*: δ 6.12 – 6.05 (m, 2H), 3.74 – 3.67 (m, 1H), 3.58 – 3.50 (m, 1H), 2.81 (br s, 1H), 2.75 (br s, 1H), 1.65 – 1.57 (m, 1H), 1.36 – 1.21 (m, 3H), 1.14 – 1.08 (m, 1H).

¹³C NMR (126 MHz, CDCl₃) δ 137.58, 136.91, 136.58, 132.25, 67.65, 66.65, 49.66, 45.09, 43.70, 43.39, 42.33, 41.99, 41.81, 41.64, 29.64, 28.90.

HRMS (DART) *m/z* calculated for C₈H₁₃O⁺ [M + H]⁺ 125.09609, found 125.09625.

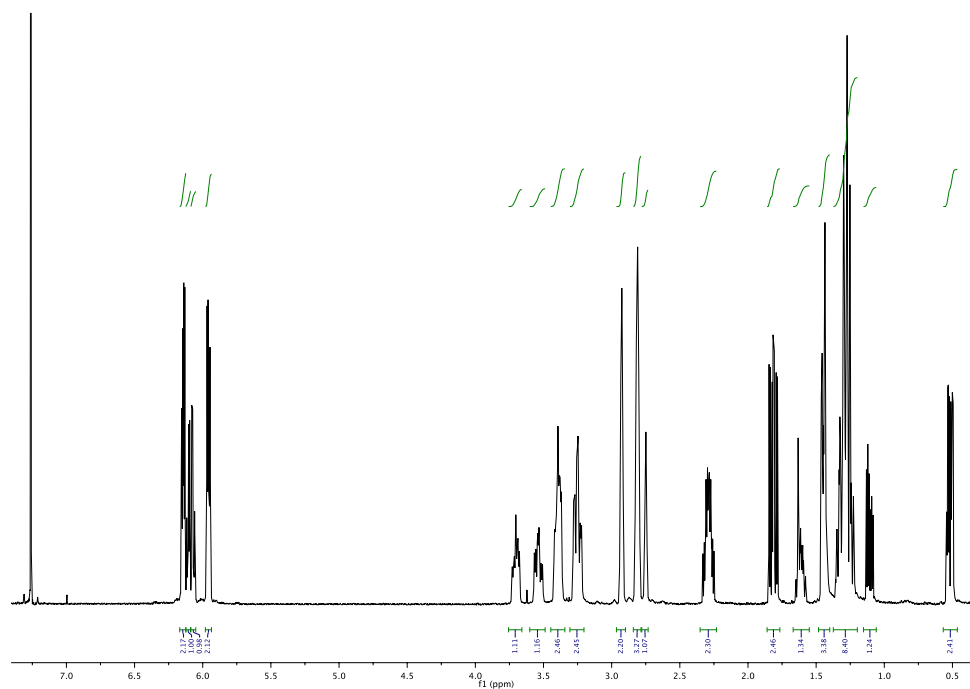


Figure 2.10 ^1H NMR spectrum of **2** in CDCl_3 . Signal at 7.26 ppm is the residual CHCl_3 .

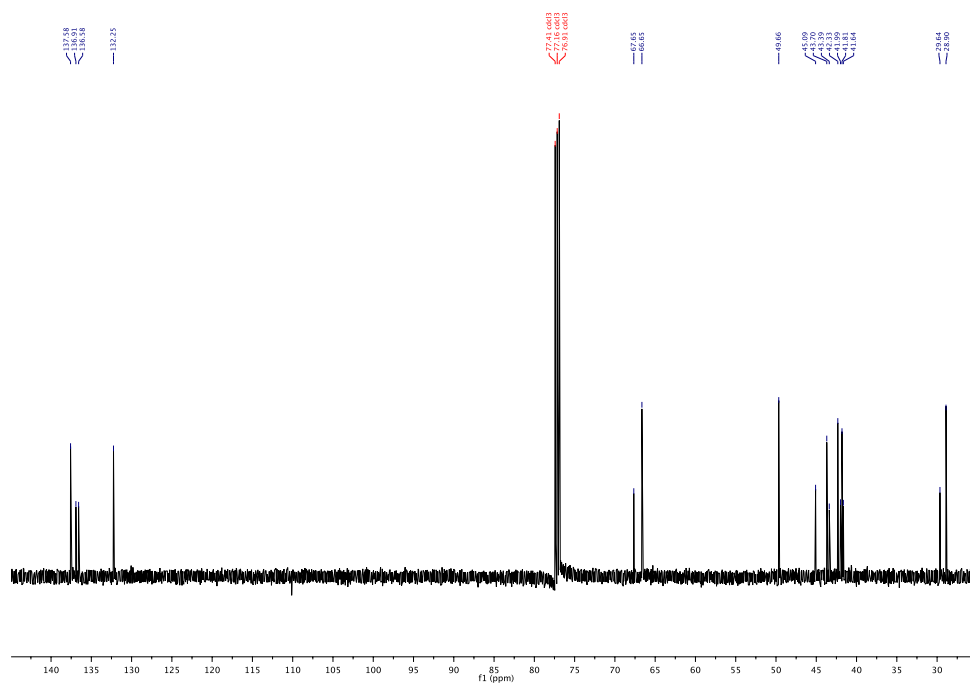


Figure 2.11 ^{13}C NMR spectrum of **2** in CDCl_3 . Signal at 77.16 ppm is the residue CHCl_3 .

2.5.3.2 Preparation of endo/exo-5-(((4-(bromomethyl)benzyl)oxy)methyl)bicyclo[2.2.1]hept-2-ene (3)

To a suspension of NaH (581 mg, 24.2 mmol) in anhydrous THF (50 mL) was added dropwise a solution of **2** (2.00 g, 16.1 mmol) in anhydrous THF (20 mL). The mixture was heated to 50 °C under N₂ for 22 h. This solution was cooled to room temperature and cannula transferred to a solution of α,α' -dibromo-*p*-xylene (6.39 g, 24.2 mmol) in anhydrous THF (50 mL) under N₂. The solution turned to bright yellow with precipitation of salts. The solution was stirred at 22 °C for 16 h and quenched with minimum amount of ethanol. The solution was filtered and the filtrate was concentrated to yield colorless oil. Hexanes (~150 mL) were added to the residue oil and the solution was kept at 0 °C to recrystallize out excess dibromo-*p*-xylene. Dibromo-*p*-xylene was removed by filtration and the filtrate was concentrated and purified by column chromatography on silica using 1:1 CH₂Cl₂/hexanes. The product was isolated as a colorless oil (2.74 g, 55%).

¹H NMR (500 MHz, CDCl₃) δ 7.40 – 7.29 (m, 4H), 6.13 – 5.86 (m, 2H), 4.53 – 4.41 (m, 4H), 3.55 – 3.50 (m, 1H *exo*), 3.40 – 3.34 (m, 1H *exo*), 3.23 – 3.17 (m, 1H *endo*), 3.09 – 3.02 (m, 1H *endo*), 2.94 (br s, 1H *endo*), 2.79 (br s, 1H *endo*+2H *exo*), 2.44 – 2.34 (m, 1H *endo*), 1.86 – 1.79 (m, 1H *endo*), 1.77 – 1.70 (m, 1H *exo*), 1.45 – 1.40 (m, 1H *endo*), 1.35 – 1.22 (m, 1H *endo*+3H *exo*), 1.15 – 1.09 (m, 1H *exo*), 0.52 – 0.46 (m, 1H *endo*).

¹³C NMR (126 MHz, CDCl₃) δ 139.37, 139.29, 137.33, 137.16, 137.05, 136.79, 136.70, 132.52, 129.23, 129.19, 128.05, 128.02, 75.27, 74.34, 72.68, 72.57, 49.54, 45.16, 44.11,

43.87, 42.32, 41.67, 39.85, 38.95, 33.56, 33.53, 29.86, 29.27.

HRMS (DART) m/z calculated for $\text{C}_{16}\text{H}_{20}\text{BrO}^+ [\text{M} + \text{H}]^+$ 307.06920, found 307.06923.

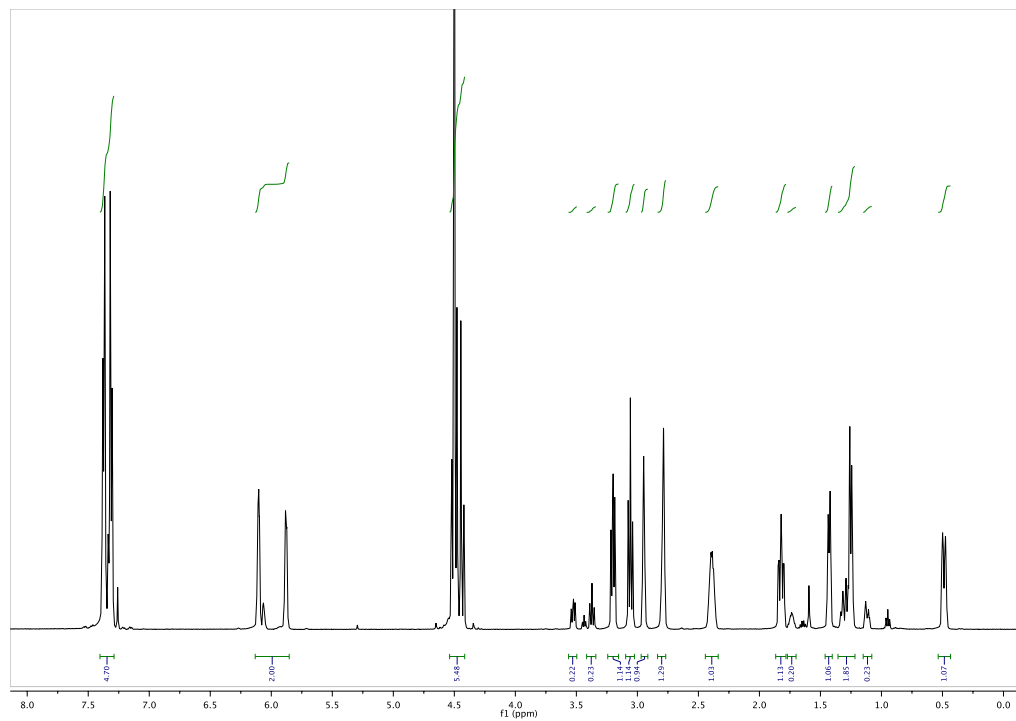


Figure 2.12 ^1H NMR spectrum of **3** in CDCl_3 . Signal at 7.26 ppm is the residual CHCl_3 .

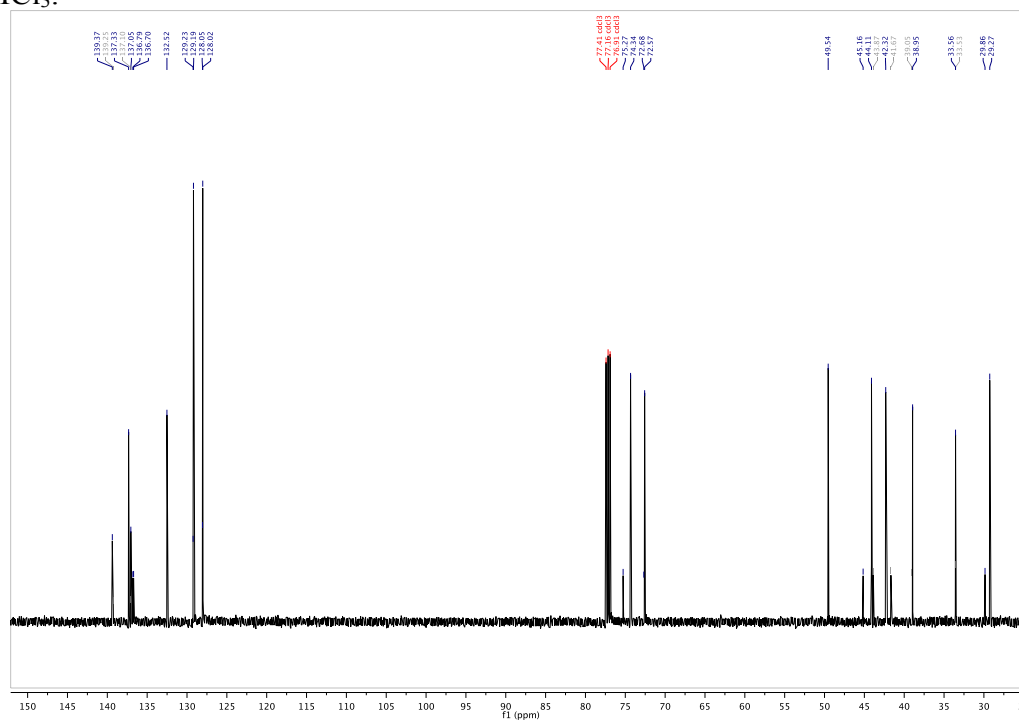


Figure 2.13 ^{13}C NMR spectrum of **3** in CDCl_3 . Signal at 77.16 ppm is the residual CHCl_3 .

2.5.3.3 Preparation of bis-norbornene terminated PEO crosslinker (1a)

In a N₂ glovebox, a Fischer-Porter bottle was charged with THF (2.0 mL) solution of **2** (108.5 mg, 0.8737 mmol). To this solution was added dropwise 0.31 M THF solution of potassium naphthalenide (2.82 mL, 0.87 mmol) leading to a dark green solution. The bottle was sealed with the reactor head, removed from the glove box and stirred at 22 °C for 1 h. The mixture was cooled with liquid nitrogen and ethylene oxide (1.54 g, 35.0 mmol) was condensed into it. The solution was allowed to warm to room temperature and stirred for 16 h. A THF (0.5 mL) solution of **3** (403 mg, 1.31 mmol) was added under nitrogen to cap the living alkoxide, resulting in immediate precipitation of KBr salt. The mixture was stirred at 50 °C for 6 h, cooled to room temperature and filtered through Celite plug to remove the fine powder salt. The filtrate was concentrated to about 5 mL and added dropwise into hexanes (~200 mL) to precipitate the PEO crosslinker out and remove excess **3**. The white powder was collected by filtration and dried under vacuum overnight (1.70 g, 88%).

¹H NMR (500 MHz, CDCl₃) δ 7.31 – 7.28 (m, 4H), 6.12 – 5.82 (m, 4H), 4.56 – 4.38 (m, 4H), 3.63 (s, 202H), 3.38 – 0.43 (m, 18H).

¹³C NMR (126 MHz, CDCl₃) δ 138.28, 137.59, 137.25, 137.22, 136.75, 136.71, 132.60, 132.55, 127.94, 127.90, 127.78, 127.76, 76.16, 75.19, 75.05, 74.11, 73.15, 72.89, 72.78, 70.69, 70.38, 70.35, 69.48, 49.52, 45.14, 45.11, 44.08, 44.05, 43.85, 43.73, 42.30, 41.64, 39.03, 38.93, 38.88, 38.79, 29.85, 29.82, 29.26.

MS (MALDI-TOF) *m/z* calculated for C₁₀₄H₁₉₀O₄₂Na⁺ [M (n=40) + Na]⁺ 2134.26, found 2134.58.

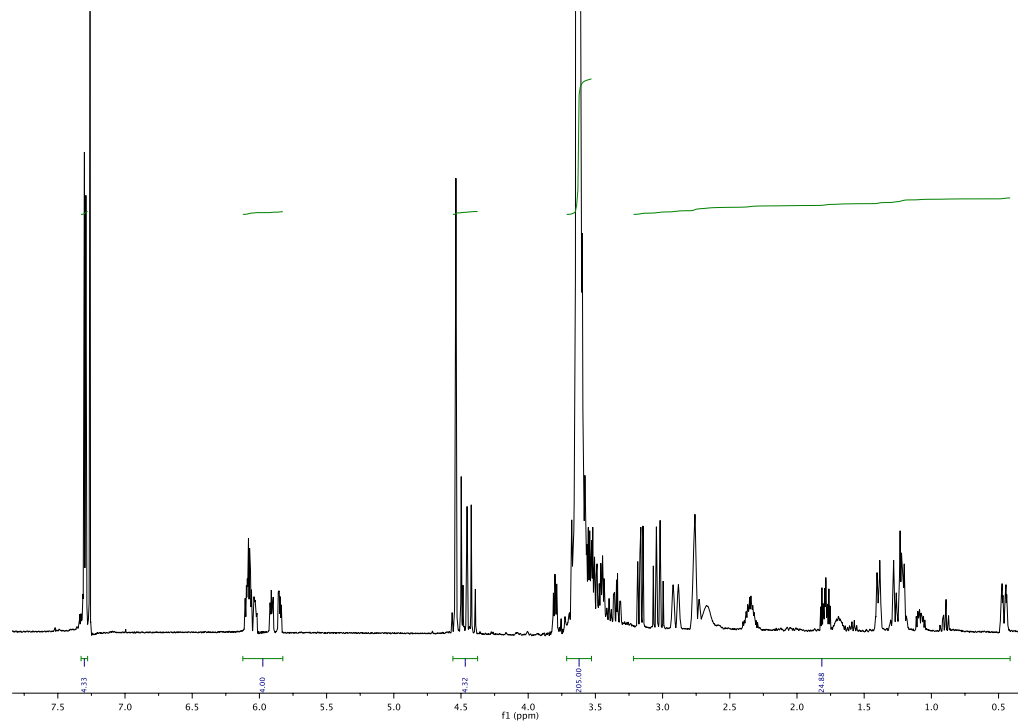


Figure 2.14 ^1H NMR spectrum of **1a** in CDCl_3 . Signal at 7.26 ppm is the residual CHCl_3 .

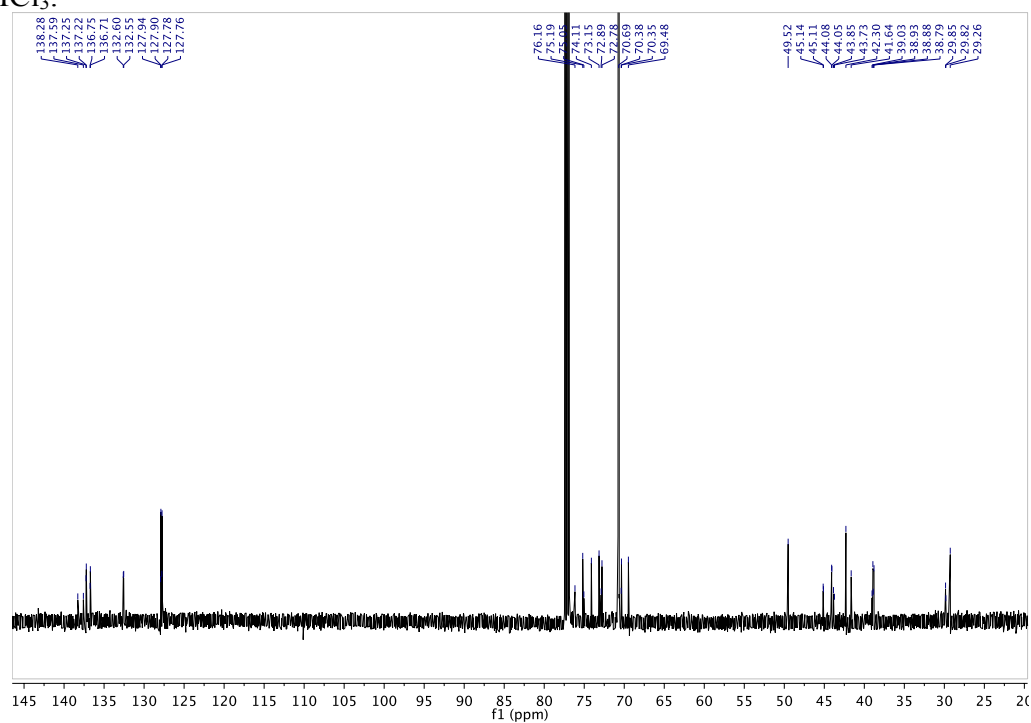


Figure 2.15 ^{13}C NMR spectrum of **1a** in CDCl_3 . Signal at 77.16 ppm is the residual CHCl_3 .

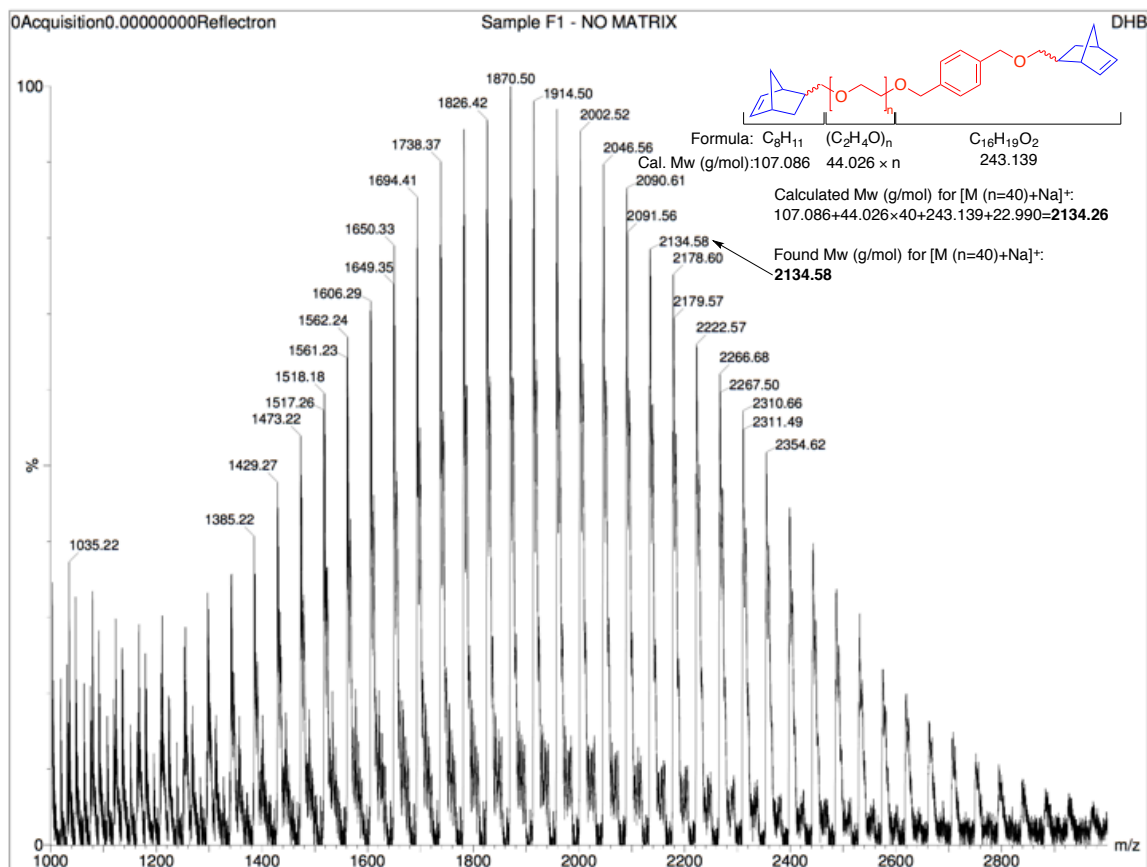
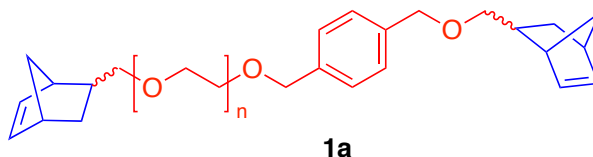


Figure 2.16 MALDI-TOF mass spectrum of **1a** with dithranol as the matrix.

2.5.4 Synthesis of the Cross-Linked Solid Polymer Electrolytes (SPEs)

2.5.4.1 Di-Norbornene Terminated PEO Crosslinker



The effect of crosslinker length on ionic conductivity was studied by synthesizing three crosslinkers with different molecular weights using the procedure described above (section 2.5.3.3). The molecular weight and polydispersity index (PDI) are described in Table 2.2.

Table 2.2 Di-norbornene terminated PEO crosslinker.

Entry No.	EO units in the crosslinker ^a	M_n -NMR ^a (kg/mol)	M_n -GPC ^b (kg/mol)	PDI ^b
1	52	2.6	2.1	1.3
2	88	4.2	3.2	1.3
3	120	5.5	3.9	1.4

^aDetermined by ^1H NMR spectroscopy. ^bDetermined by THF gel permeation chromatography with polystyrene standards at 30 °C.

2.5.4.2 Nomenclature of hPNB-PEO, PCOD-PEO Cross-Linked Solid Polymer

Electrolyte

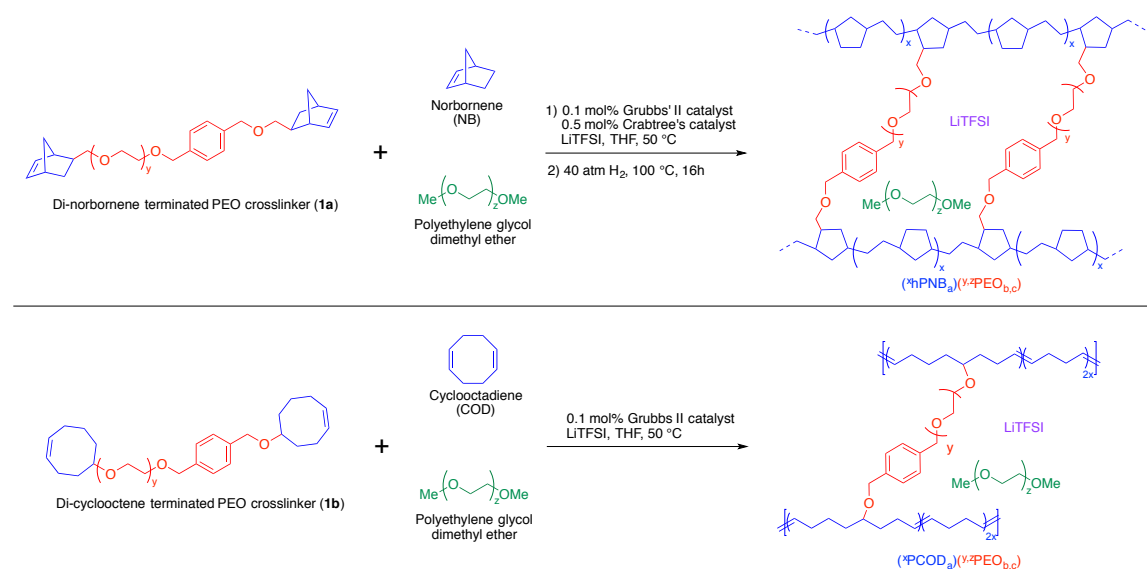
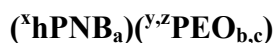


Figure 2.17 General scheme for the synthesis of hPNB-PEO, PCOD-PEO cross-linked system.

Nomenclature of hPNB-PEO system



where

hPNB: hydrogenated polynorbornene; **PEO**: poly(ethylene oxide); **x**: average number

of hydrogenated norbornene (hNB) units between two cross-linkers; **y**: average number of ethylene oxide(EO) units in the cross-linker; **z**: average number of EO units in the plasticizer (omitted for unplasticized system); **a**: mole of hNB/ total moles of hNB and EO; **b**: mole of EO from cross-linkers/ total moles of hNB and EO; **c**: mole of EO from plasticizers/ total moles of hNB and EO.

Calculation:

Define

$$m = (\text{mmols of norbornene (NB)}) + 2 \times \text{mmols of } \mathbf{1a}$$

$$x = m / (2 \times \text{mmols of } \mathbf{1a})$$

$$y = \text{average number of EO in } \mathbf{1a}$$

$$z = 5 \text{ (if plasticized)}$$

$$a = m / (m + y \times \text{mmols of } \mathbf{1a} + z \times \text{mmols of plasticizer})$$

$$b = y \times \text{mmols of } \mathbf{1a} / (m + y \times \text{mmols of } \mathbf{1a} + z \times \text{mmols of plasticizer})$$

$$c = z \times \text{mmols of plasticizer} / (m + y \times \text{mmols of } \mathbf{1a} + z \times \text{mmols of plasticizer})$$

Nomenclature of PCOD-PEO system

$$(\mathbf{xPCOD}_a)(\mathbf{y,zPEO}_{b,c})$$

where

PCOD: polycyclooctadiene; **PEO**: poly(ethylene oxide); **x**: average number of cyclooctadiene (COD) units between two cross-linkers; **y**: average number of ethylene oxide (EO) units in the cross-linker; **z**: average number of EO units in the plasticizer (omitted for unplasticized system); **a**: mole of COD/ total moles of COD and EO; **b**: mole of EO from cross-linkers/ total moles of COD and EO; **c**: mole of EO from plasticizers/ total moles of COD and EO.

Calculation:

Define

$$m = (\text{mmols of cyclooctadiene (COD)}) + 2 \times \text{mmols of } \mathbf{1b}$$

$$x = m / (2 \times \text{mmols of } \mathbf{1b})$$

$$y = \text{average number of EO in } \mathbf{1b}$$

$$z = 5 \text{ (if plasticized)}$$

$$a = m / (m + y \times \text{mmols of } \mathbf{1b} + z \times \text{mmols of plasticizer})$$

$$b = y \times \text{mmols of } \mathbf{1b} / (m + y \times \text{mmols of } \mathbf{1b} + z \times \text{mmols of plasticizer})$$

$$c = z \times \text{mmols of plasticizer} / (m + y \times \text{mmols of } \mathbf{1b} + z \times \text{mmols of plasticizer})$$

2.5.4.3 Sample procedure for the synthesis of hPNB-PEO, PCOD-PEO cross-linked system:

The procedure is similar as reported for PE-PEO system. In a N₂ filled glove box, cross-linker **1a** (130.8 mg, 0.03305 mmol) with 90 EO units in the cross-linker was dissolved in 1.0 mL of THF. To this solution was subsequently added norbornene (46.2 mg, 0.491 mmol, in 1 mL THF), LiTFSI (83.3 mg, 0.290 mmol, in 1 mL THF), PEG 275 (123 mg, 0.447 mmol, in 0.5 mL THF, if plasticized), Crabtree's catalyst (2.2 mg, 2.8×10^{-3} mmol, in 0.4 mL CHCl₃) and Grubbs' 2nd generation catalyst (0.5 mg, 6×10^{-4} mmol, in 0.5 mL THF). The resulting solution was quickly poured into a cut regular metal pan (Teflon coated, diameter of 5.25 cm and depth of 3.0 cm). The mixture gelled up in less than 1 minute. The teflon-coated metal pan was then covered with the top part of a volume glass chamber and placed on top of the hot plate with a metal plate in between to ensure uniform heating. The film was casted in the glove box at 50 °C for 4

h. After all the solvent evaporated off, ~5 mL hexanes was added to the metal pan to help peeling the film off. The film was dried under vacuum at 22 °C for 24 h and then placed in a Parr reactor and sealed. The Parr reactor was pressurized to 40.8 atm with hydrogen and vented down to 3.4 atm. This process was repeated twice to purge the air out. The Parr reactor was then pressurized to 40.8 atm and heat to 100 °C. After 16 h, the reactor was cooled and vented. The film was dried under vacuum at 22 °C for 24 h. No solvent peak was seen from the CDCl₃ extracting of the film, proving there is no remaining solvent. A residue water content of < 0.01 wt % was determined by Karl-Fisher analysis from a THF extraction of the film. Open-circuit voltage for a Li/SPE/Li symmetric coin cell was measured to be 0.0 V, further proving no remaining solvent and water. A control experiment with films without rigorous drying step showed a 0.4 V open-circuit voltage for the symmetric cell, indicating reactions between Li metal and the residue solvent or water. Films of PCOD-PEO cross-linked systems were cast the same way except Crabtree's catalyst was not added and hydrogenation was not performed.

2.5.5 Control Experiment

In order to prove Crabtree's catalyst results in complete hydrogenation of main-chain alkenes, a PEG-grafted NB comonomer was used instead of **1a** during film cast to obtain a soluble hydrogenated copolymer. The synthesis of PEG grafted NB was similar as **1a** except the living alkoxide was quenched by benzyl bromide instead of **3**. In a N₂ glovebox, a Fischer-Porter bottle was charged with THF (2.0 mL) solution of **2** (57.5 mg, 0.463 mmol). To this solution was added dropwise 0.31 M THF solution of

potassium naphthalenide (1.49 mL, 0.46 mmol) leading to a dark green solution. The bottle was sealed with the reactor head, removed from the glove box and stirred at 22 °C for 1 h. The mixture was cooled with liquid nitrogen and ethylene oxide (1.63 g, 37.0 mmol) was condensed into it. The solution was allowed to warm to room temperature and stirred for 16 h. Benzyl bromide (0.082 mL, 0.69 mmol) was added under nitrogen to cap the living alkoxide, resulting in immediate precipitation of KBr salt. The mixture was stirred at 50 °C for 6 h, cooled to room temperature and filtered through Celite plug to remove the fine powder salt. The filtrate was concentrated to about 5 mL and added dropwise into hexanes (~200 mL) to precipitate the PEO crosslinker out. The white powder was collected by filtration and dried under vacuum overnight (1.41 g, 87%). Film cast procedure was similar to hPNB-PEO and PCOD-PEO systems as described in Section 4.3 except PEG-grafted NB was used instead of **1a**. The ¹H NMR of hydrogenated film is shown in Figure S8. It can be seen that no peaks were seen at the alkene range (δ 5–6 ppm). All the norbornene units were reduced to saturated hydrocarbons, corresponding to the peaks between δ 0.5 to 2.0 ppm. The peak at δ 3.7 ppm was from PEO. The sharp singlet at δ 4.6 ppm corresponded to the benzylic hydrogens. This result showed that the Crabtree's catalyst gave complete hydrogenation of the polynorbornene backbones.

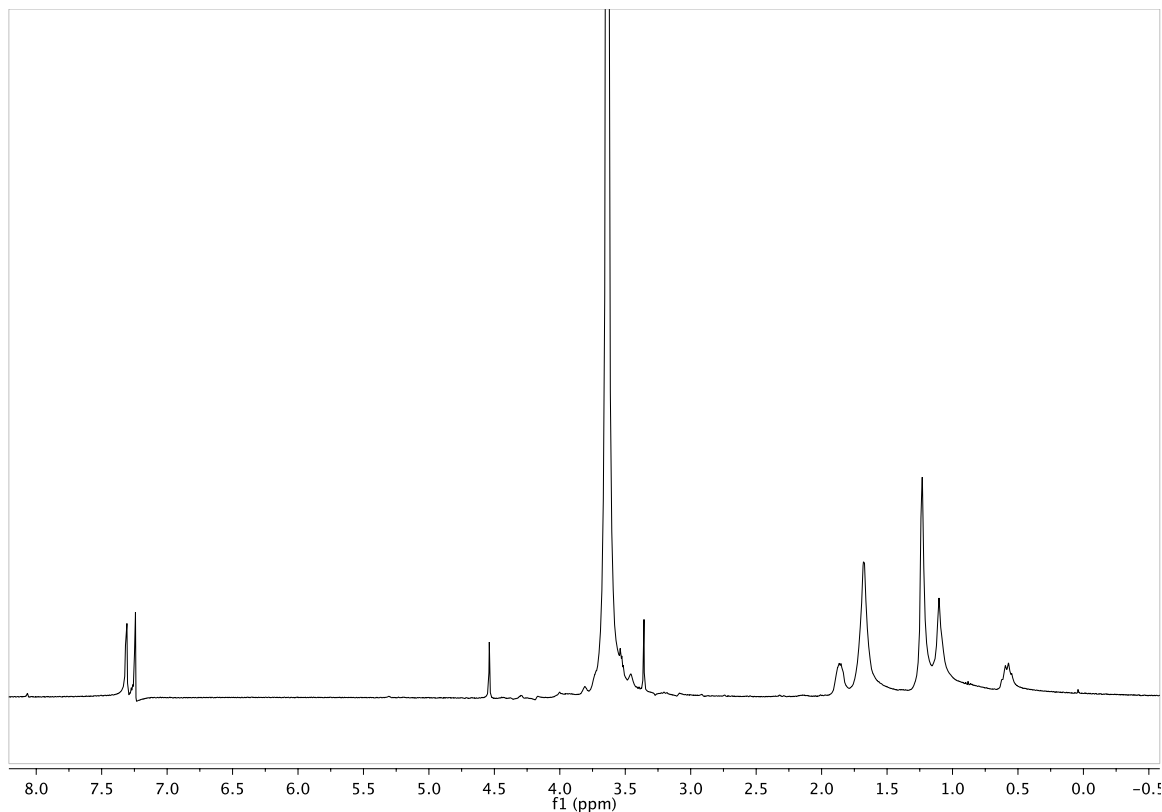


Figure 2.18 ^1H NMR spectrum of hydrogenated film in CDCl_3 . Signal at 7.26 ppm is the residual CHCl_3 .

2.5.6 Differential Scanning Calorimetry (DSC)

DSC analysis was performed using a TA Instruments Q1000 instrument equipped with liquid nitrogen cooling system and automated sampler. Typical DSC samples were made in aluminum pans and the method used was 10 $^{\circ}\text{C}/\text{min}$ ramp, with one cycle of heat, cool, and heat again. The DSC data of plasticized hPNB-PEO and PCOD-PEO systems were shown in the main paper. Unplasticized DSC data were shown in Table 2.3 and 2.4.

Table 2.3 Composition and thermal properties of Unplasticized hPNB-PEO Cross-Linked SPEs^a

Entry	Unplasticized SPE	[NB]:[1] ratio	hPNB segments ^b			PEO segments ^c		
			T_m^d (°C)	ΔH_{fus}^d (J/g)	T_g^d (°C)	T_c^d (°C)	T_m^d (°C)	ΔH_{fus}^d (J/g)
1	(^{8.5} hPN _{0.25})(⁵² PEO _{0.75})	15:1	97	8.8	-46	<i>n.d.</i> ^e	<i>n.d.</i> ^e	<i>n.d.</i> ^e
2	(⁶ hPN _{0.19})(⁵² PEO _{0.81})	10:1	93	3.8	-45	<i>n.d.</i> ^e	<i>n.d.</i> ^e	<i>n.d.</i> ^e
3	(^{4.5} hPN _{0.15})(⁵² PEO _{0.85})	7:1	<i>n.d.</i> ^e	<i>n.d.</i> ^e	-47	<i>n.d.</i> ^e	23	1.1
4	(^{8.5} hPN _{0.16})(⁸⁸ PEO _{0.84})	15:1	92	2.8	-48	-6	32	27.9
5	(⁶ hPN _{0.12})(⁸⁸ PEO _{0.88})	10:1	<i>n.d.</i> ^e	<i>n.d.</i> ^e	-49	-5	32	31.3
6	(^{4.5} hPN _{0.09})(⁸⁸ PEO _{0.91})	7:1	<i>n.d.</i> ^e	<i>n.d.</i> ^e	-50	-6	32	38.5
7	(^{8.5} hPN _{0.12})(¹⁴⁰ PEO _{0.89})	15:1	<i>n.d.</i> ^e	<i>n.d.</i> ^e	-36	-7	36	49.0
8	(⁶ hPN _{0.09})(¹⁴⁰ PEO _{0.92})	10:1	<i>n.d.</i> ^e	<i>n.d.</i> ^e	-39	-6	36	49.8
9	(^{4.5} hPN _{0.07})(¹⁴⁰ PEO _{0.94})	7:1	<i>n.d.</i> ^e	<i>n.d.</i> ^e	-39	-9	37	60.7

^aAll films have [EO]:[Li] composition of 20:1, where EO means ethylene oxide units in the crosslinker.^bhPNB segments: hydrogenated polynorbornene domains in the polymer electrolytes. ^cPEO segments: polyethylene oxide domains in the polymer electrolytes. ^dGlass transition temperature (T_g), cold crystallization temperature (T_c), melting temperature (T_m) and enthalpy of fusion (ΔH_{fus}) were determined by differential scanning calorimetry from the second heat cycle. ^eNot detected.

Table 2.4 Composition and thermal properties of Unplasticized PCOD-PEO Cross-Linked SPEs^a

Entry	Unplasticized SPE	[COD]:[2] ratio	PEO segments ^b		
			T_g^c (°C)	T_m^c (°C)	ΔH_{fus}^c (J/g)
1	(^{8.5} PCOD _{0.30})(⁴⁰ PEO _{0.70})	15:1	-21	<i>n.d.</i> ^d	<i>n.d.</i> ^d
2	(⁶ PCOD _{0.23})(⁴⁰ PEO _{0.77})	10:1	-30	<i>n.d.</i> ^d	<i>n.d.</i> ^d
3	(^{4.5} PCOD _{0.28})(⁴⁰ PEO _{0.82})	7:1	-34	<i>n.d.</i> ^d	<i>n.d.</i> ^d
4	(^{8.5} PCOD _{0.18})(⁷⁵ PEO _{0.82})	15:1	-41	<i>n.d.</i> ^d	<i>n.d.</i> ^d
5	(⁶ PCOD _{0.14})(⁷⁵ PEO _{0.86})	10:1	-40	<i>n.d.</i> ^d	<i>n.d.</i> ^d
6	(^{4.5} PCOD _{0.11})(⁷⁵ PEO _{0.89})	7:1	-42	<i>n.d.</i> ^d	<i>n.d.</i> ^d
7	(^{8.5} PCOD _{0.10})(¹⁶⁰ PEO _{0.90})	15:1	-39	39	68.1
8	(⁶ PCOD _{0.07})(¹⁶⁰ PEO _{0.93})	10:1	-39	39	61.5
9	(^{4.5} PCOD _{0.05})(¹⁶⁰ PEO _{0.95})	7:1	-40	39	76.1

^aAll films have [EO]:[Li] composition of 20:1, where EO means ethylene oxide units in the crosslinker. ^bPEO segments: polyethylene oxide domains in the polymer electrolytes. ^cGlass transition temperature (T_g), cold crystallization temperature (T_c), melting temperature (T_m) and enthalpy of fusion (ΔH_{fus}) were determined by differential scanning calorimetry from the second heat cycle. ^dNot detected.

2.5.7 DC Ionic conductivity and VTF fitting

Samples for DC ionic conductivity were prepared in a dry glove box. The polymer electrolyte membrane was cut into a circle with a diameter of 1 cm using hole punch. The thickness of the electrolyte was typically in the range of 150 – 200 μm . The cut membrane was then sandwiched between two gold plated stainless steel electrodes to form a symmetric cell. The DC ionic conductivity was determined from the plateau value of the conductivity as a function of frequency as reported for PE-PEO system.

Figure 2.19 shows one example of the plots of the real part of the ionic conductivity and $\tan(\delta)$ vs. frequency. The conductivity was recorded at the frequency when $\tan(\delta)$ reached the maximum. Each sample was measured three times at each temperature and took an average. DC ionic conductivity data for unplasticized and plasticized hPNB-PEO and PCOD-PEO systems were reported in Table 2.5, 2.6, 2.7, 2.8. VTF fitting in the main text was done using the variable temperature DC ionic conductivity.

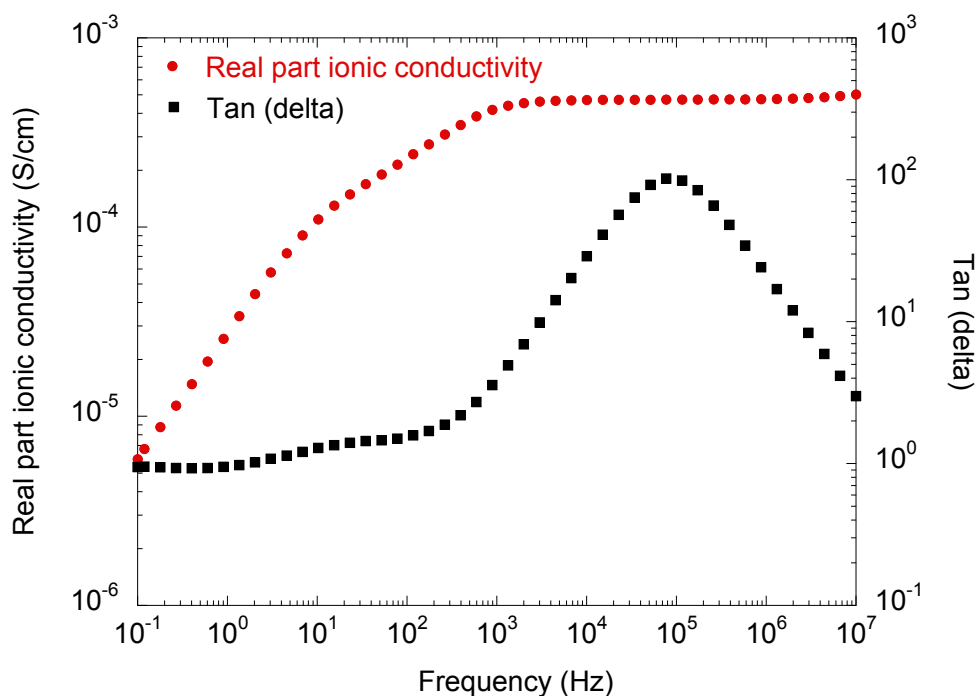


Figure 2.19 Real part of the ionic conductivity and $\tan(\delta)$ vs. frequency plot for $(^{8.5}\text{hPNB}_{0.11})(^{88.5}\text{PEO}_{0.46,0.43})$.

Table 2.5 DC ionic Conductivities of Unplasticized hPNB-PEO Cross-Linked SPEs^a

Entry	Unplasticized SPE	DC Ionic Conductivity (S/cm)						
		10 °C	25 °C	40 °C	55 °C	70 °C	85 °C	100 °C
1	(^{8.5} hPN _{0.25})(⁵² PEO _{0.75})	2.4 × 10 ⁻⁶	1.1 × 10 ⁻⁵	3.6 × 10 ⁻⁵	8.8 × 10 ⁻⁵	1.8 × 10 ⁻⁴	3.3 × 10 ⁻⁴	5.2 × 10 ⁻⁴
2	(⁶ hPN _{0.19})(⁵² PEO _{0.81})	2.3 × 10 ⁻⁶	1.2 × 10 ⁻⁵	4.4 × 10 ⁻⁵	1.2 × 10 ⁻⁴	2.4 × 10 ⁻⁴	4.6 × 10 ⁻⁴	7.4 × 10 ⁻⁴
3	(^{4.5} hPN _{0.15})(⁵² PEO _{0.85})	3.6 × 10 ⁻⁶	1.7 × 10 ⁻⁵	5.6 × 10 ⁻⁵	1.4 × 10 ⁻⁴	2.8 × 10 ⁻⁴	4.9 × 10 ⁻⁴	7.8 × 10 ⁻⁴
4	(^{8.5} hPN _{0.16})(⁸⁸ PEO _{0.84})	6.3 × 10 ⁻⁶	2.8 × 10 ⁻⁵	8.5 × 10 ⁻⁵	2.0 × 10 ⁻⁴	3.8 × 10 ⁻⁴	6.6 × 10 ⁻⁴	1.0 × 10 ⁻³
5	(⁶ hPN _{0.12})(⁸⁸ PEO _{0.88})	6.3 × 10 ⁻⁶	3.0 × 10 ⁻⁵	1.2 × 10 ⁻⁴	2.6 × 10 ⁻⁴	5.0 × 10 ⁻⁴	8.5 × 10 ⁻⁴	1.3 × 10 ⁻³
6	(^{4.5} hPN _{0.09})(⁸⁸ PEO _{0.91})	3.7 × 10 ⁻⁶	2.3 × 10 ⁻⁵	1.1 × 10 ⁻⁴	2.7 × 10 ⁻⁴	5.3 × 10 ⁻⁴	9.1 × 10 ⁻⁴	1.4 × 10 ⁻³
7	(^{8.5} hPN _{0.12})(¹⁴⁰ PEO _{0.89})	9.3 × 10 ⁻⁷	6.8 × 10 ⁻⁶	7.7 × 10 ⁻⁵	2.4 × 10 ⁻⁴	4.5 × 10 ⁻⁴	7.5 × 10 ⁻⁴	1.1 × 10 ⁻³
8	(⁶ hPN _{0.09})(¹⁴⁰ PEO _{0.92})	2.3 × 10 ⁻⁶	1.5 × 10 ⁻⁵	1.0 × 10 ⁻⁴	3.3 × 10 ⁻⁴	6.3 × 10 ⁻⁴	1.1 × 10 ⁻³	1.6 × 10 ⁻³
9	(^{4.5} hPN _{0.07})(¹⁴⁰ PEO _{0.94})	2.4 × 10 ⁻⁶	1.5 × 10 ⁻⁵	1.0 × 10 ⁻⁴	3.6 × 10 ⁻⁴	6.8 × 10 ⁻⁴	1.1 × 10 ⁻³	1.8 × 10 ⁻³

^aAll films had [EO]:[Li] composition of 20:1; where EO means ethylene oxide units in the cross-linker. Conductivities were determined by dielectric spectroscopy measurements.

Table 2.6 DC ionic Conductivities of Unplasticized PCOD-PEO Cross-Linked SPEs^a

Entry	Unplasticized SPE	DC Ionic Conductivity (S/cm)						
		10 °C	25 °C	40 °C	55 °C	70 °C	85 °C	100 °C
1	(^{8.5} PCOD _{0.30})(⁴⁰ PEO _{0.70})	3.5×10^{-6}	1.4×10^{-5}	3.8×10^{-5}	8.7×10^{-5}	1.6×10^{-4}	2.7×10^{-4}	4.2×10^{-4}
2	(⁶ PCOD _{0.23})(⁴⁰ PEO _{0.77})	5.2×10^{-6}	2.2×10^{-5}	6.3×10^{-5}	1.5×10^{-4}	2.8×10^{-4}	4.6×10^{-4}	7.0×10^{-4}
3	(^{4.5} PCOD _{0.28})(⁴⁰ PEO _{0.82})	6.5×10^{-6}	2.8×10^{-5}	8.1×10^{-5}	1.9×10^{-4}	3.5×10^{-4}	5.8×10^{-4}	8.6×10^{-4}
4	(^{8.5} PCOD _{0.18})(⁷⁵ PEO _{0.82})	7.2×10^{-6}	2.9×10^{-5}	8.4×10^{-5}	1.9×10^{-4}	3.5×10^{-4}	5.8×10^{-4}	8.6×10^{-4}
5	(⁶ PCOD _{0.14})(⁷⁵ PEO _{0.86})	1.1×10^{-5}	4.0×10^{-5}	1.1×10^{-4}	2.3×10^{-4}	4.2×10^{-4}	6.7×10^{-4}	9.8×10^{-4}
6	(^{4.5} PCOD _{0.11})(⁷⁵ PEO _{0.89})	1.6×10^{-5}	6.7×10^{-5}	1.9×10^{-4}	4.4×10^{-4}	8.1×10^{-4}	1.3×10^{-3}	1.9×10^{-3}
7	(^{8.5} PCOD _{0.10})(¹⁶⁰ PEO _{0.90})	5.4×10^{-7}	4.4×10^{-6}	4.8×10^{-5}	3.4×10^{-4}	6.3×10^{-4}	1.0×10^{-3}	1.6×10^{-3}
8	(⁶ PCOD _{0.07})(¹⁶⁰ PEO _{0.93})	2.6×10^{-6}	1.7×10^{-5}	1.5×10^{-4}	7.2×10^{-4}	1.3×10^{-3}	2.2×10^{-3}	3.2×10^{-3}
9	(^{4.5} PCOD _{0.05})(¹⁶⁰ PEO _{0.95})	2.0×10^{-6}	1.5×10^{-5}	1.7×10^{-4}	7.4×10^{-4}	1.4×10^{-3}	2.2×10^{-3}	3.2×10^{-3}

^aAll films had [EO]:[Li] composition of 20:1; where EO means ethylene oxide units in the cross-linker. Conductivities were determined by dielectric spectroscopy measurements.

Table 2.7 DC ionic Conductivities of Plasticized hPNB-PEO Cross-Linked SPEs^a

Entry	Plasticized SPE	DC Ionic Conductivity (S/cm)						
		10 °C	25 °C	40 °C	55 °C	70 °C	85 °C	100 °C
1	(^{8.5} hPNB _{0.25})(^{88,0} PEO _{0.75,0})	6.3×10^{-6}	2.8×10^{-5}	8.5×10^{-5}	2.0×10^{-4}	3.8×10^{-4}	6.6×10^{-4}	1.0×10^{-3}
2	(^{8.5} hPNB _{0.14})(^{88,5} PEO _{0.64,0.22})	2.8×10^{-5}	1.0×10^{-4}	2.5×10^{-4}	4.9×10^{-4}	8.4×10^{-4}	1.3×10^{-3}	1.8×10^{-3}
3	(^{8.5} hPNB _{0.13})(^{88,5} PEO _{0.57,0.30})	6.1×10^{-5}	1.9×10^{-4}	4.4×10^{-4}	8.4×10^{-4}	1.4×10^{-3}	2.2×10^{-3}	3.0×10^{-3}
4	(^{8.5} hPNB _{0.11})(^{88,5} PEO _{0.46,0.43})	1.8×10^{-4}	4.7×10^{-4}	9.9×10^{-4}	1.7×10^{-3}	2.7×10^{-3}	3.9×10^{-3}	5.3×10^{-3}
5	(^{8.5} hPNB _{0.09})(^{88,5} PEO _{0.38,0.54})	3.2×10^{-4}	8.1×10^{-4}	1.7×10^{-3}	2.9×10^{-3}	4.4×10^{-3}	6.3×10^{-3}	8.4×10^{-3}

^aAll films had [EO]:[Li] composition of 20:1; where EO means ethylene oxide units in the cross-linker and plasticizers. Conductivities were determined by dielectric spectroscopy measurements.

Table 2.8 DC ionic Conductivities of Plasticized PCOD-PEO Cross-Linked SPEs^a

Entry	Plasticized SPE	DC Ionic Conductivity (S/cm)						
		10 °C	25 °C	40 °C	55 °C	70 °C	85 °C	100 °C
1	(^{8.5} PCOD _{0.17})(^{75,0} PEO _{0.83,0})	7.2×10^{-6}	2.9×10^{-5}	8.4×10^{-5}	1.9×10^{-4}	3.5×10^{-4}	5.8×10^{-4}	8.6×10^{-4}
2	(^{8.5} PCOD _{0.13})(^{75,5} PEO _{0.66,0.21})	2.4×10^{-5}	8.0×10^{-5}	2.0×10^{-4}	4.1×10^{-4}	7.2×10^{-4}	1.1×10^{-3}	1.6×10^{-3}
3	(^{8.5} PCOD _{0.11})(^{75,5} PEO _{0.57,0.32})	4.6×10^{-5}	1.5×10^{-4}	3.7×10^{-4}	7.3×10^{-4}	1.2×10^{-3}	1.9×10^{-3}	2.6×10^{-3}
4	(^{8.5} PCOD _{0.10})(^{75,5} PEO _{0.48,0.43})	8.8×10^{-5}	2.6×10^{-4}	6.0×10^{-4}	1.1×10^{-3}	1.9×10^{-3}	2.7×10^{-3}	3.8×10^{-3}
5	(^{8.5} PCOD _{0.08})(^{75,5} PEO _{0.39,0.53})	1.1×10^{-4}	3.3×10^{-4}	7.5×10^{-4}	1.4×10^{-3}	2.3×10^{-3}	3.4×10^{-3}	4.6×10^{-3}

^aAll films had [EO]:[Li] composition of 20:1; where EO means ethylene oxide units in the cross-linker and plasticizers. Conductivities were determined by dielectric spectroscopy measurements.

2.5.8 Galvanostatic Cycling Measurements

Li/SPE/Li symmetric coin cells were assembled in an argon filled MBraun glovebox, and the galvanostatic cycling short-circuit measurements were performed using a Neware CT-3008 battery tester with wiring into (Fisher Scientific and VWR) convection ovens at a temperature of 90 °C. An initial 24 hour period of three hour charge and three hour discharge cycling at a lower current density (0.026 mA/cm^2) was performed, followed by each of half cycle of 3 h at 0.26 mA/cm^2 until a sudden drop in voltage was observed. Figure 2.20 shows the voltage profile of hPNB-PEO as an example.

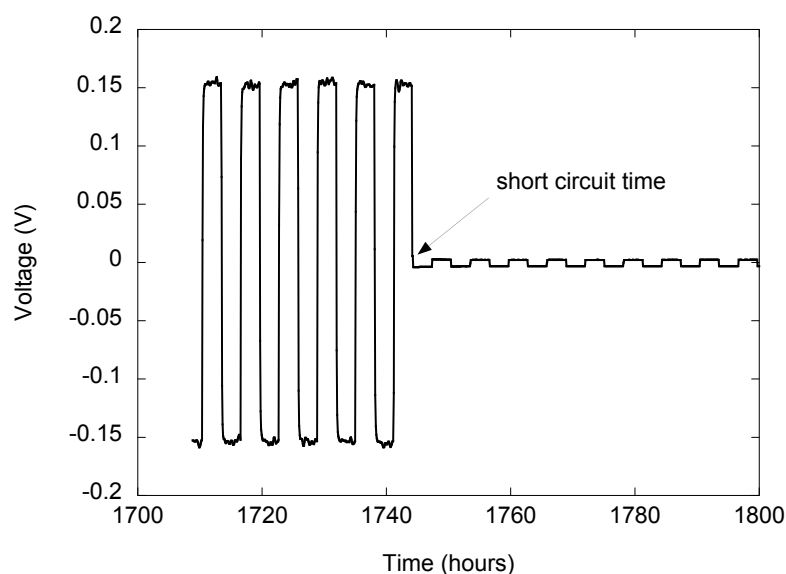


Figure 2.20 Galvanostatic cycling curve obtained for hPNB-PEO with 32 wt % plasticizer at fixed current density for 0.26 mA/cm^2 and 90 °C. The short circuit time (t_{sc}) is pointed out; C_d value is 1638 C/cm^2 .

2.5.9 Galvanostatic Polarization Measurements

Galvanostatic polarization measurements were performed on Li/SPE/Li symmetric coin cells by a Neware CT-3008 battery tester. A typical polarization curve at current density of 0.26 mA/cm^2 at 90°C is shown in Figure 2.21.

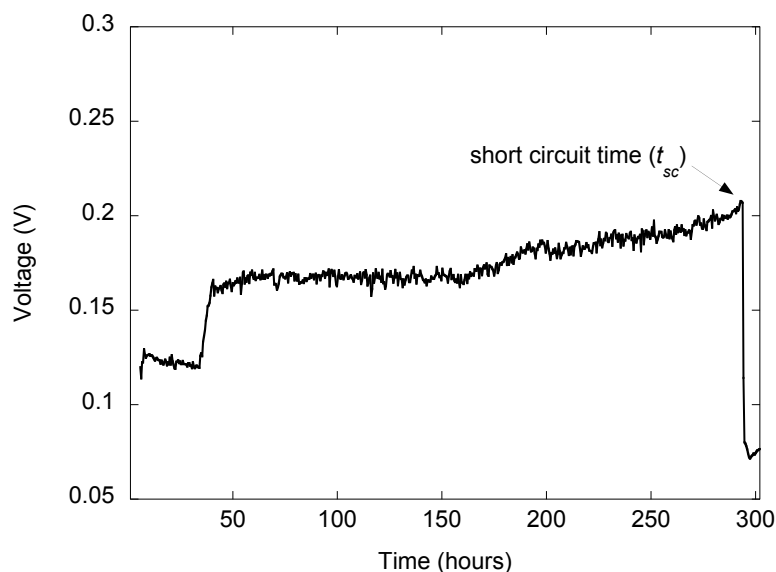


Figure 2.21 Voltage profile of galvanostatic polarization of hPNB-PEO system at fixed current density of 0.26 mA/cm^2 at 90°C . The short circuit time is determined at the moment when the sudden voltage drop is observed.

2.5.10 Rheology

Anton Paar Physica MCR 301 rheometer was used for rheological measurements with 10 mm diameter parallel plates. The storage G' and loss G'' moduli were quantified as a function of applied angular frequency at low strain (0.1%) and 90°C .

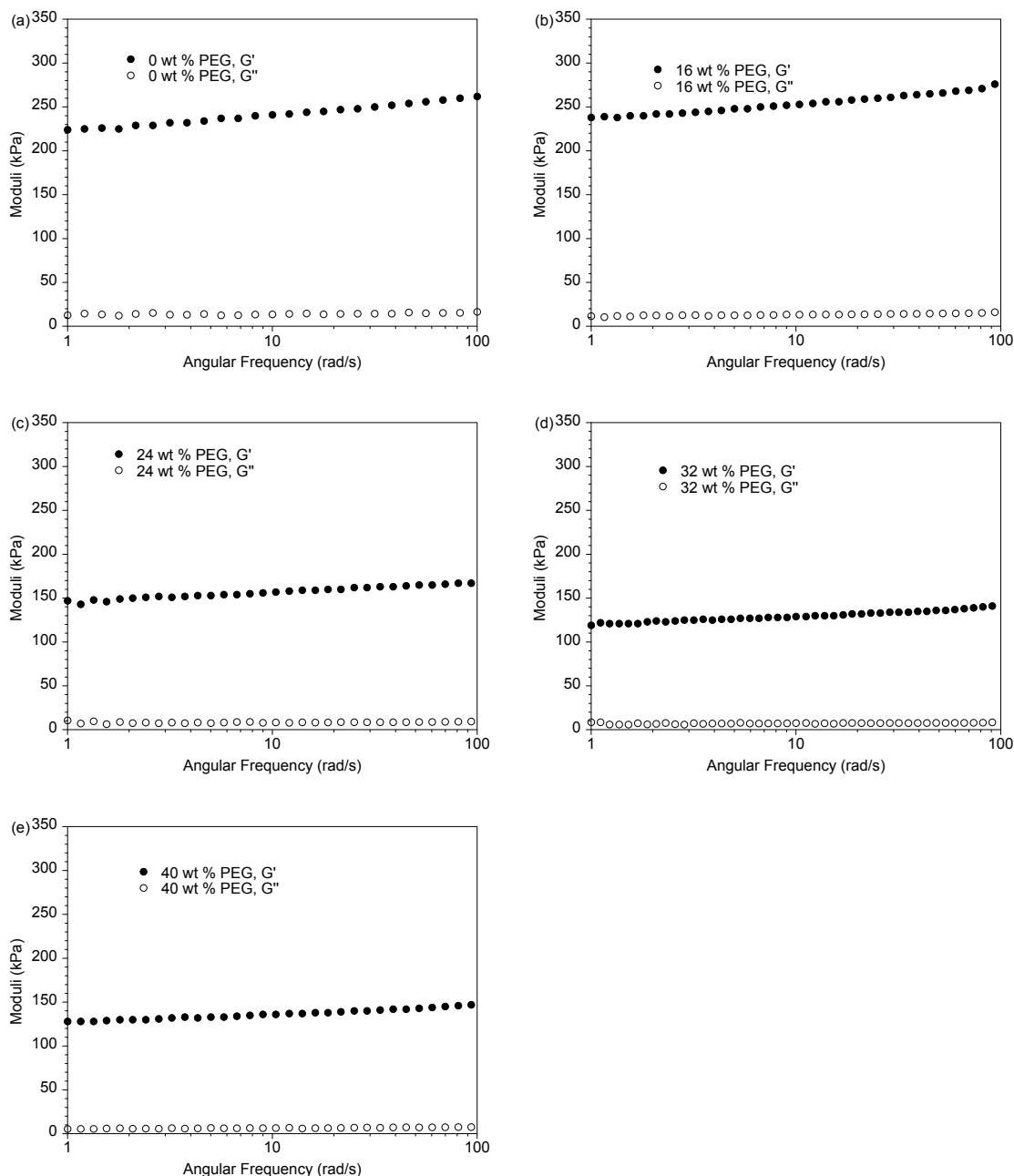


Figure 2.22 Rheological measurements on hPNB-PEO system with different weight% of the plasticizer at 90 °C. All films had [NB]:[**1a**] ratio of 15:1 and [EO]:[Li] composition of 20:1. Storage modulus $G'(\omega)$ is shown with filled symbols, and the loss modulus $G''(\omega)$ is shown with hollow symbols. (a) 0 wt %, (b) 16 wt%, (c) 24 wt %, (d) 32 wt %, and (e) 40 w % PEG275 plasticizer in the cross-linked films.

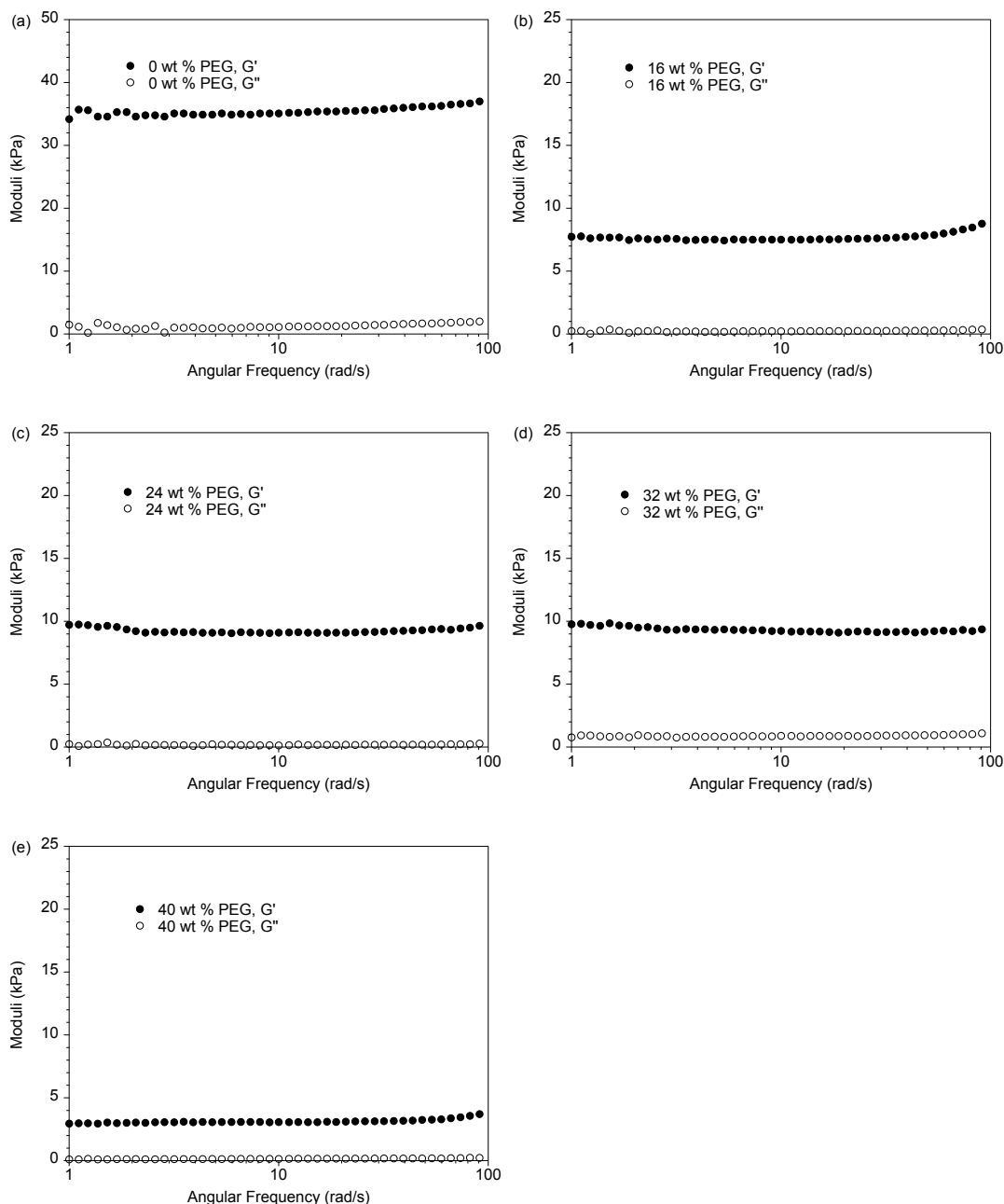


Figure 2.23 Rheological measurements on PCOD-PEO system with different weight% of the plasticizer at 90 °C. All films had [COD]:[**1b**] ratio of 15:1 and [EO]:[Li] composition of 20:1. Storage modulus $G'(\omega)$ is shown with filled symbols, and the loss modulus $G''(\omega)$ is shown with hollow symbols. (a) 0 wt %, (b) 16 wt%, (c) 24 wt %, (d) 32 wt %, and (e) 40 wt % PEG275 plasticizer in the cross-linked films.

2.5.11 SEM of the lithium metal after short-circuit

The morphology of the lithium metal in different systems after short-circuit is analyzed using Keck scanning electron microscope (SEM) at 3kV acceleration voltage. The batteries after short-circuit were disassembled in the glove box and the lithium metal was taken out for observation.

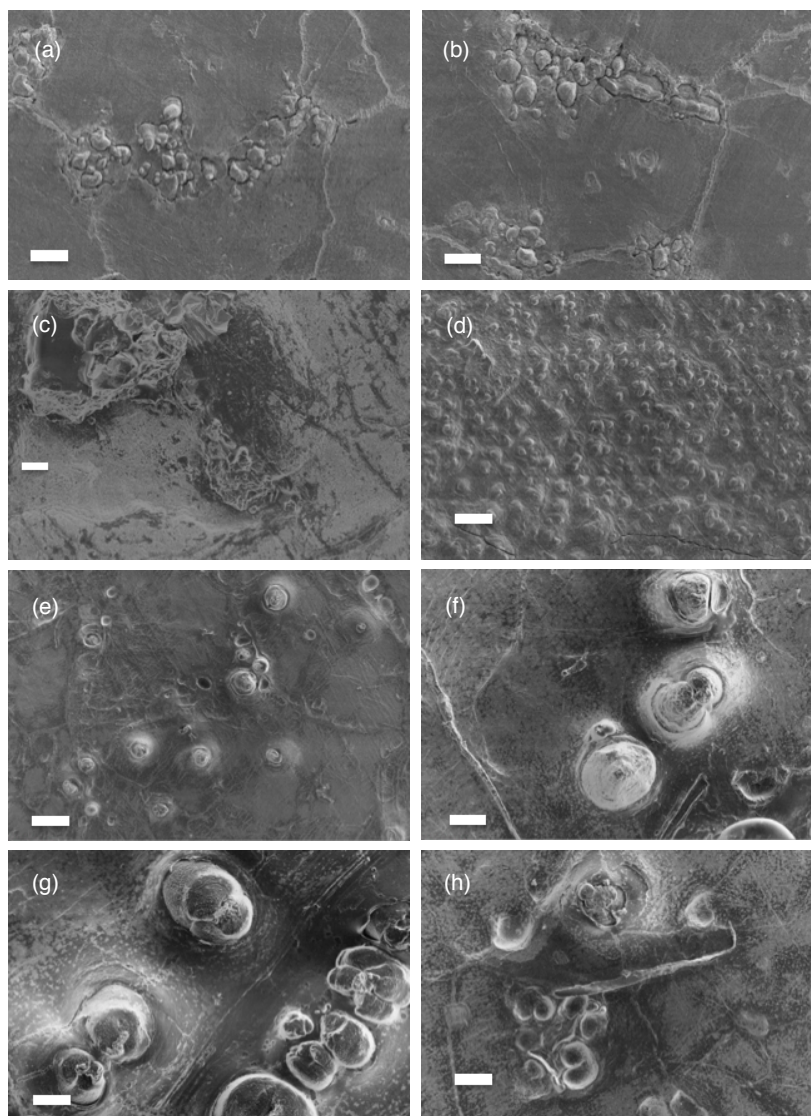


Figure 2.24 SEM images of lithium metal after short-circuit. Galvanostatic polarization of hPNB-PEO system at (a) 0.26 mA/cm²; (b) 0.4 mA/cm²; (c) 1 mA/cm²; (d) Galvanostatic cycling of hPNB-PEO system at 0.26 mA/cm²; Galvanostatic polarization of PCOD-PEO system at (e) 0.26 mA/cm²; (f) 0.4 mA/cm²; (g) 1 mA/cm²; (h) Galvanostatic cycling of PCOD-PEO system at 0.26 mA/cm². Scale bar = 20 μ m.

2.5.12 Electrochemical Impedance Spectroscopy (EIS)

The ac impedance spectroscopy measurements for the Li/SPE/Li symmetric coin cells were measured using a Novocontrol Broadband Dielectric Spectrometer, fitted with a Quatro temperature control system at frequency ranging from 2 KHz to 900 MHz and at amplitude of 10 mV. Figure 2.25 (a) shows the impedance spectra for hPNB-PEO electrolytes with varied plasticizer weight at 18 °C. With the increase in the amount of PEG275 as plasticizer in the SPEs, the bulk resistance (R_b) of the polymer electrolytes decreases significantly, which is consistent with the expectation. Also with the increase of temperature from 18 °C to 90 °C, both the bulk resistance (R_b) and interfacial resistance (R_i) shows obvious decrease. Figure 2.25 (c) and (d) shows the corresponding impedance data of the PCOD-PEO system. Consistent with the trend of the conductivity measurement of the different systems (Figure 2.25), PCOD-PEO shows lower bulk resistance compared to hPNB-PEO system.

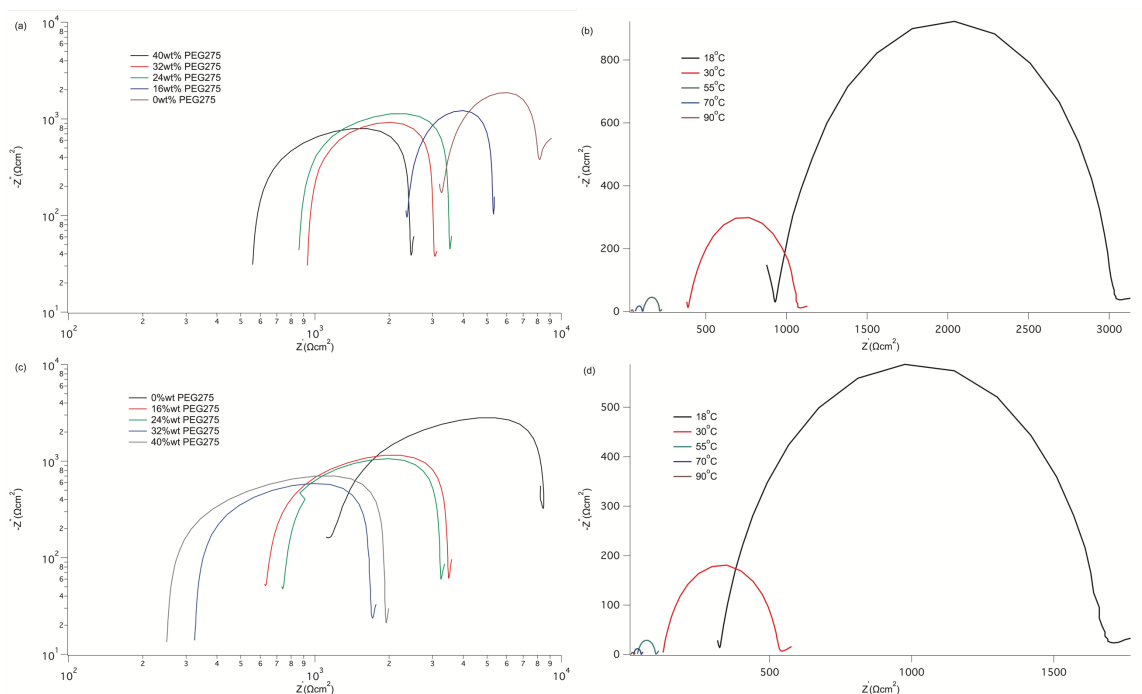


Figure 2.25 (a) Impedance spectra for hPNB-PEO electrolytes with varied plasticizer weight at 18 °C. (b) Impedance for hPNB-PEO with 32 wt % plasticizer at variable temperature. (c) Impedance spectra for PCOD-PEO electrolytes with varied plasticizer weight at 18 °C. (d) Impedance for PCOD-PEO with 32 wt % plasticizer at variable temperature.

2.5.13 Density measurements

The densities for nonplasticized and plasticized hPNB and PCOD electrolytes were measured and summarized in Table 2.9. The polymer electrolytes were cut into a circle with a hole punch. The thickness was measured using a micrometer. The volume of the membrane can then be calculated by $V = \pi r^2 h$, where V is the volume, r is the diameter of the circle and h is the thickness of the membrane. The masses of the membranes were weighted. The density can then be calculated by $\rho = m/V$, where ρ is the density and m is the mass.

Table 2.9 Density of the hPNB and PCOD SPEs

hPNB (wt % of		PCOD (wt % of	
PEG250)	Density (g/cm ³)	PEG250)	Density (g/cm ³)
0	1.27	0	1.19
16	1.25	16	1.22
24	1.25	24	1.24
32	1.28	32	1.25
40	1.20	40	1.21

The densities of the both copolymers are around 1.2 – 1.3 g/cm³ and no significant trend is seen by varying the amount of plasticizers. This result is expected because the densities of the hydrocarbon polymers are all in the range between 0.9 – 1.0 g/ml and are very close to each other (PE ~ 0.97 g/cm³, hPNB ~ 0.99 g/cm³, PCOD ~ 0.91 g/cm³). PEO has a density of about 1.2 g/cm³ and LiTFSI has a density of about 1.33 g/cm³. A density around 1.2 g/cm³ is a reasonable value. Because the densities are very close to each other in both hPNB and PCOD electrolytes, we conclude that the density should have no significant effect on dendrite suppression.

2.5.14 Li transference number

The lithium transference number of hPNB-PEO and PCOD-PEO was measured using a conventional Bruce and Vincent method.²⁸ Specifically, a lithium symmetric cell was assembled with two lithium metal pieces as electrodes and the SPE as the separator. The transference number was then determined using the equation:

$$T_+ = \frac{I^S(\Delta V - I^O R_1^O)}{I^O(\Delta V - I^S R_1^S)} \quad \text{Equation 2.2}$$

Here ΔV is the potential applied across the cell; R_1^o and R_1^s are the initial and steady state resistances of the passivating layers; I^o and I^s are the initial and steady-state currents respectively. A small $\Delta V = 20$ mV was applied and the result is summarized in Figure 2.26, which shows the impedance and current change before and after polarization of the cell with unplasticized hPNB-PEO as the separator. The Li transference number is then calculated as 0.30. A transference number of 0.32 is calculated with unplasticized PCOD-PEO as the separator using the same method.

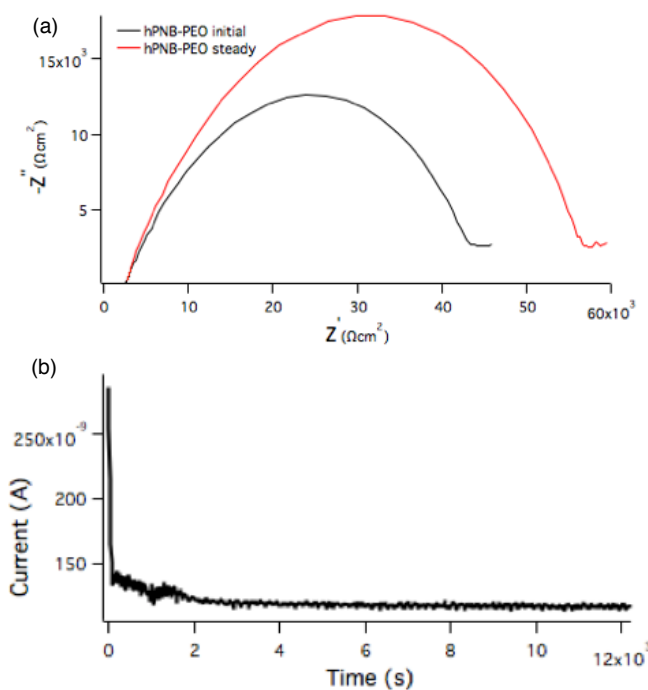


Figure 2.26 (a) Initial and steady state impedance spectra of lithium symmetric cell for unplasticized hPNB-PEO. (b) Steady state current measurement for unplasticized hPNB-PEO.

2.5.15 Battery device test

We applied the 32 wt% plasticized hPNB-PEO membrane to a half cell and the voltage profile is shown below (Figure 2.27). The half cell battery is composed of LiCoO_2 as the cathode, Li metal as the anode and hPNB as the separator. The battery

was cycled at 0.5 C. It shows that the battery device still has the feature of LiCoO_2 electrode, with a discharge plateau at ~ 3.9 V, indicating the potential application of the polymer electrolytes in practical battery devices. The capacity is lower than the theoretical capacity of LiCoO_2 , which is probably due to the limited conductivity of the membrane.

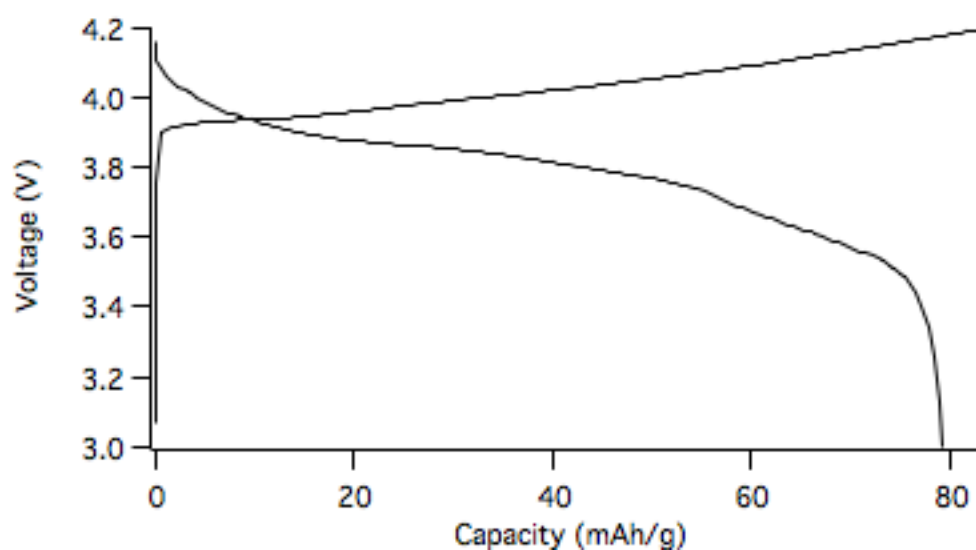


Figure 2.27 Charge/discharge profile of $\text{LiCoO}_2/\text{hPNB}/\text{Li}$ battery at a discharge rate of 0.5 C.

REFERENCES

- (1) Xu, K. *Chem. Rev.* **2004**, *104*, 4303–4418.
- (2) Xu, K. *Chem. Rev.* **2014**, *114*, 11503–11618.
- (3) Gireaud, L.; Grugeon, S.; Laruelle, S.; Yrieix, B.; Tarascon, J. M. *Electrochem. Commun.* **2006**, *8*, 1639–1649.
- (4) Harry, K. J.; Hallinan, D. T.; Parkinson, D. Y.; MacDowell, A. A.; Balsara, N. P. *Nat. Mater.* **2014**, *13*, 69–73.
- (5) Kang, I. S.; Lee, Y. S.; Kim, D. W. *J. Electrochem. Soc.* **2013**, *161*, A53–A57.
- (6) Ding, F.; Xu, W.; Graff, G. L.; Zhang, J.; Sushko, M. L.; Chen, X.; Shao, Y.; Engelhard, M. H.; Nie, Z.; Xiao, J.; Liu, X.; Sushko, P. V.; Liu, J.; Zhang, J. G. *J. Am. Chem. Soc.* **2013**, *135*, 4450–4456.
- (7) Ota, H.; Wang, X.; Yasukawa, E. *J. Electrochem. Soc.* **2004**, *151*, A427.
- (8) Lu, Y.; Tu, Z.; Archer, L. A. *Nat. Mater.* **2014**, *13*, 961–969.
- (9) Zheng, G.; Lee, S. W.; Liang, Z.; Lee, H. W.; Yan, K.; Yao, H.; Wang, H.; Li, W.; Chu, S.; Cui, Y. *Nat. Nanotechnol.* **2014**, *9*, 618–623.
- (10) Khurana, R.; Schaefer, J. L.; Archer, L. A.; Coates, G. W. *J. Am. Chem. Soc.* **2014**, *136*, 7395–7402.
- (11) Stone, G. M.; Mullin, S. A.; Teran, A. A.; Hallinan, D. T.; Minor, A. M.; Hexemer, A.; Balsara, N. P. *J. Electrochem. Soc.* **2012**, *159*, A222–A227.
- (12) Sadoway, D. R. *J. Power Sources* **2004**, *129*, 1–3.
- (13) Ghosh, A.; Kofinas, P. *J. Electrochem. Soc.* **2008**, *155*, A428–A231.
- (14) Choudhury, S.; Mangal, R.; Agrawal, A.; Archer, L. A. *Nat. Commun.* **2015**, *6*, 10101.

- (15) Pan, Q.; Smith, D. M.; Qi, H.; Wang, S.; Li, C. Y. *Adv. Mater.* **2015**, *27*, 5995–6001.
- (16) Monroe, C.; Newman, J. J. *J. Electrochem. Soc.* **2003**, *150*, A1377–A1384.
- (17) Monroe, C.; Newman, J. J. *J. Electrochem. Soc.* **2005**, *152*, A396–A404.
- (18) Brissot, C.; Rosso, M.; Chazalviel, J. N.; Baudry, P.; Lascaud, S. *Electrochim. Acta* **1998**, *43*, 1569–1574.
- (19) Lee, L.-B. W.; Register, R. A. *Macromolecules* **2005**, *38*, 1216–1222.
- (20) Rupp, B.; Schmuck, M.; Balducci, A.; Winter, M.; Kern, W. *Eur. Polym. J.* **2008**, *44*, 2986–2990.
- (21) Gnanou, Y.; Hild, G.; Rempp, P. *Macromolecules* **1984**, *17*, 945–952.
- (22) Robertson, N. J.; Kostalik, H. A. t.; Clark, T. J.; Mutolo, P. F.; Abruna, H. D.; Coates, G. W. *J. Am. Chem. Soc.* **2010**, *132*, 3400–3404.
- (23) Kuo, C. W.; Huang, C. W.; Chen, B. K.; Li, W. B.; Chen, P. R.; Ho, T. H.; Tseng, C. G.; Wu, T. Y. *Int. J. Electrochem. Sc.* **2013**, *8*, 3834–3850.
- (24) Lu, Y.; Das, S. K.; Moganty, S. S.; Archer, L. A. *Adv. Mater.* **2012**, *24*, 4430–4435.
- (25) Lu, Y.; Korf, K.; Kambe, Y.; Tu, Z.; Archer, L. A. *Angew. Chem. Int. Ed.* **2014**, *53*, 488–492.
- (26) Tu, Z.; Kambe, Y.; Lu, Y.; Archer, L. A. *Adv. Energy Mater.* **2014**, *4*, 1300654.
- (27) Blanco, J. M.; Fernández, F.; García-Mera, X.; Rodríguez-Borges, J. E. *Tetrahedron* **2002**, *58*, 8843–8849.
- (28) Bruce, P. *Solid State Ionics* **1988**, *28-30*, 918–922.

CHAPTER 3

Alternating and random copolymers of ethylene oxide and trimethylene oxide as solid
polymer electrolytes for lithium batteries

Chapter 3

Alternating and random copolymers of ethylene oxide and trimethylene oxide as solid polymer electrolytes for lithium batteries

3.1 Abstract

Polyethylene oxide (PEO) and PEO based polymers have been the predominantly studied polymers as candidates for solid electrolytes for lithium batteries. The modification on PEO, either by doping with additives or copolymerizing with hard blocks, did not improve the lithium ion conductivities significantly. Searching new targets other than PEO using theoretical simulations have identified a target polymer – poly(ethylene oxide-*alt*-trimethylene oxide) as a promising candidate with higher ionic conductivity than that of PEO. Inspired by this prediction, we successfully synthesized this polymer and systematically compared its ionic conductivity with PEO and random copolymers of ethylene oxide (EO) and trimethylene oxide (TMO). The conductivities of both alternating and random copolymers were higher than that of PEO at room temperature. One random copolymer with 61 mol% EO content reached a conductivity of 1×10^{-4} S/cm at room temperature, among the highest values reported for polymer electrolytes. Although the prediction was not completely validated, the results reported in this study demonstrated that theoretical simulation, together with polymer synthesis and electrochemical characterization, could be a useful tool in discovering new polymer electrolytes with promising properties.

3.2 Introduction

Polyethylene oxide (PEO) has been extensively studied as a solid polymer electrolyte (SPE) for lithium-ion batteries since Wright's discovery of its capability to dissolve lithium salt in 1970s.¹ After four decades of research, PEO is still largely considered to be the state-of-the-art for SPEs because of its low cost, high ionic conductivity ($\sim 10^{-3}$ S/cm) at elevated temperature and chemical stability. However, one significant barrier for the commercial application of PEO is its low ionic conductivity ($\sim 10^{-7}$ – 10^{-6} S/cm) at ambient temperatures. The significant decrease of the conductivity is caused by the crystallinity of PEO at room temperature. Two main strategies have been taken to reduce the crystallinity of PEO. One strategy was doping additives to PEO. The additives can be either liquid plasticizers²⁻¹⁰ (alkyl carbonate, oligo(ethylene glycol), ionic liquids) or solid inorganic fillers¹¹ (mostly metal oxide nanoparticles). The liquid plasticizers helped to partially or completely reduce the crystallinity of PEO and dramatically increased the ionic conductivity to $\sim 10^{-4}$ S/cm at room temperature. However, the mechanical properties of the SPE was significantly compromised by the addition of plasticizers. The solid inorganic fillers maintained the mechanical properties of the SPE but the increase in conductivity was marginal compared to liquid plasticizers, mostly at 10^{-5} S/cm. Moreover, the addition of inorganic fillers did not improve the adhesion properties of PEO-based electrolytes (good contact between electrodes and electrolytes was essential for optimal battery performance). The other strategy was incorporating PEO into copolymers. Linear block copolymers of PEO have been reported with either rigid polymers, such as polystyrene;¹² or soft polymers, including poly(dimethyl siloxane) and poly(propylene oxide).¹³ Grafted copolymers of PEO have

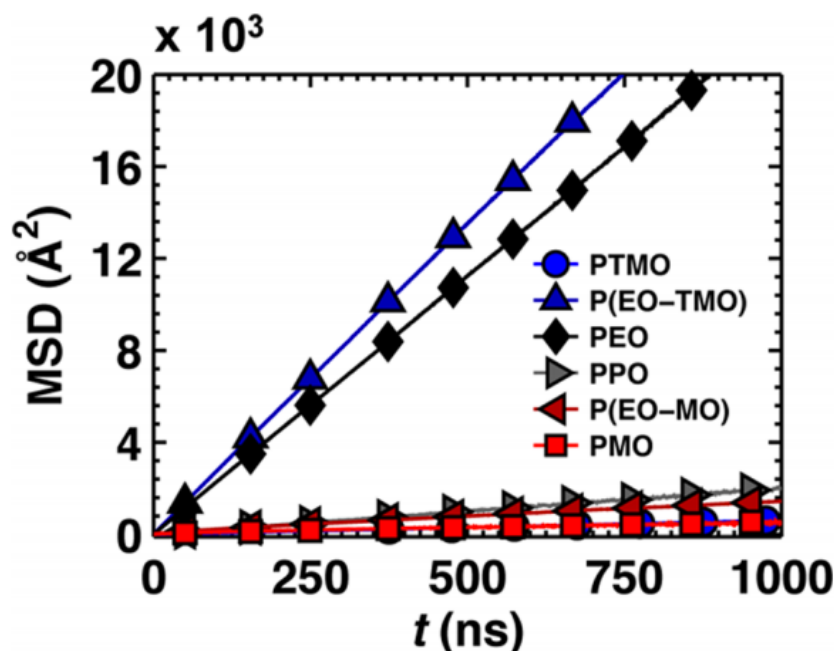


Figure 3.1 Mean-square displacement (MSD) of a lithium cation obtained from KMC trajectories using the CS-DBP model. (adapted from reference 1).

also been synthesized with the expectation that grafted polymer chains would have larger segmental movement than that of backbone polymer chains. The highest room temperature conductivities achieved for both linear and grafted PEO copolymers were in the range of 10^{-4} – 10^{-3} S/cm, whereas the intrinsic trade-off between conductivities and mechanical properties held true for most of these copolymers.

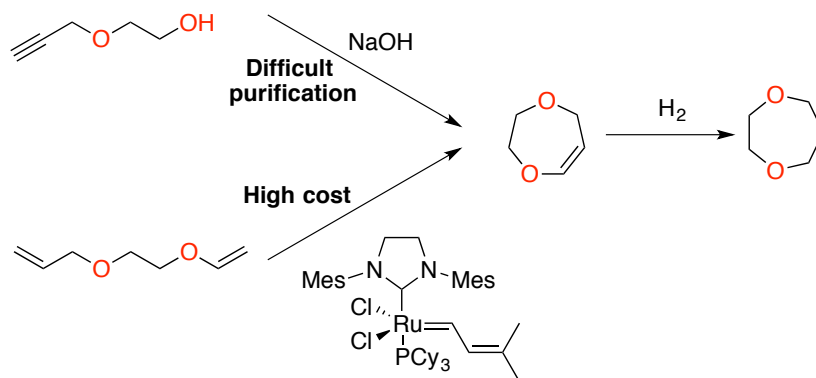
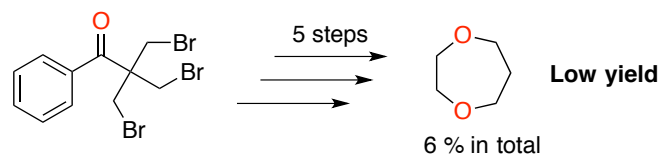
For over four decades of studies on SPEs, researchers have mostly used their empirical experiences in developing new polymer electrolytes and their works have been focused on PEO and PEO derivatives. There were few examples on applying polyethers other than PEO as SPEs for lithium-ion batteries. A collaboration among theoretical chemist Miller, synthetic chemist Coates and material scientist Balsara was aiming to systematically screen polyethers other than PEO with computer simulation using a chemically specific dynamic bond percolation (CS-DBP) model. Miller and

coworkers¹⁴ recently reported that an alternating copolymer of ethylene oxide (EO) and trimethylene oxide (TMO) will have higher ionic conductivity than PEO based on their simulation results (Figure 3.1). Herein, we report the synthesis of the copolymer of EO and TMO and characterized its ionic conductivity. We further synthesized random copolymers of EO and TMO with variable EO content and compared their conductivities with the alternating copolymer.

3.3 Results and Discussions

To our best knowledge, the synthesis of the alternating copolymer of EO and TMO has not been reported before. There are two potential routes to synthesize this polymer. One is by step-growth polymerization of disodium salt of ethylene glycol with 1,3-dibromopropane or 1,3-dimesyloxypropane. However, the step-growth polymerization is known to achieve high molecular weight only with high conversions. The nucleophilic substitution (S_N2) between alkoxide and bromide or mesyl group is also competing with the corresponding elimination reactions (E2). Once the elimination reaction happens, the growth of the polymer chain will be terminated. The alternative route is by ring-opening polymerization of 1,4-dioxepane through chain growth mechanism to reach high molecular weight. The synthesis of 1,4-dioxepane has been reported but none of them is scalable (Figure 3.2). Weyerstahl and co-workers¹⁵ reported a five-step synthesis from 3-bromo-2,2-bis(bromomethyl)-1-phenylpropan-1-one with an overall yield of 6% and the ketone starting material was not commercially available. The monomer can also be synthesized by hydrogenating the unsaturated cyclic enol ether – 2,3-dihydro-1,4-dioxepine. Böttner and co-workers¹⁶ reported a one-step base-induced cyclization from propargyloxyethanol to the enol ether in 48% yield. However, it was difficult to separate the product from other cyclized by-products because of similar boiling points. Recently, Grubbs and co-workers reported a ring-closing metathesis of 1-allyloxy-2-vinyloxyethane to the enol ether in 49% yield with a modified alkylidene ruthenium-based olefin metathesis catalyst. The high cost of the ruthenium catalyst precluded large scale synthesis of the enol ether. A high-yield and low-cost synthesis of the monomer needs to be developed.

Previous work:



This work:

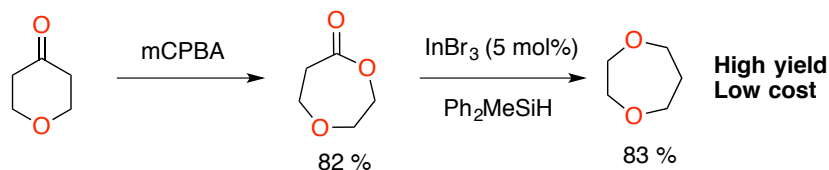


Figure 3.2 Synthesis of 1,4-dioxepane

In contrast to reported cyclization reactions, we were interested in synthesizing the monomer by keeping the ring structure from the starting material. Reductions of lactones to cyclic ethers have been known for decades. Pettit *et al.*¹⁷ first observed reductions of lactones to cyclic ethers on some natural products by using boron trifluoride etherate and lithium aluminum hydride as the reducing reagents back in the 1960s. This reduction was further improved by Kraus and co-workers¹⁸ to a milder two-step conversion with diisobutylaluminum hydride, followed by Et₃SiH/BF₃·Et₂O. However, reductions with metal hydrides were limited to certain substrates and a mixture of ether and diol products were usually afforded. Cutler and co-workers¹⁹ first

reported reduction of esters to ethers with catalytic hydrosilylation under manganese-based catalyst, eliminating the use of metal hydrides. The yield of the reaction on lactones were all below 70% and the manganese acetyl catalyst was not commercially available. Recently, Sakai *et al.*²⁰ greatly improved the hydrosilane-induced reactions using commercially available InBr_3 as the catalyst and the yield was as high as 99 % by GC analysis. Inspired by this improvement, we sought to apply this methodology to the synthesis of 1,4-dioxepane. Bayer-Villiger oxidation was performed on commercially available tetrahydro-4H-pyran-4-one to yield 1,4-dioxepan-5-one, which was further reduced to 1,4-dioxepane using indium-catalyzed hydrosilane-induced reduction. The yields of both steps were above 80% and the overall yield was about 70% over two steps. (Figure 3.2) No column chromatography purification was needed for either step and the reaction could be scaled up easily in gram scale.

Cationic ring-opening polymerization (cROP) was then conducted on the monomer and the results are summarized in Table 3.1. Cationic polymerization of trimethylene oxide or tetrahydrofuran using alkylating reagent, such as methyl trifluoromethanesulfonate (MeOTf), as initiator has been well studied. The cROP of oxepane, the seven-membered cyclic ether, has been reported by Saegusa *et al.*²¹ The polymerization was conducted in CH_2Cl_2 and initiated with trialkyloxonium salts such as Et_3OBF_4 , which was a stronger alkylating reagent than MeOTf . The polymerization rate was found to be extremely slow with full conversion attained after about one month at ambient temperature. Saegusa suggested that the slow propagation rates were largely due to the weak nucleophilic reactivity of oxepane as well as the increased stability of seven-membered oxonium ion intermediate. We observed similar results in the cROP

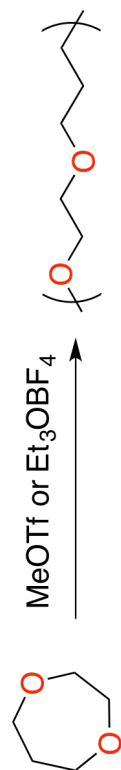


Table 3.1 Regio-selective cationic ring-opening polymerization of 1,4-dioxepane

Init. loading									
Entry	Initiator	(mol %)	Solvent	Temperature (°C)	Time (d)	Conversion % ^b	<i>M_n</i> (kDa)	PDI	Alternating% ^c
1	MeOTf	1	CH ₂ Cl ₂ ^a	22	3	0	—	—	—
2	MeOTf	1	neat	22	20	13	3.4	1.8	—
3	MeOTf	3	neat	22	10	>99	2.6	2.1	85
4	Et ₃ OBF ₄	1	CH ₂ Cl ₂ ^a	20	7	48	4.6	2.1	82
5	Et ₃ OBF ₄	1	CH ₂ Cl ₂ ^a	-20	60	51	7.2	1.6	91
6	Et ₃ OBF ₄	1	neat	22	7	21	4.1	1.9	83
7	Et ₃ OBF ₄	2	neat	22	7	79	7.7	1.8	82

^aSolvent was introduced from the stock solution of the initiators (0.5M for MeOTf and 1.0M for Et₃OBF₄). ^bConversion was determined by ¹H-NMR. ^cAlternating percentage was determined by ¹³C-NMR.

of 1,4-dioxepane as shown in Table 3.1. Polymerizations were generally slower when initiated with MeOTf compared to Et₃OBF₄. Higher initiator loading and more concentrated monomer helped to increase the polymerization rate but both initiators still needed more than one week to reach acceptable conversions.

There were two possible repeating unit configurations for the synthesized poly(1,4-dioxepane). One was the desired head-to-tail (alternating EO/TMO) and the other one was head-to-head (tail-to-tail) configuration which would give two EOs or two TMOs consecutively. Figure 3.3 demonstrated the mechanism to reach the two configurations. If the incoming monomer consistently attacked the trimethylene or the dimethylene side of the oxonium intermediate, the polymer would have the alternating configuration. On the opposite, if the incoming monomer alternately attacked the trimethylene and the dimethylene side of the intermediate, head-to-head (tail-to-tail) configuration would be formed. Quantitative ¹³C-NMR was utilized to determine the percentage of alternating configurations in the polymer. As seen from Figure 3.3, the alternating structure had three different carbons: two ether carbons next to ether oxygens and one middle methylene carbon from the trimethylene unit. On the other hand, the head-to-head configuration had five different carbons: four ether carbons and one middle methylene carbon. Figure 3.4 (a) showed the quantitative ¹³C-NMR spectrum of the poly(1,4-dioxepane) initiated from Et₃OBF₄ and more alternating percentage of the

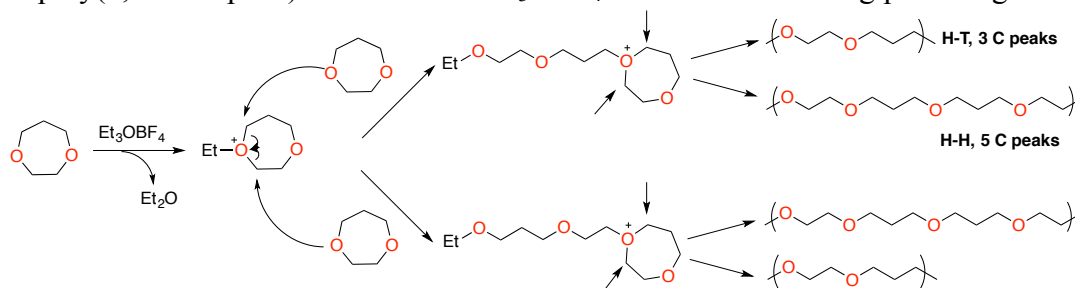


Figure 3.3 Mechanism of the cationic ring-opening polymerization of 1,4-dioxepane

polymers are summarized in Table 3.1. Three main singlets and five smaller peaks were observed for the pol(1,4-dioxepane) from the quantitative ^{13}C -NMR spectrum. As discussed above, the three main peaks corresponded to the alternating structures while the five small peaks matched the head-to-head configuration. To our surprise, the integrations of the middle methylene peaks near 30 ppm demonstrated that the polymer initiated from Et_3OBF_4 had high alternating configurations above 80 % and no significant effects were seen from different initiators. The alternating percentage can be greatly improved to over 90 % by decreasing the reaction temperature from ambient temperature to $-20\text{ }^\circ\text{C}$ with slower polymerization rate. Further decrease to $-40\text{ }^\circ\text{C}$ yielded no polymer after one week of the reaction. A 90 % alternating polymer corresponded to roughly 19:1 selectivity during the propagation. This regio-selective cROP was rarely seen in other cyclic ethers except for cyclic acetals.²² We hypothesized that the seven-membered ring was opened on the trimethylene side of the oxonium intermediate because of its better electrophilicity than the dimethylene side. Penczek and co-workers²³ also reported that 1,4-dioxane and other crown ethers, instead of polymers, were the main products when cROP were conducted on EO, further suggesting that the opening on the dimethylene side was unlikely.

To gain better understand whether the alternating sequence was necessary, we were interested in synthesizing random copolymers of EO and TMO to compare with the alternating copolymer. Keul et al.²⁴ first reported the cationic ring-opening copolymerization of EO and THF. They reported more than 90 % conversion after 6 hours and no 1,4-dioxane or other cyclic oligomers of EO were observed. No synthesis of random copolymers of EO and TMO has been reported but we expected the synthesis

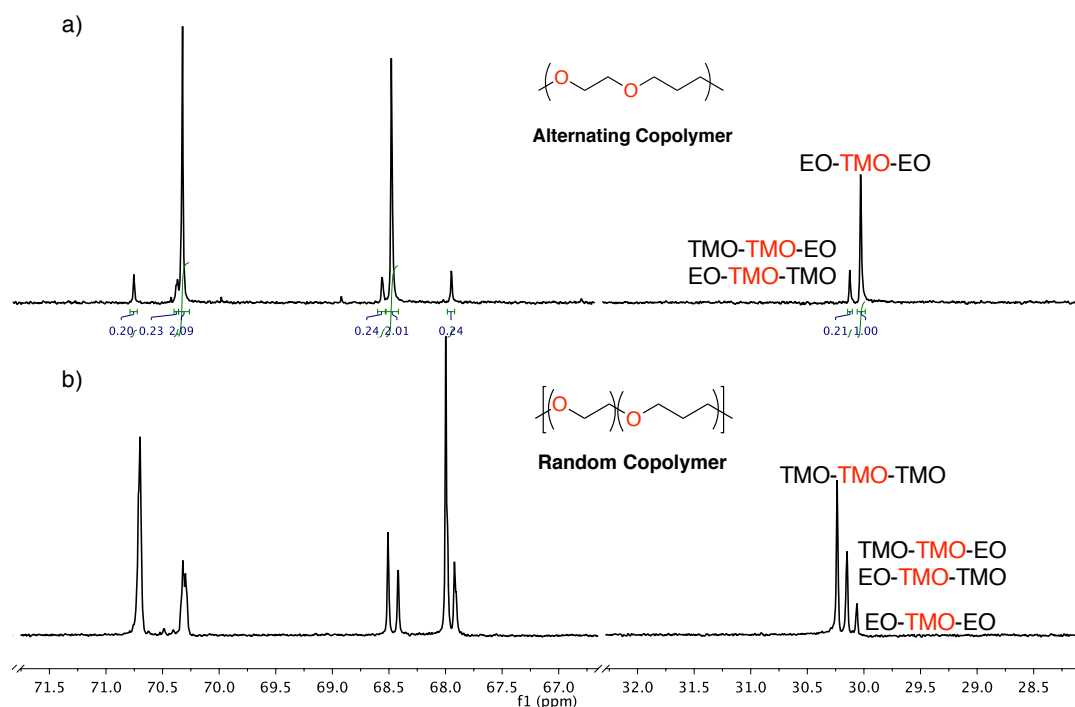


Figure 3.4 Quantitative ^{13}C -NMR of alternating (a) and random (b) copolymers of EO and TMO

would be similar to that of the EO/THF random copolymers. We synthesized a range of random copolymers by copolymerizing EO and TMO with $\text{BF}_3 \cdot \text{Et}_2\text{O}$ as the initiator. The synthesis conditions as well as thermal properties of the synthesized polymers are summarized in Table 3.2. All polymerization achieved more than 99% conversion for TMO after 16 hours at ambient temperature. However, unlike what was reported for the synthesis of EO/THF random copolymers, formation of large quantities of 1,4-dioxane was observed from the ^1H -NMR of the crude reaction mixture for EO/TMO polymerization, suggesting competing reactions between polymerization and cyclization of EO. The EO content in the EO/TMO polymer were significantly lower than that in the monomer but did increase with increasing EO mol% in the monomer. However, the molecular weight of the random copolymer decreased with increasing EO

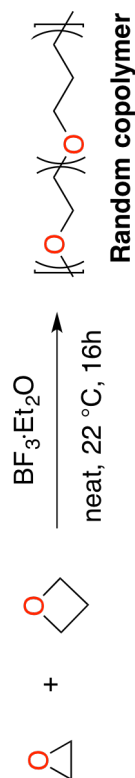


Table 3.2 Synthesis and thermal properties of EO-TMO copolymers

Entry	Polymer	[EO]:[TMO]:[Init.]	Conversion % ^a	EO mol% in polymer ^b	M_n (kDa) ^c	PDI ^c	T_g (°C) ^d	T_m (°C) ^d	$T_{g,I=0.08}$ (°C) ^e	$T_{m,I=0.08}$ (°C) ^e
1	PEO	–	–	100	5.0	1.1	–60	65	–43	41
2	PTMO	0:50:1	> 99	0	32.4	2.2	–70	19	–55	n.d.
3	P(EO ₄₀ –TMO ₆₀)	200:100:1	> 99 for TMO	40	10.1	1.7	–70	–14	–53	n.d.
4	P(EO ₆₁ –TMO ₃₉)	500:100:1	> 99 for TMO	61	5.5	1.9	–70	9	–49	n.d.
5	P(EO ₇₄ –TMO ₂₆)	1000:100:1	> 99 for TMO	74	3.0	2.1	–66	18	–58	n.d.
6	P(EO- <i>alt</i> -TMO)	–	–	50	7.7	1.8	–71	n.d.	–56	n.d.

^aConversion were determined by ¹H-NMR from the crude reaction mixture. ^bEO mol% in the polymer were determined by ¹H-NMR of the polymer. ^cNumber average molecular weight (M_n) and polydispersity index (PDI) were determined by THF gel permeation chromatography calibrated with polystyrene. ^dGlass transition temperature (T_g) and melting temperature (T_m) of the neat polymer were determined by differential scanning calorimetry of the second heat cycle. ^eThe electrolytes were prepared by mixing the polymer with lithium bis(trifluoromethane)sulfonimide (LiTFSI) and had a salt concentration $r([Li]:[O]) = 0.08$.

content from 10.1 kDa (40% EO) to 3.0 kDa (74% EO) because of the cyclization side-reaction of EO. In order to confirm the randomness of the synthesized polymer, quantitative ^{13}C -NMR were conducted on the sample entry 3 of Table 3.2 and the spectra were shown in Figure 3.4 (b). Three singlets were observed in the ^{13}C -NMR spectra between 30.0–30.5 ppm and they corresponded to the middle methylenes in TMO units. Unlike in the alternating copolymer, where only two TMO-centered sequences were possible (EO-TMO-EO and TMO-TMO-EO), there were three sequences available for the random copolymers (EO-TMO-EO, TMO-TMO-EO and TMO-TMO-TMO). The TMO-TMO-TMO sequence had the highest population among the three sequences even if the polymer had higher EO mol%. We hypothesized that this was due to the higher electrophilicity of TMO. Glass transition temperatures for both the random and alternating copolymers were lower than PEO at around $-70\text{ }^{\circ}\text{C}$ and no significant differences were observed between random and alternating copolymers, or among copolymers with different EO contents. The melting points of random copolymers increased with increasing EO contents because the polymer became more rigid with higher EO contents. Surprisingly, the alternating copolymer had no melting point possibly due to the regio-defects in the polymer. We further doped both the random and alternating copolymers with lithium bis(trifluoromethane)sulfonimide (LiTFSI) to prepare the electrolytes for ionic conductivity measurements. The thermal properties of the electrolytes were significantly different compared to those of the neat polymers. When the salt concentration r ($[\text{Li}]:[\text{O}] = 0.08$), the melting points of all polymers were no longer existed except for PEO. As expected, T_g s of all electrolytes

were higher than those of the neat polymers because of the rigidity from physically cross-linking the polymer chains with lithium ions.

The ionic conductivities of both the random and alternating copolymers were based on ac impedance spectroscopy and were measured as a function of temperature from 27 to 110 °C. The results were shown in Figure 3.5 with a fixed salt concentration $r = 0.08$, which was where PEO ionic conductivity reaches maximum.²⁵ The conductivities of both random and alternating EO/TMO copolymers had higher conductivities than that of PEO at room temperature. At high temperature (90 °C), the conductivity of PEO surpassed all the copolymers, reaching 2×10^{-3} S/cm. In order to elucidate the effects of salt concentrations, we further measured ionic conductivities at different salt concentrations and both the room temperature (27 °C) and high temperature (90 °C) results are summarized in Figure 3.6. Similar to what was overserved for $r = 0.08$, the conductivities of both random and alternating copolymers

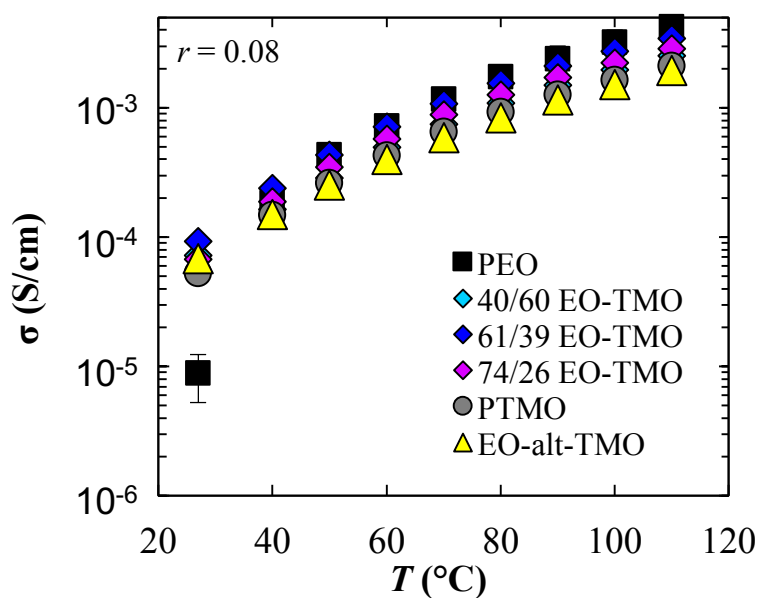


Figure 3.5 Ionic conductivity of PEO, PTMO and EO-TMO copolymers with variable temperatures at $r = 0.08$.

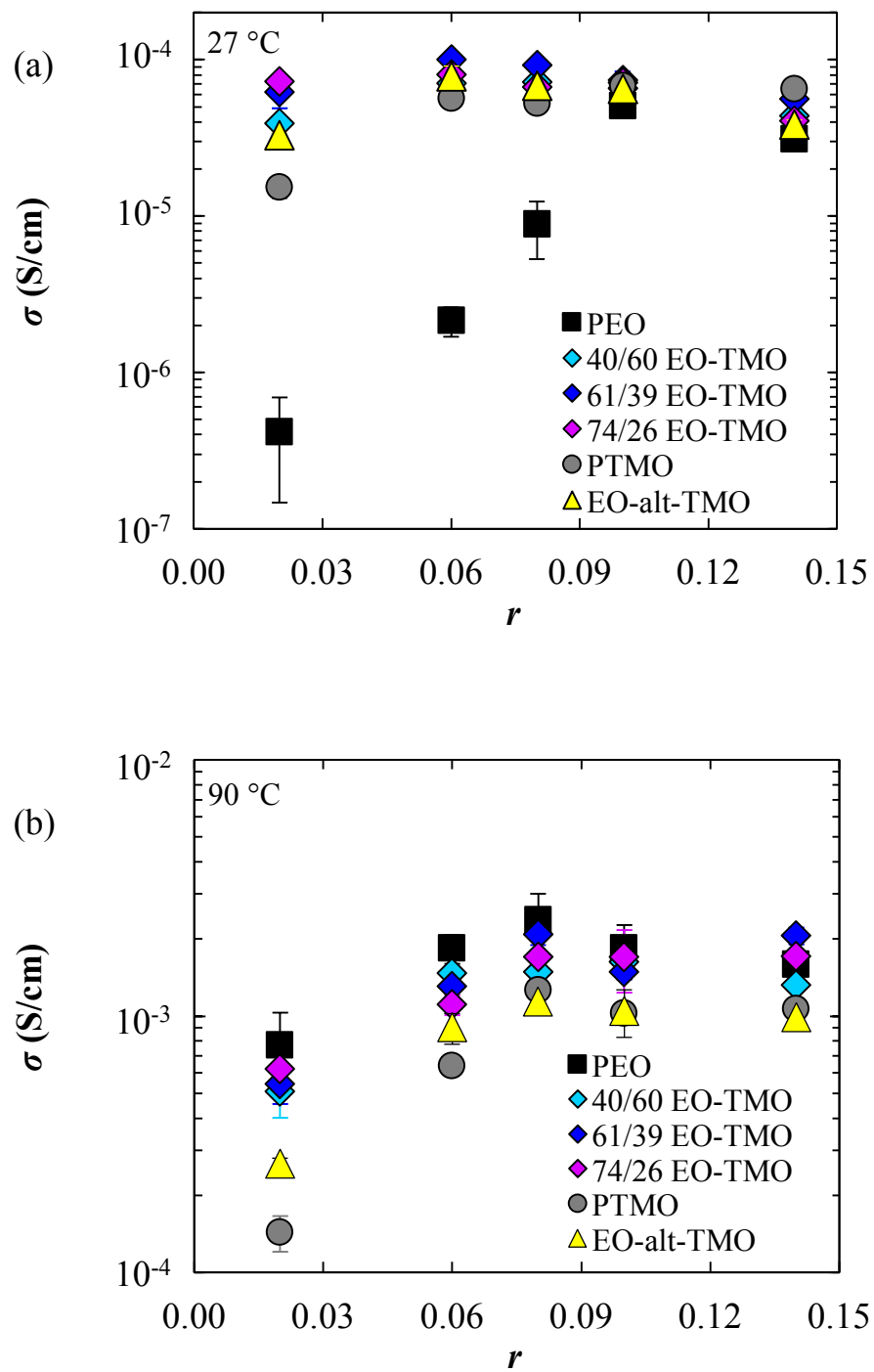


Figure 3.6 Ionic conductivity of PEO, PTMO and EO-TMO copolymers with different salt concentrations at 27 °C (a) and 90 °C (b).

were significantly higher than that of PEO at low Li salt concentrations at room temperature. But when the Li salt concentration was increased from $r = 0.08$ to $r = 0.10$, the conductivity of PEO was improved by almost an order of magnitude to reach the maximum at 5.1×10^{-3} S/cm and then plateaued out when r was further increased. We hypothesized that this improvement was achieved by breaking the crystallinity of PEO. Unlike PEO, no significant improvement on conductivities were observed for EO/TMO copolymers across the Li salt concentrations from $r = 0.02$ to $r = 0.14$. We believe this difference was caused by weaker crystallinity of EO/TMO copolymers. All the copolymers had lower melting points than that of PEO and all the EO/TMO copolymers became completely amorphous at $r = 0.08$ (see Table 3.2). The conductivities of most of the copolymers reached the maximum with $r = 0.06$, with the highest (1.0×10^{-4} S/cm) achieved by the random copolymer of EO/TMO with 61 mol% EO content (Table 3.2, entry 4). This was one of the highest conductivities obtained for polyether based polymer electrolytes. Niitani *et al.*²⁶ reported a PEO-grafted poly(methyl methacrylate) (PMMA) block copolymer with polystyrene. They obtained ionic conductivity of 2×10^{-4} S/cm at room temperature, which was the highest room temperature conductivity reported for PEO based copolymers as far as we know. However, their PEO polymers were grafted on the side chains and the molecular weight was around only 1 kDa, both of which helped to conduct lithium ions.²⁷ Examples of polymer electrolytes based on polyoxetane were far more less than those based on PEO, likely due to the less accessibility to oxetane monomers. Tsutsumi *et al.*²⁸⁻²⁹ recently reported a series of poly(oxetane) based polymer electrolytes. Lithium conducting functional groups were attached to oxetane monomers, such as phosphate ester group²⁸ and cyanoethoxymethyl

group²⁹. The monomers were then either crosslinked with oxetane-based cross-linker, or homopolymerized and mixed with PVDF-HFP (poly(vinylidene fluoride-*co*-hexafluoropropylene)) binder. The conductivities of these oxetane-based polymer electrolytes were in the range of 10^{-5} to 10^{-4} S/cm at room temperature. The author claimed that the enhanced conductivities of these materials were because of improved lithium ion solvation by side groups and the role of poly(oxetane) backbones in conducting lithium ions were not discussed. It's worth noting that in the examples mentioned above, all the lithium solvation sites were on the side chains instead of the backbones. Our EO/TMO copolymers provided a rare example to have both high room temperature conductivities and solvation sites on the backbones.

The high temperature (90 °C) conductivities of EO/TMO copolymers showed similar salt concentration trend as PEO. The conductivities enhanced with increasing salt concentrations and plateaued after $r = 0.08$. The highest conductivity at 90 °C were again achieved by the random copolymer of EO/TMO with 61 mol% EO content at 1.7×10^{-4} S/cm with $r = 0.08$, slightly lower than that of PEO (2.1×10^{-4} S/cm). Contrary to the prediction by Miller *et al.*,¹⁴ the conductivity of the alternating EO/TMO copolymer was lower than that of PEO at both room temperature and high temperature (90 °C), and even lower than those of the random EO/TMO copolymer. We hypothesize that the well-organized alternating structures may contribute to strong chelation to lithium ions, preventing them from moving in the polymers, while the chelation may not be stable because of the irregular sequences in the random copolymers. Theoretical simulations are currently underway to prove this hypothesis and the results will be applied to improve the prediction model.

3.4 Conclusions

Inspired by theoretical predictions, we successfully synthesized the alternating copolymer of EO and TMO by cationic ring-opening polymerization of 1,4-dioxepane. The monomer was synthesized by indium-catalyzed ester-to-ether reduction. The alternating structure of the synthesized polymer was confirmed by ^{13}C -NMR. Ionic conductivities of the alternating copolymer were compared with that of PEO and random copolymers of EO and TMO. Both the random and alternating copolymers of EO and TMO had higher room-temperature conductivities than that of PEO but PEO surpassed both copolymers in conductivities at high temperature (90 °C). The highest ionic conductivity value of 1×10^{-4} S/cm at room temperature was observed for the random copolymer of EO and TMO with 61 mol% EO content. Theoretical simulations to rationalize these results are currently under way. We believe that these random and alternating copolymers are an interesting class of materials in both synthesis and lithium ion conductive properties. The three-way collaboration of simulation-synthesis-characterization will provide useful insights for the future design of polymer electrolytes.

3.5 Experimental

3.5.1 General

All air and water sensitive reactions were carried out under dry nitrogen conditions using standard Schlenk techniques or MBraun UniLab dry glove box. ^1H NMR spectra were collected on a Bruker AV 500MHz spectrometer equipped with liquid nitrogen cooled cryoprobe and referenced with residue non-deuterated solvent shifts ($\text{CHCl}_3 = 7.26$ ppm). ^{13}C NMR spectra were collected on a Bruker AV 500 MHz (^{13}C , 125 MHz) spectrometer liquid nitrogen cooled cryoprobe and referenced to chloroform (δ 77.16 ppm). High resolution mass spectrometry (DART-HRMS) analyses were performed on a Thermo Scientific Exactive Orbitrap MS system equipped with an Ion Sense Direct Analysis in Real Time (DART) ion source.

Gel permeation chromatography (GPC) analyses were carried out using an Agilent PL-GPC 50 integrated system, equipped with UV and refractive index detectors, and 2 PL gel Mini-MIX C columns (5 micron, 4.6 mm ID). The GPC columns were eluted with tetrahydrofuran at 30 °C at 0.3 mL/min and were calibrated with monodisperse polystyrene standards. Differential scanning calorimetry (DSC) analyses of polymer samples were performed on a TA Instruments Q1000 instrument equipped with liquid nitrogen cooling system. Polymer samples were made in aluminum pans and heated under nitrogen from -100 °C to 180 °C at a rate of 10 °C per minute and then cooled to -100 °C at a rate of 10 °C per minute, followed heating to 180 °C at a rate of 10 °C per minute. The glass transition temperature (T_g) and the melting temperature (T_m) were recorded from the second heating run.

3.5.2 Materials

Tetrahydro-4H-pyran-4-one and methyl trifluoromethanesulfonate were purchased from Matrix Scientific. Indium bromide and triethyloxonium tetrafluoroborate were purchased from Alfa Aesar. Diphenylmethylsilane was purchased from Gelest. Meta-chloroperoxybenzoic acid (77 %) and boron trifluoride diethyl etherate were purchased from Sigma-Aldrich. All the above chemicals were used as received. Ethylene oxide was purchased from Sigma-Aldrich and dried over *n*-BuLi before use. Bis(trifluoromethane)sulfonimide lithium salt (LiTFSI) was purchased from Sigma-Aldrich and dried under vacuum at 90 °C for 24 h and transferred into the glove box. Oxetane was purchased from Alfa Aesar and dried over CaH₂ for 2 days and distilled before use. Dichloromethane was purchased from Fisher Scientific and dried using a Phoenix solvent drying system and degassed by freeze-pump-thaw method for three cycles before use. NMR solvent (CDCl₃) was purchased from Cambridge Isotope Laboratories (CIL) and used as received. Polyethylene oxide (PEO) with an M_n of 5.0 kDa was purchased from Polymer Source and dried under vacuum before use. Polytrimethylene oxide (PTMO) was synthesized as reported³⁰ by cationic ring-opening polymerization of oxetane with BF₃·OEt₂ as the initiator.

3.5.3 Synthesis

3.5.3.1 Synthesis of 1,4-dioxepan-5-one

To a solution of meta-chloroperoxybenzoic acid (mCPBA, 77 wt%, 38.0 g, 169.3 mmol) in 300 mL dichloromethane was added anhydrous Na₂SO₄ to remove the water. The mixture was filtered to obtain dry solution of mCPBA. To this solution was added tetrahydro-4H-pyran-4-one (15.0 g, 150 mmol) at 0 °C and the resulting mixture was refluxed at 40 °C for 20 h. The mixture was cooled to 0 °C and the precipitate was filtered off. The filtrate was washed with aqueous solution of NaHSO₃ followed by NaHCO₃ powder until no bubble was formed anymore. The organic layer was separated and washed with saturated NaHCO₃ aqueous solution. The organic layer was dried over anhydrous Na₂SO₄. Solvent was removed and the residue was distilled under reduced pressure (0.2 torr, b.p. 64 °C) to yield a colorless viscous oil (14.3 g, 82 %) which solidified gradually at room temperature.

¹H NMR (500 MHz, CDCl₃) δ 4.31 – 4.27 (m, 2H), 3.90 – 3.86 (m, 2H), 3.84 – 3.79 (m, 2H), 2.91 – 2.86 (m, 2H).

¹³C NMR (125 MHz, CDCl₃) δ 174.07, 70.73, 70.30, 64.72, 39.28.

HRMS (DART) *m/z* calculated for C₅H₉O₃⁺ [M + H]⁺ 117.05462, found 117.05461.

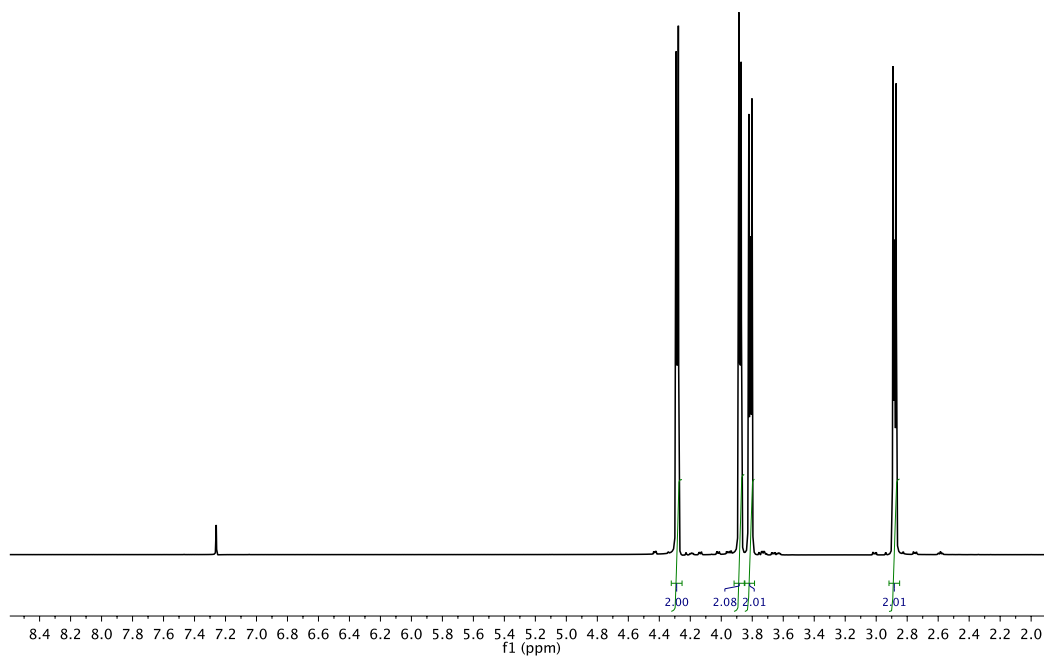


Figure 3.7 ^1H -NMR spectrum of 1,4-dioxepan-5-one. Signal at 7.26 ppm is the residue CHCl_3 .

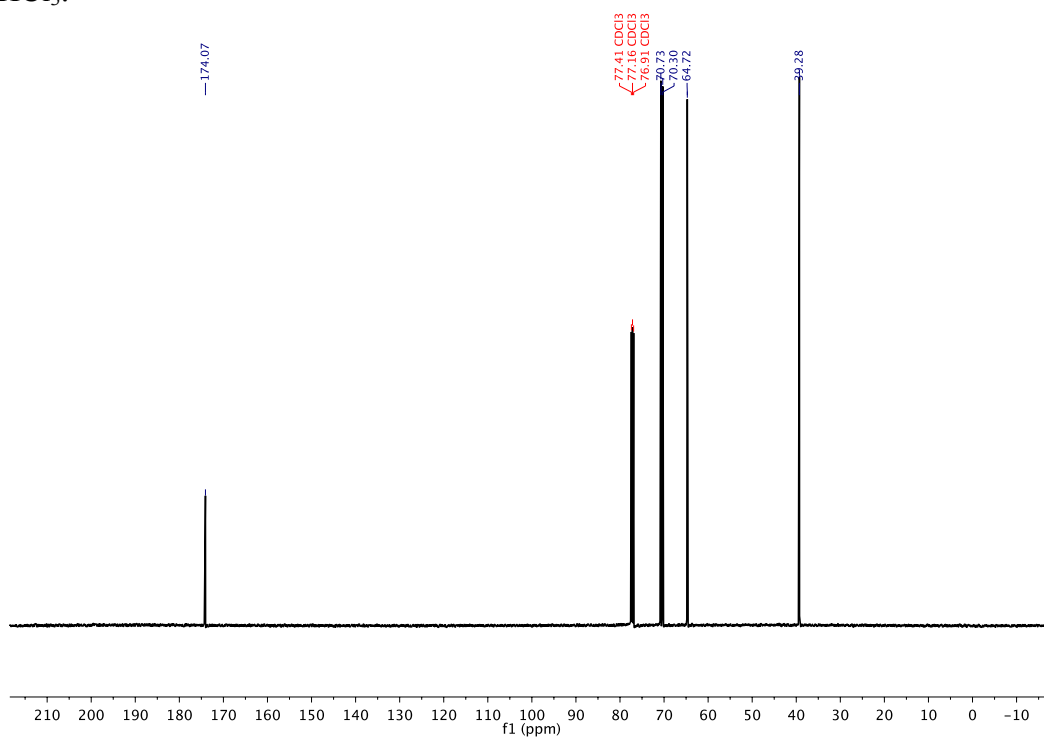


Figure 3.8 ^{13}C -NMR spectrum of 1,4-dioxepan-5-one. Signal at 77.16 ppm is the residue CHCl_3 .

3.5.3.2 Synthesis of 1,4-dioxepane

To a suspension of InBr_3 (1.06 g, 2.98 mmol) in dichloromethane (30 mL) was added 1,4-dioxepan-5-one (6.93 g, 59.67 mmol). The mixture was stirred for 5 min. To this mixture was added dropwise diphenylmethyilsilane (24.8 mL, 125 mmol). The resulting mixture was stirred at room temperature for 18 h. The reaction mixture was quenched with water and separated. The aqueous phase was washed with dichloromethane twice and the combined organic phase was dried over anhydrous Na_2SO_4 . The resulting solution was vacuum transferred under reduced pressure (0.2 torr, static vacuum) at 70 °C to collect the volatiles and separate 1,4-dioxepane from the non-volatile disiloxane by-product. The collected volatiles were further distilled to remove the dichloromethane and yield the product as a colorless liquid (4.79 g, 79%).

^1H NMR (500 MHz, CDCl_3) δ 3.82 (t, J = 6.0 Hz, 4H), 3.72 (s, 4H), 1.99 (p, J = 6.0 Hz, 4H).

^{13}C NMR (125 MHz, CDCl_3) δ 72.36, 68.89, 70.30, 32.46.

HRMS (DART) m/z calculated for $\text{C}_5\text{H}_{11}\text{O}_2^+$ [$\text{M} + \text{H}$] $^+$ 103.07536, found 103.07549.

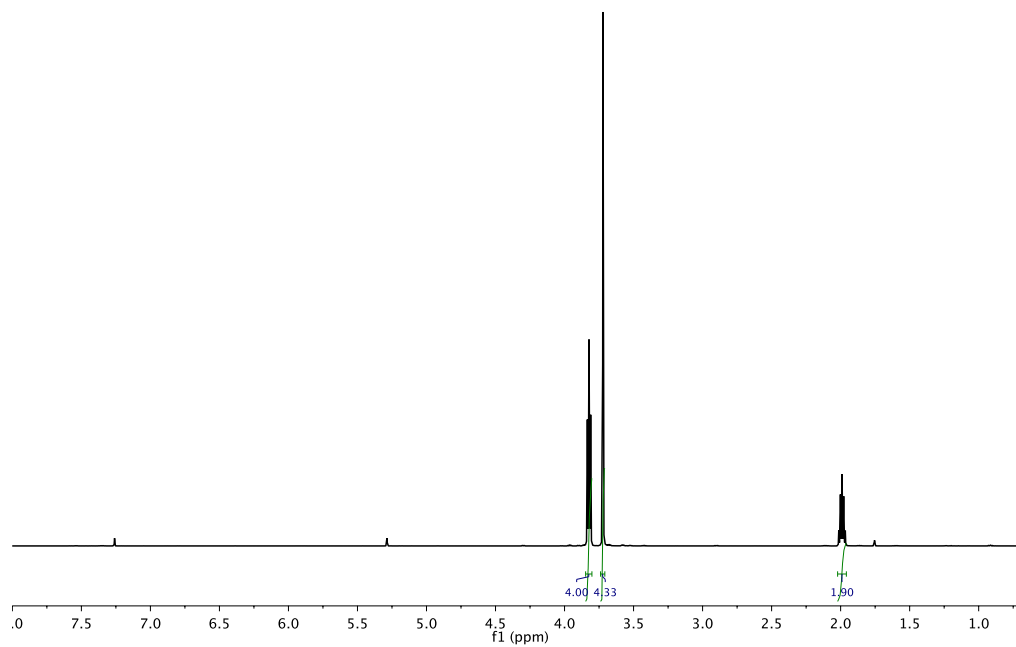


Figure 3.9 ^1H -NMR spectrum of 1,4-dioxepane. Signal at 7.26 ppm is the residue CHCl_3 .

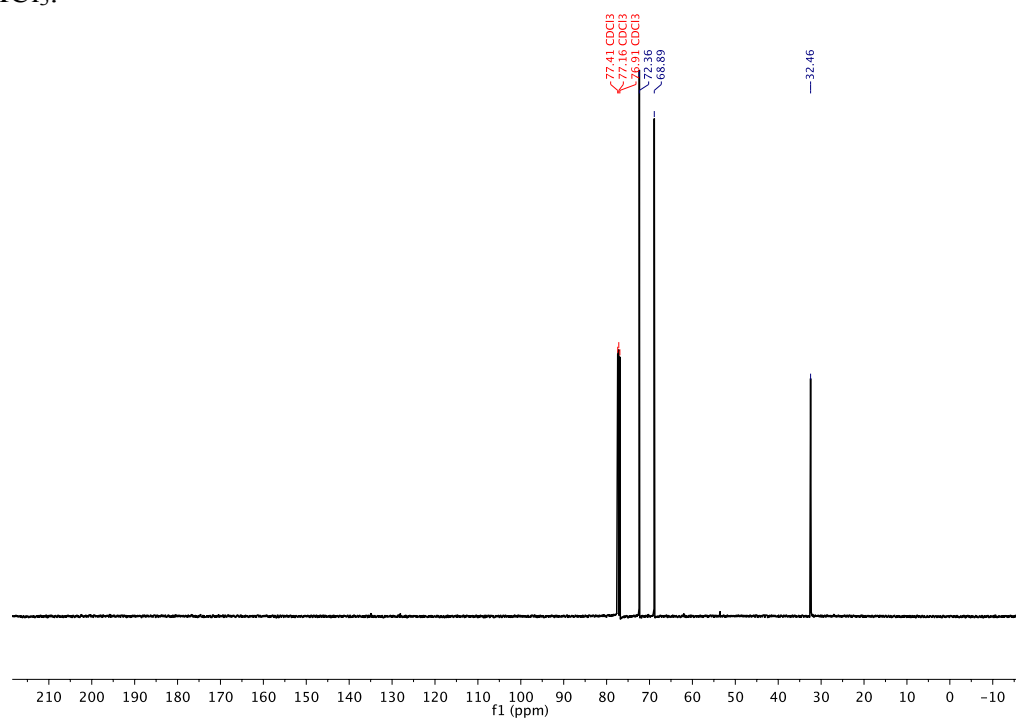


Figure 3.10 ^{13}C -NMR spectrum of 1,4-dioxepane. Signal at 77.16 ppm is the residue CHCl_3 .

3.5.3.3 Polymerization of 1,4-dioxepane

In a dry glove box, to a vial with triethyloxonium tetrafluoroborate (37.2 mg, 0.196 mmol) was added 1,4-dioxepane (1.00 g, 9.79 mmol). The vial was sealed and the mixture was stirred at room temperature for one week. The mixture turned viscous after ~ 6 h and a 79 % conversion was recorded from ^1H -NMR after one week. The reaction mixture was quenched with water and extracted with dichloromethane. The organic layer was dried over anhydrous Na_2SO_4 . The solvent was removed and the residue was dried under vacuum to yield the polymer as a viscous material (698 mg, 70 %).

^1H NMR (500 MHz, CDCl_3) δ 3.63 – 3.44 (m, 8H), 1.91 – 1.80 (m, 2H).

^{13}C NMR (125 MHz, CDCl_3) δ 70.69, 70.31, 70.27, 68.52, 68.43, 67.91, 30.11, 30.01.

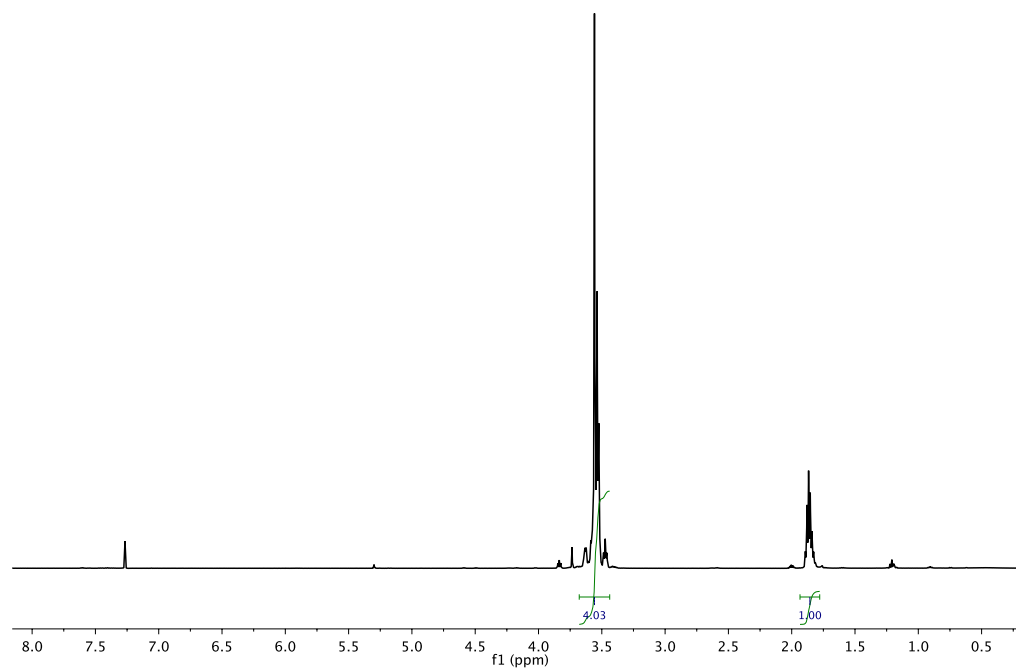


Figure 3.11 ^1H -NMR spectrum of poly(1,4-dioxepane). Signal at 7.26 ppm is the residue CHCl_3 .

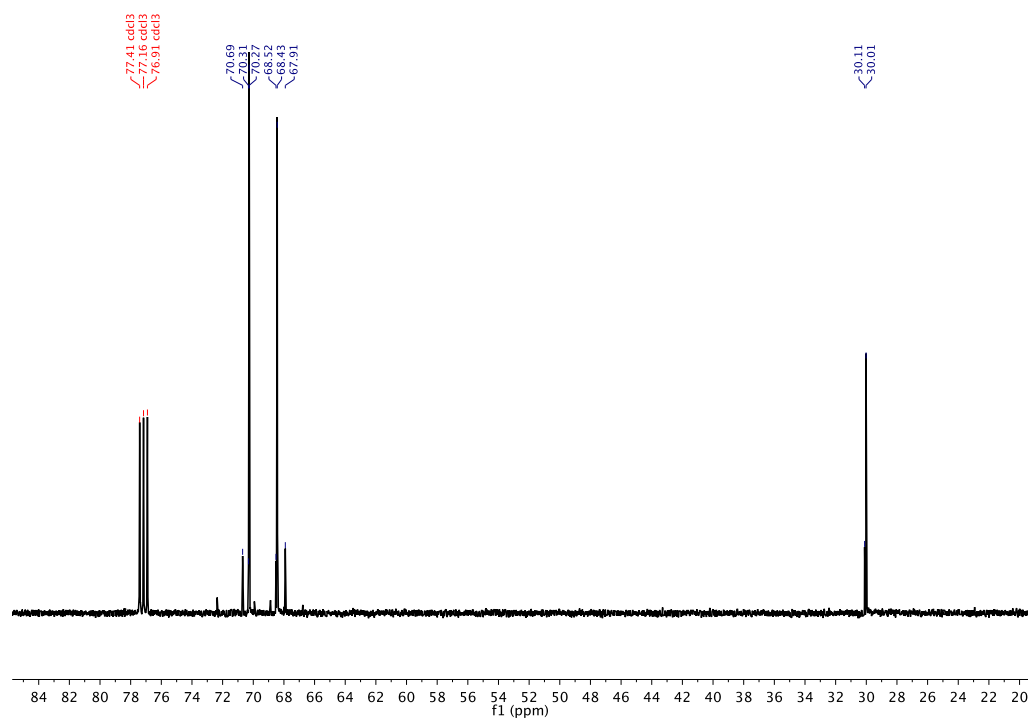


Figure 3.12 ^{13}C -NMR spectrum of poly(1,4-dioxepane). Signal at 77.16 ppm is the residue CHCl_3 .

3.5.3.4 Copolymerization of ethylene oxide (EO) and trimethylene oxide (TMO)

In a dry glove box, a Fischer-Porter bottle was charged with dry trimethylene oxide (TMO) (0.85 mL, 13 mmol). The vessel was sealed with the reactor head and removed from the box. Dry ethylene oxide (1.15 g, 26.1 mmol) was then condensed into the Fischer-Porter bottle at $-78\text{ }^{\circ}\text{C}$. The mixture was warmed to $0\text{ }^{\circ}\text{C}$ and a stock solution of boron trifluoride etherate (0.5 M in dichloromethane, 0.26 mL, 0.13 mmol) was added under nitrogen. The mixture was immediately frozen with liquid nitrogen and the vessel was evacuated to 0.2 torr. The vessel was sealed, warmed to room temperature and stirred under static vacuum for 15 h. The reaction mixture was quenched by water and extracted with dichloromethane. The organic layer was further washed with saturated aqueous solution of NaHCO_3 . The washed organic layer was dried over anhydrous Na_2SO_4 . The solvent was removed and the residue was dried under vacuum to yield the polymer as a viscous material (1.36 g, 71 %).

^1H NMR (500 MHz, CDCl_3) δ 3.67 – 3.40 (m), 1.89 – 1.75 (m).

^{13}C NMR (125 MHz, CDCl_3) δ 70.70, 70.32, 70.30, 68.51, 68.42, 68.00, 67.92, 67.90, 30.24, 30.15, 30.06.

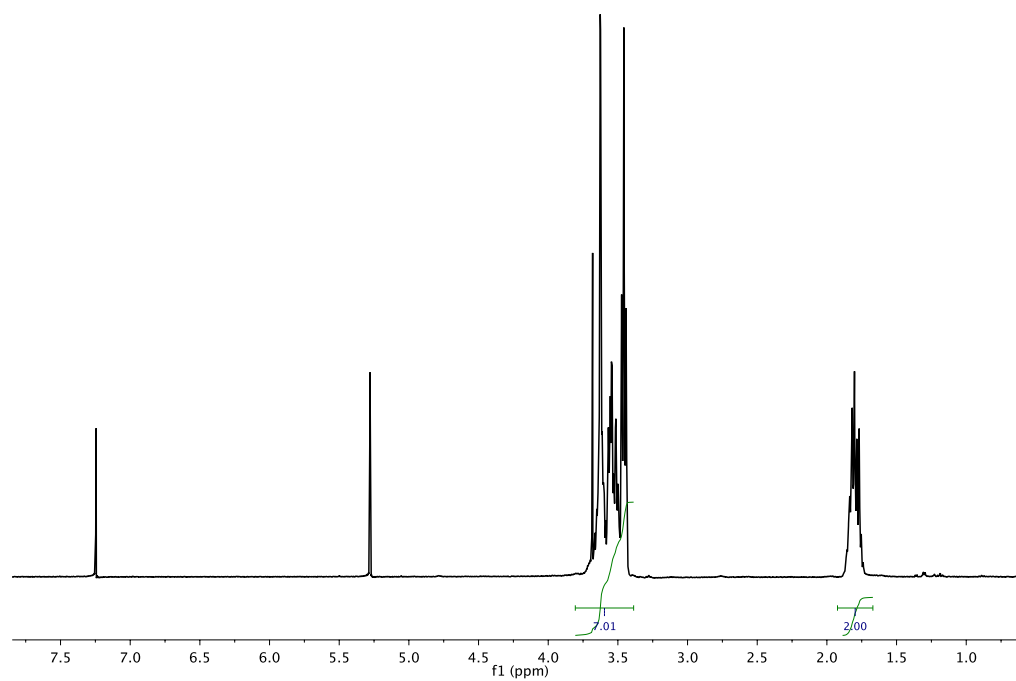


Figure 3.13 ^1H -NMR spectrum of poly(EO-*co*-TMO). Signal at 7.26 ppm is the residue CHCl_3 .

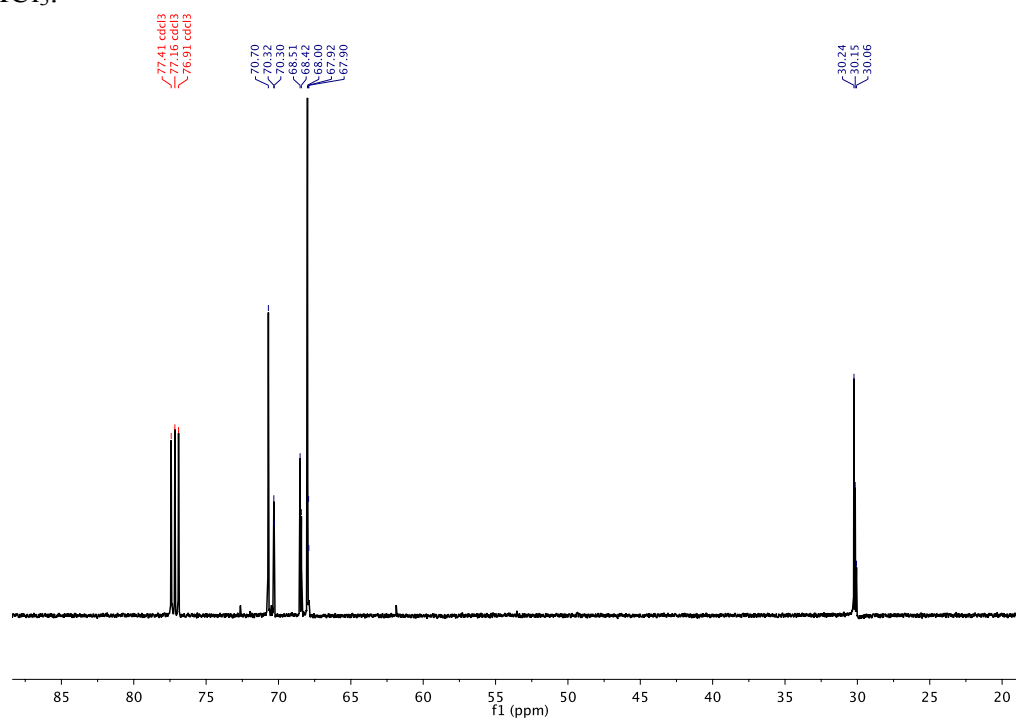


Figure 3.14 ^{13}C -NMR spectrum of poly(EO-*co*-TMO). Signal at 77.16 ppm is the residue CHCl_3 .

3.5.4 Thermal properties of the polymers and the electrolytes

The synthesized polymers were dried under vacuum at 90 °C and transferred into a nitrogen dry glove box. The polymer and lithium bis(trifluoromethane)sulfonimide (LiTFSI) were dissolved in anhydrous N,N-dimethylformamide (DMF). The resulting mixture was stirred at 90 °C for 3 h to yield a homogeneous solution. The solvent was evaporated and the residue was dried under vacuum at 90 °C for 8 h to remove trace leftover solvent. Glass transition temperatures were determined from the second heating run of differential scanning calorimetry (DSC).

Table 3.3 Glass transition temperatures of EO-TMO polymer and electrolytes

Polymer	Glass transition temperature, T_g (°C) ^a					
	$r = 0^b$	$r = 0.02^b$	$r = 0.06^b$	$r = 0.08^b$	$r = 0.1^b$	$r = 0.14^b$
PEO	−60.0	−55.5	−47.2	−42.5	−38.5	−30.9
PTMO	−70.2	−68.6	−62.6	−57.7	−57.5	−51.8
P(EO ₄₀ –TMO ₆₀)	−69.2	−68.6	−62.6	−55.2	−52.7	−46.3
P(EO ₆₁ –TMO ₃₉)	−70.4	−64.0	−55.7	−52.8	−48.9	−43.8
P(EO ₇₄ –TMO ₂₆)	−65.9	−62.1	−53.1	−48.8	−46.4	−39.2
P(EO- <i>alt</i> -TMO)	−71.0	<i>n.d.</i> ^c	−60.4	−56.2	<i>n.d.</i> ^c	−45.4

^aThe glass transition temperature was determined from differential scanning calorimetry.

^b r was the Li salt concentration ([Li]:[O]). ^cNot determined due to limited amount of samples.

3.5.5 Ionic conductivities

The conductivity measurements were conducted in a similar way as reported in our previous paper.³¹ The sample was prepared in the same way as described in section 3.5.4. The sample was then transferred into a 254 μm thick silicon spacer and sandwiched between two 200 μm stainless steel electrodes. The thickness of the sample was taken the same as the thickness of the silicon spacer. The sample cell was secured with aluminum tabs to provide electrical contacts, vacuum sealed in a laminated aluminum pouch material (Showa-Denko), and removed from the glove box for electrochemical characterization.

Conductivity measurements were based on ac impedance spectroscopy acquired with a Biologic VMP3 potentiostat. The complex impedance measurements were performed for a frequency range of 1 Hz – 1 MHz at an amplitude of 80 mV. The low-frequency minimum on the Nyquist impedance plot was treated as the electrolyte resistance (R_b) and the ionic conductivity (σ) can be calculated according to Equation 3.1:

$$\sigma = \frac{l}{aR_b} \quad \text{Equation 3.1}$$

whereas a is the electrolyte area, which can be calculated from the inner diameter of the silicon spacer; l is the thickness of the electrolyte. After the measurement, the sample cells were disassembled to inspect that no defects were exhibited during the measurement, such as bubbles or voids. The defected cells, which were less than 5 % of all the samples prepared, were discarded from the data set. The reported conductivity was taken as the average of the results from three different samples and the error bars were deduced from the standard deviation of these measurements.

Table 3.4 DC ionic Conductivities of Unplasticized PCOD-PEO Cross-Linked SPEs^a

Entry	Polymer	DC Ionic Conductivity (S/cm)								
		27 °C	40 °C	50 °C	60 °C	70 °C	80 °C	90 °C	100 °C	110 °C
1	PEO	8.9×10^{-6}	1.8×10^{-4}	4.3×10^{-4}	7.2×10^{-4}	1.2×10^{-3}	1.7×10^{-3}	2.4×10^{-3}	3.2×10^{-3}	4.2×10^{-3}
2	PTMO	5.3×10^{-5}	1.5×10^{-4}	2.6×10^{-4}	4.2×10^{-4}	6.5×10^{-4}	9.2×10^{-4}	1.3×10^{-3}	1.6×10^{-3}	2.1×10^{-3}
3	P(EO ₄₀ -TMO ₆₀)	7.2×10^{-5}	1.6×10^{-4}	2.9×10^{-4}	4.9×10^{-4}	7.4×10^{-4}	1.1×10^{-3}	1.5×10^{-3}	2.0×10^{-3}	2.5×10^{-3}
4	P(EO ₆₁ -TMO ₃₉)	9.3×10^{-5}	2.4×10^{-4}	4.3×10^{-4}	7.1×10^{-4}	1.1×10^{-3}	1.5×10^{-3}	2.1×10^{-3}	2.7×10^{-3}	3.4×10^{-3}
5	P(EO ₇₄ -TMO ₂₆)	6.7×10^{-5}	1.9×10^{-4}	3.5×10^{-4}	5.8×10^{-4}	8.8×10^{-4}	1.3×10^{-3}	1.7×10^{-3}	2.2×10^{-3}	2.9×10^{-3}
6	P(EO- <i>alt</i> -TMO)	6.8×10^{-5}	1.5×10^{-4}	2.5×10^{-4}	4.0×10^{-4}	5.9×10^{-4}	8.3×10^{-4}	1.1×10^{-3}	1.5×10^{-3}	1.9×10^{-3}

^aConductivities were determined with $r = 0.08$.

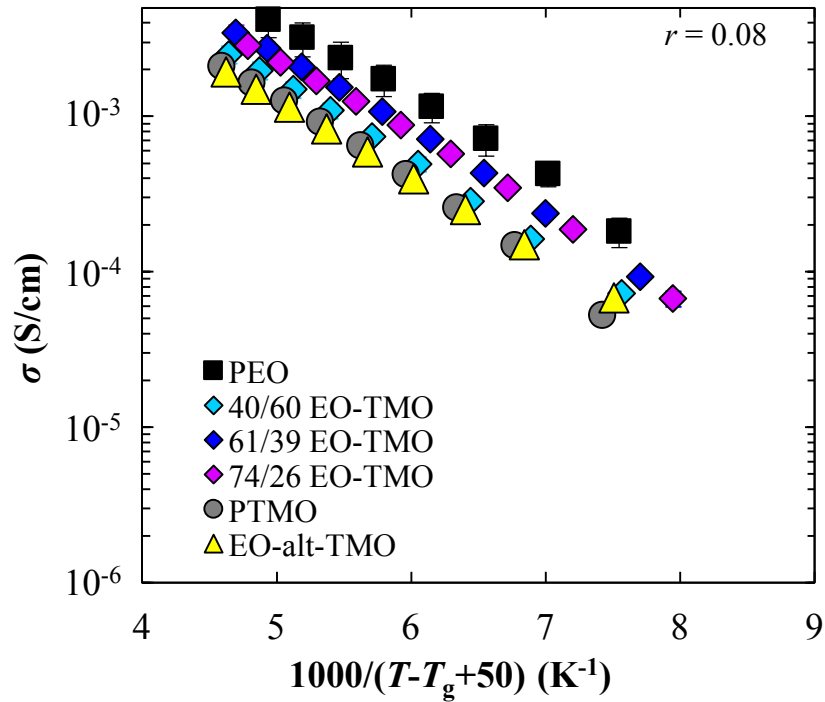


Figure 3.15 Ionic conductivity of EO-TMO polymers as a function of $1000/(T-T_g+50)$ with $r = 0.08$.

Variable temperature ionic conductivities are summarized in Table 3.4. The ionic conductivities were known to get affected by the glass transition temperature (T_g) with low T_g generally favored high conductivity. One method to remove the effects from T_g was to deduce the reduced conductivity (σ_r). The ionic conductivity was plotted as a function of $1000/(T-T_g+50)$, where T was the temperature at which the conductivity was measured and T_g was obtained from Table 3.3 for each sample. The plot was shown in Figure 3.15 for $r = 0.08$.

The data was then linear fitted and the reduced conductivity (σ_r) was determined as the conductivity at $T = T_g + 75\text{K}$. The σ_r s for all Li salt concentrations are summarized in Figure 3.16. The σ_r of all the EO-TMO copolymers were significantly lower than that of PEO at all Li concentrations.

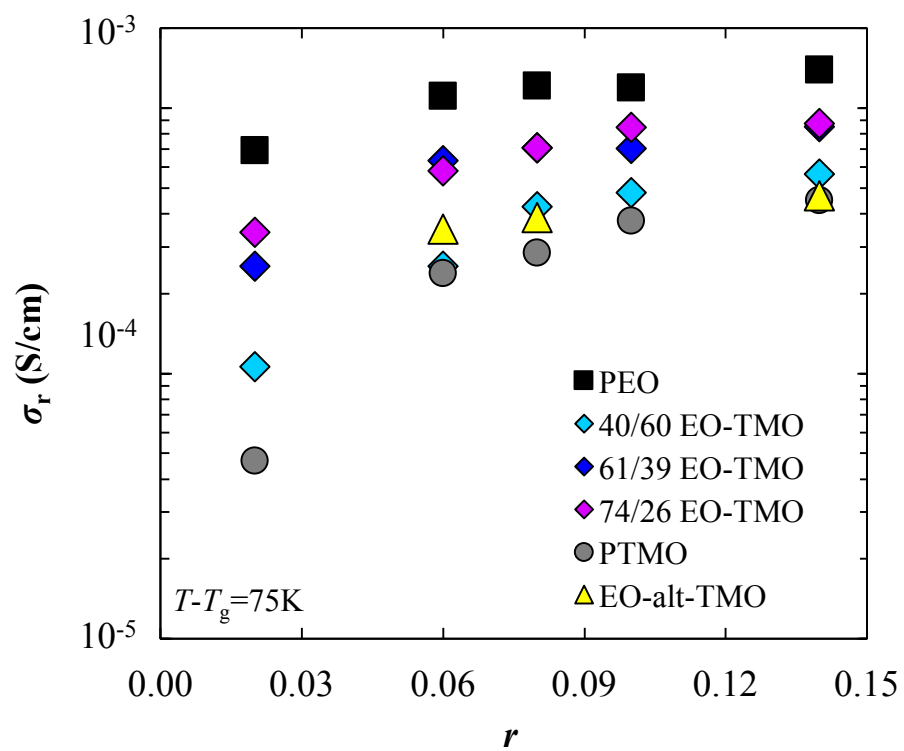


Figure 3.16 Reduced ionic conductivity of EO-TMO polymers as a function of Li salt concentrations.

REFERENCES

- (1) Fenton, D. E.; Parker, J. M.; Wright, P. V. *Polymer* **1973**, *14*, 589.
- (2) Chintapalli, S.; Frech, R. *Macromolecules* **1996**, *29*, 3499–3506.
- (3) Frech, R.; Chintapalli, S. *Solid State Ionics* **1996**, *85*, 61–66.
- (4) Bandara, L. R. A. K.; Dissanayake, M. A. K. L.; Mellander, B. E. *Electrochim. Acta* **1998**, *43*, 1447–1451.
- (5) Fan, L.; Dang, Z.; Nan, C.-W.; Li, M. *Electrochim. Acta* **2002**, *48*, 205–209.
- (6) Alarco, P. J.; Abu-Lebdeh, Y.; Abouimrane, A.; Armand, M. *Nat. Mater.* **2004**, *3*, 476–481.
- (7) Fan, L.-Z.; Maier, J. *Electrochem. Commun.* **2006**, *8*, 1753–1756.
- (8) Lee, Y. M.; Ko, D.-H.; Lee, J. Y.; Park, J.-K. *Electrochim. Acta* **2006**, *52*, 1582–1587.
- (9) Shin, J.; Henderson, W. A.; Passerini, S. *Electrochem. Commun.* **2003**, *5*, 1016–1020.
- (10) Zhu, C.; Cheng, H.; Yang, Y. *J. Electrochem. Soc.* **2008**, *155*, A569–A575.
- (11) Scrosati, B.; Croce, F.; Appetecchi, G. B.; Persi, L. *Nature* **1998**, *394*, 456–458.
- (12) Singh, M.; Odusanya, O.; Wilmes, G. M.; Eitouni, H. B.; Gomez, E. D.; Patel, A. J.; Chen, V. L.; Park, M. J.; Fragouli, P.; Iatrou, H.; Hadjichristidis, N.; Cookson, D.; Balsara, N. P. *Macromolecules* **2007**, *40*, 4578–4585.
- (13) Przyłuski, J.; Wieczorek, W. *Solid State Ionics* **1992**, *53-56*, 1071–1076.
- (14) Webb, M. A.; Savoie, B. M.; Wang, Z.-G.; Miller Iii, T. F. *Macromolecules* **2015**, *48*, 7346–7358.
- (15) Nerdel, F.; Mamluk, M.; Weyerstahl, P. *Liebigs Ann.* **1970**, *736*, 75–87.

- (16) Bottini, A. T.; Corson, F. P.; Böttner, E. F. *J. Org. Chem.* **1965**, *30*, 2988–2994.
- (17) Pettit, G.; Ghatak, U.; Green, B.; Kasturi, T.; Piatak, D. *J. Org. Chem.* **1961**, *26*, 1685–1686.
- (18) Kraus, G. A.; Frazier, K. A.; Roth, B. D.; Taschner, M. J.; Neuenschwander, K. *J. Org. Chem.* **1981**, *46*, 2417–2419.
- (19) Mao, Z.; Gregg, B. T.; Cutler, A. R. *J. Am. Chem. Soc.* **1995**, *117*, 10139–10140.
- (20) Sakai, N.; Moriya, T.; Konakahara, T. *J. Org. Chem.* **2007**, *72*, 5920–5922.
- (21) Saegusa, T.; Shiota, T.; Matsumoto, S.-i.; Fujii, H. *Polym. J.* **1972**, *3*, 40–43.
- (22) Kawakami, Y.; Yamashita, Y. *Macromolecules* **1977**, *10*, 837–839.
- (23) Libiszowski, J.; Szymanski, R.; Penczek, S. *Die Makromol. Chem.* **1989**, *190*, 1225–1232.
- (24) Hövetborn, T.; Hölscher, M.; Keul, H.; Höcker, H. *Rev. Roum. Chim.* **2006**, *51*, 781–793.
- (25) Lascaud, S.; Perrier, M.; Vallee, A.; Besner, S.; Prud'homme, J.; Armand, M. *Macromolecules* **1994**, *27*, 7469–7477.
- (26) Niitani, T.; Shimada, M.; Kawamura, K.; Dokko, K.; Rho, Y.-H.; Kanamura, K. *Electrochem. Solid-State Lett.* **2005**, *8*, A385–A388.
- (27) Timachova, K.; Watanabe, H.; Balsara, N. P. *Macromolecules* **2015**, *48*, 7882–7888.
- (28) Shibutani, R.; Tsutsumi, H. *J. Power Sources* **2012**, *202*, 369–373.
- (29) Nakano, Y.; Tsutsumi, H. *Solid State Ionics* **2014**, *262*, 774–777.
- (30) Luan, B.; Yuan, Q.; Pan, C.-Y. *Macromol. Chem. Phys.* **2004**, *205*, 2097–2104.

- (31) Pesko, D. M.; Webb, M. A.; Jung, Y.; Zheng, Q.; Miller, T. F.; Coates, G. W.; Balsara, N. P. *Macromolecules* **2016**, *49*, 5244–5255.

CHAPTER 4

Indium catalyzed reduction of polyesters to polyethers

Chapter 4

Indium catalyzed reduction of polyesters to polyethers

4.1 Abstract

The synthesis of aliphatic polyethers were limited by available monomers and polymerization methods while the aliphatic polyesters can be synthesized with variable monomers and polymerization techniques. A direct synthesis of polyethers by reducing the corresponding polyesters were pursued with indium-catalyzed reduction using hydrosilanes. The model reaction on poly(ϵ -caprolactone) successfully yielded the poly(hexamethylene oxide) product in high conversion. However, chain scission was observed but can be significantly suppressed by introducing bulkier silane reagents or lowering the reaction temperature. The polyester substrate scope was examined and new polyethers including poly(tetrahydropyran) and poly(2-methyloxepane) were synthesized for the first time from readily available polyesters. Various indium based catalysts were screened and InBr_3 remained the most reactive catalyst for this reaction. This is the first report on obtaining polyethers directly from polyesters and the results demonstrated that new polyethers can be synthesized from easily accessible polyesters. This work showed great potential to discover new polyethers with promising properties that can have applications in polymer electrolytes or drug delivery.

4.2 Introduction

Aliphatic polyethers have been widely used in polyurethane foam, lubricant, and medical applications.¹ However, most of the aliphatic polyethers synthesized were polyethylene oxide (PEO), its derivatives, and polytetrahydrofuran (PTHF).² The polymerization was mostly limited on ring-opening polymerization of the corresponding cyclic ethers. On the other hand, polyesters are another large family of polymers with applications in food containers and clothing. The synthesis of polyesters can be achieved by both step-growth polymerizations and ring-opening polymerizations with a variety of available monomers. Synthesizing polyethers directly from polyesters by ester to ether reduction will yield polyethers that have never been accessed before. As far as we know, there has been no report on polyester to polyether synthesis before. The direct synthesis from polyester to polyether will require no side reaction of the reduction, especially side reactions that can break the polymer chain.

The first example of ester to ether reduction was reported by Pettit *et al.*³ where they used boron trifluoride etherate and lithium aluminum hydride to reduce lactones to cyclic ethers on natural products. However, the reduction with metal hydrides gave mixed products including both ether and diol and the reaction scope was also limited. Cutler and co-workers⁴ improved the reduction by applying hydrosilylation catalyzed by manganese-based catalyst to remove the use of metal hydrides. However, the yield of the reaction was low and the catalyst was not commercially available, both of which prevented wide applications of the reduction. Recently, Sakai *et al.*⁵ significantly improved the hydrosilylation reaction by using inexpensive InBr_3 catalyst. The yields of some substrates were as high as 99 %. Inspired by Sakai and co-workers' work, we

were interested to apply the indium catalyzed ester-to-ether reduction to polyesters to synthesize corresponding polyethers. Herein, we report the first example of direct synthesis from polyester to polyether through indium catalyzed hydrosilane-induced reduction.

4.3 Results and Discussions

4.3.1 Model reaction on poly(ϵ -caprolactone) (PCL)

Initially, we sought to apply the ester to ether reduction reaction onto a simple model polyester to both examine the reactivity and optimize the reaction conditions. Poly(ϵ -caprolactone) (PCL) was selected as the model polyester because it is one of the simplest aliphatic polyesters and commercially available. We performed the reduction reaction following the same protocols Sakai *et al.* reported. To our surprise, the reaction (Table 4.1, entry 1) gave full conversion and PCL was fully reduced to the corresponding polyether – poly(hexamethylene oxide) based on ^1H -NMR spectroscopy. Poly(hexamethylene oxide) can be obtained by cationic ring opening polymerization of the expensive hexamethylene oxide monomer⁶ while PCL was inexpensive. However, the molecular weight of the synthesized poly(hexamethylene oxide) was 1.1 kDa and significantly lower than theoretical molecular weight (15.4 kDa), suggesting that chain scission happened during the reduction.

A plausible mechanism for this reaction on polyester was shown in Figure 4.1 based on the work by Sakai,⁵ Baba⁷ and Hosomi.⁸ The first step was a transmetalation between silane and InBr_3 to generate an indium hydride. An indium radical was then formed by abstracting the proton from the hydride and the radical was consecutively

added to the ester group to form the key acetal radical intermediate. The second step was a metathesis between the intermediate and another equivalence of silane. There were two possibilities for this reaction to happen. One possibility was the silane trapped the indium alkoxide group to form $R_3SiOInBr_2$ and an ether radical, where the polymer chain was preserved. The other possibility was the silane trapped the alkoxide group from the ester to scissor the polymer chain into two parts, which subsequently caused the decrease on M_n . The last step was the attack from another equivalence of silane to generate the corresponding products and the indium radical. In order to improve the M_n of the polyether, a better selectivity on the second step needed to be achieved. It is worth noting that even with a selectivity as high as 19:1, one will yield a polyether with an M_n of 2 kDa in the case of PCL.

In order to eliminate the chain scission, we first screened various silane species with different bulkiness, expecting the bulkiness of the silane may influence the selectivity of the reaction on the key intermediate and thereby affect the M_n of the polyether. The results are summarized in Table 4.1. When the bulkiness of the silane was increased from Et_3SiH to $PhMe_2SiH$ (Table 4.1, entries 1 and 4), a significant increase on the polyether M_n was observed from 1.1 kDa to 2.3 kDa. The M_n of the polyether was further increased to a maximum at 14.0 kDa when Ph_3SiH was used (Table 4.1, entry 8). Notably, the reactivity dropped slightly when bulkier silanes were used as in the case of Ph_3SiH , where the conversion reached 90 % while all the other silanes had a full conversion under the same reaction condition. When bulkier silane such as iPr_3SiH was tested (Table 4.1, entry 10), no reduction was observed and the polyester was recovered, suggesting that isopropyl group was too bulky to let the

metathesis happen between the acetal radical intermediate and the silane. In addition to silane bulkiness, reaction temperature was another condition that influenced the M_n of the polyether. We investigated the temperature effects by keeping the silane as Et_3SiH and conducted the reaction under various temperatures (Table 4.1, entries 1 to 3). The M_n of the polyether increased from 1.1 kDa to 8.7 kDa when the reaction temperature was decreased from 60 °C to 0 °C. Similar trend was found on PhMe_2SiH with an increase of M_n from 5.4 kDa (60 °C) to 9.6 kDa (22 °C). It's noteworthy that the reaction no longer proceeded at ambient temperature when Ph_3SiH was used as the silane, further suggesting the low reactivity of bulky silanes. Judging from the mechanism discussed above, it is likely that energy differences existed between the two radical intermediates of the two routes (polymer-kept and polymer-broken). Lower temperature would make the reaction favor the more stable intermediate, which was the radical intermediate from polymer-kept route in this reaction. Thus, the selectivity was shifted to the polymer-kept route, resulting in higher M_n .

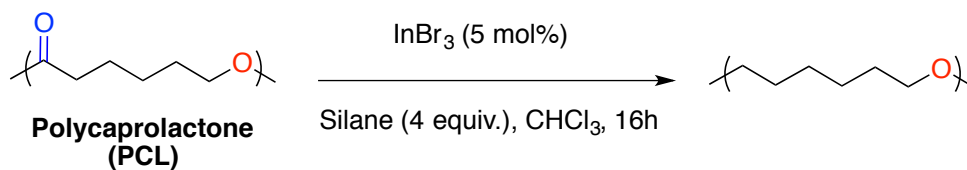


Table 4.1 Polyester to polyether reduction on poly(ϵ -caprolactone)^a (PCL) through indium catalyzed hydrosilylation

Temperature					
Entry	Silanes	(°C)	Conversion % ^b	M_n (kDa) ^c	PDI ^c
1	Et_3SiH	60	>99	1.1	1.9
2	Et_3SiH	22	>99	3.2	2.1
3	Et_3SiH	0	>99	8.7	2.1
4	PhMe_2SiH	60	>99	2.3	1.7
5	PhMe_2SiH	22	>99	2.2	1.8
6	Ph_2MeSiH	60	>99	5.4	2.0
7	Ph_2MeSiH	22	>99	9.6	2.0
8	Ph_3SiH	60	90	14.0	2.0
9	Ph_3SiH	22	0	—	—
10	iPr_3SiH	60	0	—	—
11	iPr_3SiH	22	0	—	—

^aThe polycaprolactone was purchased from Aldrich with a M_n of 17.5 kDa and PDI of 2.1. ^bThe conversion of the polymerization was determined from ^1H -NMR from the crude reaction mixture. ^cNumber average molecular weight (M_n) and polydispersity index (PDI) were determined by THF gel permeation chromatography calibrated with polystyrene.

4.3.2 Substrate scope

After conducting and optimizing the proof-of-concept model reaction on polycaprolactone, the polyester substrate scope was examined for the polyester to polyether reaction. Although bulkier silanes were proven to yield polyethers with higher M_n , the removal of the disiloxane byproduct from polyethers was more difficult. In order to obtain pure polyether samples, we conducted the reaction with Et_3SiH as the silane reagent because the byproduct $\text{Et}_3\text{SiOSiEt}_3$ was relatively volatile and can be removed under vacuum. The equivalence of the silane reagent was also dropped from 4 equivalences to 2.1 equivalences to ease the purification. There was no substantial change on both the reactivity and the M_n of the polyether with decreased silane equivalence. The screening reactions were conducted at 0 °C to maximize the M_n of the polyethers expect for poly(1,4-dioxepan-5-one), where the reaction was performed at 22 °C to enhance the reactivity. The results of the substrate scope screening are summarized in Table 4.2.

We first explored the reduction reactions on linear aliphatic polyesters, including poly(γ -butyrolactone) (PBL, **1a**), poly(δ -valerolactone) (PVL, **1b**), poly(ϵ -caprolactone) (PCL, **1c**) and poly(1,4-dioxepan-5-one) (PDXO, **1d**). The reaction on PBL, PVL and PCL all proceeded as expected to yield the corresponding polyethers with high conversions. The M_n s of all polyethers were lower than theoretical M_n s, suggesting that chain scissions still took place in the reaction. A limitation of this reaction was revealed when PDXO was submitted to the reaction, the reactivity was significantly lower than other linear polyesters, thus we had to elevate the reaction temperature to 22 °C and let

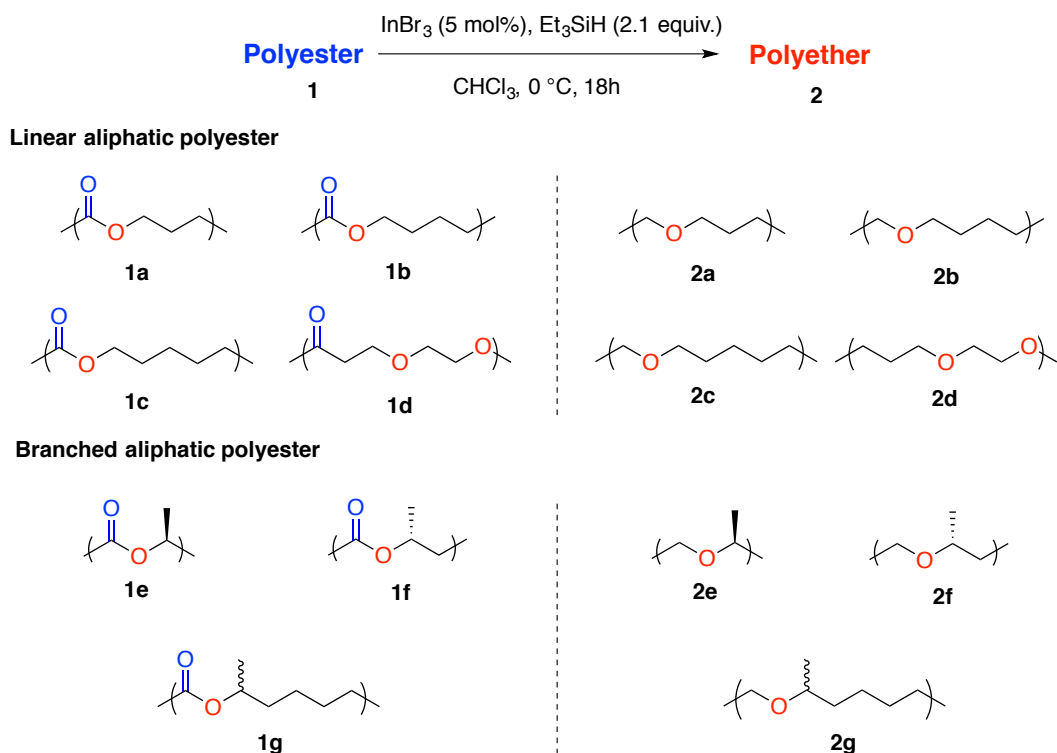


Table 4.2 Substrate scope of polyester to polyether reduction

Entry	Polyester	Polyether	Conversion % ^a	Polyester M_n (kDa) ^b	Polyester PDI ^b	Polyether M_n (kDa) ^b	Polyether PDI ^b
1	1a	2a	>99	8.4	1.4	2.8	1.6
2	1b	2b	>99	44.6	2.2	7.2	1.6
3	1c	2c	>99	17.5	2.1	7.3	1.7
4 ^c	1d	2d	57	18.1	1.6	3.4	1.9
5	1e	2e	0	<i>n.d.</i> ^d	<i>n.d.</i> ^d	<i>n.d.</i>	<i>n.d.</i>
6	1f	2f	0	<i>n.d.</i> ^d	<i>n.d.</i> ^d	<i>n.d.</i>	<i>n.d.</i>
7	1g	2g	>99	46.4	1.2	5.4	1.7

^aThe conversion of the polymerization was determined from ¹H-NMR from the crude reaction mixture. ^bNumber average molecular weight (M_n) and polydispersity index (PDI) were determined by THF gel permeation chromatography calibrated with polystyrene. ^cThe reaction was conducted at 22 °C for 7 days. ^dNot determined because the polymer was insoluble in THF.

the reaction run longer. Even with optimized conditions, the conversion was only 57 % after 1 week with M_n dropped to 3.4 kDa. When comparing the structures of PDXO with PCL, the only difference was an ether linkage on PDXO instead of methylene linkage on PCL. We hypothesized that the ether linkage binded to the indium in the acetal radical intermediate to form a chelation structure that prevented the silane attack to happen.

In addition to linear aliphatic polyesters, we further expanded the substrate scope to branched aliphatic polyesters. Attempts to conduct the reaction on polylactic acid (PLA, **1e**) and poly-3-hydroxybutyrate (P3HB, **1f**) resulted in no conversion and the polyesters were recovered. However, when poly(6-methyl- ϵ -caprolactone) (**1g**) was tested as the substrate, the corresponding polyether was achieved in full conversion. We hypothesized that the steric effects played an important role in determining the reactivity and longer spacers between ester groups tended to favor the reduction reaction.

Many polyethers synthesized in this substrate scope screening have been either synthesized with very expensive monomers or never synthesized before. Reichert *et al.*⁶ has reported the synthesis of poly(hexamethylene oxide) (**2c**) through cationic ring-opening polymerization. However, the expensive monomer, hexamethylene oxide, was synthesized from 1,6-hexanediol in low yield due to the unfavorability of forming a seven-membered ring. The synthesis of poly(2-methyloxepane) (**2g**) has never been reported largely because of the difficulty in acquiring the monomer,⁹ which requires Lawesson's reagent and highly reactive methyl lithium in four steps from ϵ -caprolactone. Even if the 2-methyloxepane monomer was polymerized, the resulting polymer would be regio-irregular with a mixture of both head-to-head (tail-to-tail) and

head-to-tail sequences. The most interesting example was on the synthesis of poly(tetrahydropyrane) (**2b**). Unlike other cyclic ethers such as oxetane and tetrahydrofuran, the 6-membered tetrahydropyrane has never been polymerized under a wide range of reaction conditions.² This ester to ether reduction made it possible to access this missing piece of cyclic ether homopolymers through PVL reduction for the first time. Unexpectedly, the synthesized poly(tetrahydropyrane) was stable at room temperature and did not depolymerize into tetrahydropyrane.

4.3.3 Catalyst screening

Various of catalysts were then screened to improve the reactivity and suppress chain scission. Sakai and co-workers⁵ have screened other indium based catalysts, including InCl_3 , $\text{In}(\text{OTf})_3$ and $\text{In}(\text{OAc})_3$. All of these catalysts were either unreactive or gave trace amount of products. We expanded the indium catalyst scope to include InI_3 , monovalent InBr and (*rac*-tBuSalcy) InBr with salen ligand on indium. A recent report by Metzger *et. al.*¹⁰ suggested that similar ester to ether reduction can be achieved in high conversion by gallium based catalyst (GaCl_3 and GaBr_3) with 1,1,3,3-tetramethyldisiloxane as the reductant. Thus, GaCl_3 was included in our catalyst screening to examine if metals other than indium will act as effective catalyst. The screening reactions were performed on PCL with Et_3SiH as the silane reagent. The results are summarized in Table 4.3. As expected, InI_3 catalyzed the reaction in full conversion to yield the polyether but with an M_n of 1.9 kDa, significantly lower than that of the polyether from InBr_3 catalyst. Reactions with InBr , (*rac*-tBuSalcy) InBr and GaCl_3 were all unreactive and the PCL was recovered.

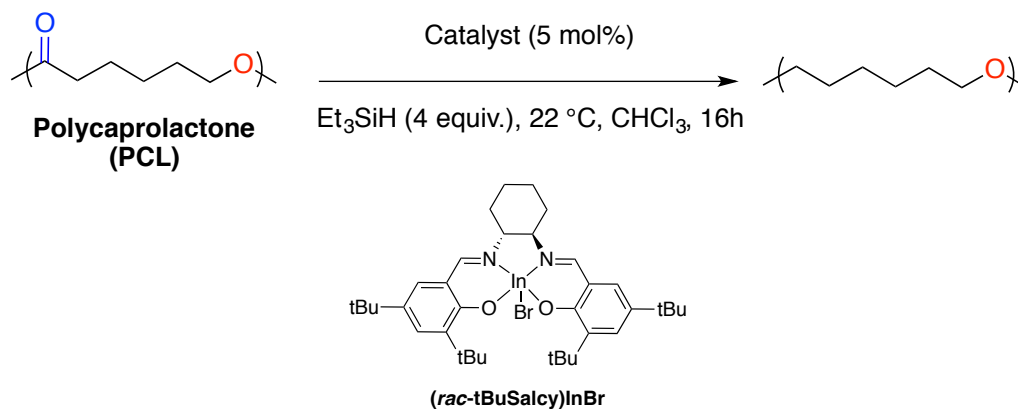


Table 4.3 Catalyst screening on polyester to polyether reduction on poly(ϵ -caprolactone)^a (PCL)

Entry	Catalyst	Conversion % ^b	M_n (kDa) ^c	PDI ^c
1	InBr ₃	>99	3.2	2.1
2	InI ₃	>99	1.9	1.8
3	InBr	0	—	—
4	(<i>rac</i> -tBuSalcy)InBr	0	—	—
5	GaCl ₃	0	—	—

^aThe polycaprolactone was purchased from Aldrich with a M_n of 17.5 kDa and PDI of 2.1. ^bThe conversion of the polymerization was determined from ¹H-NMR from the crude reaction mixture. ^cNumber average molecular weight (M_n) and polydispersity index (PDI) were determined by THF gel permeation chromatography calibrated with polystyrene.

4.4 Conclusions

In conclusion, we have developed a polyester to polyether synthesis with indium catalyzed hydrosilane-induced reduction. This synthesis enables researchers to gain access to various polyethers that are either difficult to synthesize with conventional methods or never synthesized before, which will help to discover new materials. To the best of our knowledge, this is the first time that the synthesis of poly(tetrahydropyrane), a missing piece of linear aliphatic polyethers, was reported.

Chain scission remains a major limitation of this reduction reaction but improvements were achieved with bulkier silanes and lower reaction temperatures. However, we saw a trade-off on reactivity when polyethers with higher M_n were pursued. Catalysts other than InBr_3 were screened but no significant improvements were obtained on either reactivity or chain scission. We are currently exploring other potential silanes and catalyst to increase the M_n s of the synthesized polyethers. Investigations on the reaction mechanisms are also in progress.

4.5 Experimental

4.5.1 General

All air and water sensitive reactions were carried out under dry nitrogen conditions using standard Schlenk techniques or MBraun UniLab drybox. ^1H NMR spectra were collected on a Bruker AV 500MHz spectrometer equipped with liquid nitrogen cooled cryoprobe and referenced with residue non-deuterated solvent shifts ($\text{CHCl}_3 = 7.26$ ppm). ^{13}C NMR spectra were collected on a Bruker AV 500 MHz (^{13}C , 125 MHz) spectrometer liquid nitrogen cooled cryoprobe and referenced to chloroform (δ 77.16 ppm). High resolution mass spectrometry (DART-HRMS) analyses were performed on a Thermo Scientific Exactive Orbitrap MS system equipped with an Ion Sense Direct Analysis in Real Time (DART) ion source.

Gel permeation chromatography (GPC) analyses were carried out using an Agilent PL-GPC 50 integrated system, equipped with UV and refractive index detectors, and 2 PL gel Mini-MIX C columns (5 micron, 4.6 mm ID). The GPC columns were eluted with tetrahydrofuran at 30 °C at 0.3 mL/min and were calibrated with monodisperse polystyrene standards.

4.5.2 Materials

Poly(ϵ -caprolactone) (M_w : 10000 Da, GPC M_n : 17.5 kDa) was purchased from Polysciences, Inc. and dried under vacuum before use. CHCl_3 was purchased from Fisher Scientific and dried over P_2O_5 before use. Tetrahydrofuran (THF) was purchased from Fisher Scientific and dried using a Phoenix solvent drying system and degassed by freeze-pump-thaw method for three cycles before use. Et_3SiH was purchased from Sigma-Aldrich and stored in a sure-seal bottle. InBr_3 was purchased from Alfa-Aesar and dried under vacuum before use. *rac*-tBuSalcy ligand was synthesized as reported.¹¹ All the other chemicals were purchased from commercial vendors and used as received unless otherwise noted. NMR solvent (CDCl_3) was purchased from Cambridge Isotope Laboratories (CIL) and used as received.

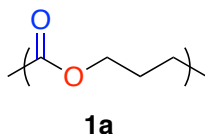
4.5.3 Synthesis

General reduction protocols:

To a suspension of InBr_3 (0.05 mmol) in CHCl_3 (0.6 mL) was added polyester (1 mmol in ester groups). Silane (2.1 mmol) was then added and the resulting mixture was stirred at 0 °C for 16 h. The reaction was quenched by water and extracted by CH_2Cl_2 . The organic layer was dried over anhydrous Na_2SO_4 . Solvent was removed and the residue was dried under vacuum at 60 °C to yield the polyether product.

4.5.3.1 Reduction on poly(γ -butyrolactone) (PBL, 1a)

4.5.3.1.1 Synthesis of poly(γ -butyrolactone) (PBL, 1a)



In a dry N_2 glove box, NaOMe (10.8 mg, 0.2 mmol) and 4-methylbenzyl alcohol (24.4 mg, 0.2 mmol) was dissolved in 0.5 mL anhydrous THF. The solution was stirred for 10 min and cooled to -40 °C for another 10 min. To this solution was added γ -butyrolactone (1.72 g, 20 mmol) and the mixture was stirred for 4 h at -40 °C. The reaction was quenched by adding a THF solution of benzoic acid (5 mg, 10 mg/mL) at -40 °C. The resulting solution was added dropwise to 100 mL MeOH and a white solid precipitated out. The solid was filtered and dried under vacuum to yield the polymer as a white solid (0.33 g, 20 %).

^1H NMR (500 MHz, CDCl_3) δ 4.12 (t, 2H), 2.39 (t, 2H), 2.01 – 1.92 (m, 2H).

^{13}C NMR (125 MHz, CDCl_3) δ 172.80, 63.67, 30.80, 24.14.

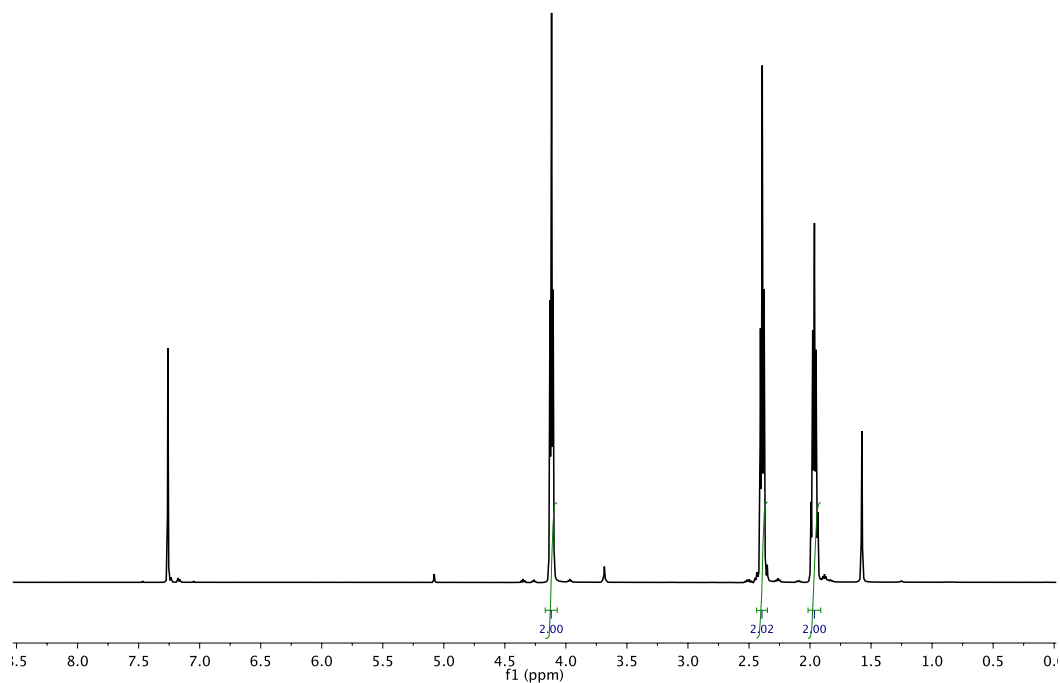


Figure 4.2 ^1H -NMR spectrum of **1a**. Signal at 7.26 ppm is the residue CHCl_3 .

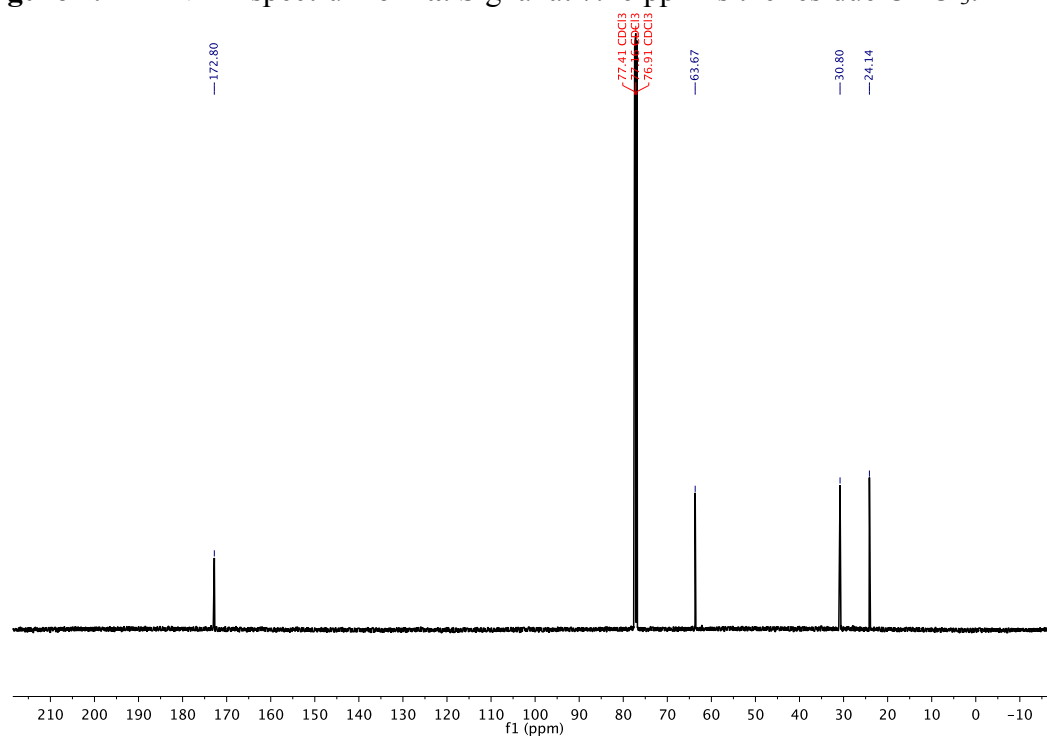
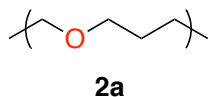


Figure 4.3 ^{13}C -NMR spectrum of **1a**. Signal at 77.16 ppm is the residue CHCl_3 .

4.5.3.1.2 Synthesis of poly(tetrahydrofuran) (2a)



Following the general protocol, to a suspension of InBr_3 (17.7 mg, 0.05 mmol) in CHCl_3 (0.6 mL) was added poly(γ -butyrolactone) (86.1 mg, 1 mmol in ester groups). Et_3SiH (0.34 mL, 2.1 mmol) was then added and the resulting mixture was stirred at 0 °C for 16 h. The reaction was quenched by water and extracted by CH_2Cl_2 . The organic layer was dried over anhydrous Na_2SO_4 . Solvent was removed and the residue was dried under vacuum at 60 °C to yield poly(tetrahydrofuran) as a white solid (35 mg, 49 %).

^1H NMR (500 MHz, CDCl_3) δ 4.39 – 4.35 (m, 4H), 1.73 – 1.55 (m, 4H).

^{13}C NMR (125 MHz, CDCl_3) δ 70.76, 26.65.

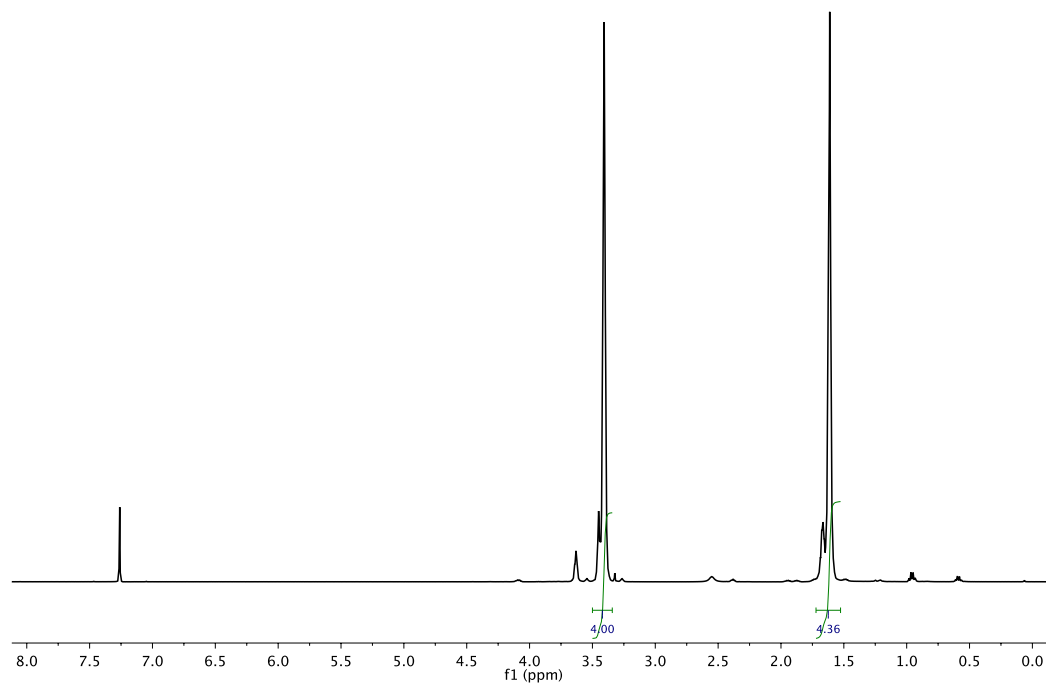


Figure 4.4 ^1H -NMR spectrum of **2a**. Signal at 7.26 ppm is the residue CHCl_3 .

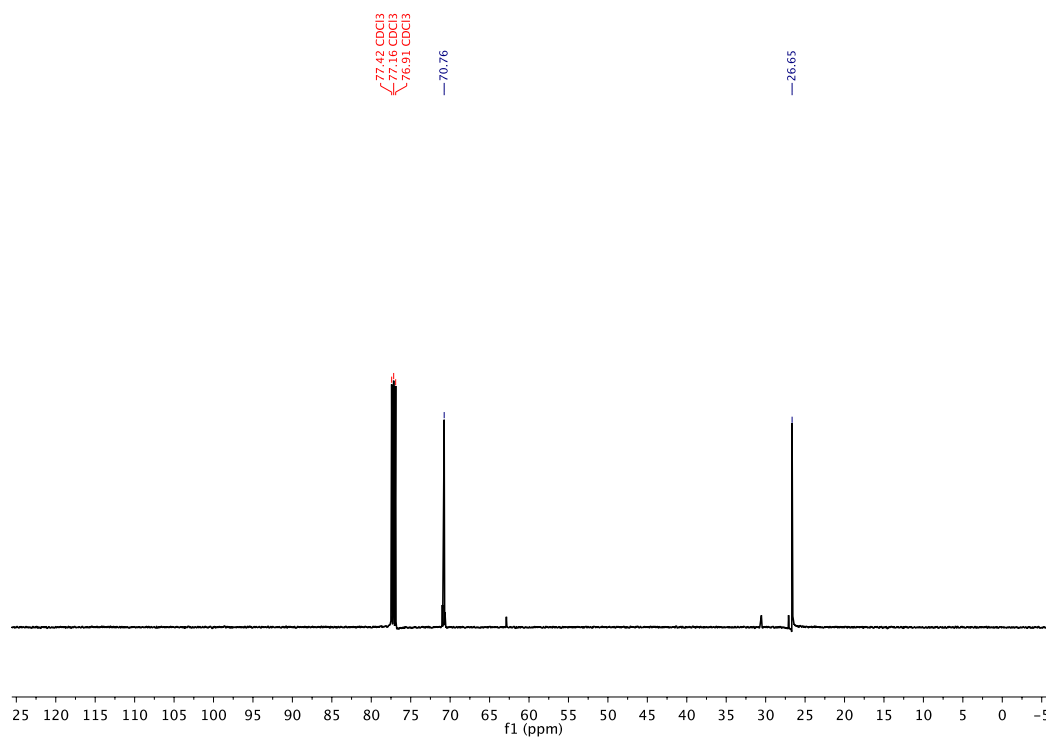
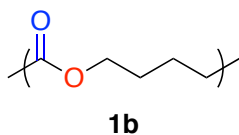


Figure 4.5 ^{13}C -NMR spectrum of **2a**. Signal at 77.16 ppm is the residue CHCl_3 .

4.5.3.2 Reduction on poly(δ -valerolactone) (PVL, 1b)

4.5.3.2.1 Synthesis of poly(δ -valerolactone) (PVL, 1b)



δ -Valerolactone (2.0 g, 19.98 mmol) was added to the organocatalyst triazabicyclodecene (TBD) (28.0 mg, 0.200 mmol) in neat. The resulting mixture was stirred at room temperature for 16 h. The solution gelled up after 10 min and turned into a white solid after overnight reaction. The solid was dissolved in CH_2Cl_2 and added dropwise into MeOH to precipitate the polymer out as a white solid (1.75 g, 88 %).

^1H NMR (500 MHz, CDCl_3) δ 4.11 – 4.05 (m, 2H), 2.39 – 2.28 (m, 2H), 1.74 – 1.60 (m, 4H).

^{13}C NMR (125 MHz, CDCl_3) δ 173.39, 64.05, 33.83, 28.22, 21.56.

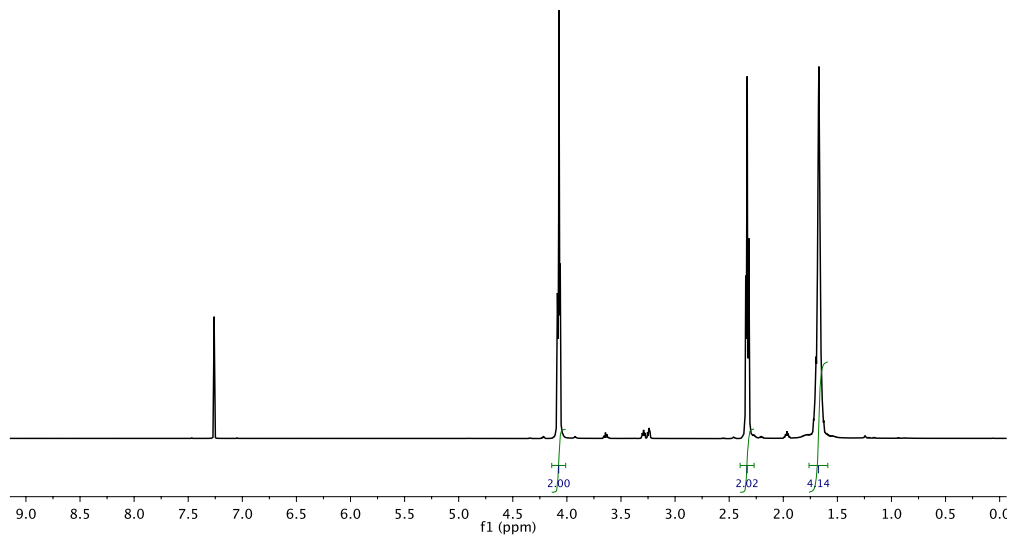


Figure 4.6 ^1H -NMR spectrum of **1b**. Signal at 7.26 ppm is the residue CHCl_3 .

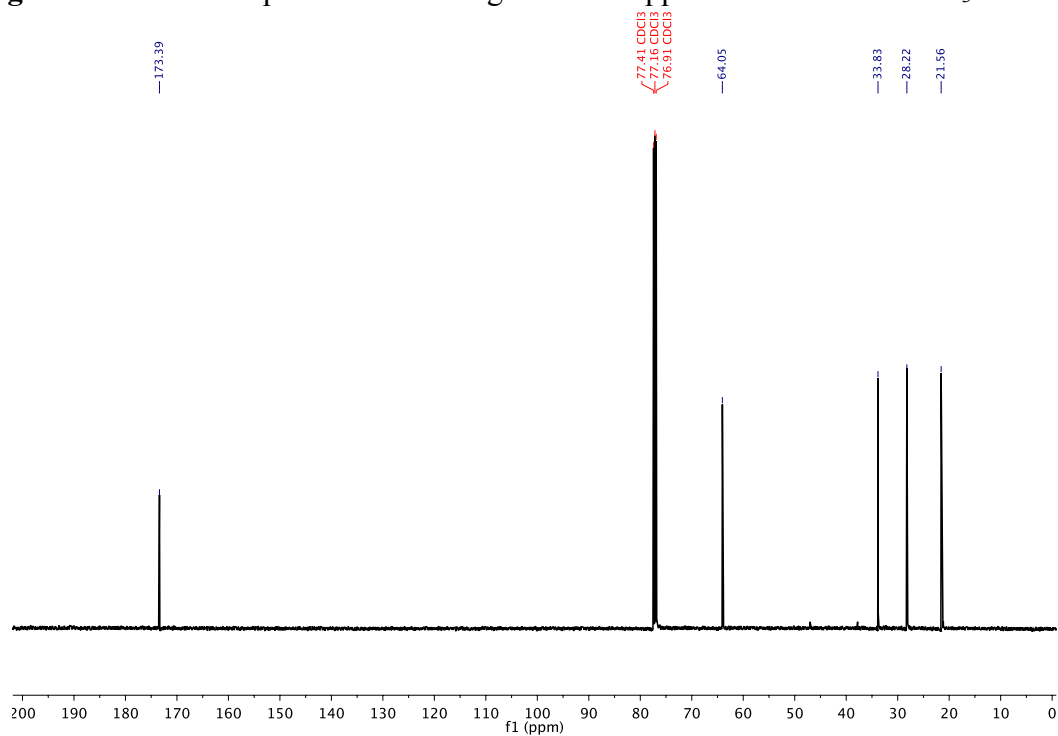
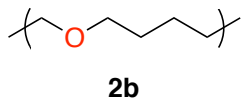


Figure 4.7 ^{13}C -NMR spectrum of **1b**. Signal at 77.16 ppm is the residue CHCl_3 .

4.5.3.2.2 Synthesis of poly(tetrahydropyrane) (2b)



Following the general protocol, to a suspension of InBr_3 (17.7 mg, 0.05 mmol) in CHCl_3 (0.6 mL) was added poly(δ -valerolactone) (100.1 mg, 1 mmol in ester groups). Et_3SiH (0.34 mL, 2.1 mmol) was then added and the resulting mixture was stirred at 0 °C for 16 h. The reaction was quenched by water and extracted by CH_2Cl_2 . The organic layer was dried over anhydrous Na_2SO_4 . Solvent was removed and the residue was dried under vacuum at 60 °C to yield poly(tetrahydropyrane) as a white solid (70 mg, 92 %).

^1H NMR (500 MHz, CDCl_3) δ 3.45 – 3.34 (m, 4H), 1.64 – 1.52 (m, 4H), 1.47 – 1.33 (m, 2H).

^{13}C NMR (125 MHz, CDCl_3) δ 70.99, 29.76, 22.97.

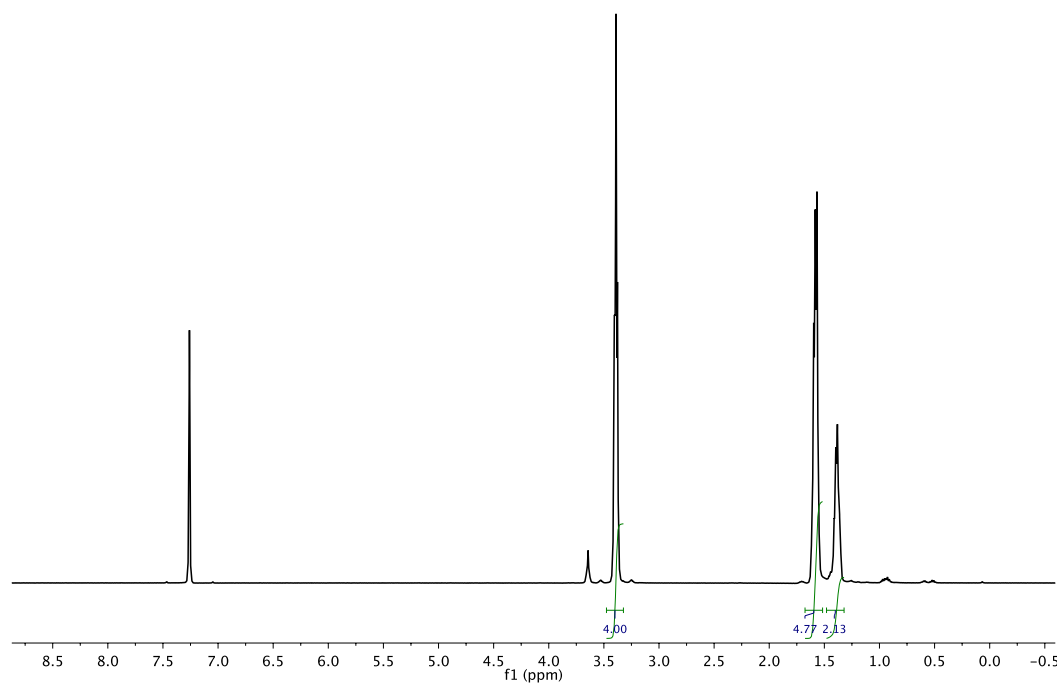


Figure 4.8 ¹H-NMR spectrum of **2b**. Signal at 7.26 ppm is the residue CHCl₃.

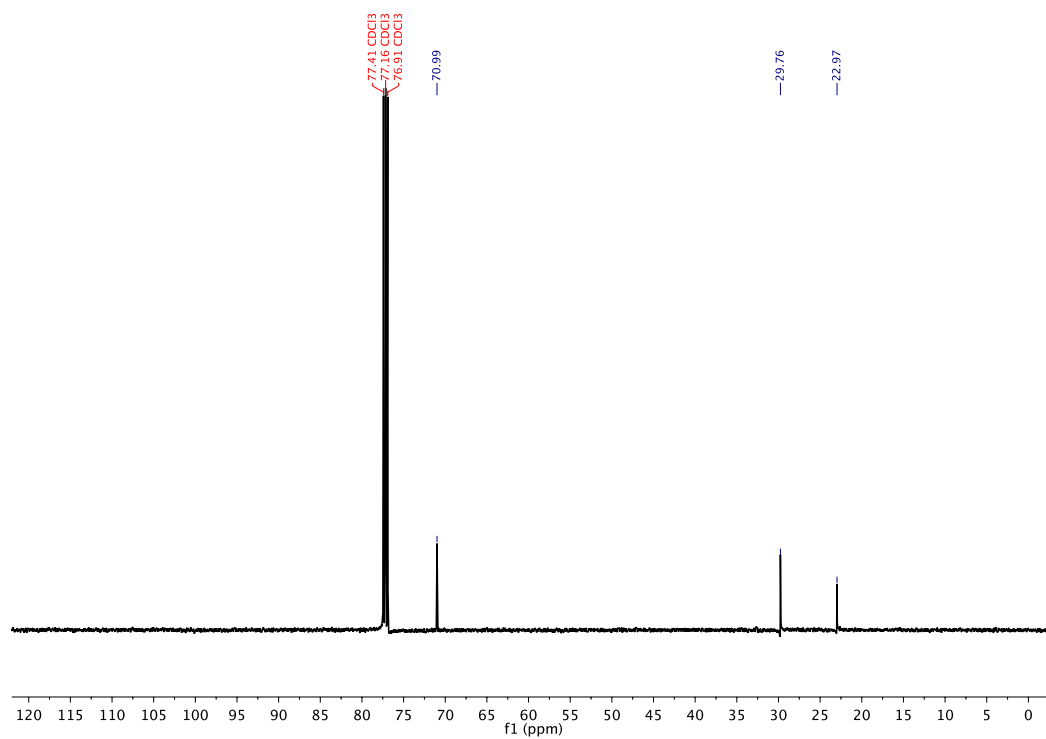
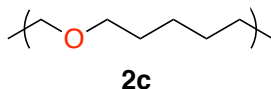


Figure 4.9 ¹³C-NMR spectrum of **2b**. Signal at 77.16 ppm is the residue CHCl₃.

4.5.3.3 Reduction on poly(ϵ -caprolactone) (PCL, 1c)

4.5.3.3.1 Synthesis of poly(hexamethylene oxide) (2c)



Following the general protocol, to a suspension of InBr_3 (17.7 mg, 0.05 mmol) in CHCl_3 (0.6 mL) was added poly(ϵ -caprolactone) (114.1 mg, 1 mmol in ester groups). Et_3SiH (0.34 mL, 2.1 mmol) was then added and the resulting mixture was stirred at 0 °C for 16 h. The reaction was quenched by water and extracted by CH_2Cl_2 . The organic layer was dried over anhydrous Na_2SO_4 . Solvent was removed and the residue was dried under vacuum at 60 °C to yield poly(hexamethylene oxide) as a white solid (79 mg, 69 %).

$^1\text{H NMR}$ (500 MHz, CDCl_3) δ 3.45 – 3.34 (m, 4H), 1.64 – 1.52 (m, 4H), 1.47 – 1.33 (m, 2H).

$^{13}\text{C NMR}$ (125 MHz, CDCl_3) δ 70.99, 29.76, 22.97.

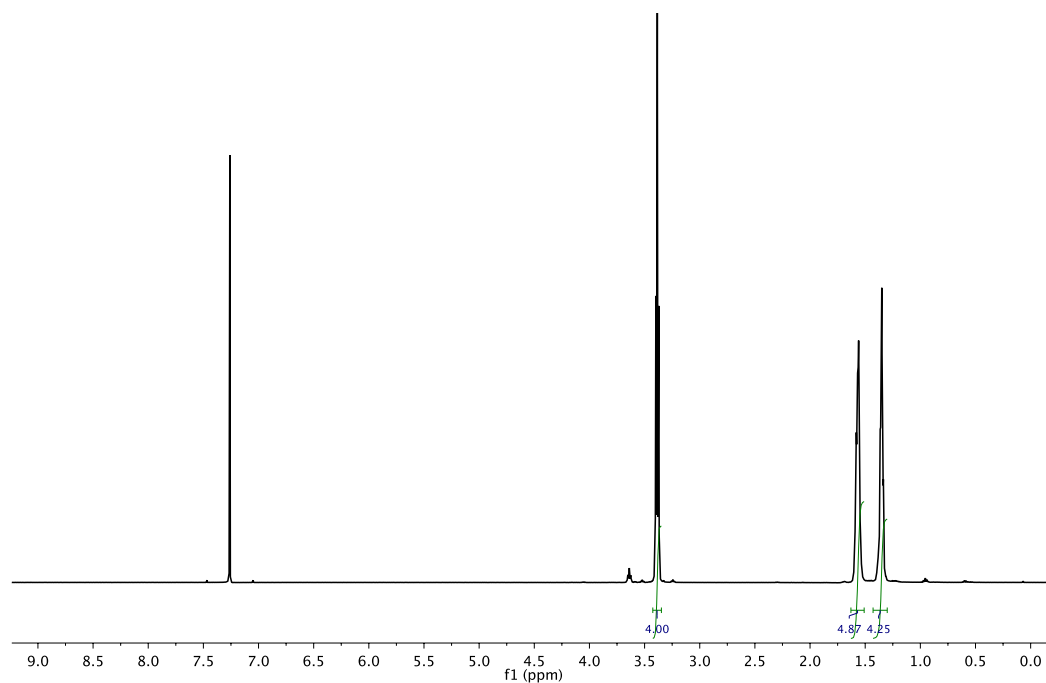


Figure 4.10 ^1H -NMR spectrum of **2c**. Signal at 7.26 ppm is the residue CHCl_3 .

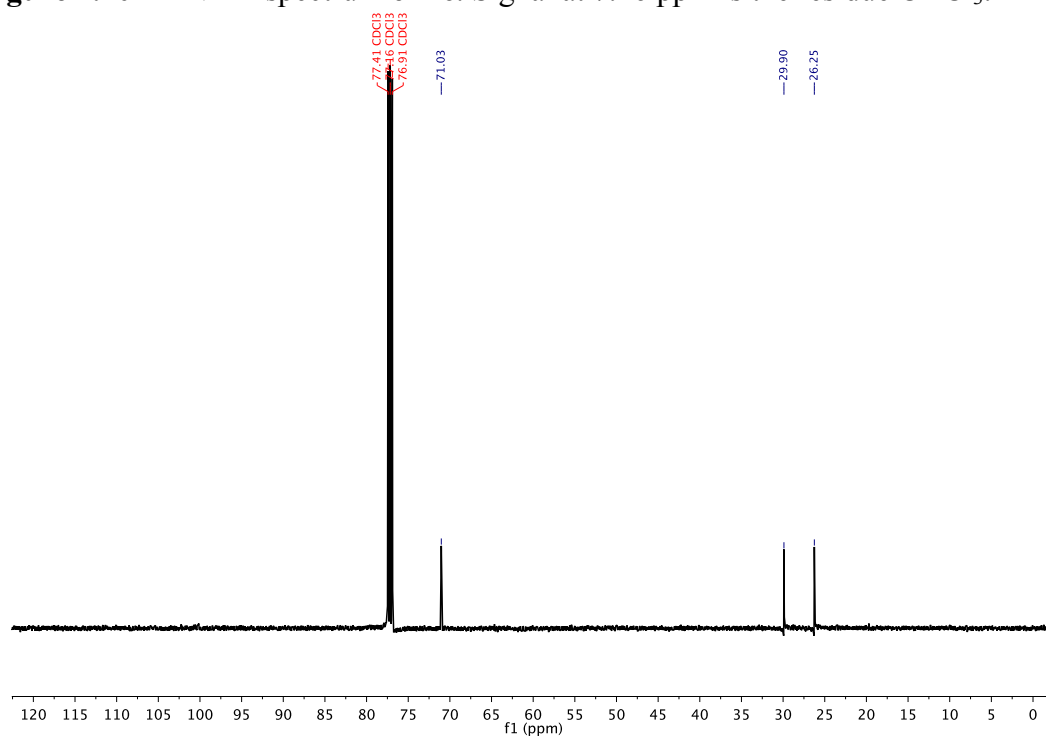
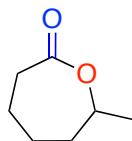


Figure 4.11 ^{13}C -NMR spectrum of **2c**. Signal at 77.16 ppm is the residue CHCl_3 .

4.5.3.4 Reduction on poly(6-methyl- ϵ -caprolactone) (1g)

4.5.3.4.1 Synthesis of 6-methyl- ϵ -caprolactone



The monomer was synthesized through Bayer-Villiger oxidation of 2-methylcyclohexanone. Meta-Chloroperoxybenzoic acid (mCPBA, 77 %, stabilized with water, 38.0 g, 169.3 mmol) was dissolved in 300 mL CH_2Cl_2 . Anhydrous Na_2SO_4 was added to this solution to remove the water. The Na_2SO_4 was filtered off and the filtrate was cooled to 0 °C. To this solution was added 2-methylcyclohexanone (10.0 g, 89.2 mmol) dropwise. The mixture was reflux at 40 °C for 18 h. The mixture was then cooled to 0 °C and the precipitated solid was filtered off. The left peracid was quenched with NaHSO_3 (17 g in 50 mL H_2O). The organic layer was separated, washed with saturated NaHCO_3 solution, and dried over anhydrous Na_2SO_4 . Solvent was removed under vacuum and the residue was distilled (0.2 torr, 54 °C) to yield the product as a colorless oil (9.13 g, 80 %). It is noteworthy that the final product has ~ 4 % of the 2-methyl- ϵ -caprolactone as the minor product from the Bayer-Villiger oxidation. The product was used for the next step without separating this minor product.

^1H NMR (500 MHz, CDCl_3) δ 4.49 – 4.40 (m, 1H), 2.73 – 2.54 (m, 2H), 1.98 – 1.83 (m, 3H), 1.71 – 1.51 (m, 3H), 1.37 – 1.31 (m, 3H).

^{13}C NMR (125 MHz, CDCl_3) δ 175.75, 76.97, 36.38, 35.17, 28.44, 23.05, 22.75.

HRMS (DART) m/z calculated for $\text{C}_7\text{H}_{13}\text{O}_2^+$ [$\text{M} + \text{H}$] $^+$ 129.09101, found 129.09116.

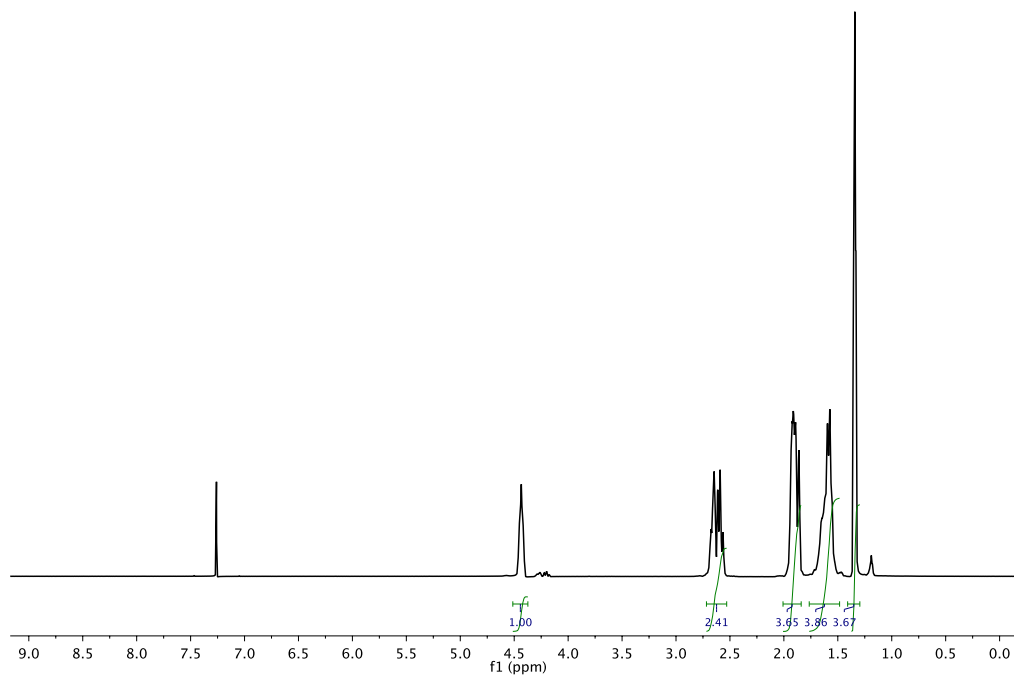


Figure 4.12 ^1H -NMR spectrum of 6-methyl- ϵ -caprolactone. Signal at 7.26 ppm is the residue CHCl_3 .

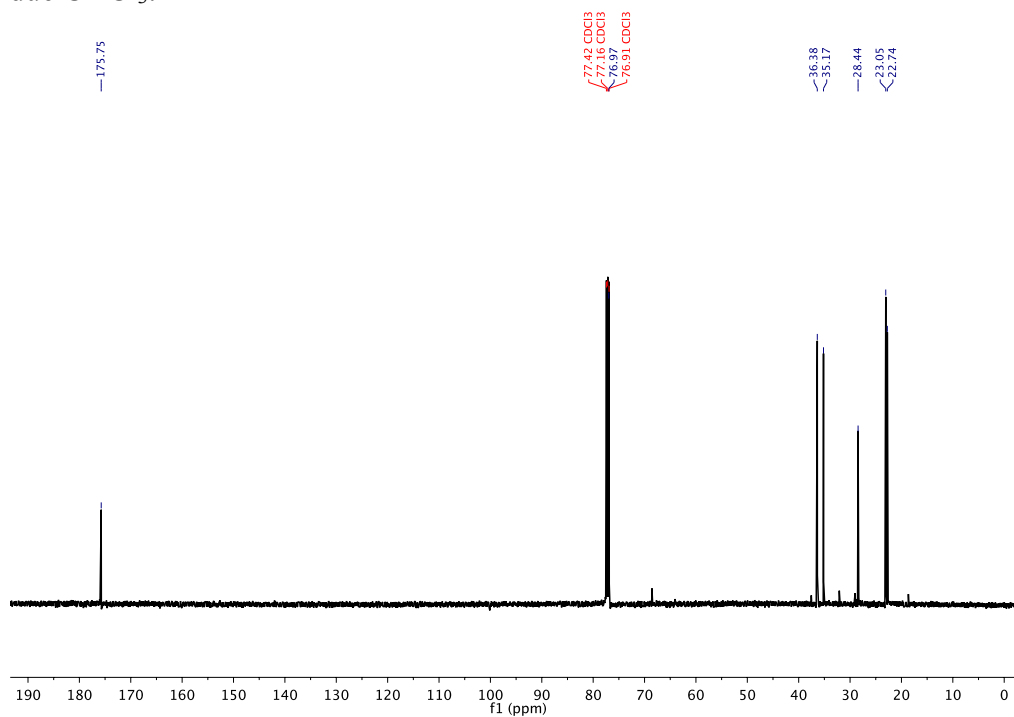
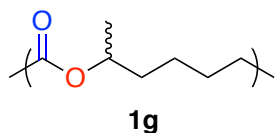


Figure 4.13 ^{13}C -NMR spectrum of 6-methyl- ϵ -caprolactone. Signal at 77.16 ppm is the residue CHCl_3 .

4.5.3.4.2 Synthesis of poly(6-methyl- ϵ -caprolactone) (1g)



The monomer (6-methyl- ϵ -caprolactone) was dried over activated 3 Å molecular sieves before use. In a dry N₂ glove box, 6-methyl- ϵ -caprolactone (2.50 g, 19.5 mmol) and Al(iPrO)₃ (39.8 mg, 0.195 mmol) were dissolved in anhydrous THF (5 mL). The resulting mixture was stirred at 0 °C for 20 h. The reaction was quenched by adding 5 mL 1M aqueous HCl solution. The mixture was diluted with THF. Solvent was removed and the residue was redissolved in CH₂Cl₂. The solution was washed with ethylenediaminetetraacetic acid (EDTA) aqueous solution (0.1 M, 25 mL \times 2), water (50 mL \times 3), and dried over anhydrous Na₂SO₄. Solvent was removed and the residue was dried under vacuum to yield the polymer product as a viscous gel (2.17 g, 87 %).

¹H NMR (500 MHz, CDCl₃) δ 4.82 (dq, J = 12.1, 6.3 Hz, 1H), 2.20 (t, J = 7.6 Hz, 2H), 1.60 – 1.48 (m, 3H), 1.47 – 1.38 (m, 1H), 1.35 – 1.20 (m, 2H), 1.12 (d, J = 6.3 Hz, 3H).

¹³C NMR (125 MHz, CDCl₃) δ 173.26, 70.71, 35.73, 34.65, 25.12, 25.00, 20.10.

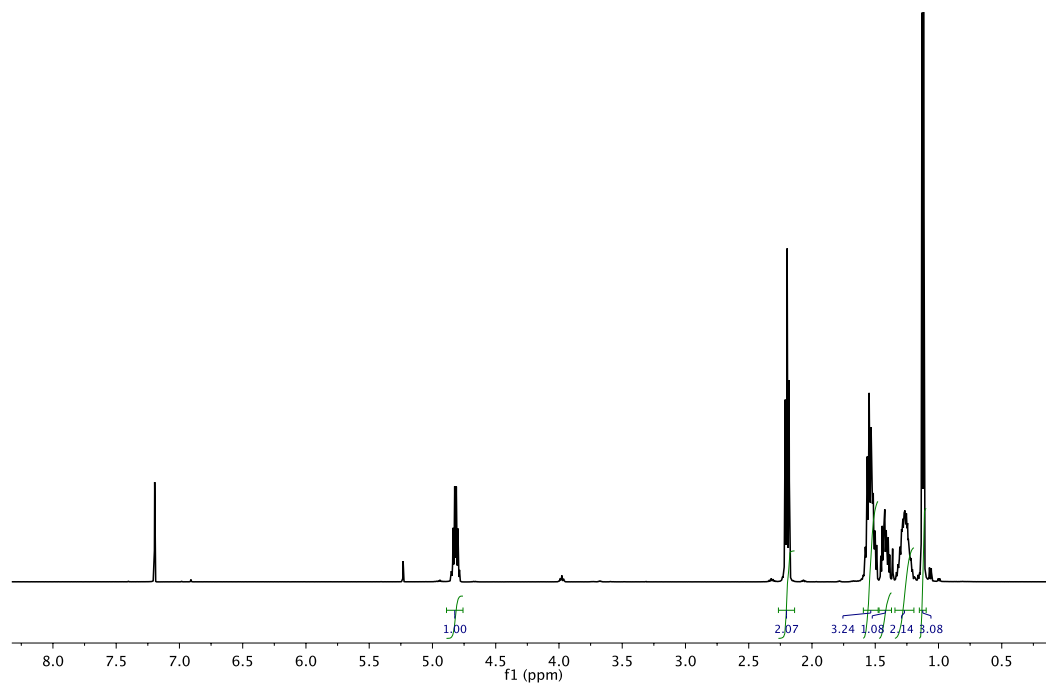


Figure 4.14 ^1H -NMR spectrum of **1g**. Signal at 7.26 ppm is the residue CHCl_3 .

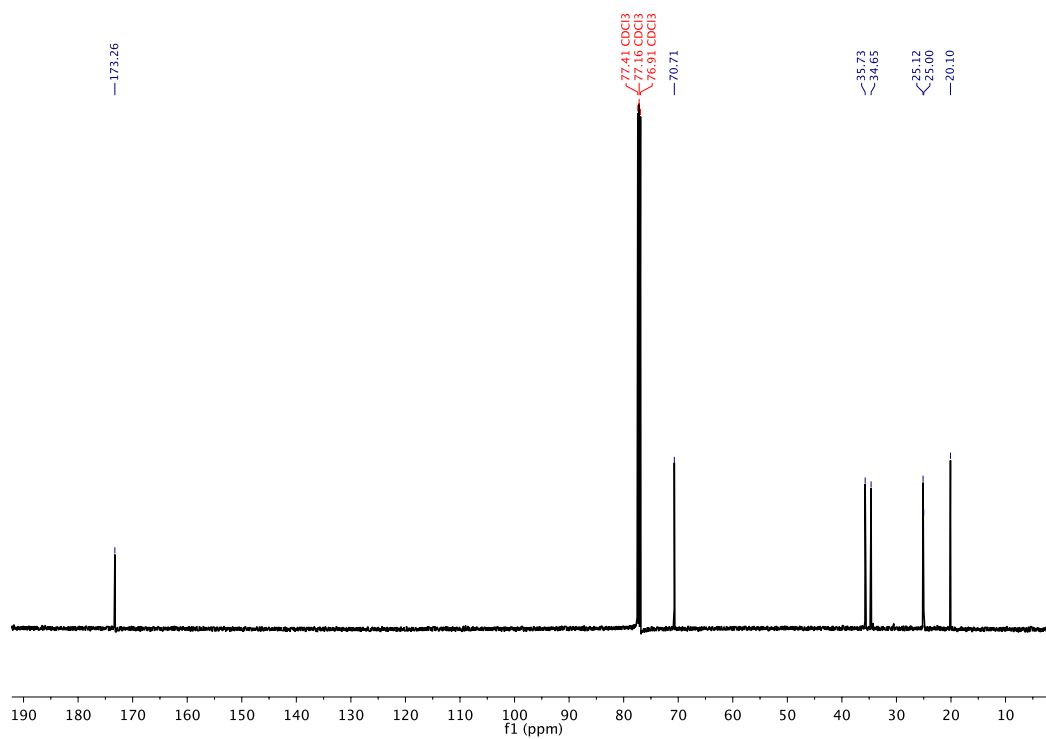
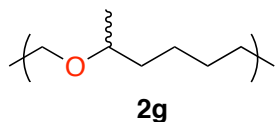


Figure 4.15 ^{13}C -NMR spectrum of **1g**. Signal at 77.16 ppm is the residue CHCl_3 .

4.5.3.4.3 Synthesis of poly(2-methyloxepane) (2g)



Following the general protocol, to a suspension of InBr_3 (17.7 mg, 0.05 mmol) in CHCl_3 (0.6 mL) was added poly(6-methyl- ϵ -caprolactone) (128.2 mg, 1 mmol in ester groups). Et_3SiH (0.34 mL, 2.1 mmol) was then added and the resulting mixture was stirred at 0 °C for 16 h. The reaction was quenched by water and extracted by CH_2Cl_2 . The organic layer was dried over anhydrous Na_2SO_4 . Solvent was removed and the residue was dried under vacuum at 60 °C to yield poly(2-methyloxepane) as a white solid (73 mg, 57 %).

^1H NMR (500 MHz, CDCl_3) δ 3.51 – 3.42 (m, 1H), 3.39 – 3.28 (m, 2H), 1.62 – 1.47 (m, 3H), 1.45 – 1.25 (m, 5H), 1.11 (d, J = 6.2 Hz, 3H).

^{13}C NMR (125 MHz, CDCl_3) δ 75.32, 68.43, 36.65, 30.21, 26.39, 25.50, 19.74.

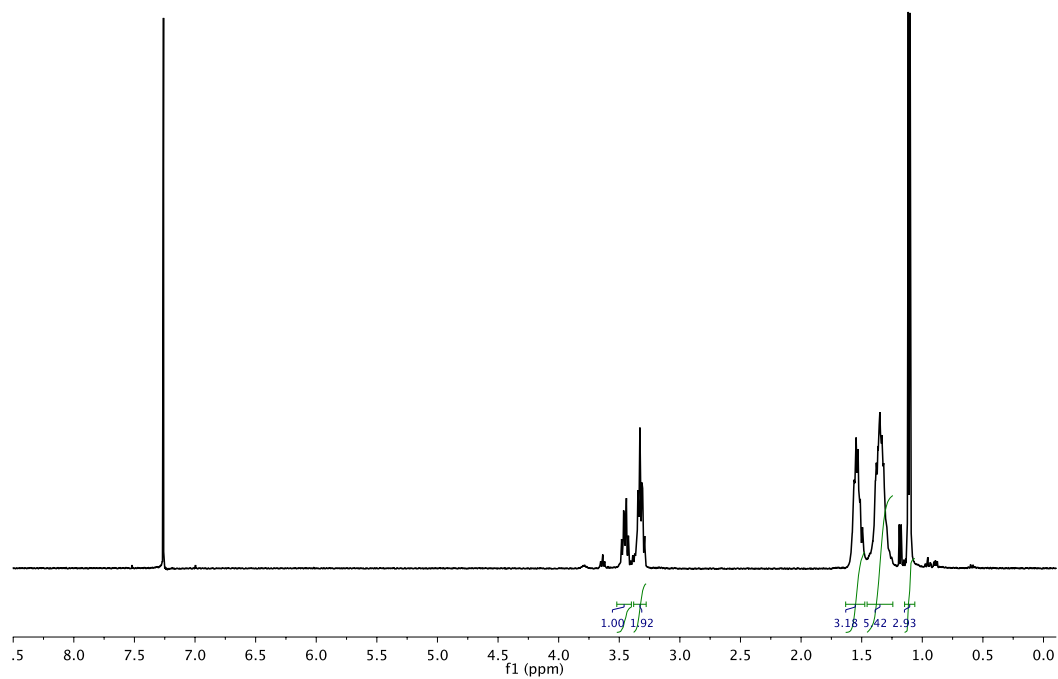


Figure 4.16 ^1H -NMR spectrum of **2g**. Signal at 7.26 ppm is the residue CHCl_3 .

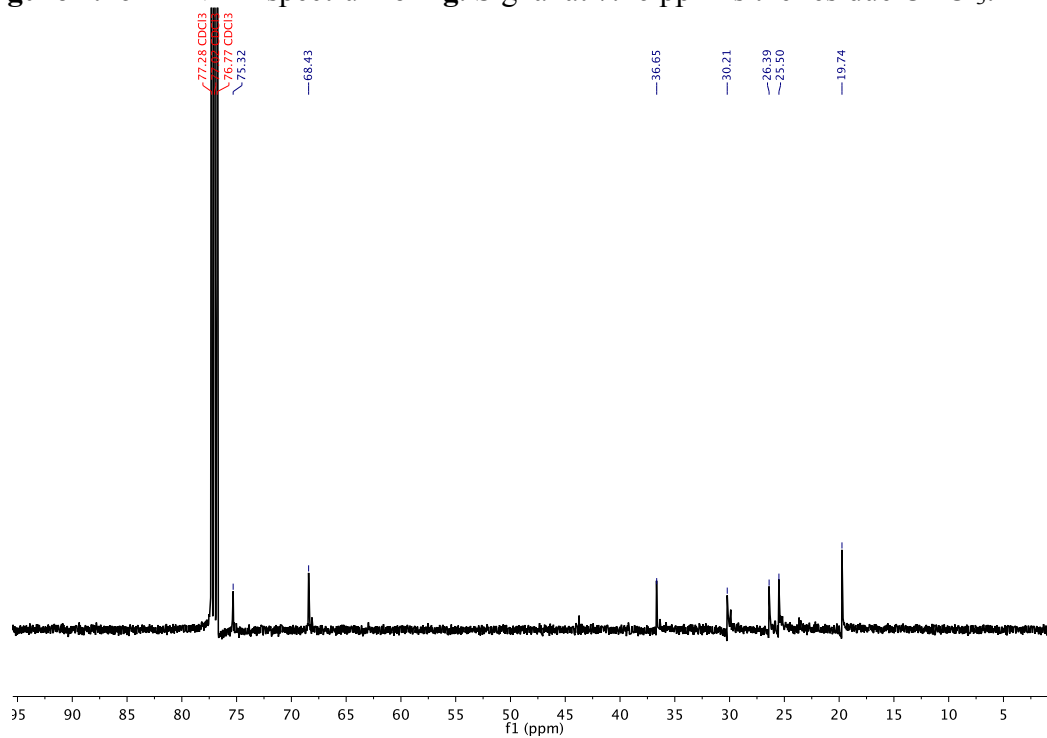
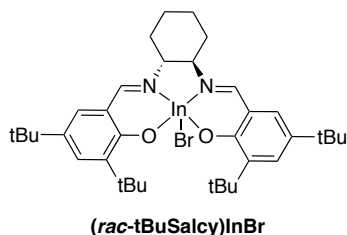


Figure 4.17 ^{13}C -NMR spectrum of **2g**. Signal at 77.16 ppm is the residue CHCl_3 .

4.5.3.5 Synthesis of (*rac*-tBuSalcy)InBr



In a dry N₂ glove box, to *rac*-tBuSalcy ligand (273.4 mg, 0.5 mmol) and NaH (27.8 mg, 1.1 mmol) was added 5 mL of anhydrous THF at 0 °C. The suspension was stirred at 45 °C for 3h under N₂. Solvent was removed under vacuum and to the residue was added InBr₃ (177.2 mg, 0.5 mmol) in 5 mL of anhydrous THF. The mixture was stirred at 22 °C for 2 d. The NaBr byproduct and unreacted NaH was removed with a micro-filter and the filtrate was concentrated under vacuum to obtain a solid. The solid was washed with hexanes and filtered to yield the product as a yellow solid (250 mg, 68 %). The ¹H NMR showed a split of two on all the proton signals because of the symmetry break by introducing the bromide on In.

¹H NMR (500 MHz, CDCl₃) δ 8.40 (s, 2H), 8.18 (s, 2H), 7.51 – 7.47 (m, 4H), 6.99 – 6.92 (m, 4H), 3.73 – 3.60 (m, 2H), 3.30 – 3.17 (m, 2H), 2.71 – 2.60 (m, 2H), 2.51 – 2.42 (m, 2H), 2.15 – 2.02 (m, 4H), 1.54 – 2.45 (m, 36H), 1.33 – 1.25 (d, 36H).

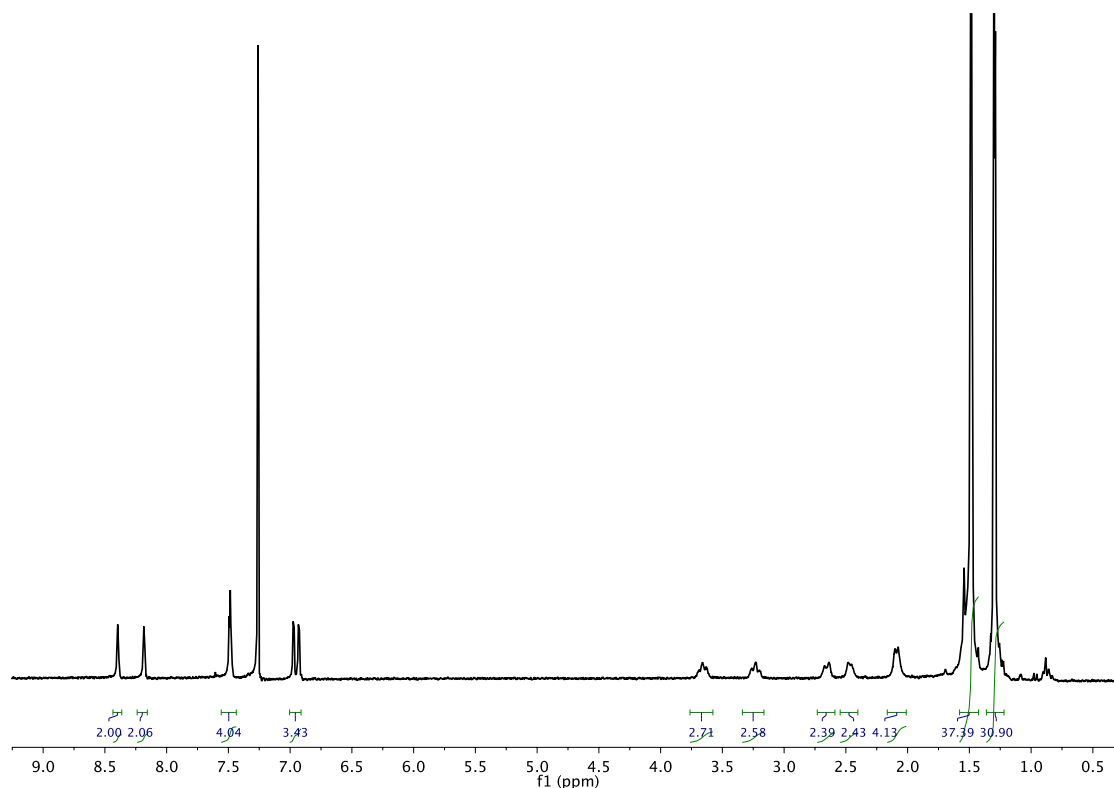


Figure 4.18 ^1H -NMR spectrum of (*rac*-tBuSalcy)InBr. Signal at 7.26 ppm is the residue CHCl_3 .

4.5.4 Reaction temperature screening

Following the general protocol, to a suspension of InBr_3 (17.7 mg, 0.05 mmol) in CHCl_3 (0.6 mL) was added poly(ϵ -caprolactone) (114.1 mg, 1 mmol in ester groups). Et_3SiH (0.64 mL, 4.0 mmol) was then added and the resulting mixture was stirred at 0 $^\circ\text{C}$, 22 $^\circ\text{C}$, or 60 $^\circ\text{C}$ for 16 h. The reaction was quenched by water and extracted by CH_2Cl_2 . The organic layer was dried over anhydrous Na_2SO_4 . Solvent was removed and the residue was dried under vacuum at 60 $^\circ\text{C}$ to yield poly(hexamethylene oxide) as a white solid. GPC analysis was performed on the product and the results are summarized in Figure 4.19.

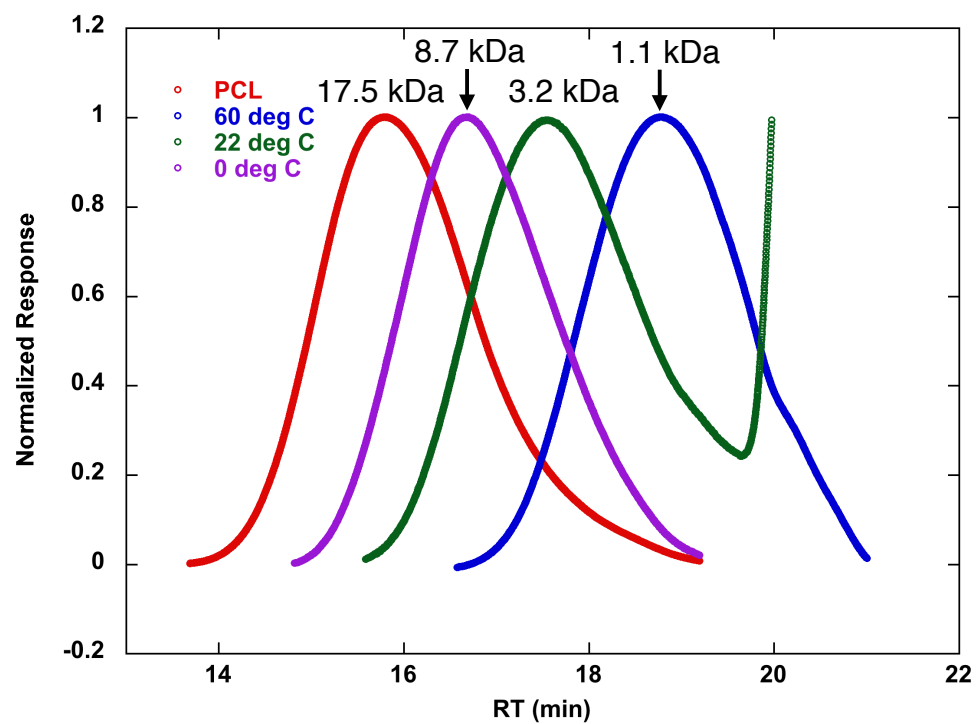


Figure 4.19 GPC traced of reaction temperature screening. The molecular weights were calibrated with monodisperse polystyrene standards.

REFERENCES

- (1) Maitz, M. F. *Biosurface and Biotribology* **2015**, *1*, 161–176.
- (2) Nuyken, O.; Pask, S. *Polymers* **2013**, *5*, 361–403.
- (3) Pettit, G.; Ghatak, U.; Green, B.; Kasturi, T.; Piatak, D. *J. Org. Chem.* **1961**, *26*, 1685–1686.
- (4) Mao, Z.; Gregg, B. T.; Cutler, A. R. *J. Am. Chem. Soc.* **1995**, *117*, 10139–10140.
- (5) Sakai, N.; Moriya, T.; Konakahara, T. *J. Org. Chem.* **2007**, *72*, 5920–5922.
- (6) Seitz, U.; Hoene, R.; Reichert, K.-H. W. *Die Makromol. Chem.* **1975**, *176*, 1689–1701.
- (7) Inoue, K.; Sawada, A.; Shibata, I.; Baba, A. *Tetrahedron Lett.* **2001**, *42*, 4661–4663.
- (8) Miura, K.; Tomita, M.; Yamada, Y.; Hosomi, A. *J. Org. Chem.* **2007**, *72*, 787–792.
- (9) Nicolaou, K. C.; McGarry, D. G.; Somers, P. K.; Veale, C. A.; Furst, G. T. *J. Am. Chem. Soc.* **1987**, *109*, 2504–2506.
- (10) Biermann, U.; Metzger, J. O. *ChemSusChem* **2014**, *7*, 644–649.
- (11) Larrow, J. F.; Jacobsen, E. N. *Org. Synth.* **1998**, *75*, 1.

APPENDIX A

Synthesis of poly(1,3,6-trioxocane), poly(styrene-*b*-1,3,6-trioxocane), and their applications as polymer electrolytes

APPENDIX A

Synthesis of poly(1,3,6-trioxocane), poly(styrene-*b*-1,3,6-trioxocane), and their applications as polymer electrolytes

A.1 Introduction

Polyethylene oxide (PEO) has been the mostly used solid polymer electrolyte since its alkali salt solubility was discovered back in the 1970s.¹ However, PEO is crystalline at room temperature and has a T_m of 65 °C, which results in low Li-ion conductivity at ambient temperature. One strategy to suppress the crystallinity is to tune the distances between oxygens in PEO to break the chain packing. Linden and Owen² reported that simply by incorporating an acetal group every ten EO units, they can increase the ionic conductivity to 10^{-5} S/cm with LiClO₄ salt. Our group³ recently reported a systematic structure-property relationship study by varying the distances (using di-, tetra-, or hexa-methylene spacers) between oligo(ethylene glycol) (tetra-, or penta-) and measuring the ionic conductivities of the corresponding polymers. A linear relationship (Figure A.1) was discovered between the temperature-dependent reduced conductivity (σ_r) and the mol% of oxygen atoms (x_O) in the polymer with higher x_O leads to increased σ_r . Inspired by this work, we expect that a polymer with even higher x_O than that of PEO ($x_O = 0.33$) should have higher σ_r compared to PEO. Poly(oxymethylene) has a x_O of 0.5 but the T_m is too high (175 °C) for the electrolyte application. In order to decrease its T_m but maintain the high x_O , we envisioned a copolymer of ethylene oxide (EO) and methylene oxide (MO) would be a good candidate. Herein, we report the synthesis and electrolyte application of poly(1,3,6-trioxocane) (or poly(oxymethylene-

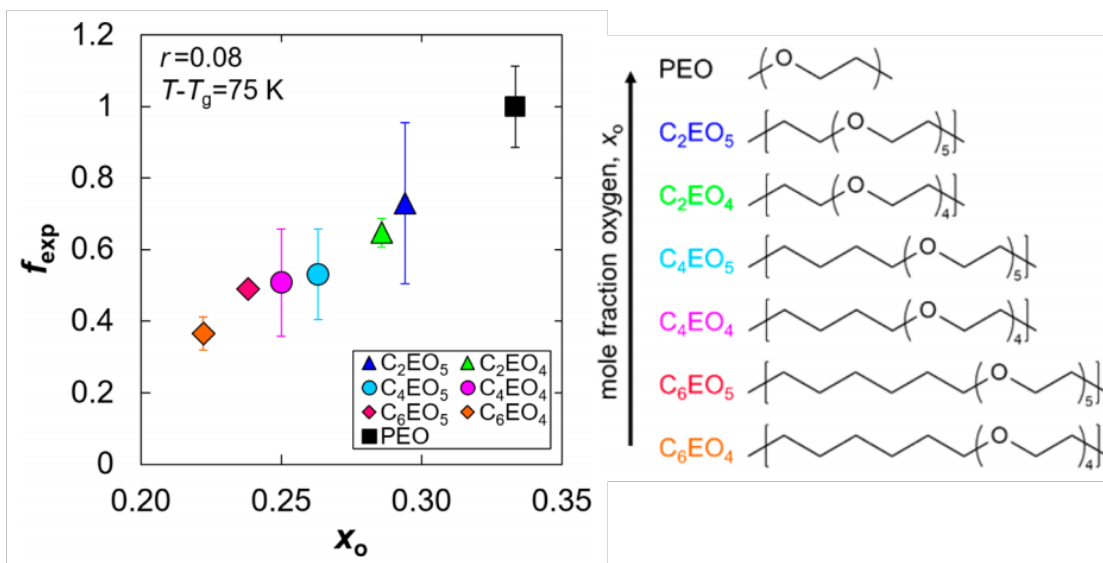


Figure A.1 Experimental connectivity, f_{exp} (defined as $f_{\text{exp}} = \sigma_r(\text{polymer})/\sigma_r(\text{PEO})$), with increasing x_O (mol% of O) at $r = 0.08$ (defined as $r = [\text{Li}]:[\text{O}]$) and $T - T_g = 75$ K. (adapted from reference 3).

alt-diethylene oxide), P(MO-2EO)) and its block copolymer with polystyrene (PS).

A.2 Results and discussions

The synthesis of P(MO-2EO) has been briefly reported back in the 1960s – 1980s⁴⁻⁶ but there was no report on its application as a polymer electrolyte to the best of our knowledge. Step-growth polymerization between diethylene glycol and paraformaldehyde was not successful in obtaining a high molecular weight polymer, instead, an oligomer was synthesized with an $M_n \sim 1$ kDa. However, the resulted oligomer can be heated under vacuum and depolymerized to yield the cyclic ether monomer, 1,3,6-trioxocane, which was polymerized subsequently under cationic conditions to yield higher molecular weight P(MO-2EO). Table A.1 summarizes the P(MO-2EO) synthesis with different mol% of $\text{BF}_3 \cdot \text{OEt}_2$ catalysts. The polymerization had very fast rates and the reaction normally started to become viscous after 30 mins and reached full conversion in 2 h. The yielded polymer had an alternating sequence of

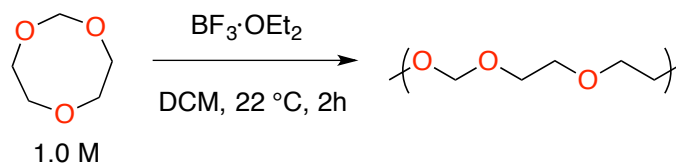


Table A.1 Synthesis of P(MO-2EO)

Initiator loading		Conversion	Theoretical	Experimental	
Entry	mol%	% ^a	M_n (kDa)	M_n (kDa) ^b	\bar{D} ^b
1	1	> 99	11.8	74.8	2.28
2	2	> 99	5.9	47.5	2.03
3	5	> 99	2.4	28.5	1.86

^aThe conversion of the polymerization was determined from ¹H-NMR from the crude reaction mixture. ^bNumber average molecular weight (M_n) and polydispersity index (PDI) were determined by THF gel permeation chromatography calibrated with polystyrene.

MO and 2EO units, and no regio-defect was observed based on ¹³C-NMR. It is noteworthy that there was an equilibrium between high molecular weight polymer and oligo-macrocycles in the cationic ring-opening polymerization (see Figure A.17 for an exemplary GPC trace of the crude reaction mixture from Table A.1 entry 3) possibly because of the backbiting from the active chain end. The oligo-macrocycles can be removed by precipitation in hexanes. The M_n s of the synthesized P(MO-2EO) were all higher than the theoretical M_n s, respectively, suggesting that not all initiators initiated the polymerization. Similar discrepancy between experimental and theoretical M_n s has been reported by Chien and co-workers⁴ in polymerizing 1,3,6-trioxocane in toluene with the $\text{BF}_3 \cdot \text{OEt}_2$ catalyst.

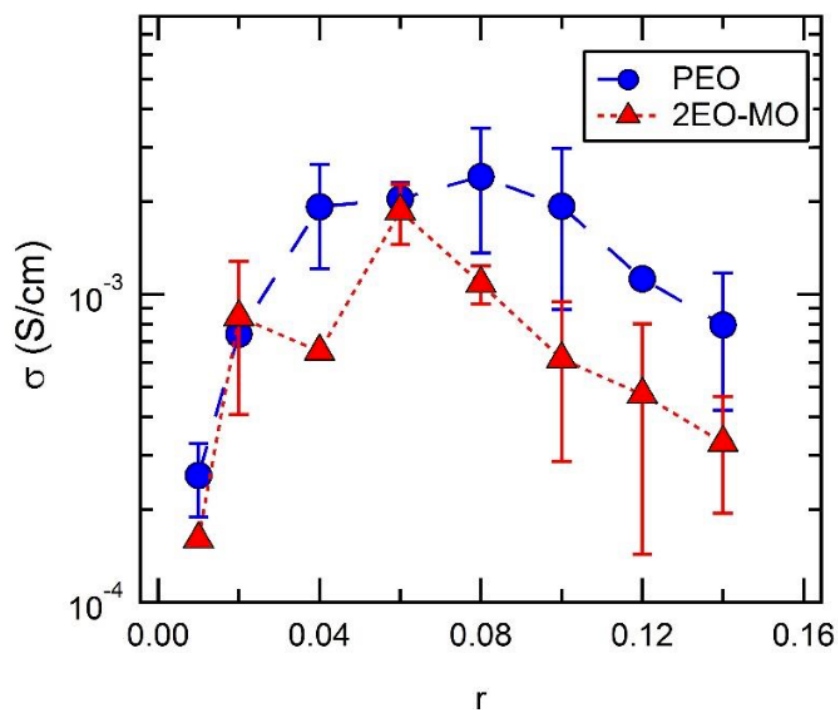


Figure A.2 Ionic conductivity of PEO and P(MO-2EO) with increasing r ([Li]:[O]) at 90 °C.

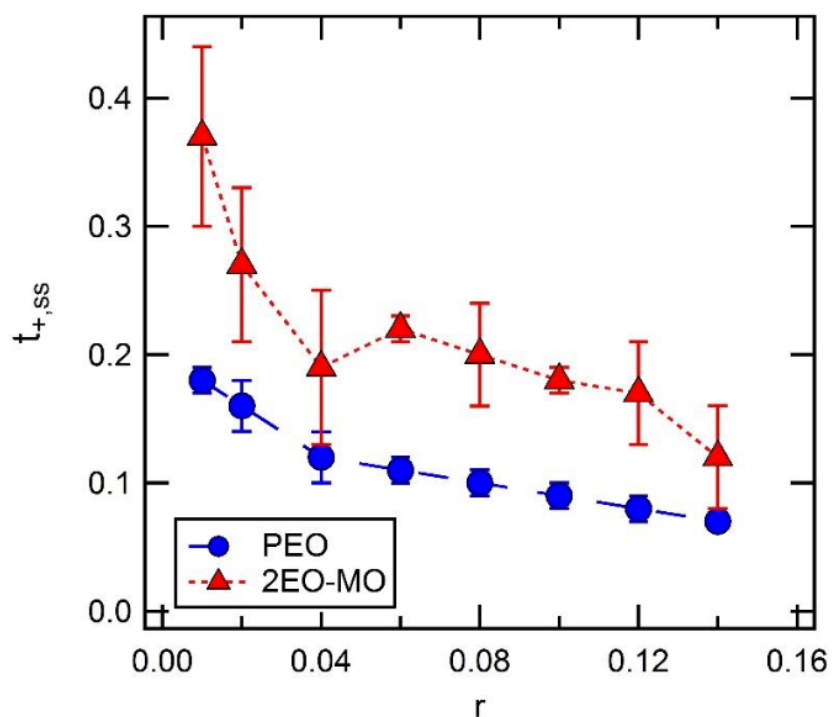


Figure A.3 Transference number t_{Li+} of PEO and P(MO-2EO) with increasing r ([Li]:[O]) at 90 °C.

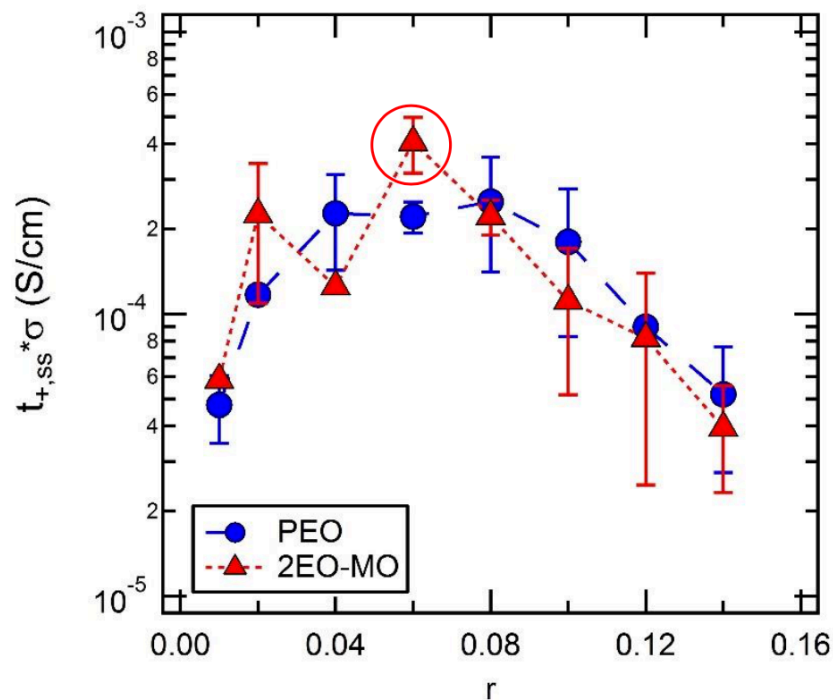


Figure A.4 Effective ionic conductivity (σ_{eff}) of PEO and P(MO-2EO) with increasing r ([Li]:[O]) at 90 °C.

The ionic conductivity (Figure A.2) was measured for one of the P(MO-2EO) samples (Table A.1, entry 1) and compared with that of PEO as well as the Li transference number (Figure A.3) and effective ionic conductivity σ_{eff} (defined as $\sigma_{\text{eff}} = \sigma \times t_{\text{Li}^+}$) (Figure A.4). The ionic conductivity of P(MO-2EO) was slightly lower than that of the PEO. However, the transference number showed a different trend with higher t_{Li^+} for P(MO-2EO) in all ranges of salt concentration. Thus, the effective ionic conductivity, which denoted the actual conductivity contributed by Li^+ transport, was higher for P(MO-2EO) in some salt concentrations, especially for $r = 0.06$. Presumably, the increase on t_{Li^+} was caused by the decreased chelation of polymer chains with Li cations due to the rigidity introduced by acetal groups. Further investigations are ongoing to elucidate the reason of high t_{Li^+} of P(MO-2EO).

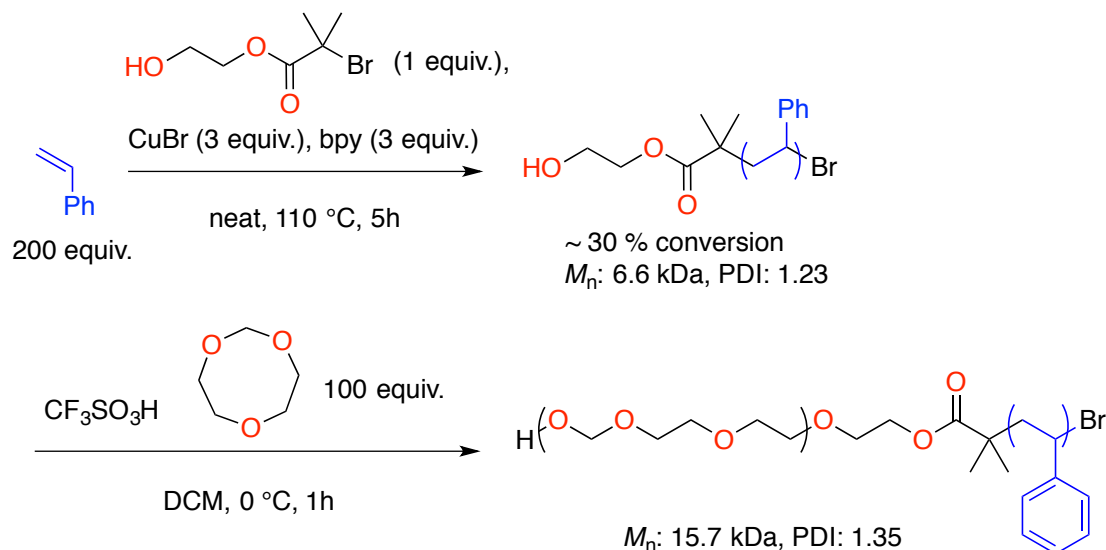


Figure A.5 Synthesis of PS-*b*-P(MO-2EO) block copolymer.

After identifying the superior conductivity of P(MO-2EO), we were interested in synthesizing a block copolymer of P(MO-2EO) and polystyrene (PS). The introduction of PS was proven to improve the mechanical properties of the polymer electrolyte and a recent report by Balsara *et al.*⁷ on PS-*b*-PEO suggested that the high shear modulus of PS helped to suppress the Li dendrite formation in Li-metal batteries. His group also reported many studies on the conductivity and morphology⁸ of PS-*b*-PEO. The PS-*b*-P(MO-2EO) block copolymer would be an interesting target to compare with the PS-*b*-PEO.

PS-*b*-P(MO-2EO) block copolymer was synthesized by a double initiator strategy (Figure A.5). The double initiator had one side (alkyl bromide) capable of initiating the atom-transfer radical polymerization (ATRP) of PS and the other side (alcohol) capable of growing the P(MO-2EO) block through cationic ring-opening polymerization. The ATRP was conducted first because the high reaction temperature of ATRP may depolymerize the P(MO-2EO) block. The yielded PS had a well-defined

M_n and a narrow PDI. The monomer, 1,3,6-trioxocane, was subsequently added with triflic acid. The triflic acid reacted with the alcohol end group of PS to form a triflic ester, which cationically polymerize the 1,3,6-trioxocane monomer. Homopolymers of 1,3,6-trioxocane and macrocycles can be removed by precipitation in methanol. GPC traces (Figure A.16) showed a clear shift to higher molecular weight region from PS to PS-*b*-P(MO-2EO), suggesting the formation of the di-block. Attempt in synthesizing PS-*b*-P(MO-2EO) with higher M_n , as well as morphology and conductivity measurements are ongoing and this new series of acetal polymers may replace PEO as a new generation of polymer electrolyte.

A.3 Experimental

A.3.1 General

All air and water sensitive reactions were carried out under dry nitrogen conditions using standard Schlenk techniques or MBraun UniLab drybox. ^1H NMR spectra were collected on a Bruker AV 500MHz spectrometer equipped with liquid nitrogen cooled cryoprobe and referenced with residue non-deuterated solvent shifts ($\text{CHCl}_3 = 7.26$ ppm). ^{13}C NMR spectra were collected on a Bruker AV 500 MHz (^{13}C , 125 MHz) spectrometer liquid nitrogen cooled cryoprobe and referenced to chloroform (δ 77.16 ppm). High resolution mass spectrometry (DART-HRMS) analyses were performed on a Thermo Scientific Exactive Orbitrap MS system equipped with an Ion Sense Direct Analysis in Real Time (DART) ion source.

Gel permeation chromatography (GPC) analyses were carried out using an Agilent PL-GPC 50 integrated system, equipped with UV and refractive index detectors, and 2 PL gel Mini-MIX C columns (5 micron, 4.6 mm ID). The GPC columns were eluted with tetrahydrofuran at 30 °C at 0.3 mL/min and were calibrated with monodisperse polystyrene standards.

The conductivity measurements were conducted in a similar way as reported in our previous paper.³ The synthesized polymers were dried under vacuum at 90 °C and transferred into a nitrogen dry glove box. The polymer and lithium bis(trifluoromethane)sulfonimide (LiTFSI) were dissolved in anhydrous THF. The resulting mixture was stirred at 90 °C for 3 h to yield a homogeneous solution. The solvent was evaporated and the residue was dried under vacuum at 90 °C for 8 h to yield the polymer electrolyte sample. The sample was then transferred into a 254 μm thick

silicon spacer and sandwiched between two 200 μm stainless steel electrodes. The thickness of the sample was taken the same as the thickness of the silicon spacer. The sample cell was secured with aluminum tabs to provide electrical contacts, vacuum sealed in a laminated aluminum pouch material (Showa-Denko), and removed from the glove box for electrochemical characterization.

Conductivity measurements were based on ac impedance spectroscopy acquired with a Biologic VMP3 potentiostat. The complex impedance measurements were performed for a frequency range of 1 Hz – 1 MHz at an amplitude of 80 mV. The low-frequency minimum on the Nyquist impedance plot was treated as the electrolyte resistance (R_b) and the ionic conductivity (σ) can be calculated according to Equation A.1:

$$\sigma = \frac{l}{aR_b} \quad \text{Equation A.1}$$

whereas a is the electrolyte area, which can be calculated from the inner diameter of the silicon spacer; l is the thickness of the electrolyte. After the measurement, the sample cells were disassembled to inspect that no defects were exhibited during the measurement, such as bubbles or voids. The defected cells, which were less than 5 % of all the samples prepared, were discarded from the data set. The reported conductivity was taken as the average of the results from three different samples and the error bars were deduced from the standard deviation of these measurements.

Transference number of the polymer electrolytes were measured based on the conventional Bruce and Vincent method.⁹ Specifically, a lithium symmetric cell was assembled with two lithium metal pieces as electrodes and the SPE as the separator. The transference number was then determined using the equation:

$$T_+ = \frac{I^s(\Delta V - I^o R_1^o)}{I^o(\Delta V - I^s R_1^s)} \quad \text{Equation A.2}$$

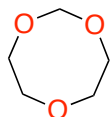
Here ΔV is the potential applied across the cell; R_1^o and R_1^s are the initial and steady state resistances of the passivating layers; I^o and I^s are the initial and steady-state currents respectively.

A.3.2 Materials

Diethylene glycol, paraformaldehyde, polyphosphoric acid, $\text{BF}_3 \cdot \text{OEt}_2$, α -bromoisobutyryl bromide was purchased from Sigma-Aldrich and used as received. *n*-Heptane was purchased from Fisher Scientific. Dichloromethane and tetrahydrofuran (THF) was purchased from Fisher Scientific and dried using a Phoenix solvent drying system and degassed by freeze-pump-thaw method for three cycles before use. All the other chemicals were purchased from commercial vendors and used as received unless otherwise noted. NMR solvent (CDCl_3) was purchased from Cambridge Isotope Laboratories (CIL) and used as received.

A.3.3 Synthesis

A.3.3.1 Synthesis of 1,3,6-trioxocane



Diethylene glycol (15.92 g, 150 mmol), paraformaldehyde (5.86 g, 195 mmol), and polyphosphoric acid (~0.2 mL) was dissolved in 30 mL *n*-heptane. The resulting mixture was refluxed at 110 °C for 16 h with a Dean-Stark head to remove the water generated from the reaction. Solvent was removed and the resulting white solid was melted by heating and distilled at 150 °C under static vacuum (0.2 torr). The collected liquid was a mixture of the desired product and diethylene glycol. The collected liquid was fractional distilled at 28 °C under static vacuum (0.2 torr) to yield the product as a colorless liquid (13.4 g, 75%).

¹H NMR (500 MHz, CDCl₃) δ 4.88 (s, 2H), 3.81 (s, 8H).

¹³C NMR (125 MHz, CDCl₃) δ 98.65, 73.29, 71.30.

HRMS (DART) *m/z* calculated for C₅H₁₁O₃⁺ [M + H]⁺ 119.07027, found 119.07095.

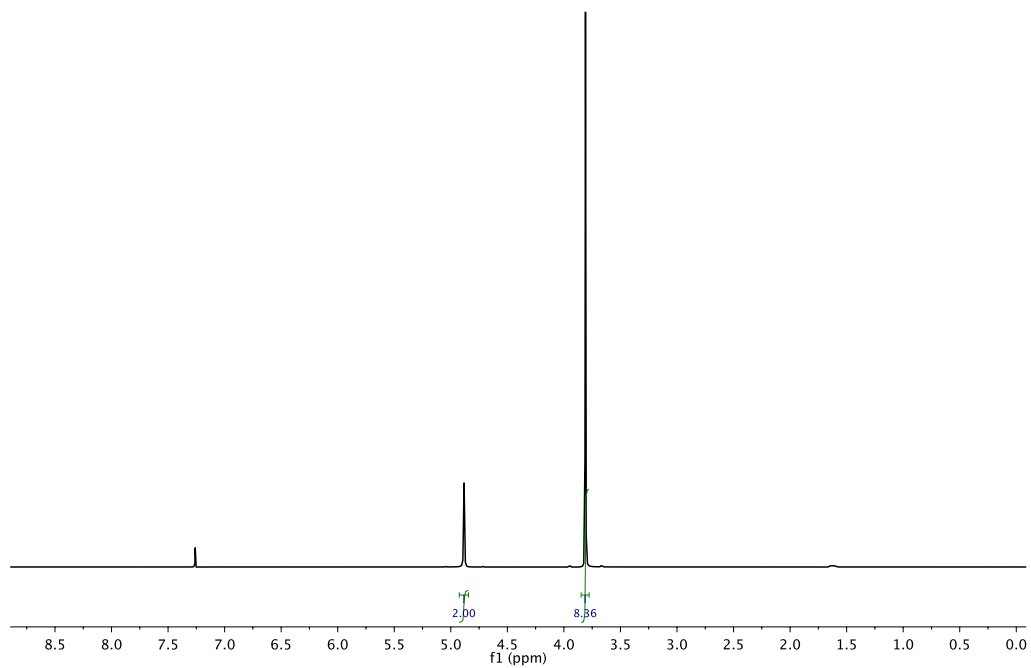


Figure A.6 ¹H-NMR spectrum of 1,3,6-trioxocane. Signal at 7.26 ppm is the residue CHCl₃.

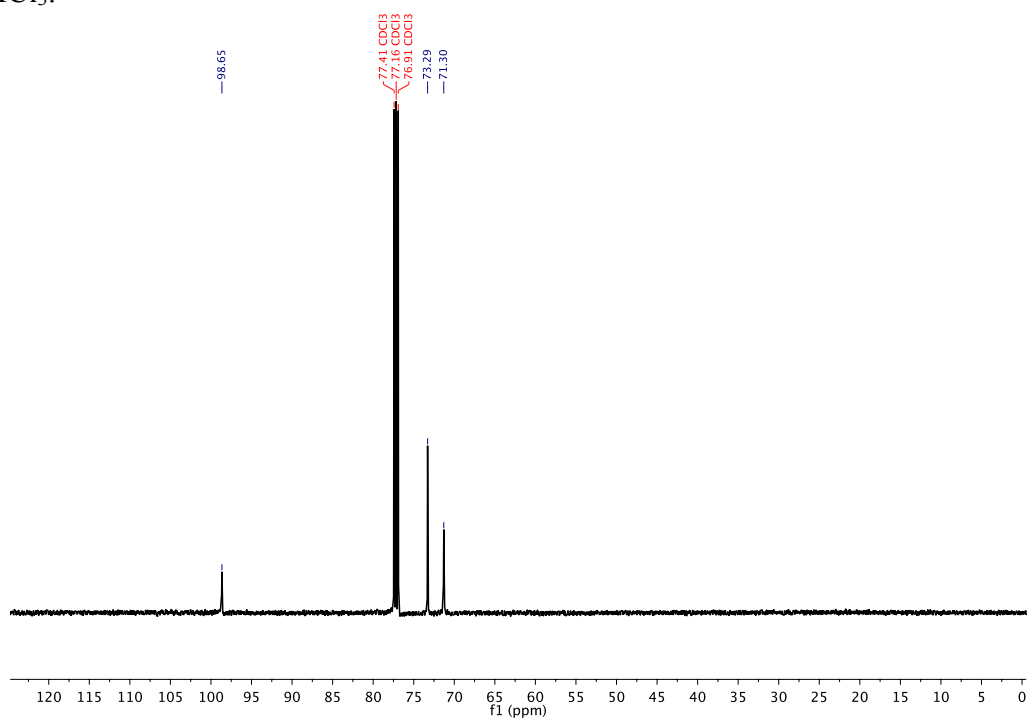
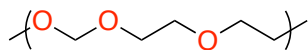


Figure A.7 ¹³C-NMR spectrum of 1,3,6-trioxocane. Signal at 77.16 ppm is the residue CHCl₃.

A.3.3.2 Synthesis of poly(1,3,6-trioxocane)



The monomer 1,3,6-trioxocane (4.00 g, 33.9 mmol) was dissolved in 10 mL dichloromethane. To this solution was added a 0.5 M stock solution of $\text{BF}_3 \cdot \text{OEt}_2$ (0.677 mL, 0.339 mmol). The mixture was stirred at room temperature for 2 h and quenched with water. The resulting mixture was washed with water and the organic layer was separated and dried over anhydrous Na_2SO_4 . The organic layer was concentrated under rotavapor and added dropwise into hexanes. A white solid was precipitated out. The solid was filtered and dried under vacuum to yield the polymer product as a white solid (3.30 g, 83 %).

^1H NMR (500 MHz, CDCl_3) δ 4.73 (s, 2H), 3.74 – 3.61 (m, 8H).

^{13}C NMR (125 MHz, CDCl_3) δ 95.73, 70.59, 67.02.

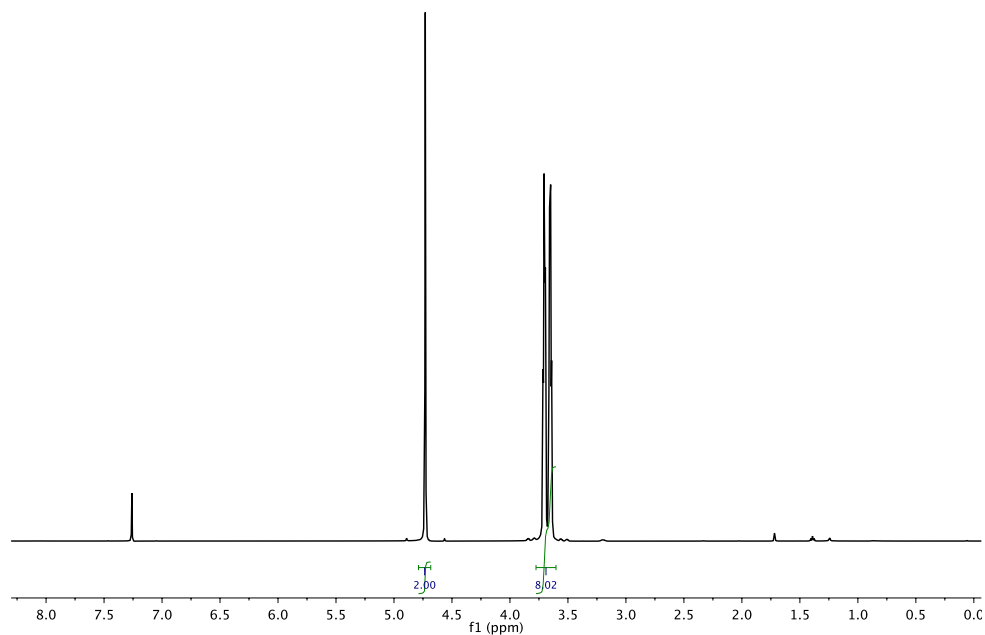


Figure A.8 ^1H -NMR spectrum of poly(1,3,6-trioxocane). Signal at 7.26 ppm is the residue CHCl_3 .

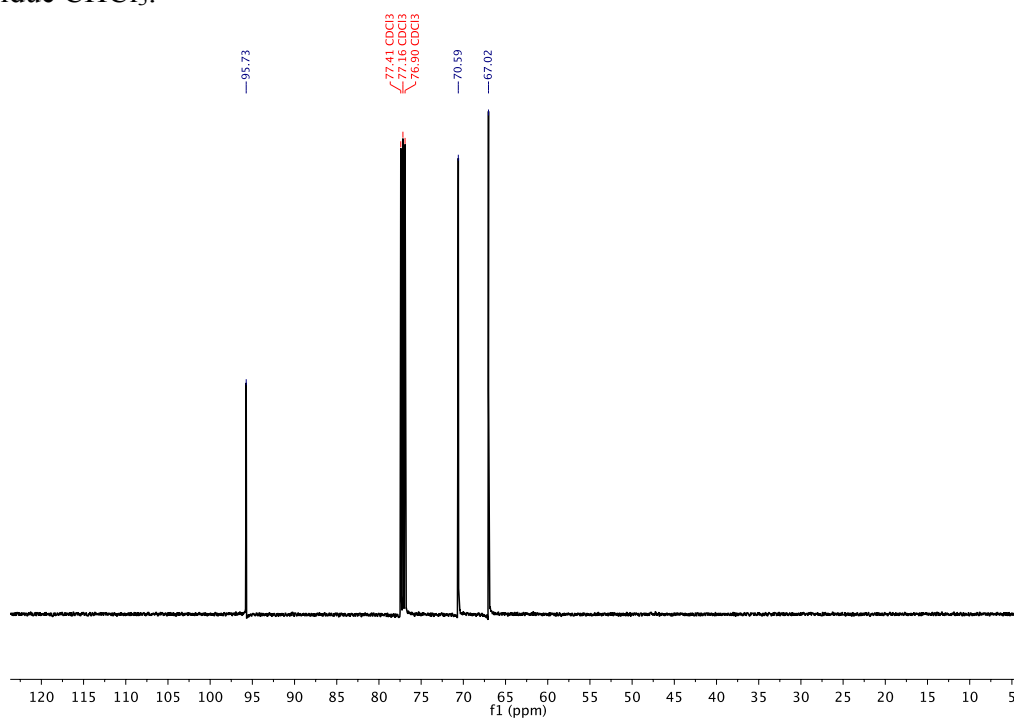
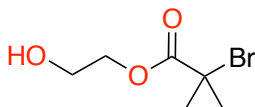


Figure A.9 ^{13}C -NMR spectrum of poly(1,3,6-trioxocane). Signal at 77.16 ppm is the residue CHCl_3 .

A.3.3.3 Synthesis of 2-hydroxyethyl 2-bromoisobutyrate (HEBI)



The double initiator HEBI was synthesized according to the literature.¹⁰ Diethylene glycol (3.82 mL, 68.4 mmol) and triethylamine (4.20 mL, 30 mmol) were dissolved in 50 mL anhydrous THF. The mixture was cooled to 0 °C and to it was added α -bromoisobutyryl bromide dropwise over 1.5 h. The mixture was stirred at 0 °C for another 1.5 h. Solvent was removed under rotavapor and the residue was dissolved in 50 mL water and extracted with dichloromethane (50 mL \times 2). The organic layer was washed with 1 M HCl aqueous solution, saturated NaHCO₃ aqueous solution, and dried over anhydrous Na₂SO₄. Solvent was removed and the residue was distilled under reduced pressure (0.2 torr, 48 °C) to yield the crude product. Redistill the crude product yielded the pure product as a colorless liquid (3.82 g, 60 %).

¹H NMR (500 MHz, CDCl₃) δ 4.36 – 4.33 (m, 2H), 3.92 – 3.88 (m, 2H), 1.98 (s, 6H).

¹³C NMR (125 MHz, CDCl₃) δ 172.05, 67.57, 61.05, 55.93, 30.84.

HRMS (DART) m/z calculated for C₆H₁₂O₃Br⁺ [M + H]⁺ 210.99643, found 210.99572.

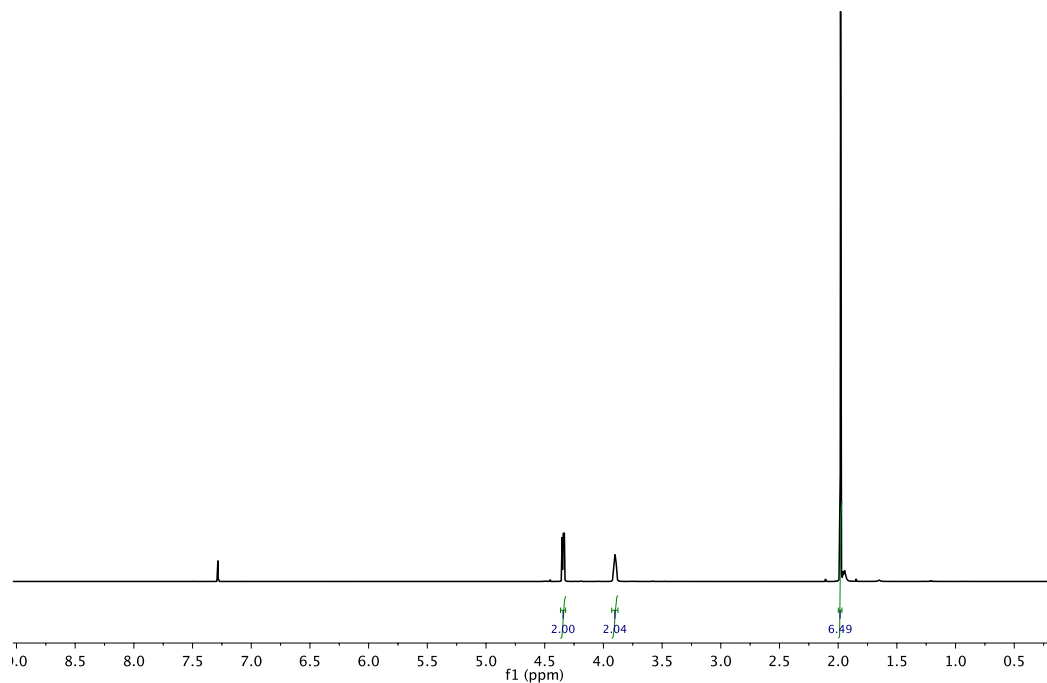


Figure A.10 ¹H-NMR spectrum of HEBI. Signal at 7.26 ppm is the residue CHCl₃.

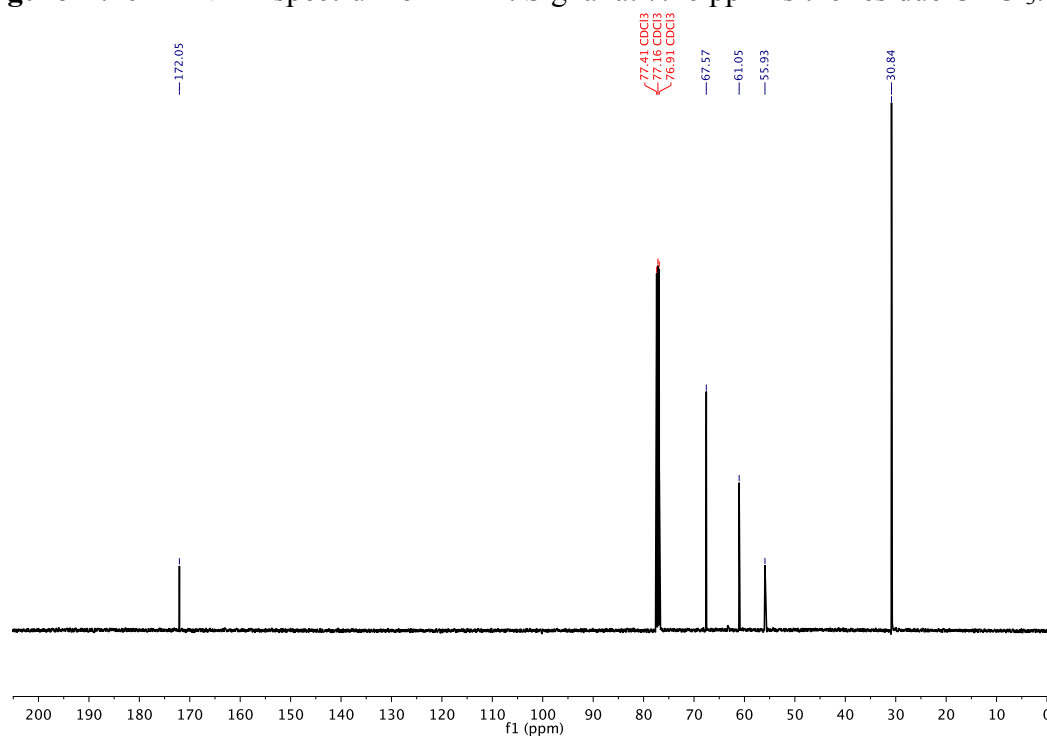
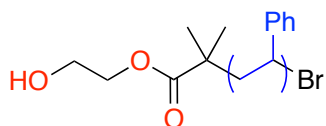


Figure A.11 ¹³C-NMR spectrum of HEBI. Signal at 77.16 ppm is the residue CHCl₃.

A.3.3.4 Synthesis of hydroxyl terminated polystyrene (PS-OH)



Hydroxyl terminated polystyrene (PS-OH) was synthesized by atom-transfer radical polymerization (ATRP).¹¹ CuBr was washed with acetic acid to remove CuBr₂ and dried under vacuum before use. Styrene was dried over CaH₂ and distilled before use. CuBr (71.7 mg, 0.5 mmol), 2,2'-bipyridine (bpy) (234 mg, 1.5 mmol), and the double initiator HEBI (105.5 mg, 0.5 mmol) was mixed in styrene (11.5 mL, 100 mmol). The resulting mixture was degassed by free-pump-thaw for 3 cycles and left sealed under static vacuum. The mixture was then heat to 110 °C and stirred for 5 h. The mixture was rapidly cooled down to room temperature and opened to air. ¹H-NMR spectroscopy of the crude mixture showed a conversion of 30 % based on integrations. The mixture was diluted with THF and passed through a plug of neutral alumina to remove the copper catalyst. The yielded colorless solution was concentrated and added dropwise to MeOH. The precipitate was collected by filtration and dried under vacuum to obtain the polymer as a white fine powder (3.13 g, 30.1 %)

GPC (calibrated to PS) M_n = 6.6 kDa, \mathcal{D} = 1.22

¹H NMR (500 MHz, CDCl₃) δ 7.30 – 6.89 (m, 3H), 6.89 – 6.29 (m, 2H), 2.14 – 1.69 (m, 1H), 1.68 – 1.26 (m, 2H).

¹³C NMR (125 MHz, CDCl₃) δ 164.96 – 144.93, 128.93 – 127.36, 126.26 – 125.46, 41.13 – 39.93.

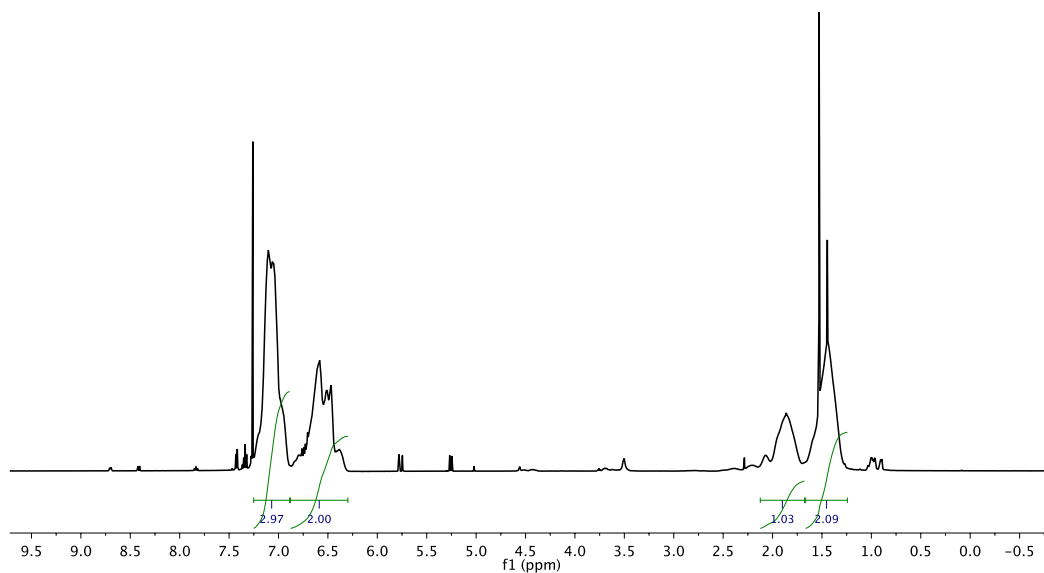


Figure A.12 ^1H -NMR spectrum of PS-OH. Signal at 7.26 ppm is the residue CHCl_3 .

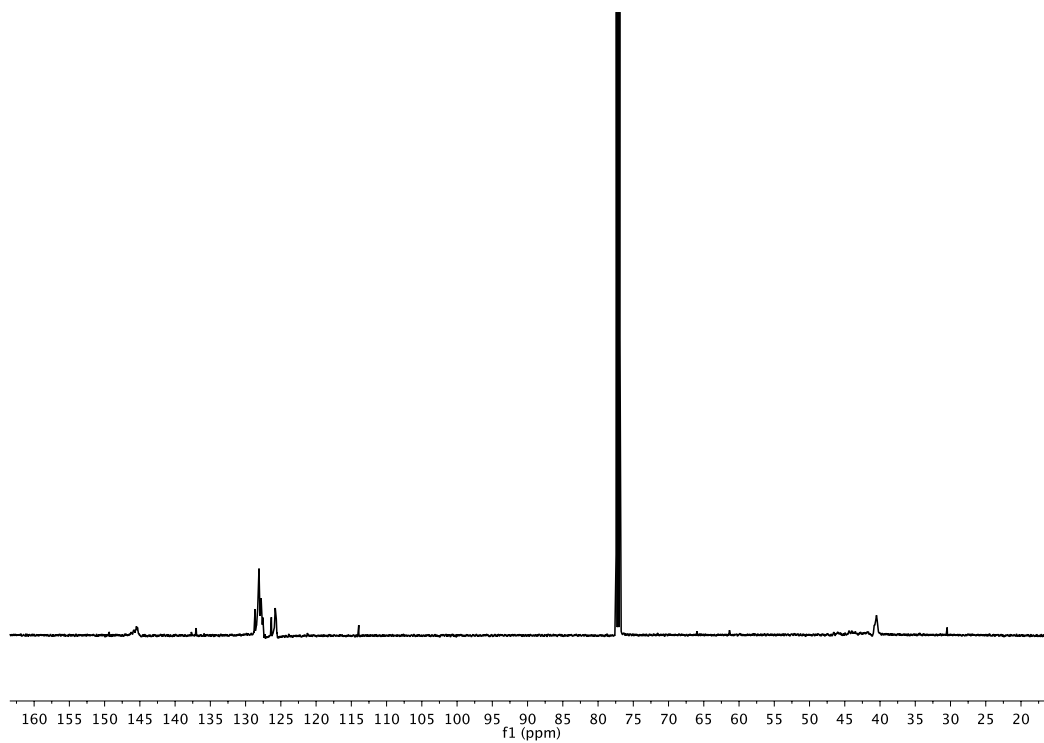
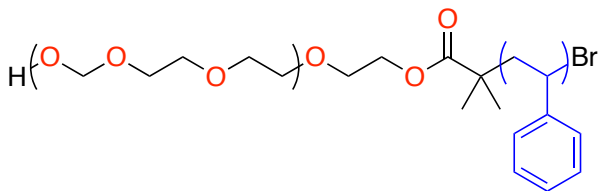


Figure A.13 ^{13}C -NMR spectrum of PS-OH. Signal at 77.16 ppm is the residue CHCl_3 .

A.3.3.5 Synthesis of polystyrene-*b*-poly(1,3,6-trioxocane) (PS-*b*-P(MO-2EO))



To a solution of 6.6 kDa PS-OH (838.2 mg, 0.127 mmol) in 2 mL dichloromethane was added trifluoromethanesulfonic acid (2 μ L) at 0 °C. A solution of 1,3,6-trioxocane (1.50 g, 12.7 mmol) in 1.5 mL dichloromethane was added to the mixture over 1 h. The mixture was stirred for another hour at 0 °C before quenching with water. The mixture was extracted with dichloromethane and the organic layer was dried over anhydrous Na₂SO₄. The solvent was removed and the concentrated solution was added to MeOH dropwise. The precipitate was filtered and dried under vacuum to yield the product as a white solid (1.39 g, 59%)

GPC (calibrated to PS) M_n = 15.7 kDa, D = 1.35

¹H NMR (500 MHz, CDCl₃) δ 7.25 – 6.87 (m, 3H of PS), 6.85 – 6.30 (m, 2H of PS), 4.74 (s, 2H of P(MO-2EO)), 3.75 – 3.63 (m, 8H of P(MO-2EO)), 2.16 – 1.73 (m, 1 H of PS), 1.66 – 1.24 (m, 2H of PS).

¹³C NMR (125 MHz, CDCl₃) δ 146.62 – 144.96, 129.29 – 127.04, 126.39 – 125.20, 95.61, 70.47, 66.90, 40.93 – 40.04.

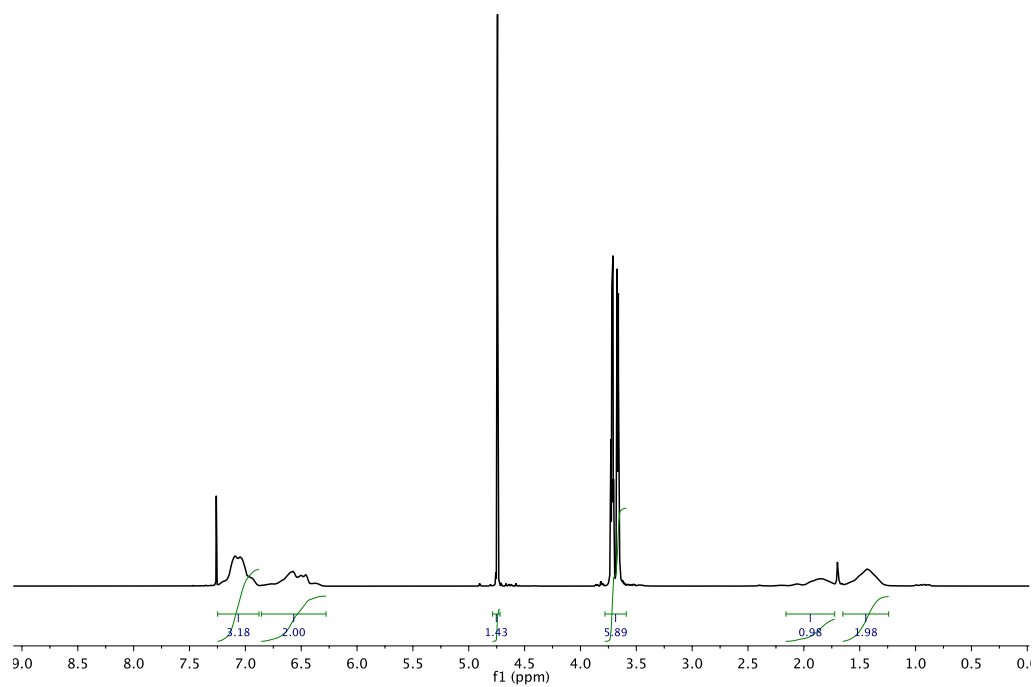


Figure A.14 ^1H -NMR spectrum of (PS-*b*-P(MO-2EO)). Signal at 7.26 ppm is the residue CHCl_3 .

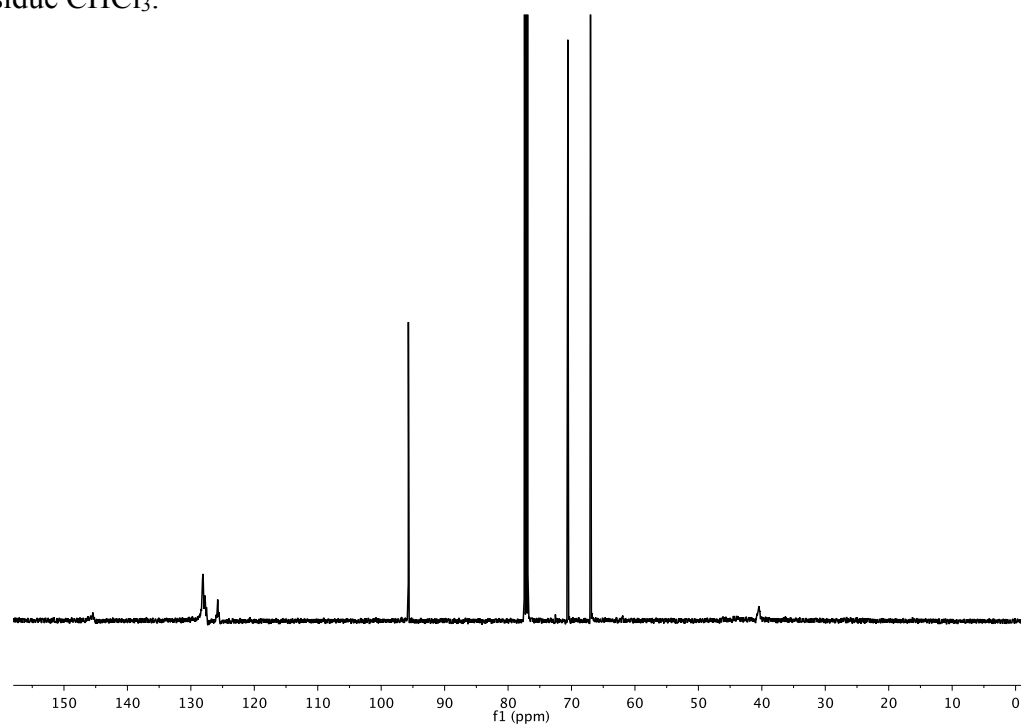


Figure A.15 ^{13}C -NMR spectrum of (PS-*b*-P(MO-2EO)). Signal at 77.16 ppm is the residue CHCl_3 .

A.3.4 GPC traces

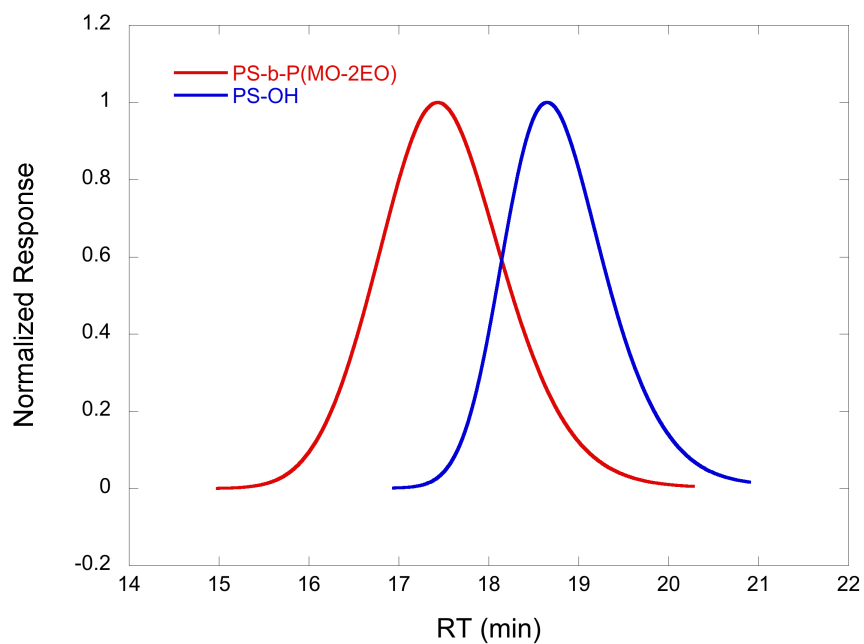


Figure A.16 GPC traces of PS-OH and PS-*b*-P(MO-2EO).

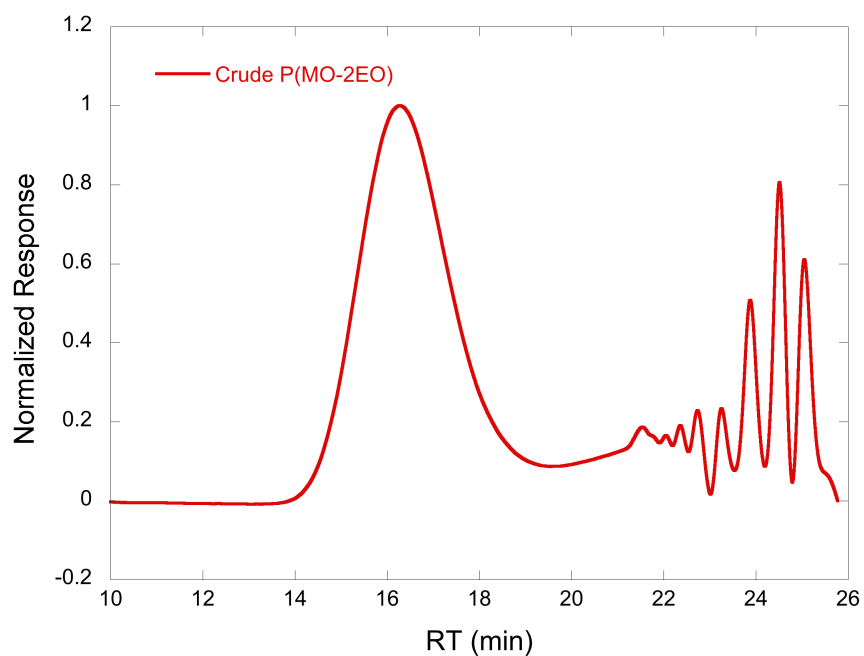


Figure A.17 The GPC trace of the crude mixture of Table A.1 entry 3.

REFERENCES

- (1) Fenton, D. E.; Parker, J. M.; Wright, P. V. *Polymer* **1973**, *14*, 589.
- (2) Linden, E.; Owen, J. R. *Solid State Ionics* **1988**, *28-30*, 994–1000.
- (3) Pesko, D. M.; Webb, M. A.; Jung, Y.; Zheng, Q.; Miller, T. F.; Coates, G. W.; Balsara, N. P. *Macromolecules* **2016**, *49*, 5244–5255.
- (4) Xu, B.; Lillya, C. P.; Chien, J. C. W. *Macromolecules* **1987**, *20*, 1445–1450.
- (5) Okada, M.; Kozawa, S.; Yamashita, Y. *Die Makromol. Chem.* **1969**, *127*, 66–77.
- (6) Kawakami, Y.; Yamashita, Y. *Macromolecules* **1977**, *10*, 837–839.
- (7) Stone, G. M.; Mullin, S. A.; Teran, A. A.; Hallinan, D. T.; Minor, A. M.; Hexemer, A.; Balsara, N. P. *J. Electrochem. Soc.* **2012**, *159*, A222–A227.
- (8) Chintapalli, M.; Le, T. N. P.; Venkatesan, N. R.; Mackay, N. G.; Rojas, A. A.; Thelen, J. L.; Chen, X. C.; Devaux, D.; Balsara, N. P. *Macromolecules* **2016**, *49*, 1770–1780.
- (9) Bruce, P. *Solid State Ionics* **1988**, *28-30*, 918–922.
- (10) Yuan, H.; Chi, H.; Yuan, W. *Polym. Chem.* **2016**, *7*, 4901–4911.
- (11) Xu, Y.; Pan, C.; Tao, L. *J. Polym. Sci. A Polym. Chem.* **2000**, *38*, 436–443.